

**INNER, OUTER AND INTRA COORDINATION
SPHERE FUNCTIONALISATION OF DIIRON
UNITS RELATED TO THE SUBSITE OF
[FeFe]-HYDROGENASES**

A thesis submitted to the University of East Anglia

For the Degree of Doctor of Philosophy

Submitted September 2016

James Richard Woods

Energy Materials Laboratory

School of Chemistry, UEA

Norwich

This copy of this thesis has been supplied on the condition that anyone who consults it is understood to recognise that its copyright rests with the author and that no quotation from the thesis, nor any information derived therefrom, may be published without the author's prior written consent. ©

Abstract

A dithiolate diiron subsite is an essential component of the H-cluster of [FeFe]-hydrogenase, it provides the centre at which protons and electrons are reversibly combined to produce dihydrogen and is fed electrons from the other component, a $4\text{Fe}4\text{S}$ cluster to which it is attached by a cysteinyl bridge. Much research has focused on developing synthetic analogues of the subsite, both to inform an understanding of the chemistry and spectroscopy of the natural system and to explore their technological potential as electrocatalysts for fuel or producer cell applications. This thesis reports new approaches for building modifications into subsite analogues which have the potential to alter their structure and function. Synthetic methods are described for: (i) introducing Lewis base or Lewis acid groups into the second coordination sphere of a diiron unit (ii) exploiting the N-basicity of coordinated cyanide to build H-bonding or bridging cyanide systems (iii) incorporating carborane structural units as part of a dithiolate diphosphine framework.

Key results include the X-ray crystallographic characterisation of a zwitterionic complex in which a Ru photosensitiser group is linked via bridging cyanide to a diiron hydrogenase subsite analogue, the characterisation of hydrogen bonding adducts of activated bis-ureas with dicyanide dithiolato diiron complexes by mass and FTIR spectroscopy, and the first example in which a borane Lewis acid is attached to a diiron unit, an approach which may presage cleavage of molecular hydrogen by a novel frustrated Lewis acid Lewis base system.

Acknowledgements

I would first like to thank my primary supervisor Prof Chris Pickett for giving me the opportunity to study for this Ph.D. His guidance and enthusiasm have been invaluable and I wish him and Mish all the very best for the future.

I would also like to thank Prof Simon Lancaster for being supportive and knowledgeable, and for always making time if I needed to chat about my chemistry and bounce ideas around.

My sincere gratitude goes to my colleague and good friend Dr Joseph Wright for X-ray crystallography, good advice, and without whom I'd still be lost somewhere in Barcelona.

I would also like to thank Prof Manfred Bochmann and his group for granting me bench space in their laboratory, and for making my time in the lab so enjoyable. I would also like to thank Dr John Fielden for his help and advice.

I have also been lucky to have two very hardworking undergraduate students, Lewis Wilkins and Lee Biggs, whose results have contributed to the work in chapters 2 and 3 of this thesis.

I would also like to thank Prof Guo-Xin Jin for hosting me at Fudan University, Shanghai for three months, and a special thank you goes to my very good friend Long Zhang who taught me how to be amazing at table tennis and swear in Mandarin.

Many thanks to my other friends and colleagues in the Chemistry department at UEA both past and present for making the duration of my Ph.D. a great experience; special mention goes to Dragos, Angel, Julio, Luca, Alex, Anna, Amanda, Mark, Farhana, Lucy, Ben and Moz.

I would like to thank my parents for always encouraging me and for being there when I need them, and to my sisters Helen and Katherine for their blunt advice and support.

Finally I would to thank my wife Rhiannon for her love and support, and always knowing if I need a hug or a kick up the backside, and then delivering it. You're the best and I'm lucky to have you.

Table of Contents

Abstract	i
Acknowledgements	ii
Abbreviations	vii
1 Introduction	1
1.1 Scope of this work	1
1.2 Background to the work	1
1.3 Methodology.....	7
2 Second coordination sphere functionalisation of a diiron subsite analogue with basic pyridine units	9
2.1 Introduction	9
2.1.1 Background	9
2.1.2 Hydroxyl-functionalised diiron subsite analogues.....	11
2.1.3 Functionalisation by ester bond formation.....	13
2.1.4 Scope of this work.....	13
2.2 Results and discussion.....	15
2.2.1 Synthesis of diiron subsite analogue	15
2.2.2 Attachment of aromatic groups by Steglich Esterification	15
2.2.3 Attachment of pyridine groups by esterification.....	21
2.2.4 Protonation of the pyridine-derived esters	26
2.2.5 Electrochemistry	31
2.2.6 Concluding remarks	38
2.3 Experimental.....	40
3 Hydrogen bonding of a diiron dicyanide subsite analogue with fluorinated bis-ureas	51
3.1 Introduction	51
3.1.1 General aspects.....	51

3.1.2	Hydrogen bonding in the natural system	51
3.1.3	Interest in the cyanide groups	52
3.1.4	Hydrogen bonding.....	57
3.1.5	Fluorinated bis-ureas to hydrogen bond cyanides.....	59
3.2	Results and discussion.....	63
3.2.1	Synthesis of diiron subsite analogues	63
3.2.2	Synthesis of fluorinated bis-ureas	65
3.2.3	The binding of fluorinated bis-ureas to $[\text{Fe}_2(\text{pdt})(\text{CO})_4(\text{CN})_2]^{2-}$	67
3.2.4	The nature of the interactions of a diiron dicyanide subsite analogue with fluorinated bis-ureas.....	92
3.2.5	Protonation of $[\text{Fe}_2(\text{pdt})(\text{CO})_4(\text{CN})_2 \cdot (\text{bis-urea})_2]^{2-}$	94
3.2.6	Concluding remarks and future work.....	97
3.3	Experimental.....	100
4	Intimate linking of a photoactive Ru(II) centre to a diiron subsite analogue via bridging cyanide	105
4.1	Introduction	105
4.1.1	General aspects.....	105
4.1.2	Photosensitised [FeFe]-hydrogenase mimic systems.....	105
4.1.3	The advantages of Ru(II)-bipyridine systems as photosensitisers	112
4.1.4	Further interest in ligated cyanide groups	113
4.1.5	Mechanistic advantages of a $[\text{Fe}_2(\text{pdt})(\text{CO})_4(\text{CN})(\mu\text{-CN})\text{Ru}(\text{tpy})(\text{bpy})]$ system.....	116
4.1.6	A photoactive unsensitised [FeFe]-hydrogenase subsite system	119
4.2	Results and discussion.....	121
4.2.1	Synthesis of the $\text{Ru}(\text{II})(\text{tpy})(\text{bpy}).\text{OH}_2$ system.....	121
4.2.2	Formation of the $[\text{Fe}_2(\text{pdt})(\text{CO})_4(\text{CN})(\mu\text{-CN})\text{Ru}(\text{tpy})(\text{bpy})]$ dyad.....	123
4.2.3	Structure and properties of $[\text{Fe}_2(\text{pdt})(\text{CO})_4(\text{CN})(\mu\text{-CN})\text{Ru}(\text{tpy})(\text{bpy})]$..	124
4.2.4	Concluding remarks and future work.....	136

4.3	Experimental.....	138
5	Incorporation of <i>ortho</i>-carboranes into the backbone structure of Fe-Fe subsite analogues	143
5.1	Introduction	143
5.1.1	General aspects.....	143
5.1.2	Interest in <i>ortho</i> -carboranes	143
5.1.3	Existing <i>ortho</i> -carborane [FeFe]-hydrogenase subsite analogue systems	145
5.1.4	Bidentate <i>ortho</i> -carborane ligands	146
5.2	Results and discussion.....	149
5.2.1	Synthesis of the bidentate <i>ortho</i> -carborane ligand.....	149
5.2.2	Reaction of the bidentate <i>ortho</i> -carborane ligand to generate diiron species	150
5.2.3	Spectroscopic properties of [Fe ₂ { <i>o</i> -carbP(Ph) ₂ S} ₂ (CO) ₄]	155
5.2.4	Concluding remarks and future work.....	159
5.3	Experimental.....	161
6	Towards heterolytic hydrogen splitting: attachment of electron-deficient boranes	165
6.1	Introduction	165
6.1.1	General aspects.....	165
6.1.2	Interest in a diiron system capable of hydrogen cleavage.....	165
6.1.3	Borane groups for hydrogen splitting	168
6.2	Results and discussion.....	172
6.2.1	Synthesis of perfluoroaryl boranes.....	172
6.2.2	Synthesis of a hydroxyl-functionalised diiron subsite analogue.....	173
6.2.3	Combination of [Fe ₂ {CH ₃ C(CH ₂ OH)(CH ₂ S) ₂ }(CO) ₆] with HB(C ₆ F ₅) ₂ ·SMe ₂	174
6.2.4	Combination of [Fe ₂ (dmp)(CO) ₆] with HB(C ₆ F ₅) ₂ ·SMe ₂	176

6.2.5	Synthesis of a diiron subsite analogue with alkene functionality	178
6.2.6	Attempted hydroboration of $[\text{Fe}_2\{\text{C}_4\text{H}_7\text{CH}(\text{S})\text{CH}_2\text{S}\}(\text{CO})_6]$ with $\text{HB}(\text{C}_6\text{F}_5)_2\cdot\text{SMe}_2$	180
6.2.7	Concluding remarks and future work.....	183
6.3	Experimental.....	184
7	References	192

Abbreviations

adt	2-Azapropan-1,3-dithiolate
CV	Cyclic voltammetry
DCC	N,N'-dicyclohexylcarbodiimide
DCM	Dichloromethane
DFT	Density functional theory
DHU	Dicyclohexylurea
DMAP	N,N-dimethyl-4-aminopyridine
DME	1,2-dimethoxyethane
DMF	<i>N,N</i> -dimethylformamide
dmp	2,3-Dimercapto-1-propanol
DMSO	Dimethyl sulfoxide
dppv	<i>cis</i> -1,2-Bis(diphenylphosphino)ethylene
EI	Electron ionisation
EPR	Electron paramagnetic resonance
Et	Ethyl
Fc	Ferrocene
FTIR	Fourier transform infrared
HOMO	Highest occupied molecular orbital
HYSCORE	Hyperfine sub-level correlation
IR	Infrared
LUMO	Lowest unoccupied molecular orbital

MeCN	Acetonitrile
mes	Mesityl
MLCT	Metal to ligand charge transfer
MS	Mass spectrometry
NMR	Nuclear magnetic resonance
<i>o</i> -carbP(Ph) ₂ S	1-SH-2-PPh ₂ -1,2- <i>closo</i> -C ₂ B ₁₀ H ₁₀
Ph	Phenyl
pdt	Propan-1,3-dithiolate
RT	Room temperature
SCE	Saturated calomel electrode
THF	Tetrahydrofuran
UV-vis	Ultraviolet-visible

1 Introduction

1.1 Scope of this work

This thesis is primarily concerned with approaches to the modification of the structure and function of [FeFe]-hydrogenase subsite analogues. Synthetic methods are described for: (i) introducing Lewis base or Lewis acid groups into the second coordination sphere of a diiron unit, (ii) exploiting the N-basicity of coordinated cyanide to build H-bonding or bridging cyanide systems, (iii) incorporating carborane structural units as part of a dithiolate diphosphine framework.

The thesis starts with this introductory **Chapter 1** which includes an overview of chemistry related to the biological [FeFe]-hydrogenase system together with a summary of the methodologies employed, and is followed by five discrete experimental chapters; each of these focussing on a separate topic with a self-contained introduction, results and discussion, conclusion and experimental sections. **Chapter 2** is concerned with the attachment of pendant pyridine groups by esterification of a diiron subsite backbone together with an investigation of protonation and electron transfer properties. **Chapter 3** explores the potential for cyanide ligands present on diiron units to engage in hydrogen bonding with fluorinated bis-ureas using FTIR and ESI-MS spectroscopy. **Chapter 4** reports the attachment of a Lewis acidic ruthenium photosensitising moiety to a diiron unit via formation of a bridging cyanide link. The electronic and photophysical properties of this novel dyad species are explored. **Chapter 5** outlines the synthesis of a diiron unit with *o*-carborane moieties incorporated into the backbone, with the key physical properties of this new species being investigated. Finally, **Chapter 6** details steps taken towards attachment of a pendant borane group, with the ultimate goal being a diiron system capable of heterolytically cleaving dihydrogen.

1.2 Background to the work

Whilst mankind has only been concerned with the production and utilisation of hydrogen as a clean energy source for the last few decades, nature has long since developed its own set of catalysts that use relatively abundant and inexpensive first-row

transition metals such as nickel and iron to metabolise hydrogen, the hydrogenase enzymes.

Characterisation of certain living organisms, such as archaea, bacteria, cyanobacteria and algae, has led to the exciting discovery that hydrogen can either be produced or utilised as a source of low-potential electrons within living cells participating in a global H₂ cycle^{1,2}. This chemical activity is made possible through the expression of a class of metalloenzymes known as 'hydrogenases'³⁻⁵, so named after Stickland and Stephenson⁶ observed bacteria consuming dihydrogen for the reduction of physiological artificial substrates, as well as demonstrating the ability to evolve dihydrogen during growth.

There are three identified classes of hydrogenase enzyme: [FeFe]-hydrogenase, [NiFe]-hydrogenase, and [Fe]-hydrogenase, referred to as such in reference to the metals located on their active sites⁷. The [Fe]-hydrogenase, also known as Hmd, catalyses the heterolytic cleavage of dihydrogen⁸⁻¹⁰ and the action of which is explained in **Chapter 6**. The [FeFe]- and [NiFe]- analogues differ in that their primary function is to catalyse the interconversion of dihydrogen into protons and electrons. They are capable of catalysing these reactions at very high rates, with one molecule of hydrogenase producing between 1,500 and 20,000 molecules of H₂ per second at the mild conditions of pH 7 and 37 °C in water^{11,12}. The [FeFe]- and [NiFe]- hydrogenases are both bi-metallic redox active systems, with the active sites being constructed of bridged thiolate groups and the metals being ligated with CO and CN⁻ ligands. Such ligands are rare in naturally-occurring biological systems, and are understood to serve as π -acceptors that stabilise the low redox states of the metal ions^{13,14}. The structures of these active sites are shown in **Figure 1.1**.

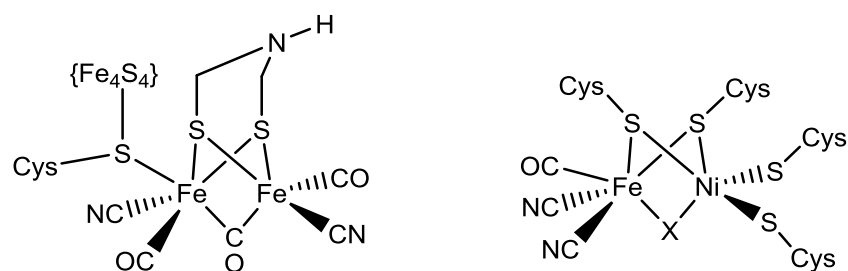


Figure 1.1 Left: active site of the [FeFe]-hydrogenase (the H-cluster). Right: active site of the [NiFe]-hydrogenase (X = HOS⁻, HO⁻ or H⁻ depending on the state). Adapted from references¹⁵⁻¹⁷.

The two systems differ in their activity and their sensitivity to inhibition by O₂ and CO. The [NiFe]-hydrogenases are less sensitive to inhibition by CO and O₂ and their biological function involves the uptake rather than generation of H₂.¹⁸ The activity of the [FeFe]-hydrogenase can be 10 to 100 times greater than [NiFe]-hydrogenases for both the oxidation of H₂ and the reduction of protons¹⁹ and as such have been extensively studied.

EPR spectroscopy of the [FeFe]-hydrogenase in the 1980s showed the presence of two {4Fe4S}-clusters often found within this enzyme²⁰, along with an unidentified 6Fe cluster. The X-ray crystal structure of this enzyme was solved independently by two groups (Peters¹⁷ and Fontecilla-Camps²¹) in 1998/1999 and demonstrated the 6Fe unit to be that which is now commonly referred to as the 'H-cluster', **Figure 1.2**.

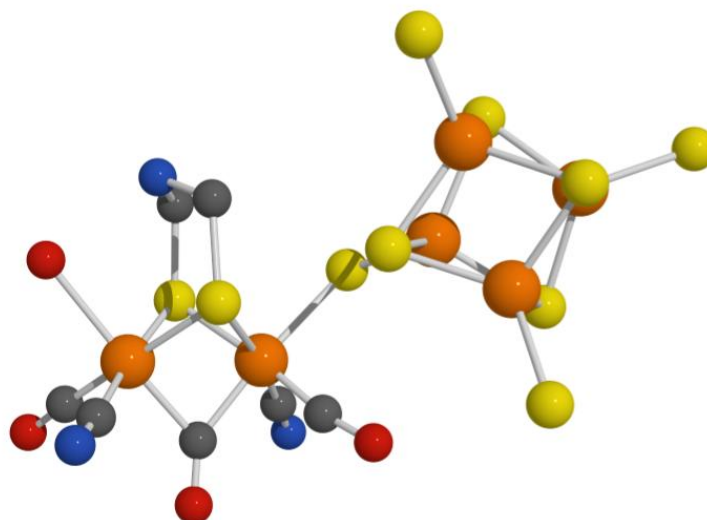


Figure 1.2 Schematic representation of the X-ray structure of the H-cluster of [FeFe]-hydrogenase from *Clostridium pasteurianum* (PDBcode: 3C8Y)¹⁷. The bridgehead atom presented here is given as a nitrogen based on current consensus, though in the original report it was modelled as an oxygen. The vacant site was occupied by a water molecule. Image reproduced from reference²².

The H-cluster consists of a cubane {4Fe4S} electronic transfer unit connected via a single bridging cysteinyl residue to a binuclear {2Fe2S} subsite, with both Fe atoms bridged by a dithiolate ligand. The Fe atom distal to the cubane unit possesses a rotated state geometry and in Peters' structure¹⁷ is coordinated by a labile water ligand in the resting state of the molecule. In the structure obtained by Fontecilla-Camps²¹ from *Desulfovibrio desulfuricans* a water molecule is not bound in this position, suggesting that this is the metal centre at which a hydride or dihydrogen may bind during catalysis. The identity of the atom in the bridgehead moiety, -SCH₂-X-CH₂S- (Xdt), has long been a point of contention. The electron density from the X-ray structure indicated atom X to either be C, N or O, with the potential of an amine function to participate in a catalytic cycle by proton trafficking making N seemingly the most likely²³. Further support of this hypothesis was provided by analysis of ¹⁴N nuclear quadrupole and hyperfine interactions of the H-cluster determined by advanced EPR spectroscopy²⁴⁻²⁶. However, this mystery was seemingly finally solved in 2013 when Berggren and coworkers²⁷ demonstrated that maturation of an apo-HydA with complexes of the three variants only

showed activity comparable to the natural system when employing an N-containing azadithiolate (adt) bridgehead.

The current consensus of the catalytic cycle of the [FeFe]-hydrogenase is given in **Figure 1.3**. The species H_{red} and H_{ox} have been isolated crystallographically and spectroscopically. Whilst there is EPR and FTIR evidence supporting the assignment of H_{sred} many of the other intermediates proposed in the cycle are subject to speculation.

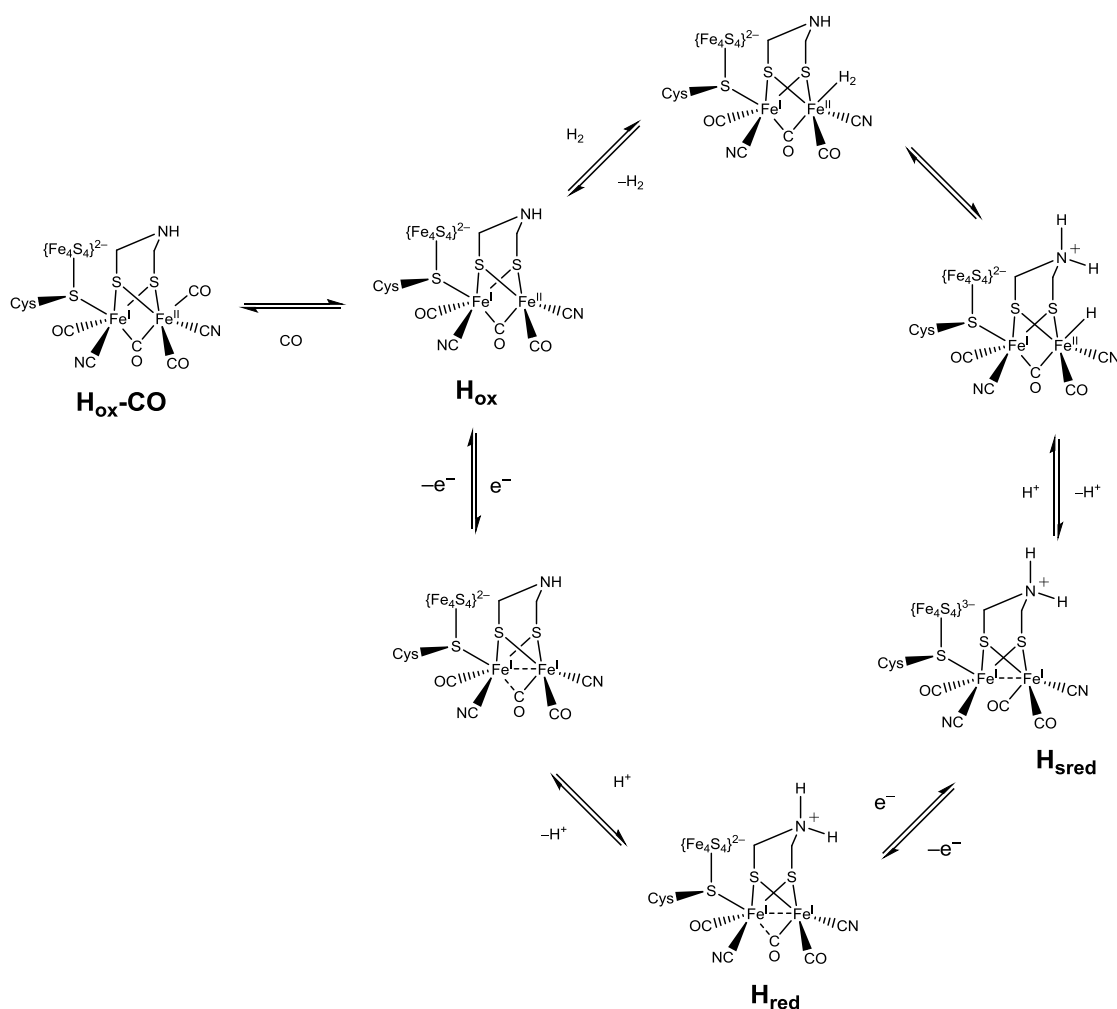


Figure 1.3 Postulated catalytic cycle for [FeFe]-hydrogenase²⁸.

The proposed oxidation of H_2 by [FeFe]-hydrogenase occurs by H_2 first binding to the vacant site of the distal Fe in H_{ox} , followed by heterolytic cleavage of the H-H bond assisted by the amine on the bridgehead and finally the transfer of two electrons

individually from the Fe bound hydride to the {4Fe4S} cluster and the distal Fe on the FeFe subsite. The release of protons and electrons from H_{sred} regenerates the starting H_{ox} state completing catalytic cycle. Each step in the cycle is reversible and thus the reduction of protons to H_2 follows the same steps but in the opposite direction.

The first crystal structures of the [FeFe]-hydrogenases prompted much chemical research on synthetic structures. This was both to aid in the understanding of the natural system and to explore the possibility of ‘stripped-down’ artificial systems for hydrogen production or uptake in reversible fuel cells²⁹. It was quickly recognised that synthetic species with some structural analogy to the diiron subsite unit were known long before the structure of the H-cluster was determined. In 1929 a study of the synthesis of bridged hexacarbonyl species by Reihlen and coworkers³⁰ included the synthesis of the diiron species $[\text{Fe}_2(\text{SEt})_2(\text{CO})_6]$, **(a)** in **Figure 1.4**, which exhibited the characteristic *butterfly* conformation observed in the S_2Fe_2 core of the natural subsite. Moreover, the structures of the H-cluster in 1998/1999 bore striking resemblance to the propanedithiolate species $[\text{Fe}_2(\text{pdt})(\text{CO})_6]$ **(b)** first reported by Winter and coworkers³¹ in 1982. This undoubtedly prompted the synthesis of the subsequent water-soluble dicyanide complex $[\text{Fe}_2(\text{pdt})(\text{CO})_4(\text{CN})_2]^{2-}$ **(c)**, which was first reported independently by three groups in 1999³²⁻³⁴.

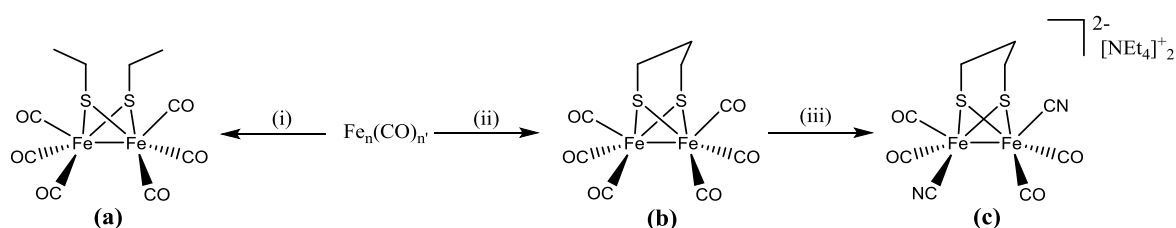


Figure 1.4 Synthesis of early [FeFe]-hydrogenase diiron subsite analogues. (i) $\text{Fe}(\text{CO})_5$, 2 EtSH, Δ ; (ii) $\text{Fe}_2(\text{CO})_9$, pdtH₂, Δ ; (iii) 2 $[\text{NEt}_4][\text{CN}]$. Adapted from references³⁰⁻³⁴.

In the last few years major advances in the chemistry of [FeFe]-hydrogenase subsite analogues have been achieved. These include; understanding factors which control protonation either on the FeFe bond or at a terminal Fe, the role of the azadithiolate group in catalysis and electrocatalysis, how structural effects influence rates of protonation, how the oxidation of dihydrogen at a synthetic diiron structure can be

achieved and how hydrogen production at diiron sites might be driven photo- or photoelectrochemically. All these aspects have been recently reviewed³⁵⁻³⁸. More recently, a research emphasis has been understanding how interactions of cyanide groups with Lewis acids effect subsite properties and how these might relate to the role of Fe-CN-Fe bridges in the biosynthesis of the H-cluster^{39,40}. As outlined above it is in the area of second coordination sphere and inter and intra-molecular interactions of subsites on which the work of this thesis is focussed.

1.3 Methodology

Unless otherwise stated chemicals were handled under an inert atmosphere of dinitrogen or argon using standard Schlenk line techniques⁴¹. Chemicals (starting materials, electrode materials, solvents) were generally purchased from Sigma-Aldrich, Alfa Aesar, Fluorochem or specialist suppliers without further purification. Solvents were freshly distilled under an inert atmosphere of dinitrogen from an appropriate dry agent using standard laboratory procedures⁴².

IR spectra were recorded using a solution Harrick cell with CaF₂ windows and spacers of 50 μm on a Bruker OPTIK GmbH XSA/B spectrometer. Signals are reported in cm^{-1} .

NMR samples were prepared using degassed deuterated solvents dried over activated 4 \AA molecular sieves. NMR spectra were obtained using a Bruker Avance DPX300 spectrometer at 25 $^{\circ}\text{C}$; J values are reported in Hz. Chemical shifts are reported in ppm. ¹H signals are referenced to residual solvent resonances; ³¹P is relative to H₃PO₄ 85% in D₂O; ¹⁹F is relative to CFCI₃; ¹¹B is relative to BF₃.Et₂O.

Regarding the mass spectrometry experiments undertaken in **Chapter 3**; electron spray ionization mass spectrometry (ESI-MS) for the small molecule complexes were carried out using a Bruker MicroTOF Q-III. Anaerobic and anhydrous MeCN was used as the solvent and samples were injected using gas tight syringes. Mass spectra were measured in negative mode. All other mass spectrometry characterisation was performed by the EPSRC UK National Mass Spectrometry Facility at Swansea University, using MAT95 spectrometers and measuring in the positive mode.

Cyclic voltammetry experiments were conducted using an Autolab PGSTAT30 potentiostat controlled by GPES software and were carried out in three compartment glass cells separated by glass frits, using a three electrode system. Specific experimental details are reported with the relevant experiments.

Individual X-ray parameters and specific experimental details are reported in the relevant Experimental sections.

Elemental analysis was carried out at London Metropolitan University using a Thermo Scientific Flash 2000 Elemental Analyser configured for %CHN.

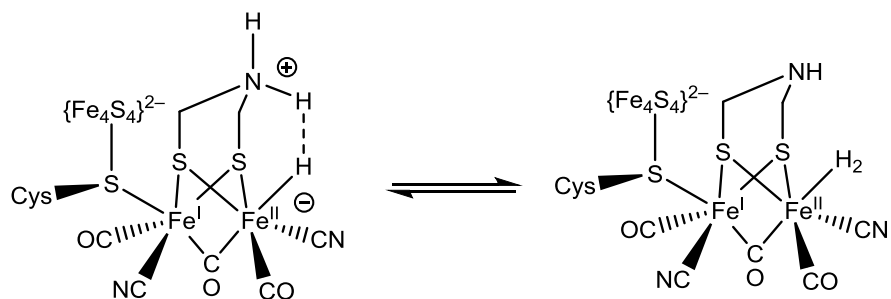
UV–visible absorption spectra were recorded using a Perkin-Elmer Lambda 35 UV/vis spectrometer. Excitation and emission spectra were measured using a (TCSPC) FluoroLog Horiba Jobin Yvon spectrofluorometer.

2 Second coordination sphere functionalisation of a diiron subsite analogue with basic pyridine units

2.1 Introduction

2.1.1 Background

It is now well-established that the naturally-occurring [FeFe]-hydrogenase possesses an azadithiolate (adt) bridgehead⁴³, and that this secondary amine is intimately involved in the catalytic cycle, acting as a proton acceptor in the heterolytic cleavage of dihydrogen and its reverse, and facilitating the shuttling of protons to and from the active site. The key reversible cleavage step in the enzyme is shown in **Scheme 2.1** and the general enzyme cycle has been outlined in **Chapter 1**.



Scheme 2.1 Putative mechanistic step for reversible formation of dihydrogen in the catalytic cycle of the [FeFe]-hydrogenase. Adapted from references^{44,45}.

The presence of an integral base in the natural system has led to recent work on the construction of synthetic subsites with appended bases proximal to the diiron unit⁴⁶⁻⁴⁸. Some examples of these are given in **Figure 2.1**.

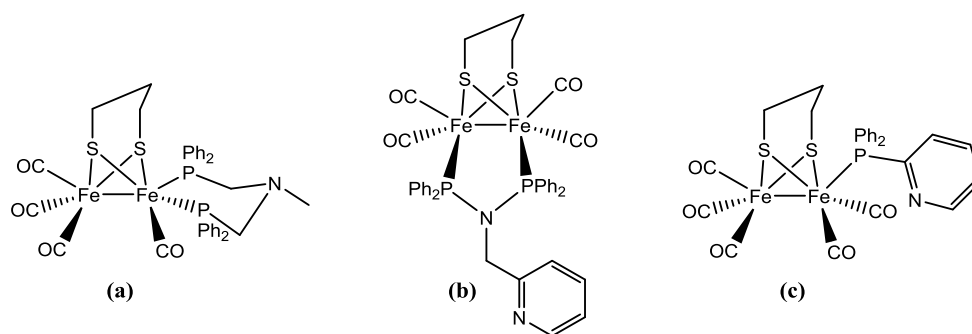
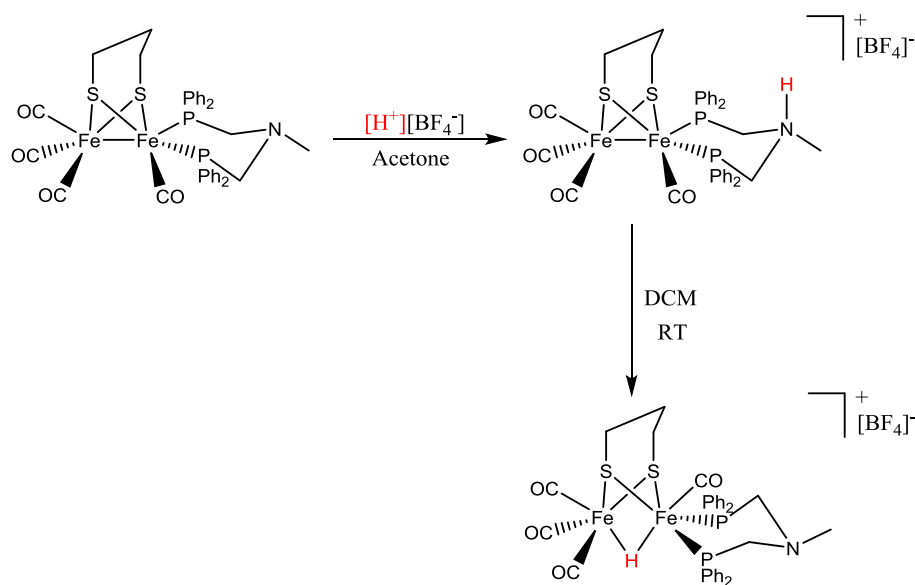


Figure 2.1. Examples of diiron systems with pendant amine groups. Adapted from references⁴⁶⁻⁴⁸.

Compound **(a)** in **Figure 2.1** is a particularly interesting example. Synthesised by Talarmin and coworkers⁴⁶ in 2009, protonation with excess $\text{HBF}_4 \cdot \text{OEt}_2$ in acetone leads to initial protonation of the NMe group in the axial position. However, upon dissolving the protonated species in dichloromethane, the compound isomerises which concomitantly forms the bridging hydride species, **Scheme 2.2**.



Scheme 2.2. Talarmin's pendant amine system acting as a proton shuttle to form bridging hydride species at the Fe-Fe bond. Adapted from reference⁴⁶.

The pyridine-derived systems **(b)** and **(c)** in **Figure 2.1** protonate on the heterocyclic N-atom on the addition of acid. The shifts in the CO region in the IR spectra as a consequence of this are *ca* 5 cm⁻¹ ^{47,48} and must arise by perturbation of electron density of the diiron core by transmission through the phosphine ligands. Not unexpectedly larger effects on the diiron core result from protonation of a bridging azadithiolate unit in synthetic complexes and this leads to a deactivation of the system with respect to subsequent protonation on the diiron unit⁴⁹.

The approach taken in the work described in this chapter was to introduce a basic pyridine function into the second coordination sphere of a subsite unit via functionalisation of the backbone of the bridging dithiolate. A possible advantage of this is that a proximal base linked through two or more saturated carbon groups would be sufficiently insulated from the diiron unit so that on protonation inductive deactivation of the diiron unit would be restricted⁴⁹; that is drift of electron density to the pyridinium centre would not be significant.

It was considered that an appropriate way of introducing pyridine units would be to esterify a hydroxyl group on the dithiolate backbone with a pyridine carboxylic acid. The type of hydroxyl functionalised dithiolate ligands deployed at a subsite unit and related esterification chemistry that has been reported in the literature, is now briefly described in the following two sections.

2.1.2 Hydroxyl-functionalised diiron subsite analogues

Despite the wide versatility of the hydroxyl group⁵⁰⁻⁵², there are surprisingly few hydroxyl-functionalised diiron subsite analogues. Some examples of such systems are given in **Figure 2.2**.

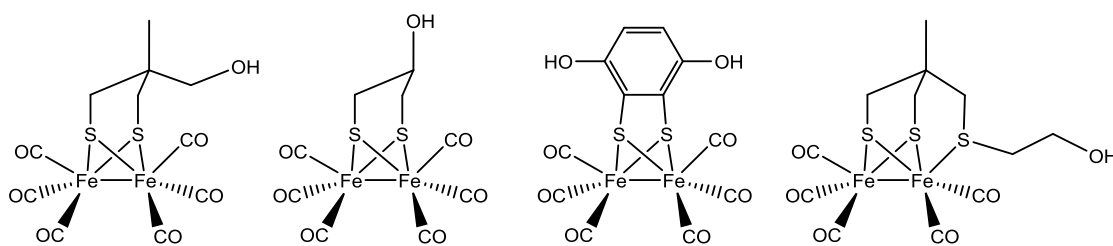
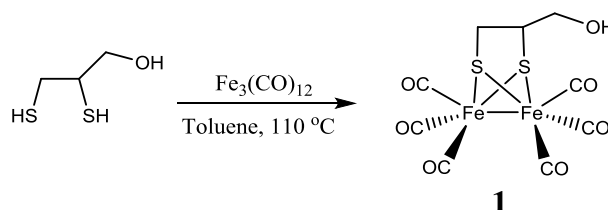


Figure 2.2. Examples of hydroxyl-functionalised diiron subsite analogues. Adapted from references⁵³⁻⁵⁶.

The few established hydroxyl-functionalised diiron dithiolate systems such as those shown in **Figure 2.2** involve multi-step processes⁵³⁻⁵⁶. However, in 2001 Pickett and coworkers⁵⁷ were able to synthesise a diiron system with a pendant OH group in a one-step reaction by refluxing commercially available 2,3-dimercapto-1-propanol (dmp) with $\text{Fe}_3(\text{CO})_{12}$ in toluene.



Scheme 2.3. One-step synthesis of $[\text{Fe}_2(\text{dmp})(\text{CO})_6]$ **1** from 2,3-dimercapto-1-propanol⁵⁷.

The synthesis is straightforward, with a column chromatography purification step allowing the product to be obtained in yields >80% as a red crystalline solid. This synthesis of $[\text{Fe}_2(\text{dmp})(\text{CO})_6]$ provides a convenient method of introducing a hydroxyl group into the outer coordination sphere of a diiron subsite. However, exploiting the reactivity of the hydroxyl group in this molecule to add other functionality has not been explored. However, esterification routes have been utilised in other hydroxyl functionalised diiron systems as noted below. In this chapter we show that esterification allows introduction of basic pyridine groups proximal to the diiron unit.

2.1.3 Functionalisation by ester bond formation

Earlier work has shown that hydroxyl groups attached to dithiolate ligands bound to diiron subsites can be readily esterified to introduce new functionality⁵⁸⁻⁶⁰. In **Figure 2.3** some example systems are given, including that of Sun and coworkers⁵⁸. This latter work was directed towards the synthesis of a photosensitised diiron subsite system (**d**) and will be discussed in more detail in **Chapter 4**. Another example is the attachment of a ferrocenyl derivative by Liu and coworkers⁵⁹ in order for the ferrocene group to act as an internal standard when probing the reduction of the diiron centre (**e**). The third example by Pickett and coworkers⁶⁰ was the attachment of a pyrrole moiety for enabling diiron subsite incorporation into polymer films (**f**).

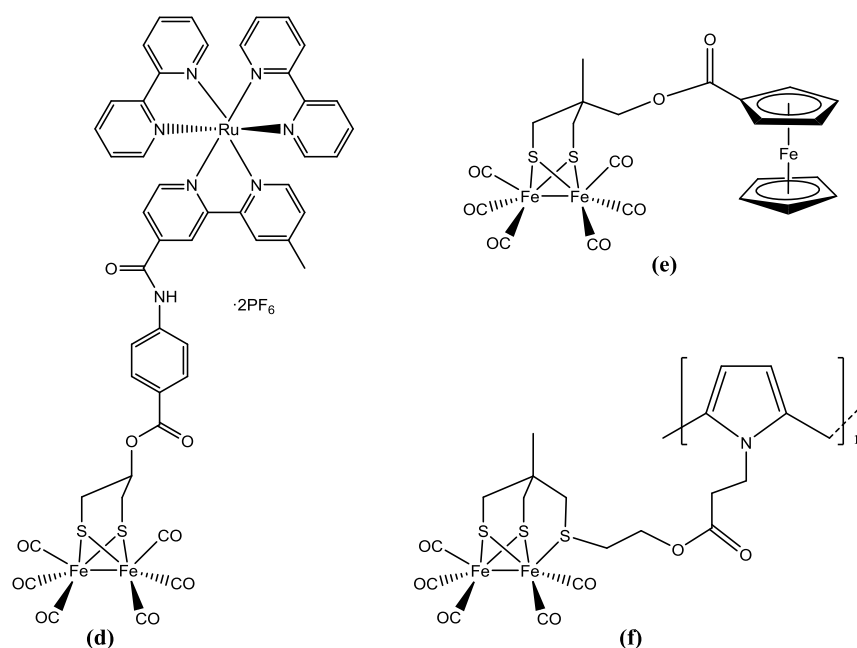


Figure 2.3. Examples of ester moieties being utilised to incorporate new functional groups. Adapted from references⁵⁸⁻⁶⁰.

2.1.4 Scope of this work

As outlined above, this work sought to evaluate systems in which a base was deployed in the second coordination sphere of a diiron unit but with its electronic influence essentially insulated from the catalytic centre; ie the effect of protonation at a basic group being largely uncoupled from the diiron core. This would minimise the effect of

deactivation of the FeFe core to subsequent protonation, but retain the advantage of vicinal protons for catalysis and proton shuttling.

To this end it was decided to take advantage of the ease of synthesis of $[\text{Fe}_2(\text{dmp})(\text{CO})_6]$ **1** and to explore esterification reactions of the hydroxyl group. Firstly the synthesis of simple benzoate and naphthoate were explored and then the synthesis of pyridine systems of the type shown in **Figure 2.4**.

The successful synthesis of such molecules should allow exploration of (i) the protonation of the anchored base group and the level of electronic influence this exerts on the diiron core (ii) electron-transfer and electrocatalytic properties, and (iii) provide precursors for mono- or di-substituted derivatives with CO replaced by donating phosphine or cyanide ligands.

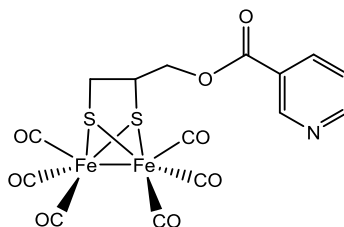
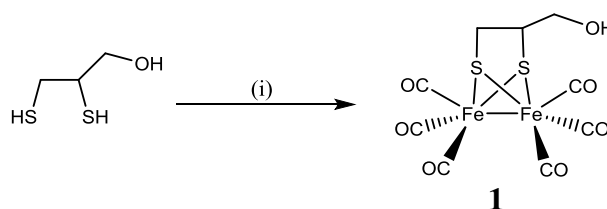


Figure 2.4. Example target diiron pyridine system.

2.2 Results and discussion

2.2.1 Synthesis of diiron subsite analogue

The hydroxyl-functionalised diiron unit $[\text{Fe}_2(\text{dmp})(\text{CO})_6]$ **1** was synthesised using a modified literature procedure⁵⁷. The synthesis follows a standard methodology for the assembly of these systems; namely heating the appropriate thiol, in this case 2,3-dimercapto-1-propanol (dmp), with a slight excess of triirondodecacarbonyl⁶¹.



Scheme 2.4. Synthesis of $[\text{Fe}_2(\text{dmp})(\text{CO})_6]$ **1**. (i) 1.2 $\text{Fe}_3(\text{CO})_{12}$, toluene, 110 °C, 1 h, 84%. Procedure modified from that outlined by Pickett and coworkers⁵⁷.

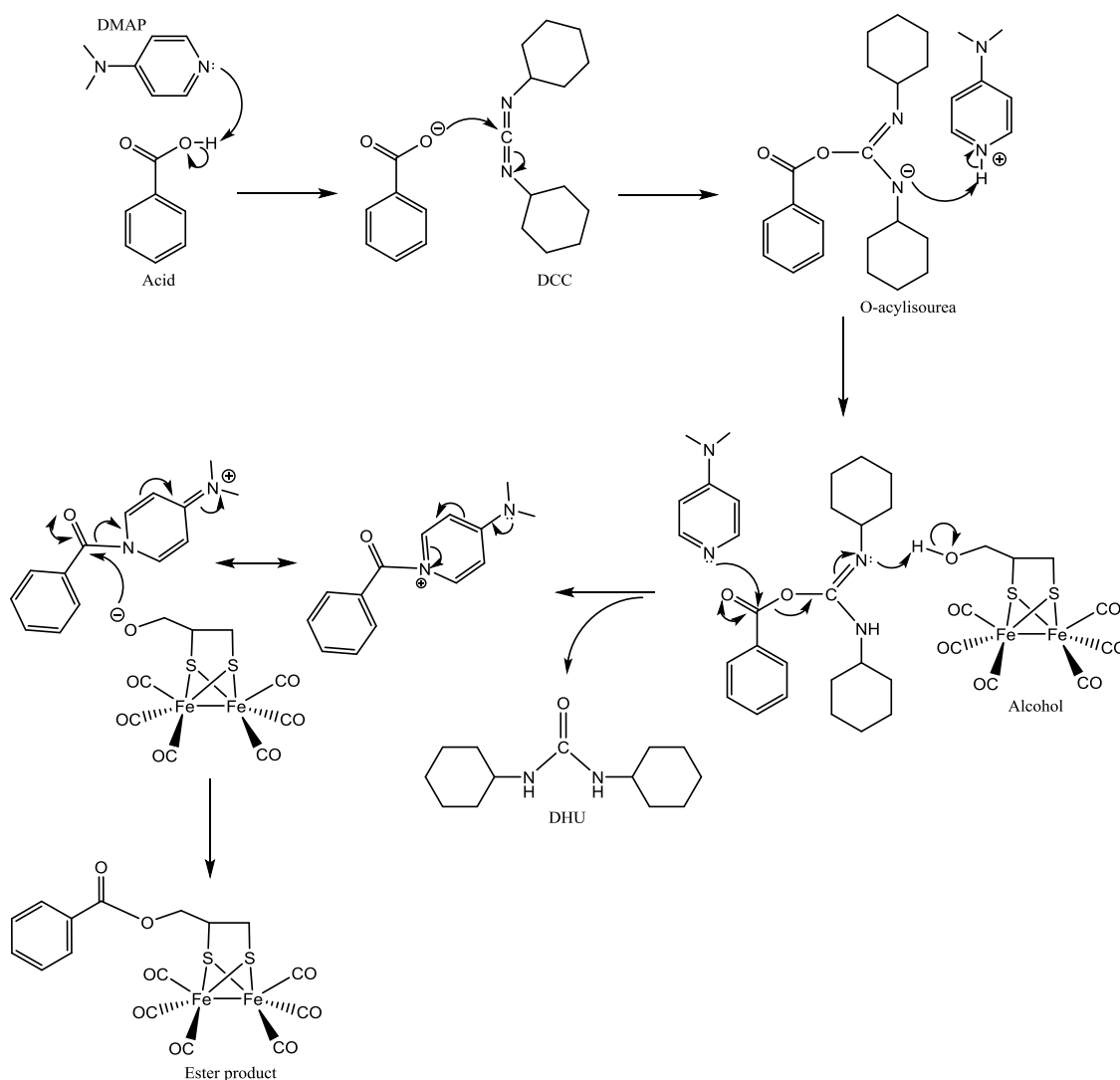
The work up is straightforward, with a column chromatography purification step using toluene eluent followed by recrystallisation from acetonitrile allowing the product to be obtained in 84% yield as a red crystalline solid.

2.2.2 Attachment of aromatic groups by Steglich Esterification

In order to appreciate and understand the effects of the incorporation of the pyridine moieties it is important to obtain control compounds without the pyridine functionality; namely the benzoic and 2-naphthoic acid ester derivatives. These were achieved by employing a Steglich Esterification.

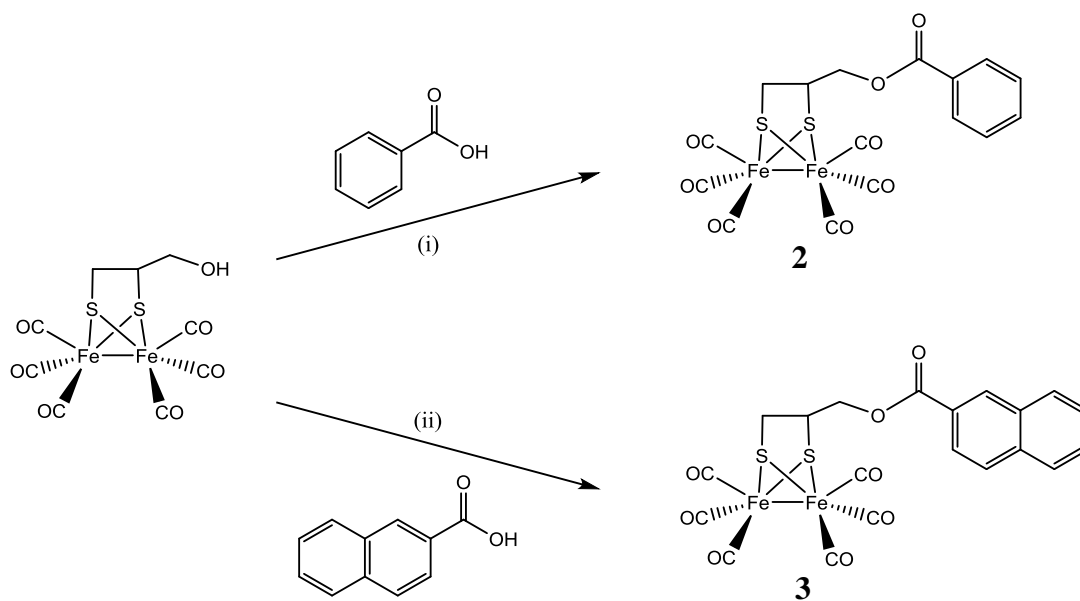
The Steglich Esterification is a mild reaction which allows the conversion of sterically demanding and acid labile substrates⁶². Dicyclohexylcarbodiimide (DCC) is employed in this reaction and forms *O*-acylisourea intermediates with carboxylic acid substrate in solution. This 'activated' carboxylic acid species can then be attacked by the alcohol to form the stable dicyclohexylurea (DHU) and the ester product. Conducting the reaction in dichloromethane helps drive towards completion as the DHU generated is insoluble.

The Steglich reaction can also be accelerated by the addition of 4-dimethylaminopyridine (DMAP)⁶³, which helps the reaction progress in two ways: firstly deprotonation of the carboxylic acid to aid formation of the *O*-acylisourea intermediate, and secondly reacting with the generated *O*-acylisourea itself to produce a reactive amide species which is readily attacked by the alcohol to form the esterified product. The mechanism for the DMAP enhanced Steglich Esterification is shown in **Scheme 2.5**.



Scheme 2.5. Mechanism of DMAP-accelerated Steglich Esterification. Adapted from references^{62,63}.

This method was employed for the synthesis of the new compounds $[\text{Fe}_2(\text{dmp-OCOC}_6\text{H}_5)(\text{CO})_6]$ **2** and $[\text{Fe}_2(\text{dmp-OCOC}_{10}\text{H}_7)(\text{CO})_6]$ **3**, as shown in **Scheme 2.6**.



Scheme 2.6. Synthesis of ester products **2** and **3**. (i) 1.2 DCC, 5 mol% DMAP, DCM, RT, 48 h, 84%; (ii) 1.2 DCC, 5 mol% DMAP, DCM, RT, 72 h, 69%.

Both esters were obtained in respectable yields, 84% and 69% respectively, after purification by column chromatography. Crystals suitable for X-ray diffraction of complexes **2** and **3** were obtained from hexane solutions.

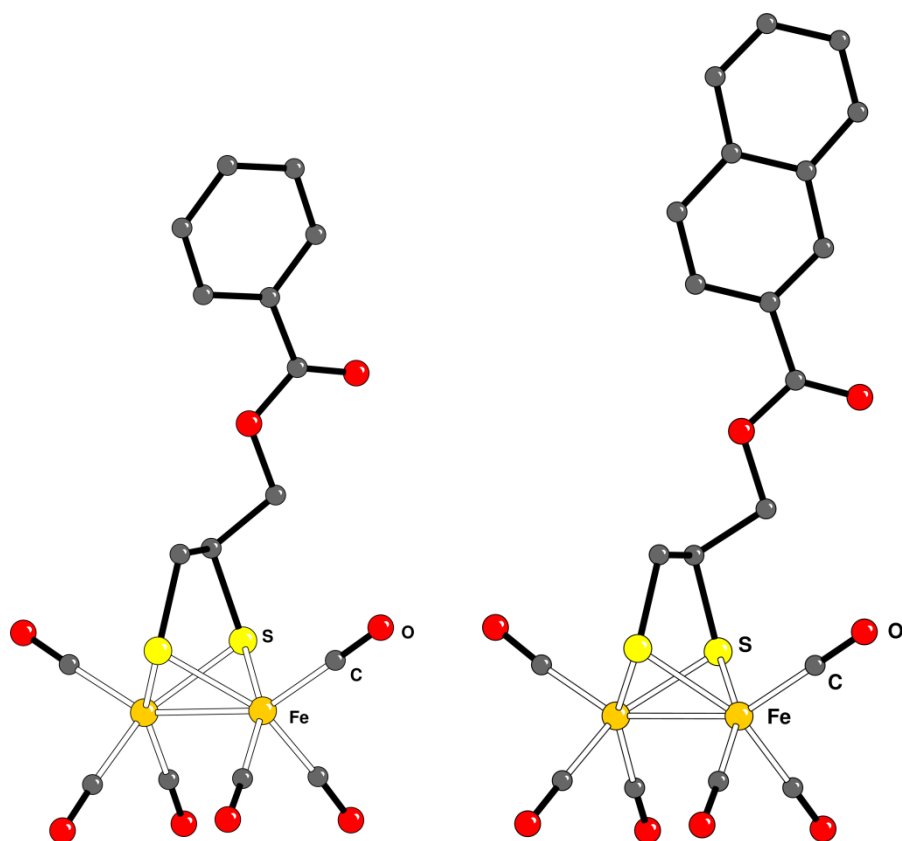
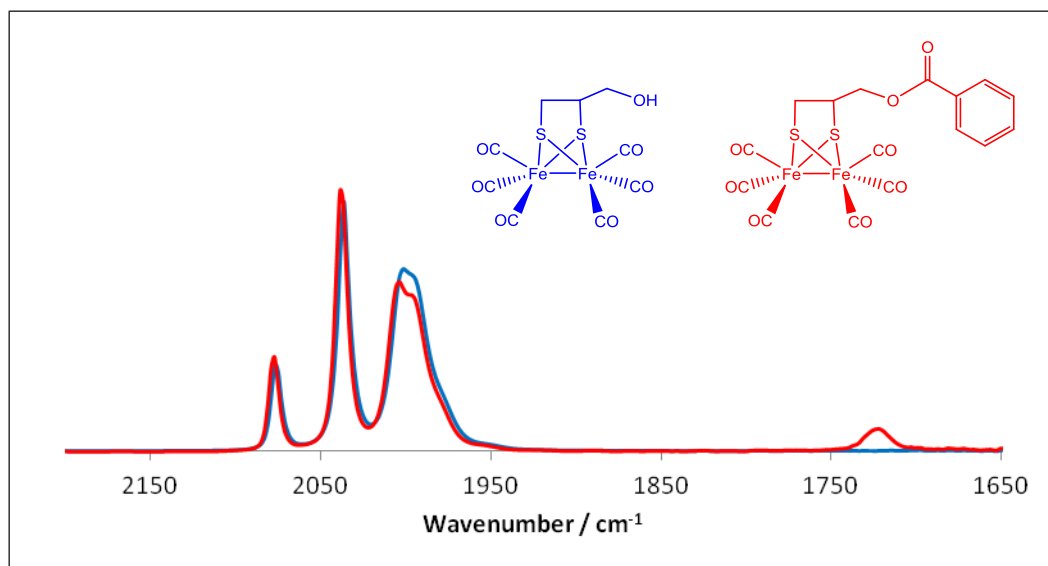


Figure 2.5. CAMERON representations of the structures of $[\text{Fe}_2(\text{dmp-OCOC}_6\text{H}_5)(\text{CO})_6]$ **2** (left) and $[\text{Fe}_2(\text{dmp-OCOC}_{10}\text{H}_7)(\text{CO})_6]$ **3** (right) with spheres of arbitrary size.

The FTIR spectra of these species show that there is minimal effect of the esterified group on the FeFe core as there is no significant change in the CO stretching region. The only obvious change is the addition of new ester CO stretches which is to be expected.



Compound	$\nu(\text{CO}) / \text{cm}^{-1}$	$\nu(\text{ester-CO}) / \text{cm}^{-1}$
$[\text{Fe}_2(\text{dmp})(\text{CO})_6]$ 1	2077, 2037, 2002, 1996	
$[\text{Fe}_2(\text{dmp-OCOC}_6\text{H}_5)(\text{CO})_6]$ 2	2077, 2039, 2004, 1996	1722
$[\text{Fe}_2(\text{dmp-OCOC}_{10}\text{H}_7)(\text{CO})_6]$ 3	2077, 2039, 2004, 1996	1720

Figure 2.6. Solution FTIR data in DCM showing the effects of esterification. Top: comparison spectra between $[\text{Fe}_2(\text{dmp})(\text{CO})_6]$ **1** and its benzoic acid ester $[\text{Fe}_2(\text{dmp-OCOC}_6\text{H}_5)(\text{CO})_6]$ **2**. Bottom: table of comparable data for the CO region.

The effects of esterification are more apparent in the ^1H -NMR spectra. The hydroxyl complex $[\text{Fe}_2(\text{dmp})(\text{CO})_6]$ **1** has been shown to exhibit strong intramolecular hydrogen bonding of the hydroxyl groups, with such intramolecular H-bonding being structurally characterised in the solid-state⁵⁷. Esterification would break up that arrangement, as is shown in **Figure 2.7**.

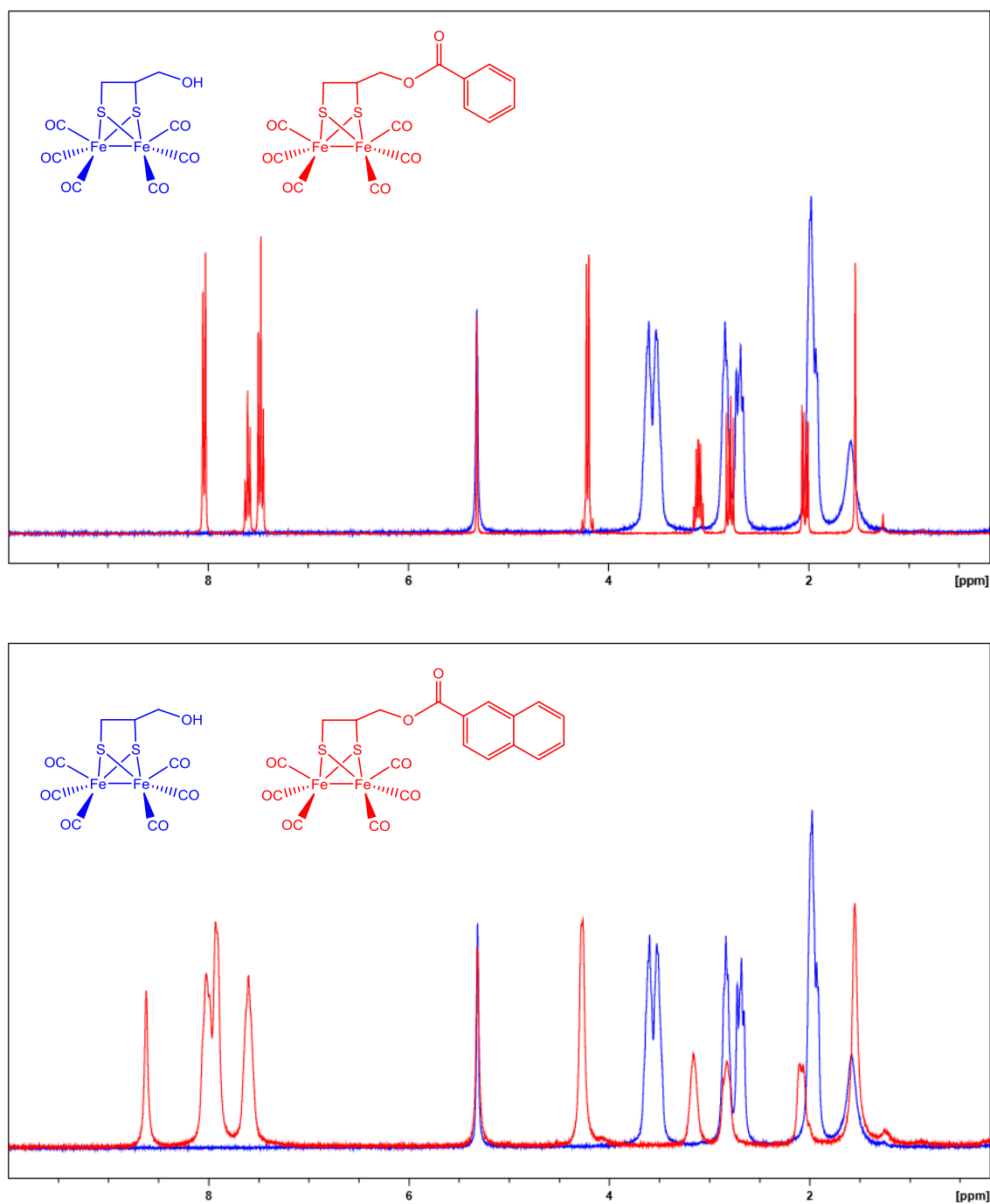
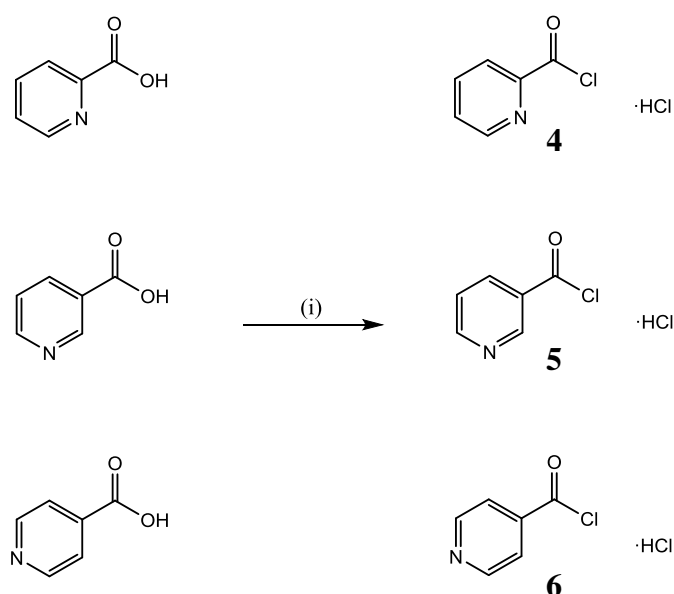


Figure 2.7. ¹H-NMR spectra (CD₂Cl₂) showing the effects of esterification. Top: comparison spectra between [Fe₂(dmp)(CO)₆] **1** and its benzoic acid ester [Fe₂(dmp-OCOC₆H₅)(CO)₆] **2**. Bottom: comparison spectra between [Fe₂(dmp)(CO)₆] **1** and its 2-naphthoic acid ester [Fe₂(dmp-OCOC₁₀H₇)(CO)₆] **3**.

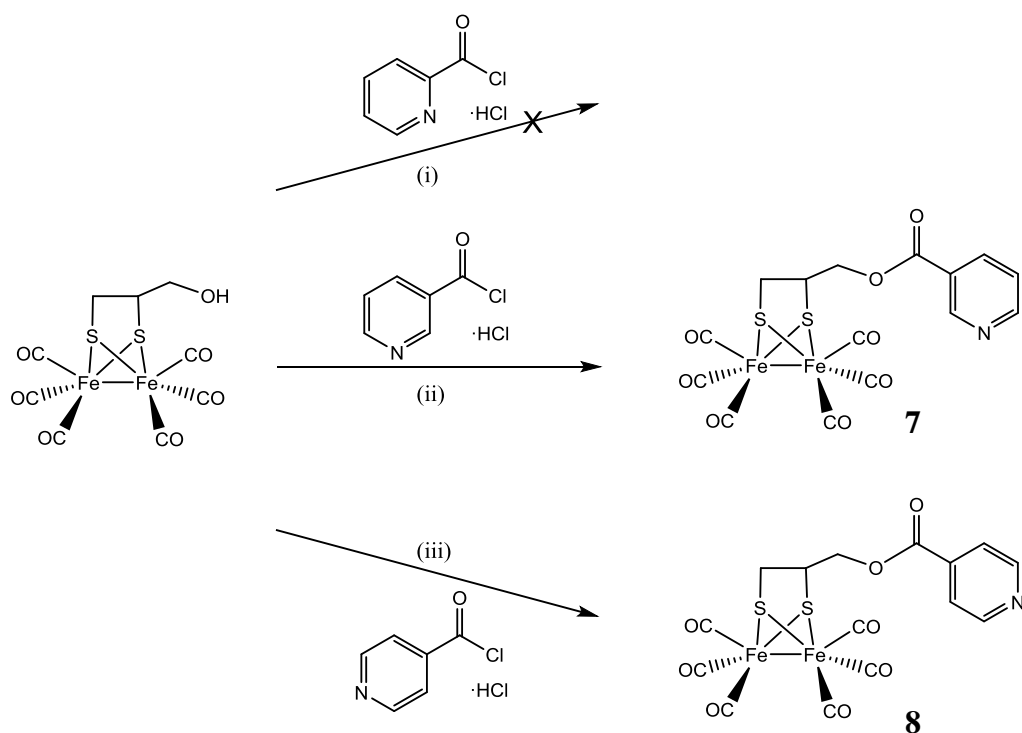
2.2.3 Attachment of pyridine groups by esterification

Due to the poor solubility of the pyridine carboxylic acids in dichloromethane, the Steglich Esterification route was not a viable option for ester coupling these acids. The use of alternative solvents (ie DMF) was attempted, but due to the pyridine carboxylic acids inherent reduced activity and the absence of dichloromethane driving the reaction by the insolubility of DHU, reactions were unsuccessful. To this end, the pyridine carboxylic acids were converted into their acyl chloride derivatives. The acyl chlorides were prepared according to the procedure outlined by Wei and coworkers⁶⁴, where the carboxylic acids are reacted with thionyl chloride in the presence of a catalytic amount of DMF.



Scheme 2.7. Synthesis of the acyl chloride derivatives of the pyridine carboxylic acids. Isolated as their HCl salts. (i)a) 9.5 SOCl₂, cat. DMF, RT, 24 h, b) 80 °C, 1.5 h. Yields: **4**: 70%, **5**: 94%, **6**: 96%. Prepared according to the procedure outlined by Wei and coworkers⁶⁴.

The acyl chloride derivatives afforded were then stirred with [Fe₂(dmp)(CO)₆] **1** in THF in the presence of triethylamine to attempt to form the subsequent esters.



Scheme 2.8. Attempted esterification by employing the appropriate acyl chlorides. (i) THF, 4.0 NEt₃, RT, 24 h, no discernible reaction; (ii) THF, 4 NEt₃, RT, 24 h, 92%; (iii) THF, 4.0 NEt₃, RT, 24 h, 17%.

The reaction with the acyl chlorides afforded the *meta*- and *para*- pyridine derivatives, $[\text{Fe}_2(\text{dmp-OCOC}_5\text{H}_4\text{N-}i{meta})(\text{CO})_6]$ **7** and $[\text{Fe}_2(\text{dmp-OCOC}_5\text{H}_4\text{N-}i{para})(\text{CO})_6]$ **8**, after purification by column chromatography. Crystals suitable for X-ray diffraction of complexes **8** and **9** were obtained from hexane solutions. However, in the case of the *ortho*-pyridine derivative, the acyl chloride was insufficiently reactive to allow esterification.

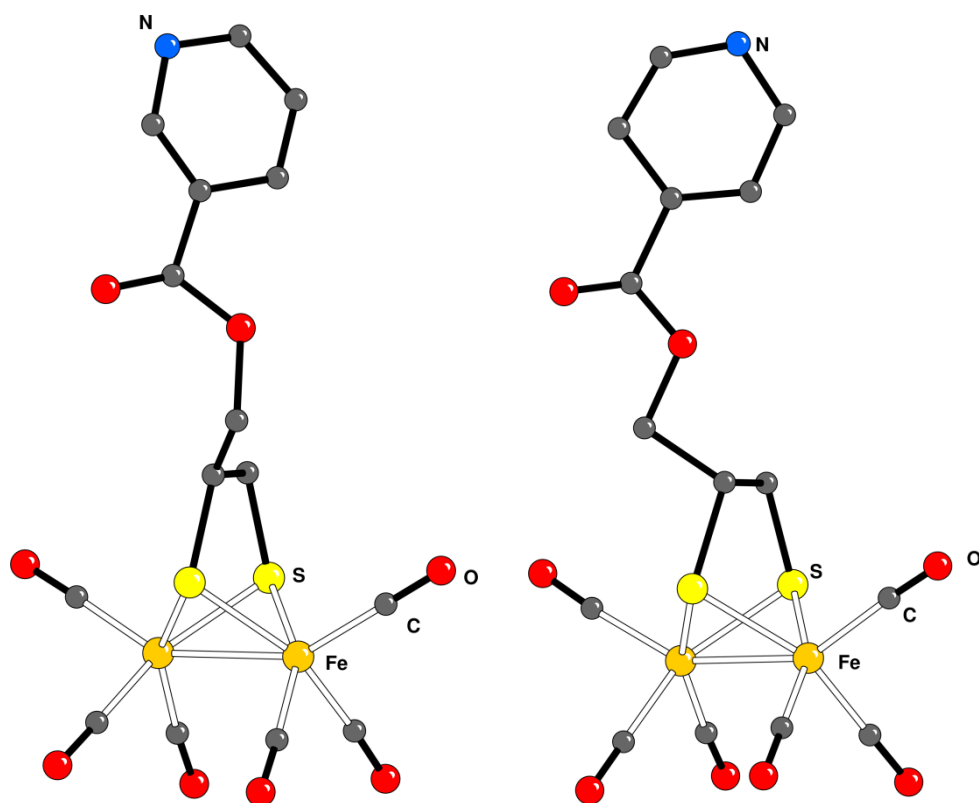
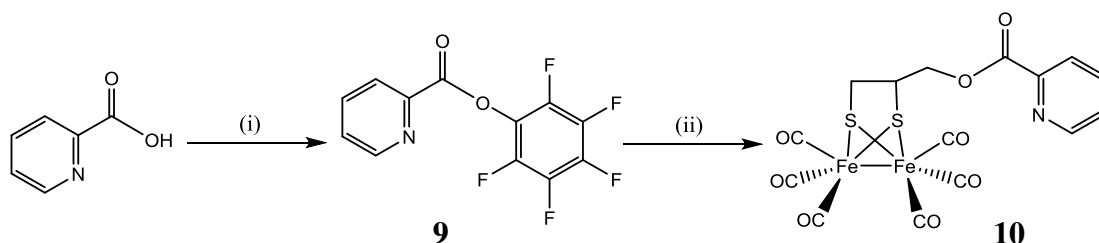


Figure 2.8. CAMERON representations of the structures of $[\text{Fe}_2(\text{dmp-OCOC}_5\text{H}_4\text{N-}i\text{meta})(\text{CO})_6]$ **7** (left) and $[\text{Fe}_2(\text{dmp-OCOC}_5\text{H}_4\text{N-}i\text{para})(\text{CO})_6]$ **8** (right) with spheres of arbitrary size.

In order to improve the reactivity of the *ortho*-pyridine derivative the activated pentafluorophenolate ester **9** was prepared. This was conducted using the method described by Yagupolskii and coworkers⁶⁵, with the subsequent activated ester undergoing reaction with $[\text{Fe}_2(\text{dmp})(\text{CO})_6]$ **1** in THF in the presence of triethylamine to attempt to form the esterified product, $[\text{Fe}_2(\text{dmp-OCOC}_5\text{H}_4\text{N-}i\text{ortho})(\text{CO})_6]$ **10** as shown in **Scheme 2.9**.



Scheme 2.9. Synthesis of ester product $[\text{Fe}_2(\text{dmp-OCOC}_5\text{H}_4\text{N-ortho})(\text{CO})_6]$ **10** by employing the pentafluorophenolate activated ester **9**. (i)⁶⁵ 1.1 $\text{C}_6\text{F}_5\text{OH}$, 1.1 DCC, dioxane, RT, 1 h, 75%; (ii) 0.7 $[\text{Fe}_2(\text{dmp})(\text{CO})_6]$ **1**, THF, 2 NEt_3 , 40 °C, 24 h, 93%.

This scheme proved successful, with the activated pentafluorophenolate ester proving sufficiently reactive to allow the ester product $[\text{Fe}_2(\text{dmp-OCOC}_5\text{H}_4\text{N-ortho})(\text{CO})_6]$ **10** to be afforded in 93% after purification by column chromatography. Crystals suitable for X-ray diffraction of complex **10** were obtained from a hexane solution cooled to 2 °C.

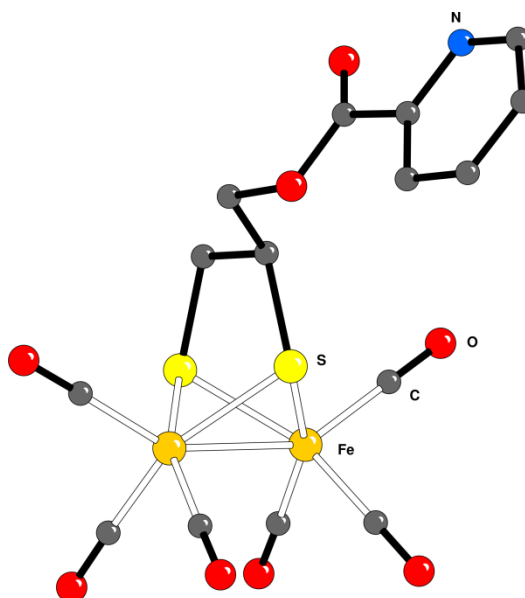
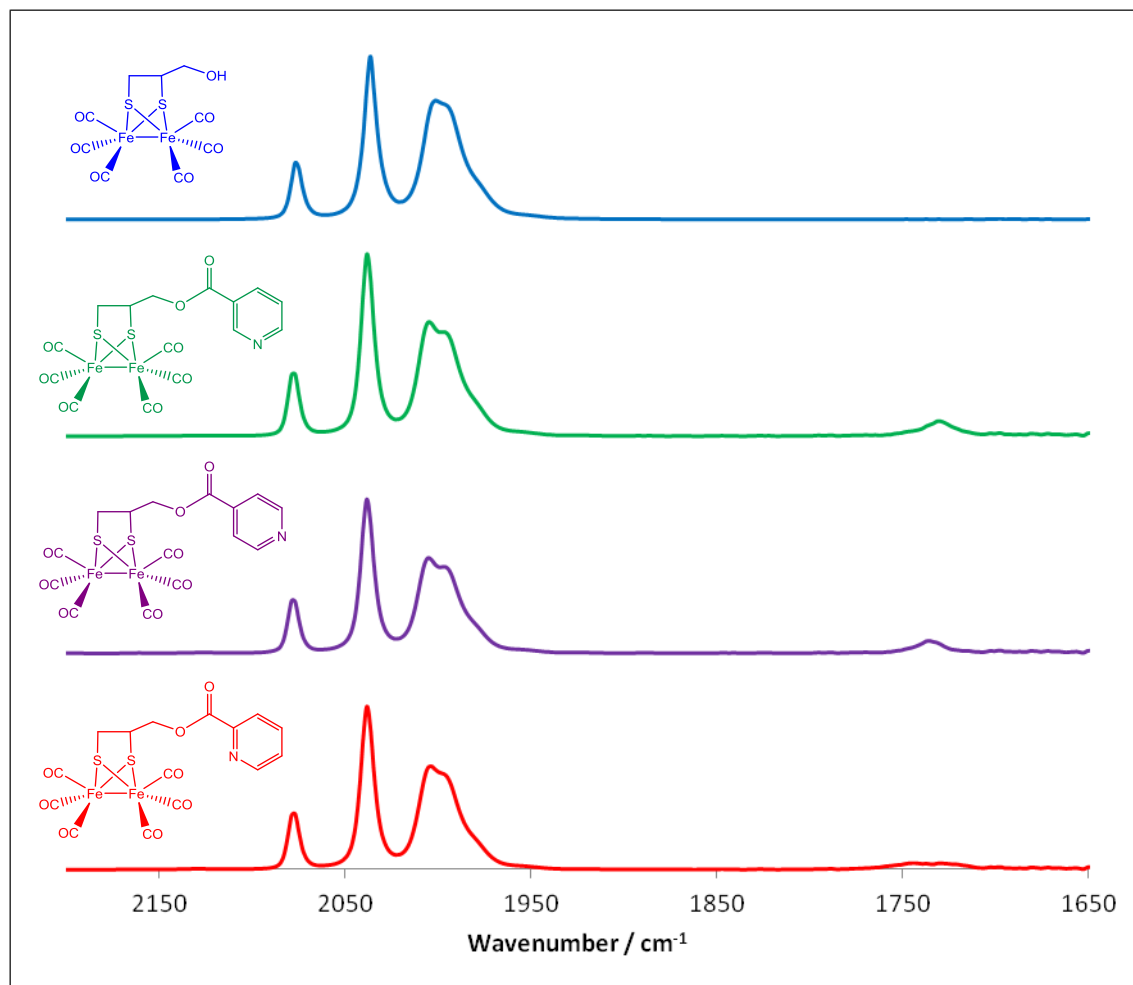


Figure 2.9. CAMERON representation of the structure of $[\text{Fe}_2(\text{dmp-OCOC}_5\text{H}_4\text{N-ortho})(\text{CO})_6]$ **10** with spheres of arbitrary size.

The FTIR spectra of the esterified pyridine species were recorded in dichloromethane and are shown in **Figure 2.10**.



Compound	$\nu(\text{CO}) / \text{cm}^{-1}$	$\nu(\text{ester-CO}) / \text{cm}^{-1}$
$[\text{Fe}_2(\text{dmp})(\text{CO})_6]$ 1	2077, 2037, 2002, 1996	
$[\text{Fe}_2(\text{dmp-OCOC}_6\text{H}_5)(\text{CO})_6]$ 2	2077, 2039, 2004, 1996	1722
$[\text{Fe}_2(\text{dmp-OCOC}_{10}\text{H}_7)(\text{CO})_6]$ 3	2077, 2039, 2004, 1996	1720
$[\text{Fe}_2(\text{dmp-OCOC}_5\text{H}_4\text{N-}i\text{meta})(\text{CO})_6]$ 7	2077, 2039, 2006, 1998	1732
$[\text{Fe}_2(\text{dmp-OCOC}_5\text{H}_4\text{N-}i\text{para})(\text{CO})_6]$ 8	2077, 2039, 2006, 1998	1736
$[\text{Fe}_2(\text{dmp-OCOC}_5\text{H}_4\text{N-}i\text{ortho})(\text{CO})_6]$ 10	2077, 2039, 2006, 1998	1743, 1730

Figure 2.10. Solution FTIR data in DCM of the esterified pyridine species. Top: comparison of the spectra of the pyridine derivatives. Bottom: table of comparable data for the CO region from all new species.

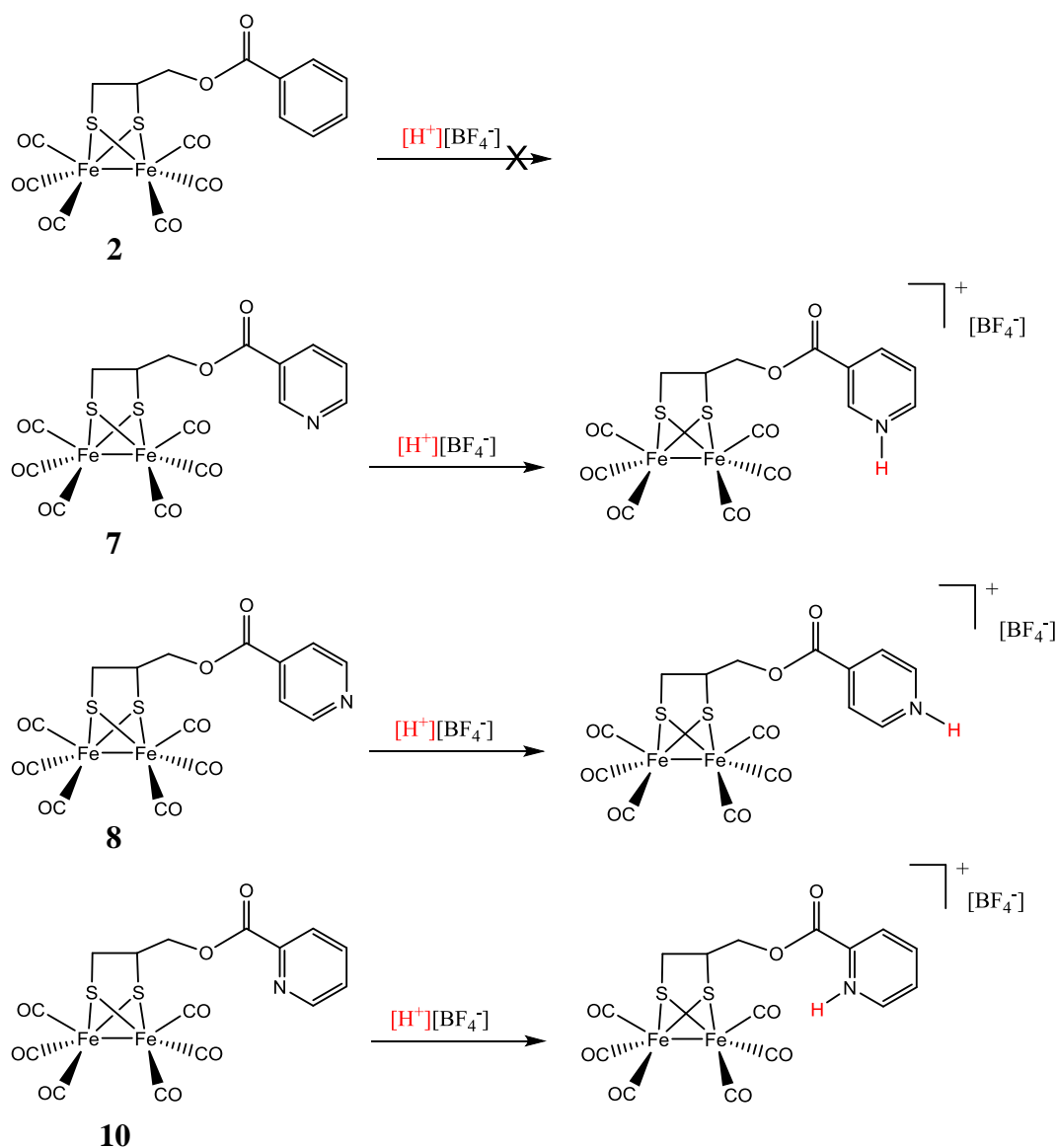
The presence of electron withdrawing groups on an ester increase the vibrational energy for the ester C=O stretch. For example, pentafluorophenolate esters typically show C=O stretches around 1780 cm^{-1} , whereas a typical alkyl ester is around $1735 - 1750\text{ cm}^{-1}$. Electron-withdrawing groups C-bonded rather than O-bonded to the carbonyl group would also be expected to similarly enhance C=O, as is observed in this example where the pyridine-derived esters have C=O stretches of *ca* 10 cm^{-1} higher than the simple arenes.

The ortho-pyridine species is interesting in that it exhibits two C=O stretches which might be attributed to cis and trans conformations. Notably on the longer timescale of ^1H -NMR resolution of the isomers is not observed.

2.2.4 Protonation of the pyridine-derived esters

As has been described previously⁴⁸, the pyridine moieties should be readily protonated upon the addition of $\text{HBF}_4\cdot\text{OEt}_2$, though protonation of the hexacarbonyl diiron centre should not occur with this acid⁶⁶, as the carbonyl electron-withdrawing groups are known to weaken the basicity of the metal-metal bond.

Stock solutions (6 mM) of the pyridine-containing systems were prepared in DCM, to which 1 equivalent of $\text{HBF}_4\cdot\text{OEt}_2$ was added. The benzoic acid derivative **2** was also subjected to the same conditions to serve as a control.



Scheme 2.10. Treatment of complexes **2**, **7**, **8** and **10** with 1.0 equivalent $\text{HBF}_4 \cdot \text{OEt}_2$.

As expected, the benzoate ester $[\text{Fe}_2(\text{dmp-OCOC}_6\text{H}_5)(\text{CO})_6]$ **2** was unaffected by addition of $\text{HBF}_4 \cdot \text{OEt}_2$. This was demonstrated by no noticeable shifts in the ^1H -NMR spectrum and no obvious perturbation of the CO bands in the FTIR.

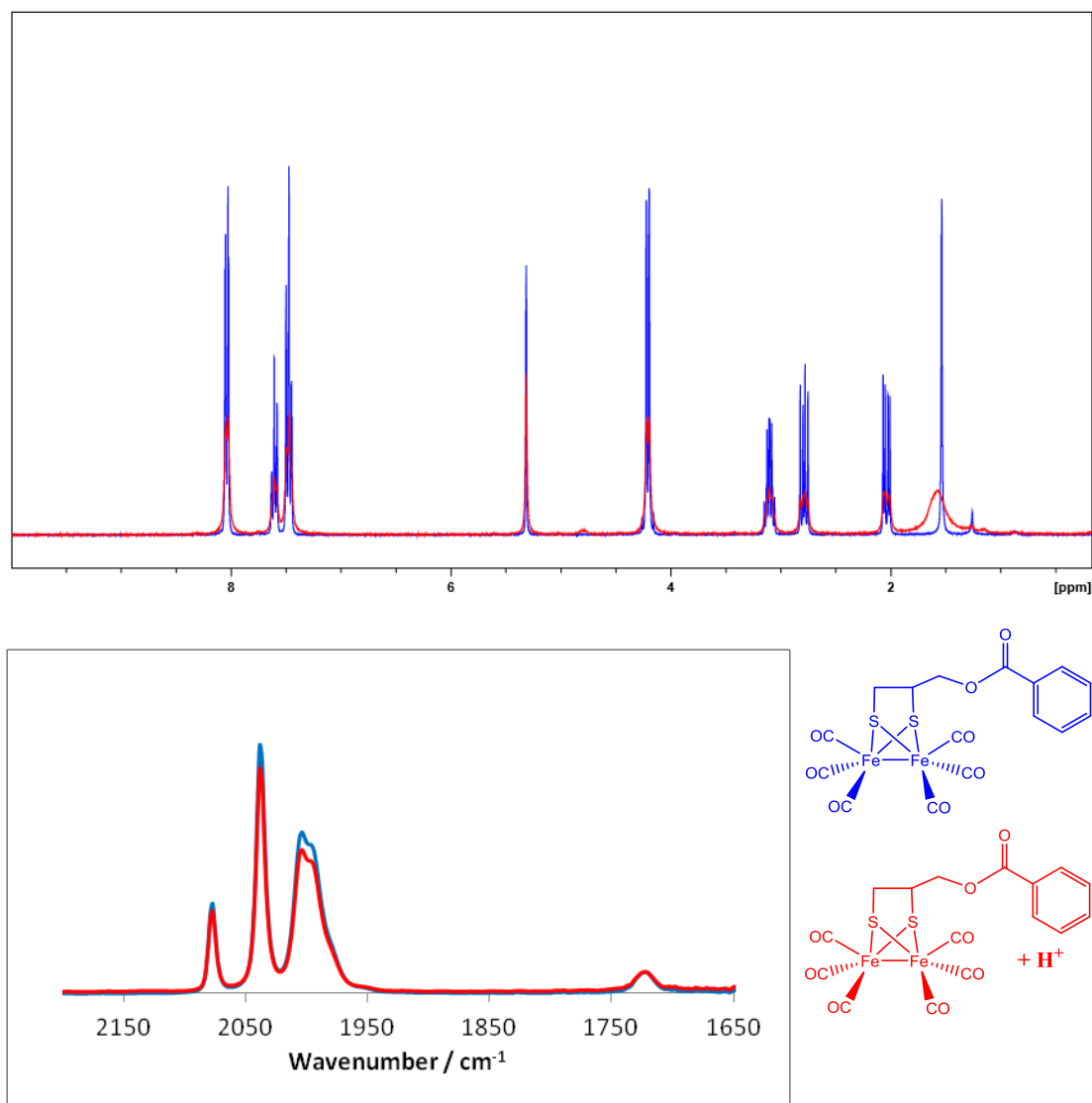
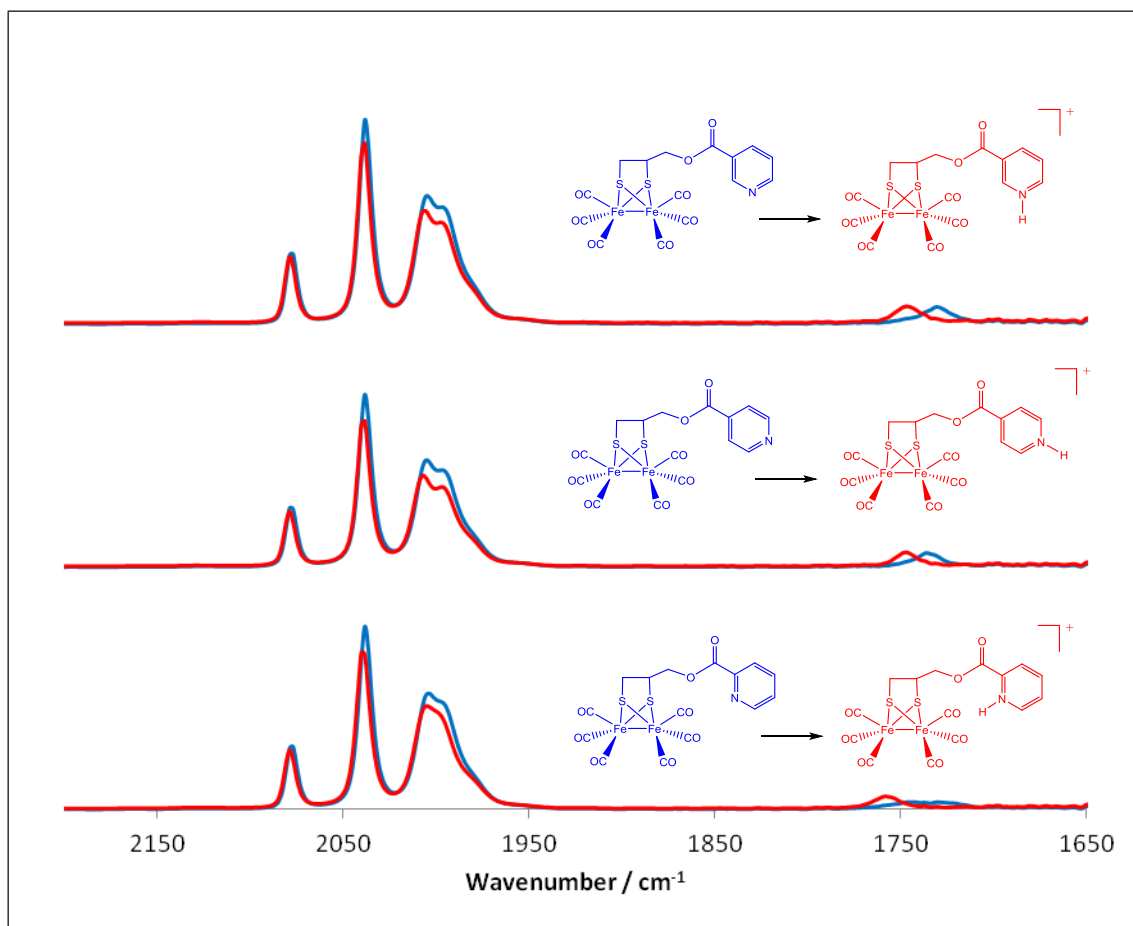


Figure 2.11. Unchanged $^1\text{H-NMR}$ (CD_2Cl_2) and solution FTIR (DCM) spectra after treatment of benzoic acid ester $[\text{Fe}_2(\text{dmp-OCOC}_6\text{H}_5)(\text{CO})_6]$ **2** with 1 equiv. $\text{HBF}_4\cdot\text{OEt}_2$.

A set of FTIR data for the three pyridine complexes before and after protonation is given in **Figure 2.12**. Consistent with the proposal that the effects of protonation on the appended pyridine group would lead to minimal perturbation of the diiron unit, shifts in the carbonyl frequencies are essentially negligible.



Compound	$\nu(\text{CO}) / \text{cm}^{-1}$	$\nu(\text{ester-CO}) / \text{cm}^{-1}$
$[\text{Fe}_2(\text{dmp-OCOC}_3\text{H}_4\text{N-}i{meta})(\text{CO})_6]$ 7	2077, 2039, 2006, 1998	1732
	2079, 2039, 2006, 1998	1747
$[\text{Fe}_2(\text{dmp-OCOC}_3\text{H}_4\text{N-}i{para})(\text{CO})_6]$ 8	2077, 2039, 2006, 1998	1736
	2079, 2039, 2007, 1998	1747
$[\text{Fe}_2(\text{dmp-OCOC}_3\text{H}_4\text{N-}i{ortho})(\text{CO})_6]$ 10	2077, 2039, 2006, 1998	1743, 1730
	2079, 2041, 2006, 2000	1759

Figure 2.12. Solution FTIR data (DCM) of the treatment of the three pyridine derivatives **7**, **8** and **10** with 1 equiv. $\text{HBF}_4 \cdot \text{OEt}_2$. **Blue**: CO bands of untreated complex. **Red**: CO bands of protonated complex.

The effect of protonation of the pyridine group on the ^1H -NMR spectra is shown by the set of spectra in **Figure 2.13**. As expected the ethane dithiolate protons experience negligible shifts in their resonances but those on the pyridine ring are dramatically shifted.

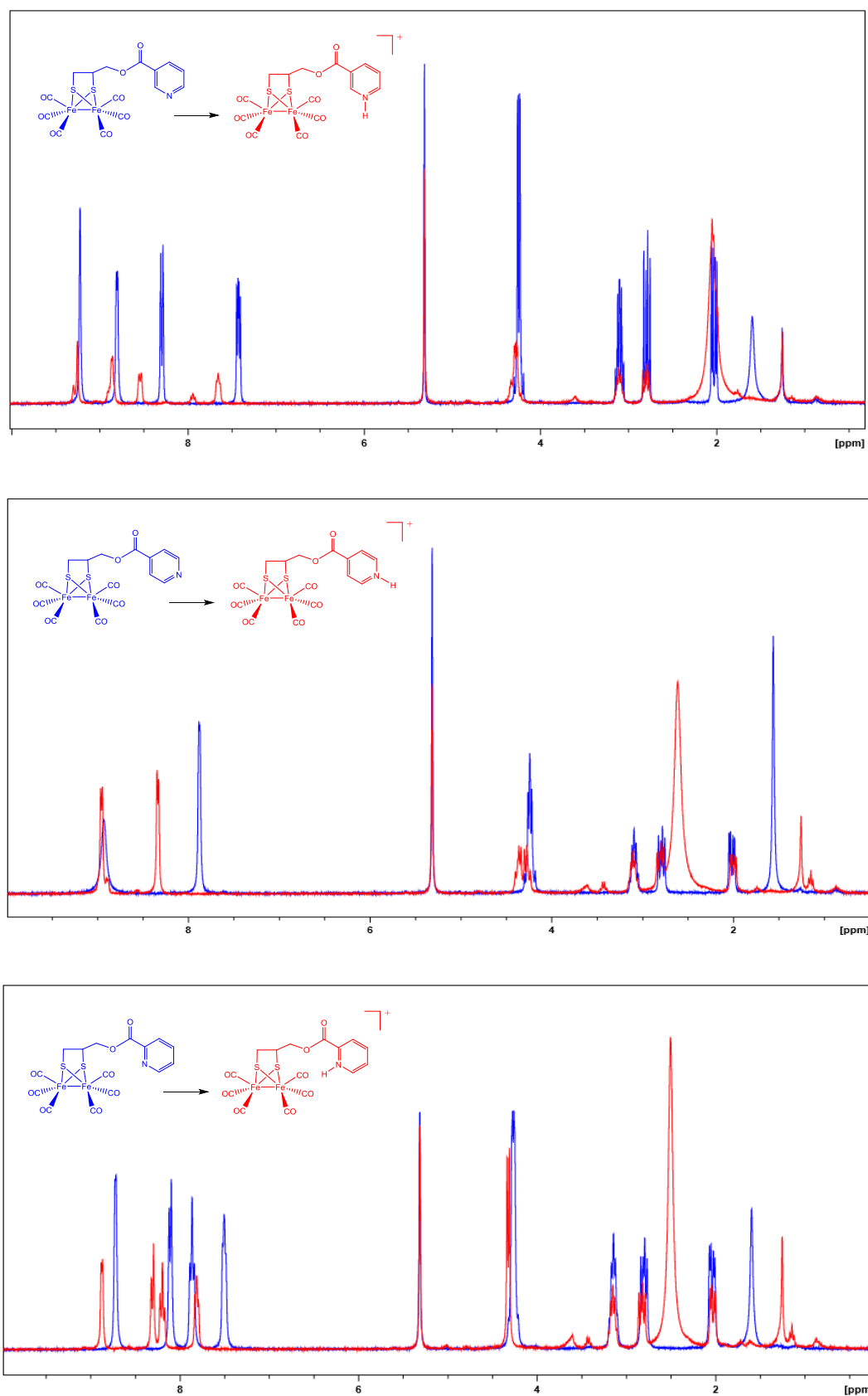


Figure 2.13. ^1H -NMR (CD_2Cl_2) of the treatment of the three pyridine derivatives **7**, **8** and **10** with 1 equiv. $\text{HBF}_4 \cdot \text{OEt}_2$.

It is quite clear that protonation occurs at the pyridine N-atom(s) but this has a minimal electronic effect on the diiron core. In summary:

- (i) The ester CO stretches are shifted substantially to higher values (*ca* 10 cm⁻¹)
- (ii) The ¹H-NMR data shows the expected shifts in the pyridine ring protons
- (iii) The corresponding FTIR and ¹H-NMR spectra of the benzoic acid ester are unperturbed upon addition of acid under the same conditions
- (iv) The *ortho*-pyridine ester shows two ester stretches in the unprotonated state attributed to geometric isomers but only shows a single band upon protonation

2.2.5 Electrochemistry

The electrochemical reduction of the diiron dithiolate bridged complexes [Fe₂(pdt)(CO)₆] and [Fe₂(edt)(CO)₆] involve a primary single electron-transfer followed by structural rearrangement(s) and a second electron-transfer. The principal reaction pathway for the propane dithiolate complex has been shown to involve decoordination of a thiolate ligand which attacks the parent complex to give a dimeric species⁶⁷. Chemical reduction has allowed isolation and structural characterisation of this species which can be reoxidised to the starting material in high yield⁶⁸. In the presence of a proton source electrocatalytic hydrogen production takes place with high turnover numbers but at high overpotentials.

A set of cyclic voltammograms for [Fe₂(dmp)(CO)₆] **1** are given in **Figure 2.14** which were recorded at a vitreous carbon electrode in MeCN containing 0.1M [NBu₄][BF₄] at room temperature.

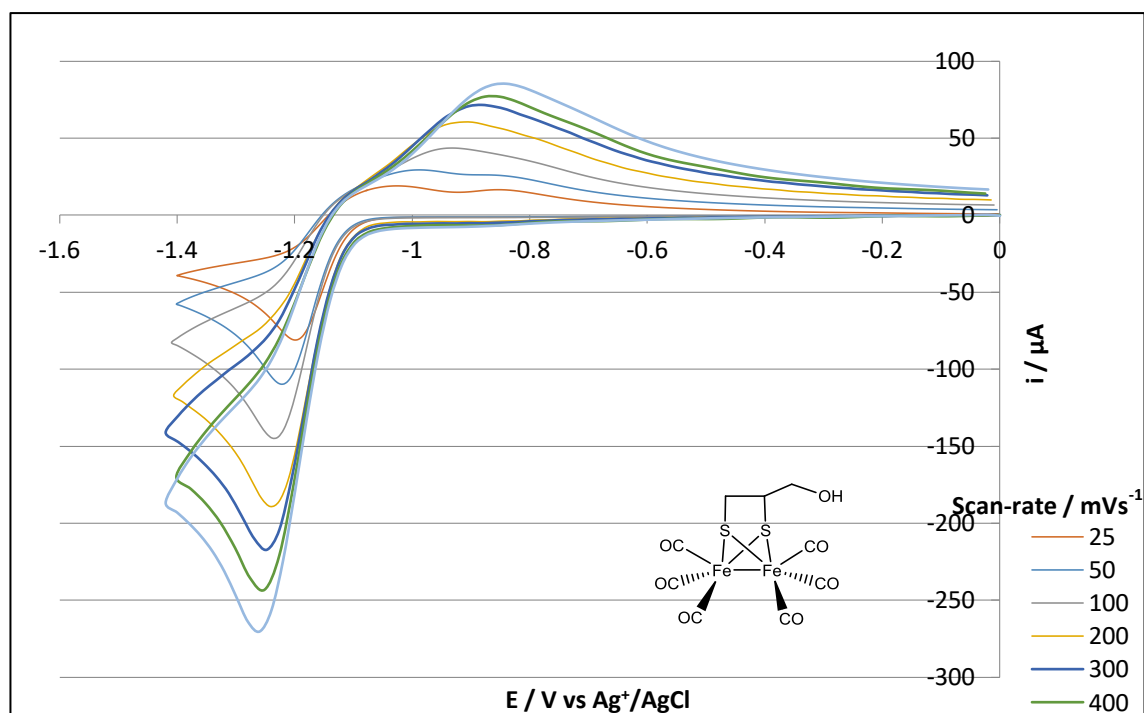


Figure 2.14. Cyclic voltammogram of $[\text{Fe}_2(\text{dmp})(\text{CO})_6]$ **1**. Conditions: 2 mM of the complex in MeCN containing 0.1 M $[\text{Bu}_4\text{N}][\text{BF}_4]$ at a vitreous carbon working electrode, area 0.7 cm^2 ; at 21°C .

The plot of the peak reduction current versus the square root of the scan-rate is linear which is consistent with a diffusion controlled reduction process, **Figure 2.15**.

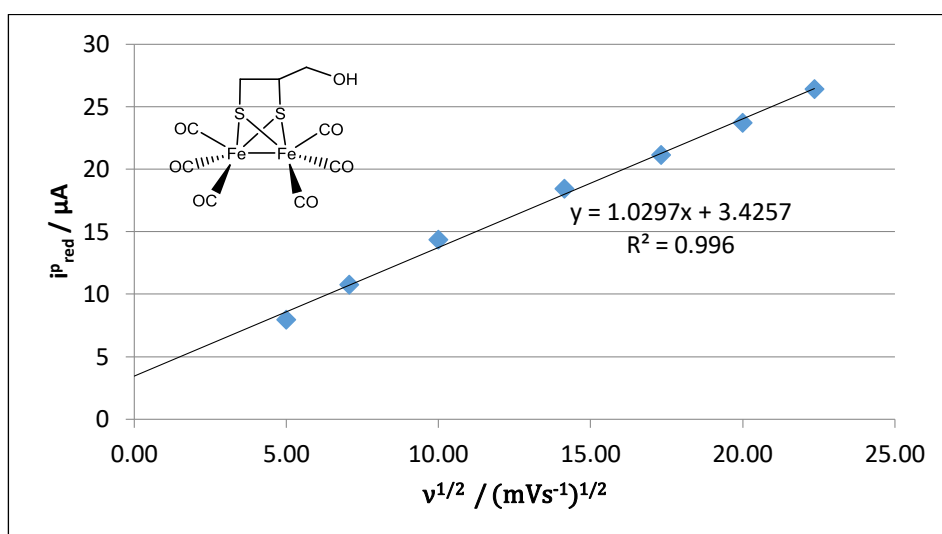


Figure 2.15. Peak current vs sq. rt. of scan-rate plot for $[\text{Fe}_2(\text{dmp})(\text{CO})_6]$ **1**. Conditions as for **Figure 2.14**.

The primary process is however essentially irreversible with fast chemistry following the initial electron-transfer. This suggests the proximal hydroxyl group might assist in cleavage of an Fe-S bond. In support of this it is found that the naphthoate ester functionalised complex shows a diffusion controlled partially reversible single electron transfer at moderate scan-rates and quasi-reversible behaviour at the faster scan-rates, **Figures 2.16 and 2.17.**

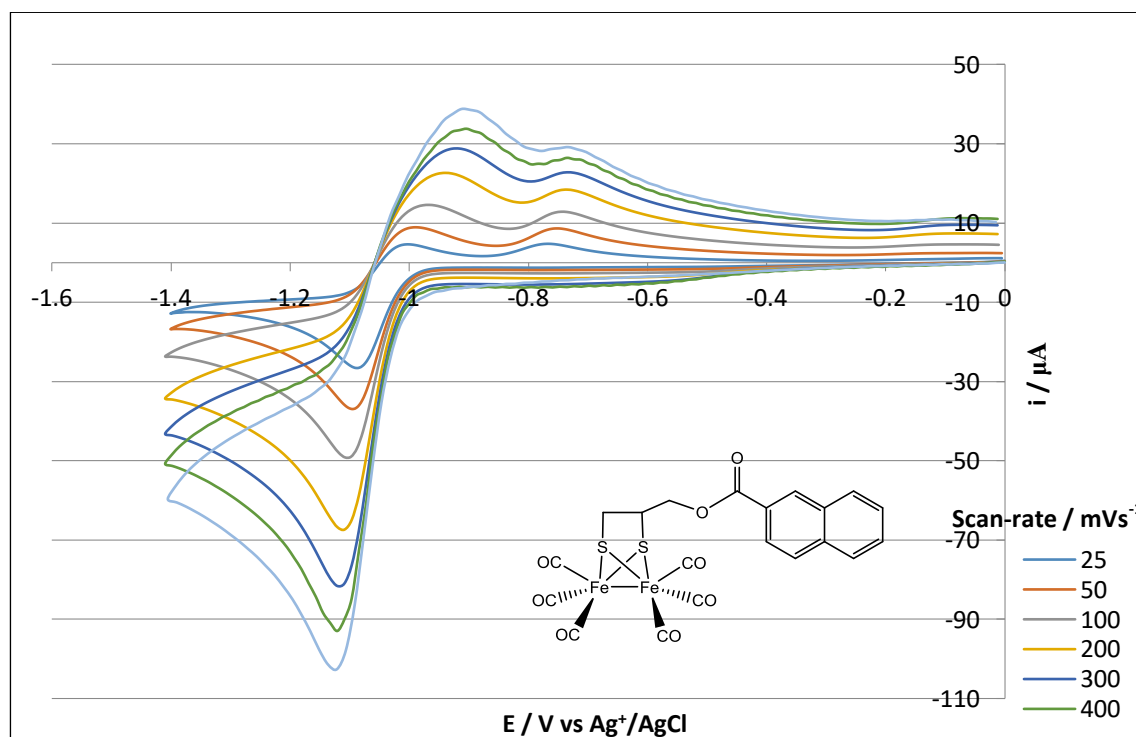


Figure 2.16. Cyclic voltammogram of $[\text{Fe}_2(\text{dmp-OCOC}_{10}\text{H}_7)(\text{CO})_6]$ **3**. Conditions: 1 mM of the complex in MeCN containing 0.1 M $[\text{Bu}_4\text{N}][\text{BF}_4]$ at a vitreous carbon working electrode, area 0.7 cm^2 ; at 21°C .

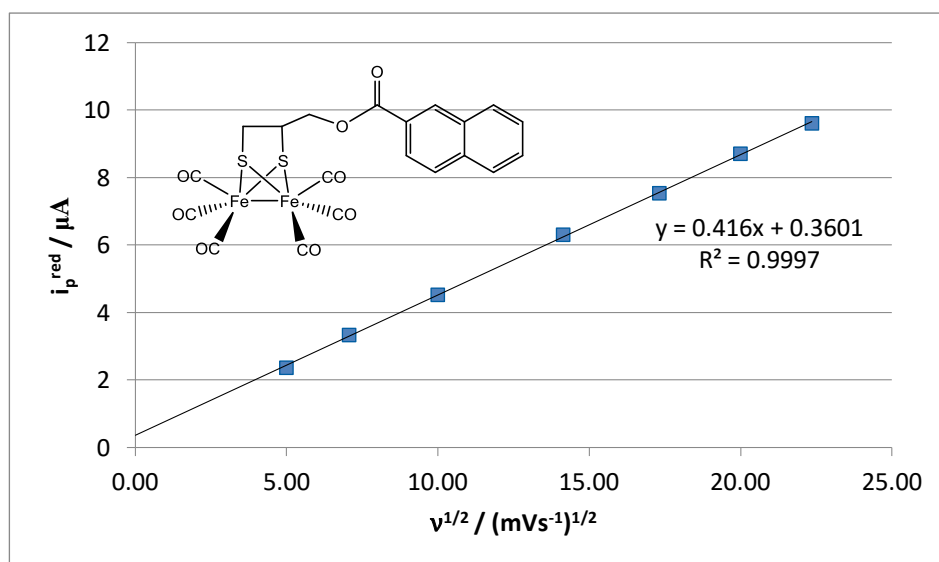


Figure 2.17. Peak current vs sq. rt. of scan-rate plot for $[\text{Fe}_2(\text{dmp-OCOC}_{10}\text{H}_7)(\text{CO})_6]$ **3**. Conditions as for **Figure 2.16**.

Clearly in this case there is not the possibility of intramolecular H-bonding assisting de-coordination of a thiolate. The set of pyridine functionalised voltammograms show essentially similar behaviour to the naphthoate species as is illustrated for the *meta*-pyridine derivative **7** shown in **Figure 2.18**. Again the process is diffusion controlled for this and the other pyridine species, **Figure 2.19**.

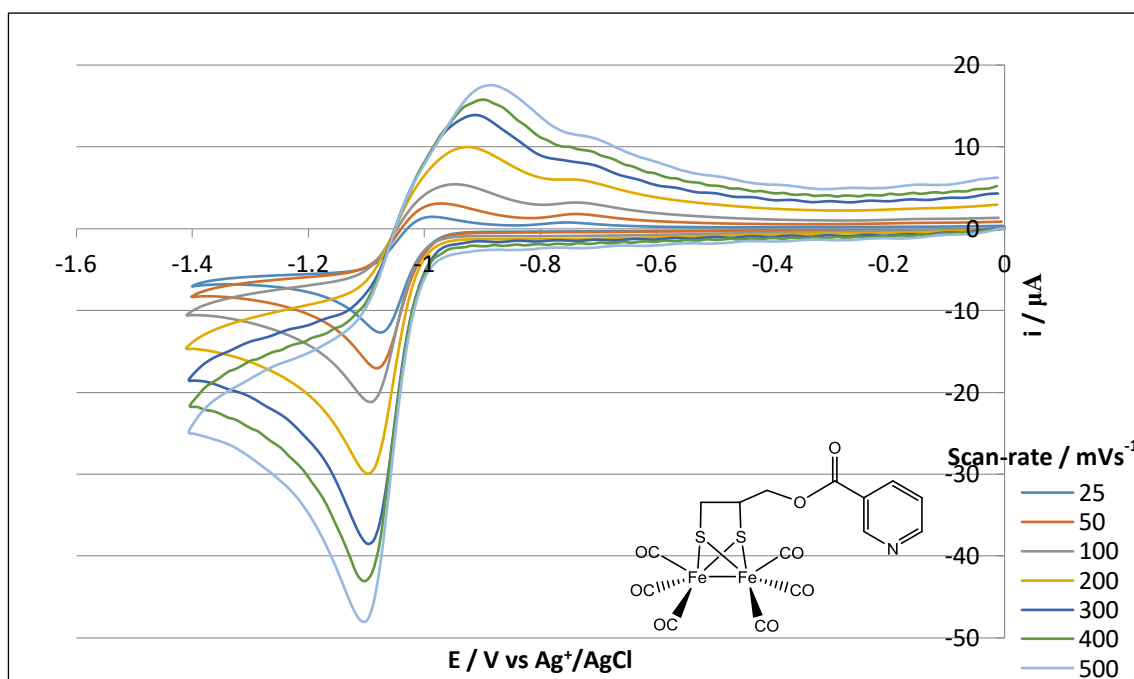


Figure 2.18. Cyclic voltammogram of $[\text{Fe}_2(\text{dmp-OCOC}_5\text{H}_4\text{N-}i\text{meta})(\text{CO})_6]$ 7. Conditions: 1 mM of the complex in MeCN containing 0.1 M $[\text{Bu}_4\text{N}][\text{BF}_4]$ at a vitreous carbon working electrode, area 0.7 cm^2 ; at 21°C .

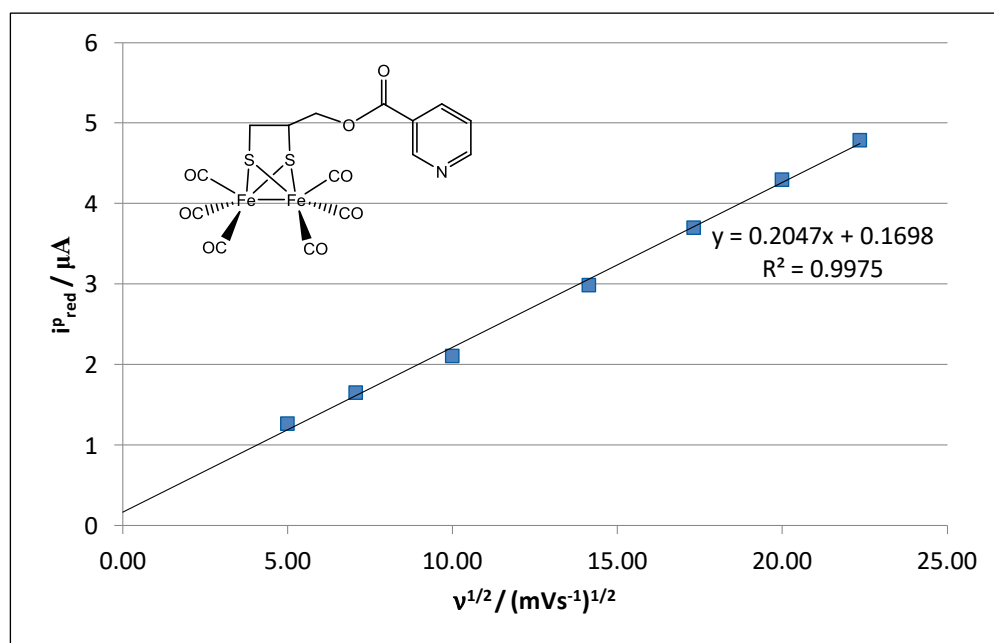


Figure 2.19. Peak current vs sq. rt. of scan-rate plot for $[\text{Fe}_2(\text{dmp-OCOC}_5\text{H}_4\text{N-}i\text{meta})(\text{CO})_6]$ 7. Conditions as for Figure 2.18.

An interesting aspect of the electrochemistry is that the peak reduction potentials E_p^{red} show a significant dependence of the nature of the pyridine with $E_p^{\text{red}} \text{ meta} > \text{ortho} \sim \text{para}$, that is the meta species is the easiest to reduce, **Figure 2.20**. This is perhaps surprising as it suggests that the LUMO of the meta species is the more stabilised (lower in energy) and that there is electronic communication between this orbital and the pyridine groups.

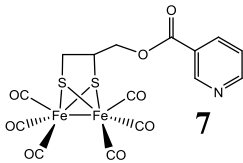
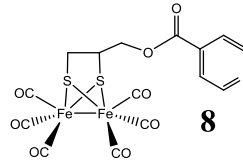
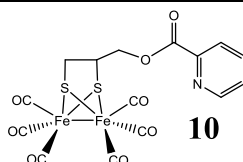
Compound	$E_p^{\text{red}} / \text{V vs Ag}^+/\text{AgCl}$
 7	-1.07
 8	-1.16
 10	-1.17

Figure 2.20. Comparison of E_p^{red} values for pyridine complexes **7**, **8** and **10**.

A preliminary investigation of the capability of the pyridine systems to electrocatalyse proton reduction was undertaken. **Figure 2.21** shows the effect of increasing lutidinium acid addition on the cyclic voltammetry of the ortho pyridine complex.

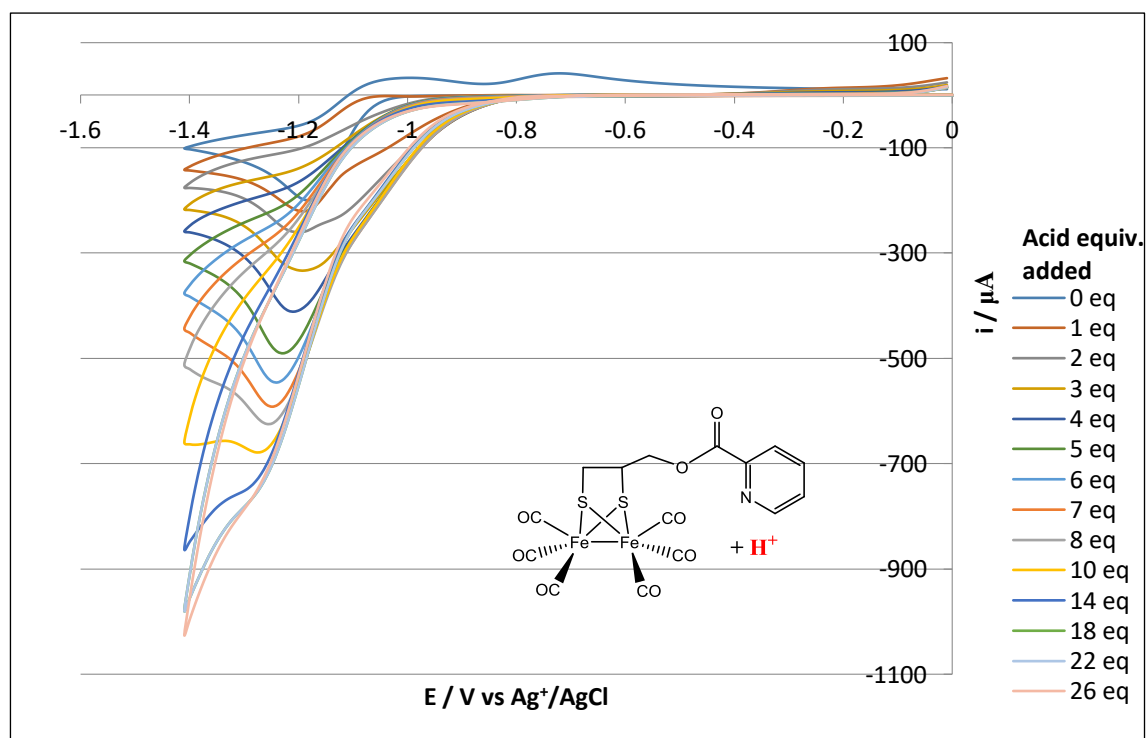


Figure 2.21. Electrocatalytic reduction of protons by $[\text{Fe}_2(\text{dmp-OCOC}_5\text{H}_4\text{N-para})(\text{CO})_6]$ **10**. Conditions: 1 mM of the complex in MeCN containing 0.1 M $[\text{Bu}_4\text{N}][\text{BF}_4]$ at a vitreous carbon working electrode, area 0.7 cm^2 ; scan-rate 50 mVs^{-1} at 21°C .

A pre-wave develops near -1.1 V which is probably associated with N-protonation of the pyridine and this is the species which is most likely engaged in electrocatalysis. Thus at higher acid concentrations the peak current increases reaching a maximum at *ca* 22 equivalents, **Figure 2.21 and 2.22**. At this concentration diffusion of protons is no longer the rate limiting step; the kinetics are limited by the turnover of the complex.

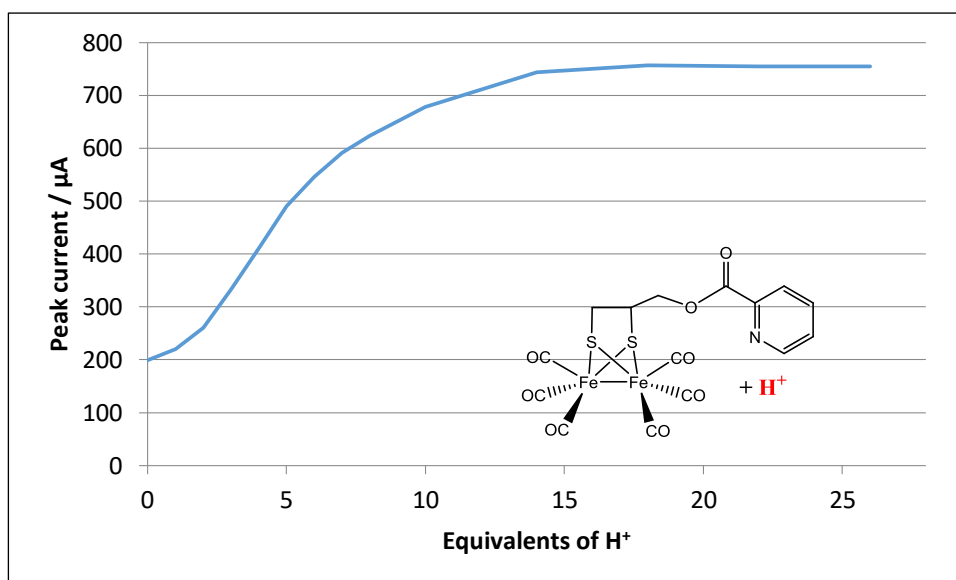


Figure 2.22. Catalytic response for reduction of protons by $[\text{Fe}_2(\text{dmp-OCOC}_5\text{H}_4\text{N-para})(\text{CO})_6]$ **10**. Conditions as for **Figure 2.21**.

The turnover frequency k_{obs} can be estimated using **Equation 1** where i_p is the magnitude of the peak current in the absence of the acid and i_{cat} is the maximum limiting current. The other symbols have their standard meanings⁶⁹.

$$\text{Equation 1: } \frac{i_{\text{cat}}}{i_p} = \frac{n}{0.4463} \sqrt{\frac{RTk_{\text{obs}}}{Fv}}$$

i_{cat} = Peak current with acid
 i_p = Peak current without acid
 n = Number of electrons involved in the process (2)
 R = Gas constant ($8.314 \text{ J K}^{-1} \text{ mol}^{-1}$)
 T = Absolute temperature (K)
 F = Faraday constant ($9.65 \times 10^4 \text{ C mol}^{-1}$)
 v = Scan-rate (Vs^{-1})
 k_{obs} = Rate constant (turnover frequency) (s^{-1})

This gives a value for the turnover frequency k_{obs} of 2.50 s^{-1} which is decidedly low and compares poorly with that of the propane dithiolate complex⁶⁷ where k_{obs} is *ca* 10^4 s^{-1} .

2.2.6 Concluding remarks

A convenient synthetic route for the introduction of pyridine groups in the second coordination sphere of a diiron dithiolate complex has been established. This uses straightforward coupling procedures to anchor the pyridine units by ester linkages. The basic methodology can be undoubtedly extended for the introduction of diverse

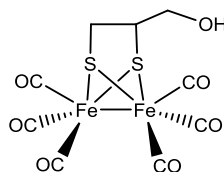
functional groups by esterification of the readily accessible diiron complex $[\text{Fe}_2(\text{dmp})(\text{CO})_6]$ **1**.

The pyridine units in the isolated complexes can be protonated but this has little effect on the IR frequencies of the metal carbonyl groups; that is N-protonation appears to have minimal electronic influence on the diiron core as reported by changes in the infrared pattern. The nature of the pyridine isomer; *ortho*-, *meta*- or *para*-, has a negligible influence on the metal carbonyl stretches, with the frequencies and intensities appearing essentially identical. Nevertheless, there is surprisingly an influence of the nature of the pyridine isomer on the peak reduction potential of the complex. The *meta*-isomer is the easiest to reduce by *ca* 100 mV, whereas the *ortho*- and *para*- isomers have comparable reduction potentials. This suggests that the pyridine can have a role in moderating the energy of the LUMO by stabilising or destabilising the mono-reduced species.

Preliminary evidence suggests that the second coordination sphere incorporation of a pyridine group as in the complexes **7**, **8** and **10** is unlikely to enhance electrocatalysis.

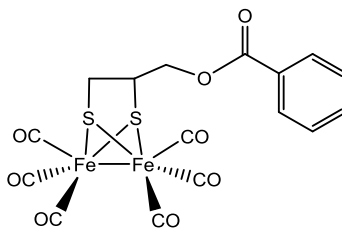
2.3 Experimental

2.3.1 Synthesis of $[\text{Fe}_2(\text{dmp})(\text{CO})_6]$ (**1**)⁵⁷



Triiron dodecacarbonyl (6.00 g, 12 mmol) was dissolved in dry degassed toluene (200 mL) to give a green/black solution. 2,3-dimercapto-1-propanol (1.0 mL, 10 mmol) was then added before the mixture was heated at 110 °C for 1 h, forming a red solution. The mixture was then purified by column chromatography using toluene eluent before the mixture was evaporated to dryness to give a red solid. Subsequent recrystallisation from MeCN gave the *title compound* (3.37 g, 8 mmol, 84%) as red crystals. ¹H-NMR (CD₂Cl₂, 300.13 MHz): δ (ppm) = 3.57 (m, 2H, CH-CH₂-OH), 2.84 (m, 1H, CH₂-CH-CH₂), 2.68 (m, 1H, S-CHH-CH), 1.96 (m, 2H, S-CHH-CH and OH). IR(DCM): ν(CO) = 2077, 2037, 2002, 1996.

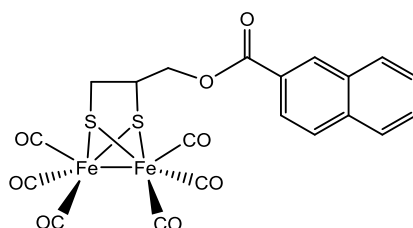
2.3.2 Synthesis of $[\text{Fe}_2(\text{dmp-OCOC}_6\text{H}_5)(\text{CO})_6]$ (**2**)



$[\text{Fe}_2(\text{dmp})(\text{CO})_6]$ **1** (0.50 g, 1.2 mmol), benzoic acid (0.16 g, 1.3 mmol), N,N'-dicyclohexylcarbodiimide (0.31 g, 1.5 mmol) and 4-(dimethylamino)pyridine (0.01 g, 0.08 mmol) were combined in a flask and dry DCM (150 mL) added. The mixture was stirred at room temperature for 48 h, with insoluble urea being precipitated. The resulting orange solution was then filtered through celite before being washed with 1 M HCl (3 x 100 mL), saturated sodium hydrogen carbonate solution (3 x 100 mL) and finally brine (3 x 100 mL). The resulting solution was dried over MgSO₄ and evaporated to dryness to give a red solid. Column chromatography (20:1 hexane/ethyl acetate) and subsequent drying in vacuo gave the *title compound* (0.53 g, 1.0 mmol,

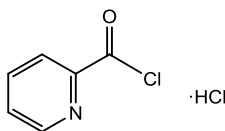
84%) as red powder. Crystals suitable for X-ray diffraction were grown from slow evaporation of a hexane solution. $^1\text{H-NMR}$ (CD_2Cl_2 , 300.13 MHz): δ (ppm) = 8.03 (m, 2H, Ar-H), 7.61 (t, $^3J_{\text{HH}} = 7.2$ Hz, 1H, Ar-H), 7.47 (t, $^3J_{\text{HH}} = 7.4$ Hz, 2H, Ar-H), 4.21 (m, 2H, CH- CH_2 -O), 3.10 (m, 1H, CH_2 -CH- CH_2), 2.79 (m, 1H, S-CHH-CH), 2.04 (m, 1H, S-CHH-CH). IR(DCM): $\nu(\text{CO}) = 2077, 2039, 2004, 1996$; $\nu(\text{ester CO}) = 1722$. Anal. Calcd. for $\text{C}_{16}\text{H}_{10}\text{O}_8\text{S}_2\text{Fe}_2$: C, 37.98; H, 1.99. Found: C, 38.08; H, 1.90. ESI-MS: m/z 523.89 $[\text{M}+\text{NH}_4]^+$.

2.3.3 Synthesis of $[\text{Fe}_2(\text{dmp-OCOC}_{10}\text{H}_7)(\text{CO})_6]$ (3)



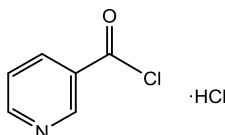
$[\text{Fe}_2(\text{dmp})(\text{CO})_6]$ **1** (0.52 g, 1.3 mmol), 2-naphthoic acid (0.25 g, 1.4 mmol), N,N'-dicyclohexylcarbodiimide (0.32 g, 1.6 mmol) and 4-(dimethylamino)pyridine (0.01 g, 0.08 mmol) were combined in a flask and dry DCM (150 mL) added. The mixture was stirred at room temperature for 72 h, with insoluble urea being precipitated. The resulting orange solution was then filtered through celite before being washed with 1 M HCl (3 x 100 mL), saturated sodium hydrogen carbonate solution (3 x 100 mL) and finally brine (3 x 100 mL). The resulting solution was dried over MgSO_4 and evaporated to dryness to give a red oily solid. Column chromatography (12:1 hexane/ethyl acetate) and subsequent drying in vacuo gave the *title compound* (0.50 g, 0.9 mmol, 69%) as red powder. Crystals suitable for X-ray diffraction were grown by cooling of a hexane solution to -20°C . $^1\text{H-NMR}$ (CD_2Cl_2 , 300.13 MHz): δ (ppm) = 8.62 (s, 1H, Ar-H), 7.96 (m, 4H, Ar-H), 7.61 (m, 2H, Ar-H), 4.27 (m, 2H, CH- CH_2 -O), 3.16 (m, 1H, CH_2 -CH- CH_2), 2.83 (m, 1H, S-CHH-CH), 2.08 (m, 1H, S-CHH-CH). IR(DCM): $\nu(\text{CO}) = 2077, 2039, 2004, 1996$; $\nu(\text{ester CO}) = 1720$. Anal. Calcd. for $\text{C}_{20}\text{H}_{12}\text{O}_8\text{S}_2\text{Fe}_2$: C, 43.19; H, 2.18. Found: C, 43.29; H, 2.11. ESI-MS: m/z 556.88 $[\text{M}+\text{H}]^+$.

2.3.4 Synthesis of 2-pyridinecarbonyl chloride hydrochloride (4)⁶⁴



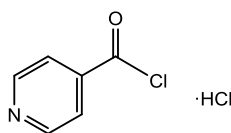
Pyridine-2-carboxylic acid (2.02 g, 16 mmol) was stirred in dry DMF (0.2 mL) for 1 h. Thionyl chloride (10 mL, 140 mmol) was then added slowly via dropping funnel. The resulting dark brown solution was stirred at room temperature for 24 h. The solution was then heated at 80 °C for 1.5 h before volatiles were removed in vacuo to give a dark brown oil. Ethyl acetate (20 mL) was then added to achieve a beige precipitate. The precipitate was washed with more ethyl acetate (20 mL) before being dried in vacuo to give the *title compound* (2.01 g, 11 mmol, 70%) as beige solid. ¹H-NMR (DMSO-*d*₆, 300.13 MHz): δ (ppm) = 8.84 (m, 1H), 8.40 (m, 1H), 8.27 (m, 1H), 7.97 (m, 1H).

2.3.5 Synthesis of 3-pyridinecarbonyl chloride hydrochloride (5)⁶⁴



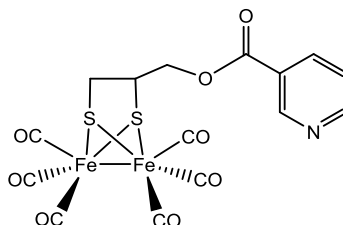
Pyridine-3-carboxylic acid (2.02 g, 16 mmol) was stirred in dry DMF (0.2 mL) for 1 h. Thionyl chloride (10 mL, 140 mmol) was then added slowly via dropping funnel. The resulting orange solution was stirred at room temperature for 24 h. The solution was then heated at 80 °C for 1.5 h before volatiles were removed in vacuo to give a pale orange oil. Ethyl acetate (20 mL) was then added to achieve a beige precipitate. The precipitate was washed with more ethyl acetate (20 mL) before being dried in vacuo to give the *title compound* (2.21g, 16 mmol, 94%) as beige solid. ¹H-NMR (D₂O, 300.13 MHz): δ (ppm) = 9.42 (m, 1H), 9.13 (m, 2H), 8.28 (m, 1H).

2.3.6 Synthesis of 4-pyridinecarbonyl chloride hydrochloride (**6**)⁶⁴



Pyridine-4-carboxylic acid (2.07 g, 17 mmol) was stirred in dry DMF (0.2 mL) for 1 h. Thionyl chloride (10 mL, 140 mmol) was then added slowly via dropping funnel. The resulting dark green solution was stirred at room temperature for 24 h. The solution was then heated at 80 °C for 1.5 h before volatiles were removed in vacuo to give a green/yellow oil. Ethyl acetate (20 mL) was then added to achieve a pale yellow precipitate. The precipitate was washed with more ethyl acetate (20 mL) before being dried in vacuo to give the *title compound* (2.87 g, 16 mmol, 96%) as pale yellow solid. ¹H-NMR (D₂O, 300.13 MHz): δ (ppm) = 8.83 (m, 2H), 8.40 (m, 2H).

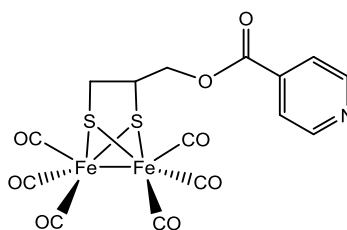
2.3.7 Synthesis of [Fe₂(dmp-OCOC₅H₄N-*meta*)(CO)₆] (**7**)



3-pyridinecarbonyl chloride hydrochloride **5** (0.32 g, 1.8 mmol) was suspended in dry THF (40 mL) to give a cloudy white suspension. Triethylamine (0.3 mL, 2.2 mmol) was then added and the mixture left to stir for 30 min. A solution of [Fe₂(dmp)(CO)₆] **1** (0.50 g, 1.2 mmol) in dry THF (40 mL) was then added, followed by more triethylamine (0.4 mL, 2.9 mmol). The resulting orange solution was then stirred at room temperature for 24 h. The volatiles were then removed in vacuo to give an orange oil before the residue was dissolved in DCM (100 mL). The resulting solution was then washed with 1 M HCl (3 x 100 mL), saturated sodium hydrogen carbonate solution (3 x 100 mL) and finally brine (3 x 100 mL) before being dried over MgSO₄ and evaporated to dryness to give an orange oily solid. Column chromatography (3:1 hexane/ethyl acetate) and subsequent drying in vacuo gave the *title compound* (0.58 g, 1.1 mmol, 92%) as orange powder. Crystals suitable for X-ray diffraction were grown by cooling of a hexane solution to -20 °C. ¹H-NMR (CD₂Cl₂, 300.13 MHz): δ (ppm) = 9.22 (s, 1H, Ar-H), 8.80

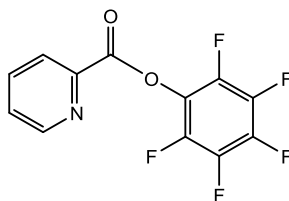
(d, $^3J_{\text{HH}} = 3.9$ Hz, 1H, Ar-H), 8.29 (d, $^3J_{\text{HH}} = 7.9$ Hz, 1H, Ar-H), 7.43 (m, 1H, Ar-H), 4.24 (m, 2H, CH-CH₂-O), 3.10 (m, 1H, CH₂-CH-CH₂), 2.79 (m, 1H, S-CHH-CH), 2.03 (m, 1H, S-CHH-CH). IR(DCM): $\nu(\text{CO}) = 2077, 2039, 2006, 1998$; $\nu(\text{ester CO}) = 1732$. Anal. Calcd. for C₁₅H₉NO₈S₂Fe₂: C, 35.53; H, 1.79; N, 2.76. Found: C, 35.66; H, 1.69; N, 2.87.

2.3.8 Synthesis of [Fe₂(dmp-OCOC₅H₄N-*para*)(CO)₆] (8)



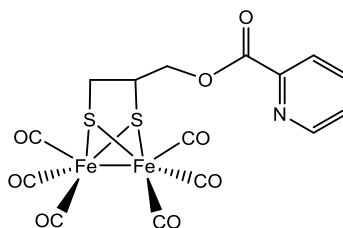
4-pyridinecarbonyl chloride hydrochloride **6** (0.37 g, 2.1 mmol) was suspended in dry THF (40 mL) to give a cloudy white suspension. Triethylamine (0.3 mL, 2.2 mmol) was then added and the mixture left to stir for 30 min. A solution of [Fe₂(dmp)(CO)₆] **1** (0.51 g, 1.3 mmol) in dry THF (40 mL) was then added, followed by more triethylamine (0.4 mL, 2.9 mmol). The resulting orange solution was then stirred at room temperature for 24 h. The volatiles were then removed in vacuo to give an orange oil before the residue was dissolved in DCM (100 mL). The resulting solution was then washed with 1 M HCl (3 x 100 mL), saturated sodium hydrogen carbonate solution (3 x 100 mL) and finally brine (3 x 100 mL) before being dried over MgSO₄ and evaporated to dryness to give an orange oily solid. Column chromatography (3:1 hexane/ethyl acetate) and subsequent drying in vacuo gave the *title compound* (0.11 g, 0.2 mmol, 17%) as orange powder. Crystals suitable for X-ray diffraction were grown from a hexane solution cooled to 2 °C. ¹H-NMR (CD₂Cl₂, 300.13 MHz): δ (ppm) = 8.93 (s, 2H, Ar-H), 7.88 (s, 2H, Ar-H), 4.24 (m, 2H, CH-CH₂-O), 3.09 (m, 1H, CH₂-CH-CH₂), 2.79 (m, 1H, S-CHH-CH), 2.02 (m, 1H, S-CHH-CH). IR(DCM): $\nu(\text{CO}) = 2077, 2039, 2006, 1998$; $\nu(\text{ester CO}) = 1736$. Anal. Calcd. for C₁₅H₉NO₈S₂Fe₂: C, 35.53; H, 1.79; N, 2.76. Found: C, 35.67; H, 1.69; N, 2.83.

2.3.9 Synthesis of pyridine-2-carboxylic acid pentafluorophenyl ester (**9**)⁶⁵



Pyridine-2-carboxylic acid (1.25 g, 10 mmol), pentafluorophenol (2.10 g, 11 mmol) and N,N'-dicyclohexylcarbodiimide (2.27 g, 11 mmol) were combined in a flask and dry dioxane (30 mL) was added to give a slightly yellow solution. The solution was stirred at room temperature for 1 hour to give a bright yellow viscous solution, which was then filtered through celite and dried in vacuo to give a dark green solid. Subsequent recrystallisation from hexane gave the title compound (2.19 g, 8 mmol, 75%) as green crystals. ¹H-NMR (CDCl₃, 300.13 MHz): δ (ppm) = 8.87 (m, 1H), 8.34 (m, 1H), 8.01 (m, 1H), 7.68 (m, 1H). ¹⁹F-NMR (CDCl₃, 282.37 MHz): δ (ppm) = -152.61 (m, 2F), -157.89 (m, 1F), -162.00 (m, 2F).

2.3.10 Synthesis of [Fe₂(dmp-OCOC₅H₄N-*ortho*)(CO)₆] (**10**)



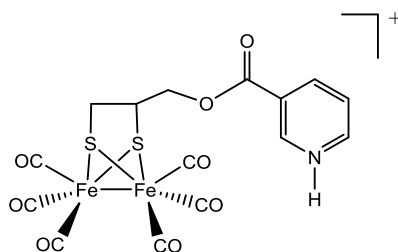
[Fe₂(dmp)(CO)₆] **1** (0.51 g, 1.3 mmol) and pyridine-2-carboxylic acid pentafluorophenyl ester **9** (0.53 g, 1.8 mmol) were dissolved in dry THF (80 mL) to give an orange solution. Triethylamine (0.4 mL, 2.9 mmol) was then added, with the subsequent mixture being heated at 40 °C for 24 h. Volatiles were then removed in vacuo to give a red oil before the residue was dissolved in DCM (100 mL). The resulting solution was then washed with 1 M HCl (3 x 100 mL), saturated sodium hydrogen carbonate solution (3 x 100 mL) and finally brine (3 x 100 mL) before being dried over MgSO₄ and evaporated to dryness to give a red solid. Column chromatography (3:1 hexane/ethyl acetate) and subsequent drying in vacuo gave the *title compound* (0.60 g, 1.2 mmol, 93%) as red powder. Crystals suitable for X-ray

diffraction were grown from a hexane solution cooled to 2 °C. $^1\text{H-NMR}$ (CD_2Cl_2 , 300.13 MHz): δ (ppm) = 9.72 (s, 1H, Ar-H), 8.11 (d, $^3J_{\text{HH}} = 7.5$ Hz, 1H, Ar-H), 7.86 (t, $^3J_{\text{HH}} = 7.5$ Hz, 1H, Ar-H), 7.50 (m, 1H, Ar-H), 4.27 (m, 2H, CH-CH₂-O), 3.15 (m, 1H, CH₂-CH-CH₂), 2.80 (m, 1H, S-CHH-CH), 2.04 (m, 1H, S-CHH-CH). IR(DCM): $\nu(\text{CO}) = 2077, 2039, 2006, 1998$; $\nu(\text{ester CO}) = 1743, 1730$.

2.3.11 General procedure for protonation of the $[\text{Fe}_2(\text{dmp})(\text{CO})_6]$ -pyridine esters

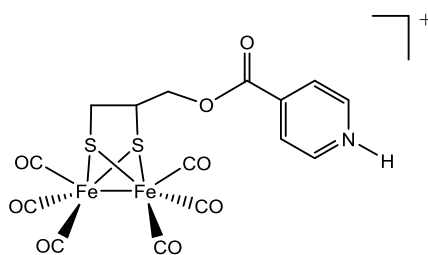
A solution of $[\text{Fe}_2(\text{dmp})(\text{CO})_6]$ -pyridine ester **7**, **8**, or **10** (15.0 mg, 0.03 mmol) in dry DCM (5 mL) was prepared, to which 1 equivalent of $\text{HBF}_4 \cdot \text{OEt}_2$ via DCM (1:99) stock solution (0.41 mL, 0.03 mmol) was added. Samples for analysis were then removed by syringe as necessary. Characterisation of individual species outlined below.

2.3.12 Characterisation of the cation $[\text{Fe}_2(\text{dmp-OCOC}_5\text{H}_4\text{N-}i{meta})(\text{CO})_6\text{H}]^+$



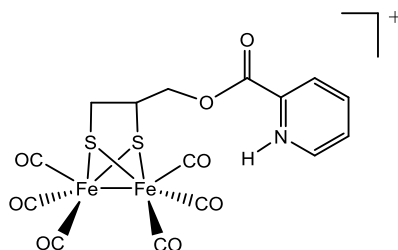
The *title cation* is formed in situ when $[\text{Fe}_2(\text{dmp})(\text{CO})_6]$ -pyridine ester **7** is combined with 1 equivalent of $\text{HBF}_4 \cdot \text{OEt}_2$ in dry DCM at room temperature. $^1\text{H-NMR}$ (CD_2Cl_2 , 300.13 MHz): δ (ppm) = 9.25 (s, 1H, Ar-H), 8.86 (m, 1H, Ar-H), 8.54 (d, $^3J_{\text{HH}} = 7.5$ Hz, 1H, Ar-H), 7.66 (m, 1H, Ar-H), 4.28 (m, 2H, CH-CH₂-O), 3.11 (m, 1H, CH₂-CH-CH₂), 2.80 (m, 1H, S-CHH-CH), 2.02 (m, 1H, S-CHH-CH, overlapped with H₂O). IR(DCM): $\nu(\text{CO}) = 2079, 2039, 2006, 1998$; $\nu(\text{ester CO}) = 1747$.

2.3.13 Characterisation of the cation $[\text{Fe}_2(\text{dmp-OCOC}_5\text{H}_4\text{N-para})(\text{CO})_6\cdot\text{H}]^+$



The *title cation* is formed in situ when $[\text{Fe}_2(\text{dmp})(\text{CO})_6]$ -pyridine ester **8** is combined with 1 equivalent of $\text{HBF}_4\cdot\text{OEt}_2$ in dry DCM at room temperature. $^1\text{H-NMR}$ (CD_2Cl_2 , 300.13 MHz): δ (ppm) = 8.96 (d, $^3J_{\text{HH}} = 5.6$ Hz, 2H, Ar-H), 8.33 (d, $^3J_{\text{HH}} = 5.6$ Hz, 2H, Ar-H), 4.32 (m, 2H, CH-CH₂-O), 3.10 (m, 1H, CH₂-CH-CH₂), 2.81 (m, 1H, S-CHH-CH), 2.00 (m, 1H, S-CHH-CH). IR(DCM): $\nu(\text{CO}) = 2079, 2039, 2007, 1998$; $\nu(\text{ester CO}) = 1747$.

2.3.14 Characterisation of the cation $[\text{Fe}_2(\text{dmp-OCOC}_5\text{H}_4\text{N-para})(\text{CO})_6\cdot\text{H}]^+$



The *title cation* is formed in situ when $[\text{Fe}_2(\text{dmp})(\text{CO})_6]$ -pyridine ester **10** is combined with 1 equivalent of $\text{HBF}_4\cdot\text{OEt}_2$ in dry DCM at room temperature. $^1\text{H-NMR}$ (CD_2Cl_2 , 300.13 MHz): δ (ppm) = 8.88 (d, $^3J_{\text{HH}} = 4.2$ Hz, 1H, Ar-H), 8.31 (d, $^3J_{\text{HH}} = 7.8$ Hz, 1H, Ar-H), 8.20 (t, $^3J_{\text{HH}} = 7.6$ Hz, 1H, Ar-H), 7.81 (m, 1H, Ar-H), 4.32 (d, $^3J_{\text{HH}} = 7.4$ Hz, 2H, CH-CH₂-O), 3.15 (m, 1H, CH₂-CH-CH₂), 2.83 (m, 1H, S-CHH-CH), 2.03 (m, 1H, S-CHH-CH). IR(DCM): $\nu(\text{CO}) = 2079, 2041, 2006, 2000$; $\nu(\text{ester CO}) = 1759$.

2.3.15 X-ray crystallography

Crystals were suspended in oil, and one was mounted on a glass fibre and fixed in the cold nitrogen stream of the diffractometer. Data were collected on a Rigaku AFC12 goniometer equipped with an enhanced sensitivity (HG) Saturn724+ detector mounted at the window of an FR-E+ SuperBright molybdenum rotating anode generator with HF

Varimax optics (**2**, **3**, **7**, **10**), or a Crystal Logic 4-circle kappa geometry goniometer with a Rigaku Saturn 724 CCD detector on beamline I19 of the Diamond Light Source (**8**). Data were process using the CrystalClear-SM Expert program⁷⁰. Structures were determined by charge flipping routines in the SUPERFLIP program⁷¹ and refined by full-matrix least-squares methods on F^2 in SHELXL-2012 (**2**, **3**)⁷² or SHELXL-2014 (**7**, **8**, **10**).⁷³ Non-hydrogen atoms were refined with anisotropic thermal parameters. Hydrogen atoms were included in idealized positions and their U_{iso} values were set to ride on the U_{eq} values of the parent carbon atoms. Complex **3** was a non-merohedral twin (a 180° rotation about [1 0 0]) with final occupancy for the minor component of 0.362. Rigid bond restraints were applied to all atoms in complex **7**, **8**, **10** with e.s.d. values of 0.004 Å both 1,2- and 1,3-distances. The benzoate ester side-chain of this complex was disordered over two positions and was models with a fixed three-quarters occupancy in the major position. Complexes **7** and **8** were subject to twin refinement using two reflection files (HKL5) with twin component values of 0.403 and 0.411, respectively. In complex **7** the CH₂O group of the ester was modelled in two positions, with occupancy of 0.56(4) for the major position at the end of the refinement. Bond distances and thermal parameters for the disordered parts were restrained to the same values with e.s.d. values of 0.02 Å and 0.04 Å, respectively. The py-CO(O) groups in the two independent molecules of complex **8** in the asymmetric unit were restrained to lie in a common plane with an e.s.d. of 0.1 Å; an extinction coefficient of 0.044(17) was also refined for this structure.

A summary of the data collection parameters is given in **Figures 2.23 and 2.24**.

	2	3	7	8
Formula	C ₁₆ H ₁₀ Fe ₂ O ₈ S ₂	C ₂₀ H ₁₂ Fe ₂ O ₈ S ₂	C ₁₅ H ₉ Fe ₂ NO ₈ S ₂	C ₁₅ H ₉ Fe ₂ NO ₈ S ₂
Molecular weight	506.06	556.12	507.05	507.05
T/K	100(2)	100(2)	100(2)	100(2)
$\lambda/\text{\AA}$	0.71075	0.71075	0.71075	0.6889
Crystal system	Triclinic	Triclinic	Monoclinic	Triclinic
Space group	$P\bar{1}$	$P\bar{1}$	$P2_1/c$	$P\bar{1}$
$a/\text{\AA}$	6.5304(5)	7.4608(8)	20.2126(16)	7.642(12)
$b/\text{\AA}$	7.5754(5)	9.3160(11)	7.4871(7)	13.21(2)
$c/\text{\AA}$	19.6740(14)	15.696(2)	12.5040(7)	20.65(4)
$\alpha/^\circ$	82.873(7)	94.355(7)	90	82.23(3)
$\beta/^\circ$	86.209(7)	98.176(7)	97.788(6)	85.01(4)
$\gamma/^\circ$	76.366(6)	94.470(7)	90	75.21(5)
$V/\text{\AA}^3$	937.86(12)	1072.4(2)	1874.8(3)	1994(6)
Z	2	2	4	4
Reflections collected	12294	5847	5651	6027
Independent reflections	4288	4901	5651	6027
R_{int}	0.040	—	—	—
$R_1 [F^2 > 2\sigma(F^2)]$	0.042	0.137	0.121	0.192
wR_2 (all data)	0.125	0.358	0.302	0.520

Figure 2.23. Summary of X-ray parameters for complexes **2**, **3**, **7** and **8**.

	10
Formula	$\text{C}_{15}\text{H}_9\text{Fe}_2\text{NO}_8\text{S}_2$
Molecular weight	507.05
T/K	100(2)
$\lambda/\text{\AA}$	0.71075
Crystal system	Triclinic
Space group	$P\bar{1}$
$a/\text{\AA}$	7.632(3)
$b/\text{\AA}$	9.536(3)
$c/\text{\AA}$	14.524(5)
$\alpha/^\circ$	92.270(6)
$\beta/^\circ$	102.425(6)
$\gamma/^\circ$	91.371(6) $^\circ$
$V/\text{\AA}^3$	1030.9(6)
Z	2
Reflections collected	18529
Independent reflections	4755
R_{int}	0.080
$R_1 [F^2 > 2\sigma(F^2)]$	0.054
wR_2 (all data)	0.153

Figure 2.24. Summary of X-ray parameters for complex **10**.

3 Hydrogen bonding of a diiron dicyanide subsite analogue with fluorinated bis-ureas

3.1 Introduction

3.1.1 General aspects

This chapter is concerned with the second coordination sphere interactions of cyanide ligands with fluorinated bis-ureas in order to demonstrate the potential for hydrogen bonding. Hydrogen bonding plays several key roles in the structure, reactivity and function of the [FeFe]-hydrogenase, so developing subsite analogue systems exhibiting significant hydrogen bonding is important for understanding the behaviour of the natural system and for directing the synthesis of future hydrogenase-inspired systems.

In the next sections the main reasons for interest in hydrogen-bonded cyanides will be outlined, along with the reasons why fluorinated bis-ureas are ideal candidates to facilitate such bonding. The combination of these bis-ureas with a cyanide-containing subsite analogue, $(\text{Et}_4\text{N})_2[\text{Fe}_2(\text{pdt})(\text{CO})_4(\text{CN})_2]$, will then be described, with the subsequent binding of the bis-ureas being demonstrated through spectroscopy and the chemical properties of the bound system being explored.

3.1.2 Hydrogen bonding in the natural system

The active site of the [FeFe]-hydrogenase as obtained by Peters and coworkers⁷⁴ from a high-resolution structure isolated from *Clostridium pasteurianum* is shown in **Figure 3.1**. The surrounding amino acid residues have been included in the structure, and they are shown to be hydrogen bonding to the cyanide ligands. The cyanide ligand at the Fe atom proximal to the 4Fe4S cluster is hydrogen bonded to proline (Pro 231) and serine (Ser 232), and the cyanide on the Fe atom distal to the cluster is hydrogen bonded to proline (Pro 324), glutamine (Gln 325). A structure showing the key hydrogen bonding interactions of the protein backbone with the cyanide ligands is also included in this figure.

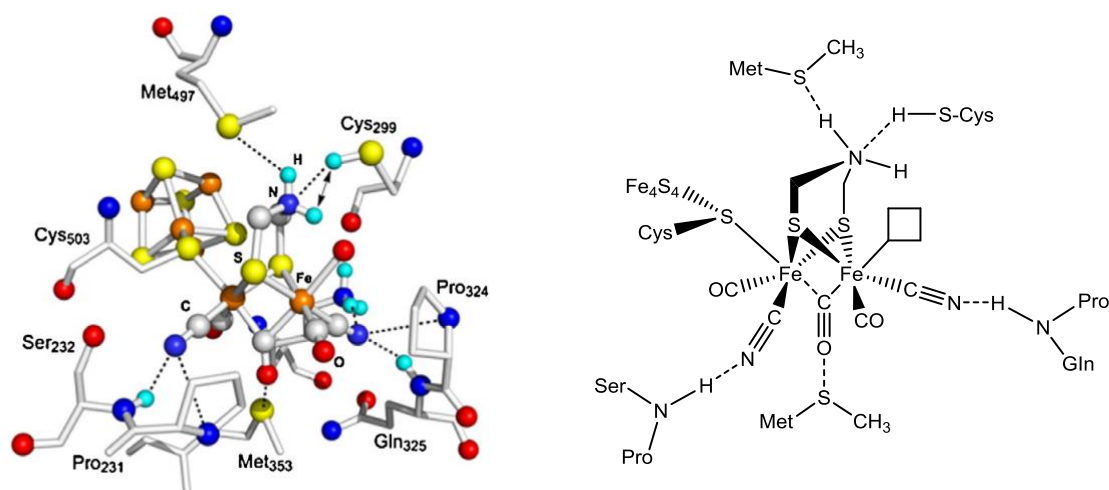


Figure 3.1. Active site of [FeFe]-hydrogenase demonstrating hydrogen bonding obtained from *Clostridium pasteurianum*. X-ray crystal structure reproduced from reference⁷⁵.

The hydrogen bonding interactions around the active site are believed to serve several important functions⁷⁶; the most basic of which is that they contribute to the binding of the subsite to the protein, which is otherwise only held by a single cysteine bridging sulfur to the 4Fe4S cluster. Secondly, they must enforce the subsite to adopt the *trans-(basal,basal)* orientation in order to favour a substrate (H^+/H_2) binding site in the turnover states. Thirdly, they help drain charge from the diiron core, allowing reduction of the $\{Fe^{II}-Fe^I\}/\{Fe^I-Fe^I\}$ couple to occur at a potential close to that of the $2H^+/H_2$ couple at neutral pH; and fourthly the hydrogen bonding plays an important role in transporting protons to and from the active site via the bridging adt ligand⁷⁷. As hydrogen bonding is so important to the structure and function of the active site of the [FeFe]-hydrogenase, and particularly through the cyanide ligands, it is clear that this is an area worthy of investigation.

3.1.3 Interest in the cyanide groups

There is much interest in the ligated cyanide groups present in [FeFe]-hydrogenase subsite analogues as they readily allow functionalisation that directly impacts on the FeFe core. The general ability of the coordinated cyanide to engage its lone pair in

bonding via acting as a Lewis base will be explained in **Chapter 4**. However, recently, a significant amount of attention regarding cyanide ligands on hydrogenase subsite mimics has been put towards a more biological context. Artero, Fontecave and collaborators⁷⁸ have recently suggested that bridging cyanide is involved in the biosynthetic pathway of the active site of [FeFe]-hydrogenase. In this pathway, a maturase enzyme, HydF, from *Thermotoga maritima*, is believed to accept a diiron unit **Figure 3.2 (a)** to form the complex **Figure 3.2 (b)**, which then gives the active H-cluster of HydA, **Figure 3.2 (c)**. It is proposed that HydF possesses a linking cyanide, but curiously, when the diiron subsite unit is bound the cyanide undergoes linkage isomerisation.

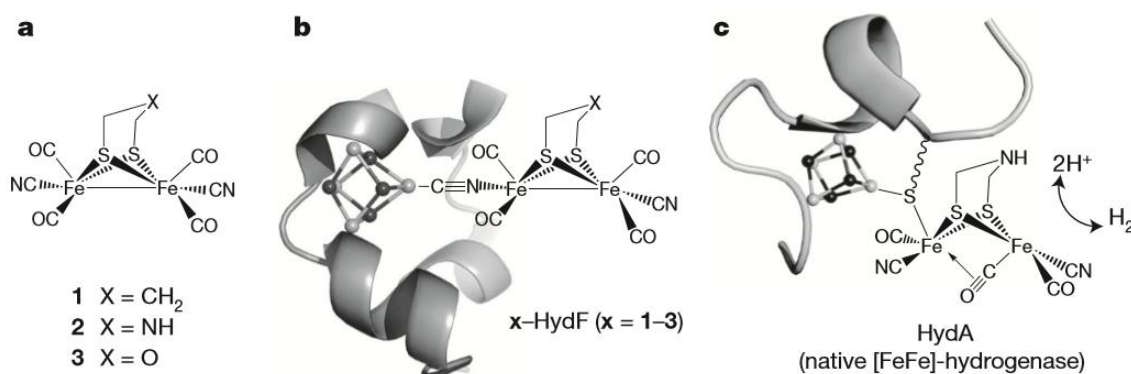
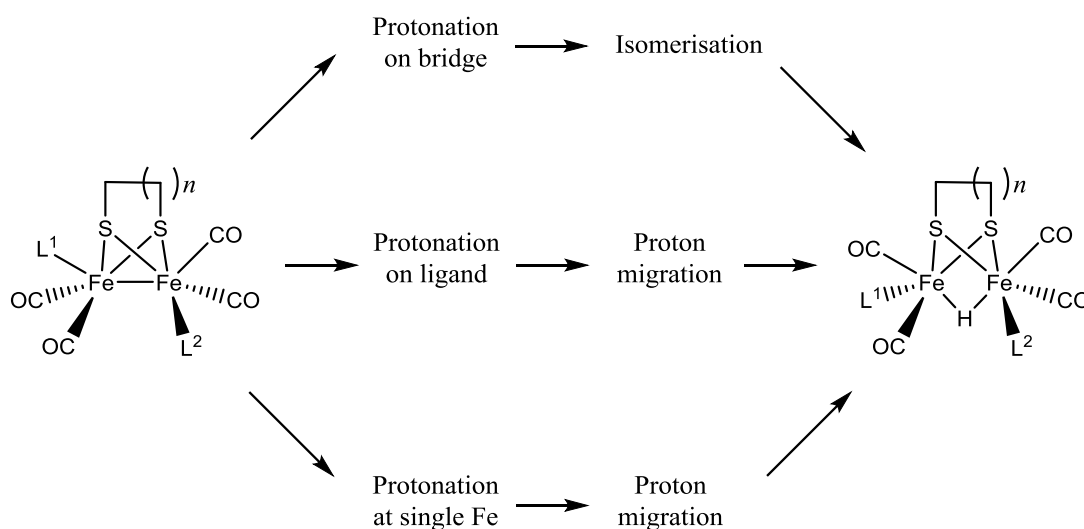


Figure 3.2. Diiron subsite analogues **(a)**, their binding to the maturase with linkage isomerisation of the CN bridge **(b)**, and **(c)** the re-flipped CN in an active hydrogenase. Image reproduced from reference⁷⁸.

This linkage isomerisation is still yet to be fully substantiated, though HYSORE experiments in combination with DFT calculations have suggested that the diiron subsite analogue incorporated into HydF is bound through a CN that has its carbon bound to the 4Fe4S cluster⁷⁹.

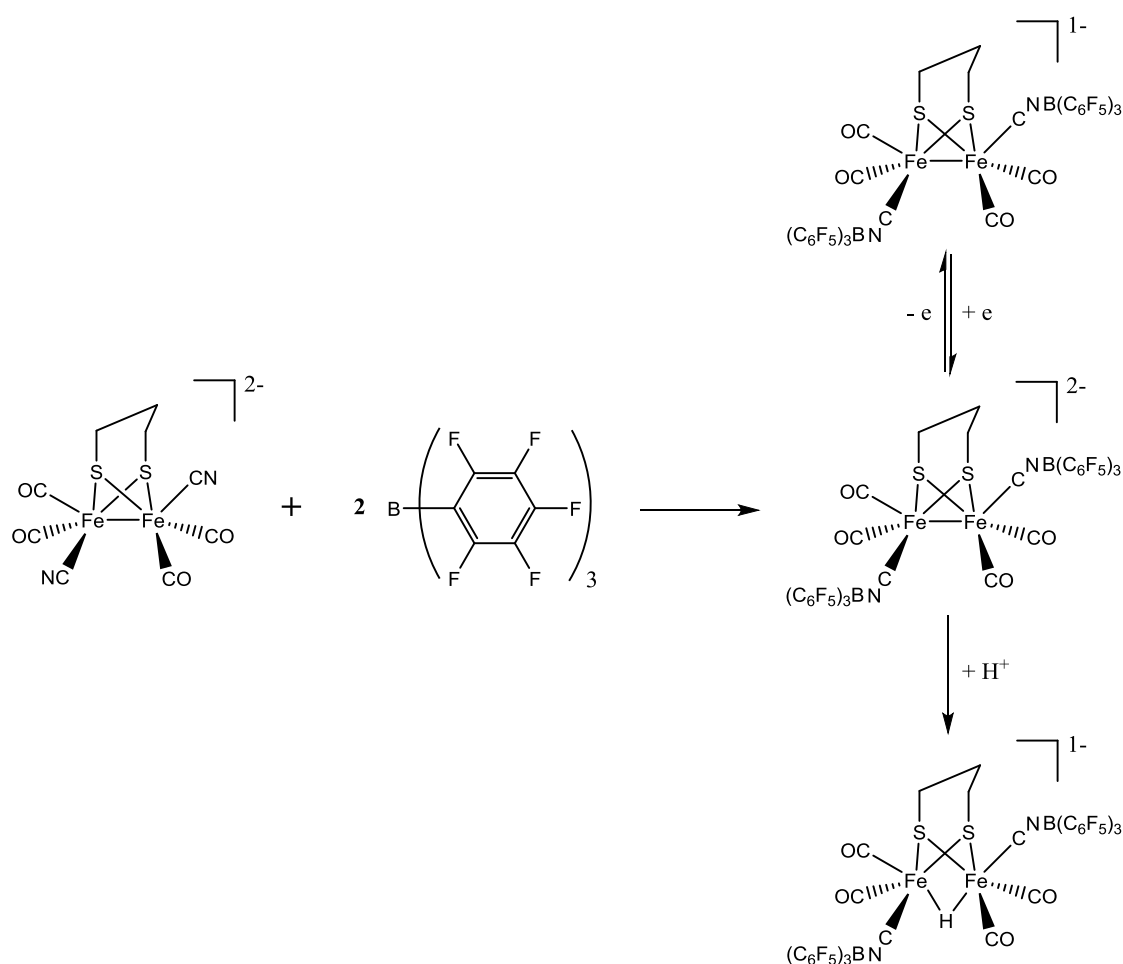
Another key area of research in regards to cyanide-containing [FeFe]-hydrogenase subsite analogues is their instability when combined with acid. As the typical use of such a hydrogenase mimic is to convert 2H^+ into H_2 , this instability presents quite a significant problem. Wright and coworkers⁸⁰ have suggested that this is caused by protonation of the cyanide ligand, forming a $-\text{CNH}^+$ species.



Scheme 3.1. Generalised protonation mechanism (L^1 and $L^2 = \text{CN}$ or PMe_3 , $n=1$ or 2). Adapted from reference⁸⁰.

With the lone pairs on the nitrogen atoms of the cyanide ligands able to readily bind protons present in solution, 'protonation on ligand' is a comparatively fast step in the proposed protonation mechanism. In order to prevent decomposition by protonation of the cyanide ligands, it would be favourable to 'tie-up' and protectively bind the cyanides prior to exposing the subsite analogue system to acid. To do this would involve striking a delicate balance; binding the cyanide so that it is suitably protected, but not so strongly so that the subsite system is drastically affected in its reactivity or chemical properties.

One attempt at such a protected system was reported by Rauchfuss and coworkers⁸¹. They attached fluorinated-aryl boranes (BAr^{F}) to the ligated cyanides via formation of Lewis adducts. The Lewis acidity of such boranes will be explained in more detail in **Chapter 6**, though it should be noted that BAr^{F} s are relatively potent Lewis acids. The fluorinated-aryl borane employed by Rauchfuss was the well-known tris(pentafluorophenyl)borane, $\text{BAr}^{\text{F}}_{15}$, and the diiron-containing adduct formed was shown to undergo a well-defined reversible one electron oxidation. In addition, protonation of the adduct species was also shown to give stable bridging hydrides, as opposed to the decomposition observed by the 'unprotected' cyanide-containing parent compound.



Scheme 3.2. Reaction of $[\text{Fe}_2(\text{pdt})(\text{CO})_4(\text{CN})_2]^{2-}$ with $\text{BAr}^{\text{F}}_{15}$ to give the 'protected' adduct $[\text{Fe}_2(\text{pdt})(\text{CO})_4(\text{CNB}(\text{C}_6\text{F}_5)_3)_2]^{2-}$. The reversible one electron oxidation and protonation chemistry of this adduct are also shown. Adapted from reference⁸¹.

As far as protecting the cyanide groups by capping them, Rauchfuss' $\text{BAr}^{\text{F}}_{15}$ experiments were a success. The parent compound, $[\text{Fe}_2(\text{pdt})(\text{CO})_4(\text{CN})_2]^{2-}$, is known to have an irreversible oxidation process⁸², and with the borane-capped version this is shown to become both stable and reversible. The protonation of the capped species, as previously stated, also gives a stable bridging hydride, being stable enough to allow structure determination by X-ray crystallography, as shown in **Figure 3.3**.

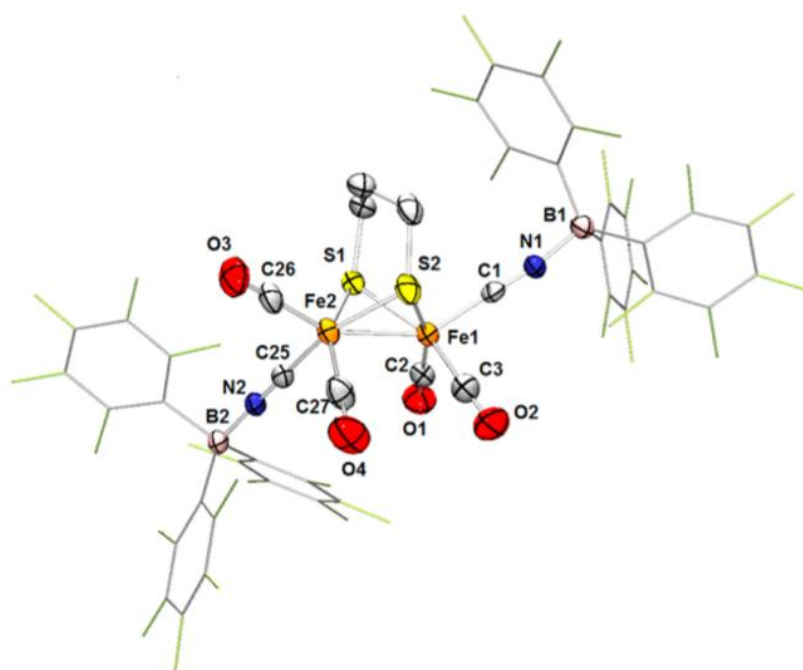
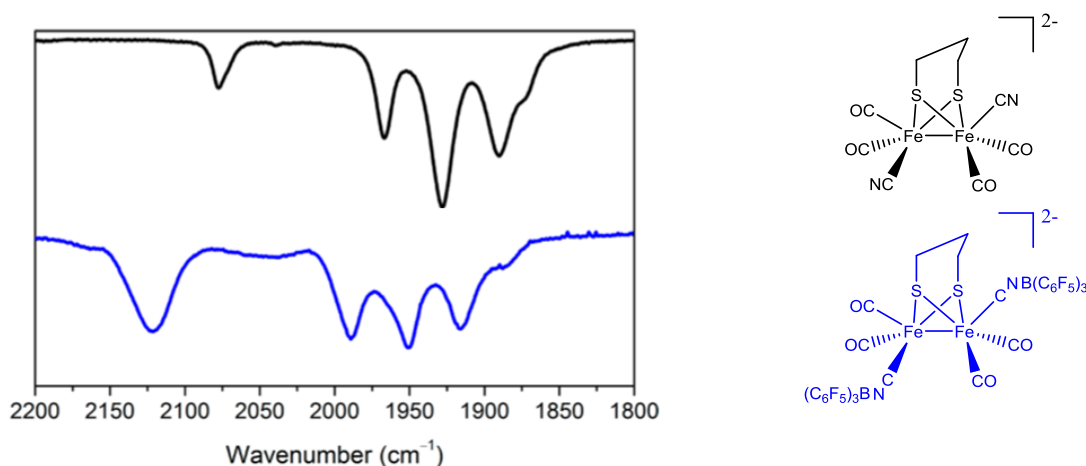


Figure 3.3. Displacement ellipsoid plot of $[\text{Fe}_2(\text{pdt})(\text{CO})_4(\text{CNB}(\text{C}_6\text{F}_5)_3)_2]^{2-}$ at 50% probability and H atoms omitted for clarity. Pentafluorophenyl groups are deemphasised for clarity. Image reproduced from reference⁸¹.

The structure of the diiron component in this adduct structure is very similar to that of the parent compound, with the CN, CO, and FeFe bond lengths being similar and the *apical-basal* geometry being retained. The FTIR spectrum, shown in **Figure 3.4.**, exhibits significant differences, however. There are substantial shifts in the CO and CN stretching frequencies, both to higher frequencies. The $\nu(\text{CO})$ stretches shift to higher values due to a reduction in the extent of back bonding into the π^* antibonding orbitals of CO, which is caused by the BAr^{F} groups withdrawing electron density from the FeFe core. The $\nu(\text{CN})$ shift to higher frequencies would also be consistent with diminished back donation into the π^* orbitals of CN.



Compound	$\nu(\text{CN}) / \text{cm}^{-1}$	$\nu(\text{CO}) / \text{cm}^{-1}$
$\text{K}_2[\text{Fe}_2(\text{pdt})(\text{CO})_4(\text{CN})_2]$	2077	1967, 1928, 1890
$\text{K}_2[\text{Fe}_2(\text{pdt})(\text{CO})_4(\text{CNB}(\text{C}_6\text{F}_5)_3)_2]$	2119	1989, 1951, 1916

Figure 3.4. Solution FTIR spectra comparing $\text{K}_2[\text{Fe}_2(\text{pdt})(\text{CO})_4(\text{CNB}(\text{C}_6\text{F}_5)_3)_2]$ with the parent compound $\text{K}_2[\text{Fe}_2(\text{pdt})(\text{CO})_4(\text{CN})_2]$. Adapted from reference⁸¹.

Although some shift in the CO and CN stretches was to be expected, as the BAr^{F} groups are attached by Lewis acid acceptance of electron density, the potency of the Lewis acid used has had a significant impact on the electron density residing at the FeFe core. The shifts of $>20 \text{ cm}^{-1}$ by the CO stretches to higher wavenumbers is substantial, and shows that the electronic properties of the FeFe centre have been altered considerably. It would therefore be more desirable to employ a less severe method of cyanide-capping; either by use of a softer Lewis acid, or another method of bonding; namely hydrogen bonding.

3.1.4 Hydrogen bonding

Hydrogen bonding is the electrostatic attraction between two polar groups when a hydrogen atom covalently bound to a highly electronegative atom, such as nitrogen or oxygen, experiences the electrostatic field of another highly electronegative atom nearby. Hydrogen bonds can occur as both intermolecular and intramolecular interactions⁸³.

Hydrogen bonding occurs due to the electronegative atom covalently attached to the hydrogen atom sharing the bonding electrons unequally; resulting in the hydrogen atom

taking on a slight positive charge. The slightly positively-charged hydrogen atom can then interact with a lone pair of electrons on a neighbouring second electronegative atom, which becomes the hydrogen bond acceptor. Mainly through electrostatic attraction, the original electronegative atom effectively shares its hydrogen with the acceptor atom, forming a bond.

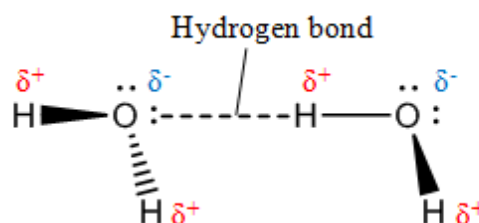


Figure 3.5. Hydrogen bonding between two water molecules.

Hydrogen bonds are weaker than ionic or covalent bonds, but are stronger than van der Waals forces. Typically hydrogen bonding strength ranges from 10-30 kJmol⁻¹, though they can be much stronger when fluorine is involved (up to 161 kJmol⁻¹), due to fluorine being very electronegative. Some example hydrogen bond strengths are given in **Figure 3.6**.

Interaction	Bond strength / kJmol ⁻¹
O-H...:N	29 kJmol ⁻¹
O-H...:O	21 kJmol ⁻¹
N-H...:N	13 kJmol ⁻¹
N-H...:O	8 kJmol ⁻¹
HO-H...:OH ₃ ⁺	18 kJmol ⁻¹
F-H...:F	161.5 kJmol ⁻¹

Figure 3.6. Example hydrogen bond strengths⁸⁴⁻⁸⁶.

Hydrogen bonds are prevalent in nature, with the hydrogen bonding lattice present in water⁸⁷ being one of the more well-known examples, along with the base-pairing present in DNA⁸⁸. Hydrogen bonding is present in many proteins, contributing to the

folding of secondary and tertiary structures, and, as explained in **Section 3.1.2.**, play several key roles in the hydrogenase enzymes.

3.1.5 Fluorinated bis-ureas to hydrogen bond cyanides

Hydrogen bonding to iron cyanides is not a new area of research, as for example White and coworkers were able to coordinate the simple $\text{K}_4[\text{Fe}(\text{CN})_6]$ to polyammonium macrocycles⁸⁹. The complex formed was sufficiently stable to be characterised by X-ray crystallography, as shown in **Figure 3.7.**, and demonstrates the capacity of cyanide ligands to engage in hydrogen bonding.

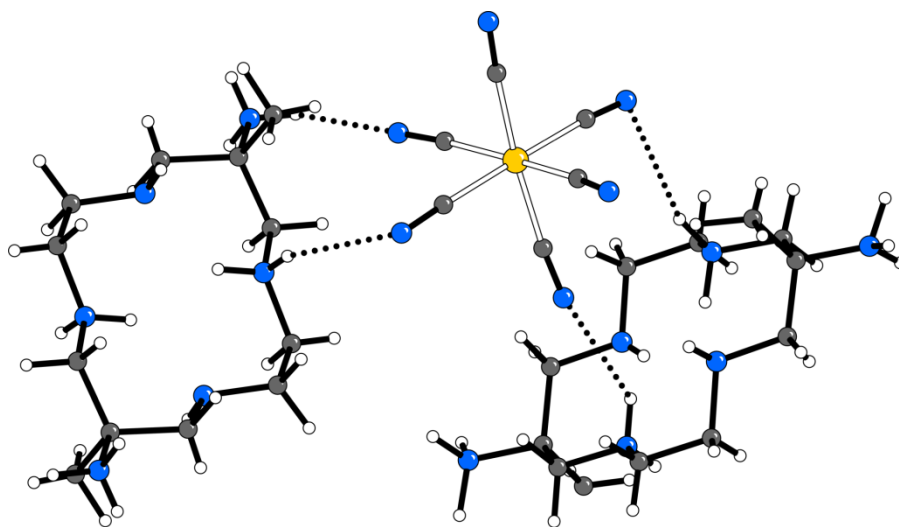


Figure 3.7. X-ray structure demonstrating hydrogen bonding interactions to cyanide ligands. Image adapted from reference⁸⁹ (white spheres H; blue spheres N; black spheres C; yellow sphere Fe).

In this work we explore the hydrogen bonding interactions between a cyanide-functionalised diiron subsite analogue with fluorinated bis-ureas. Gale and coworkers have recently developed a series of bis- and tris- ureas and thioureas to act as anion transporters across cell membranes^{90,91}.

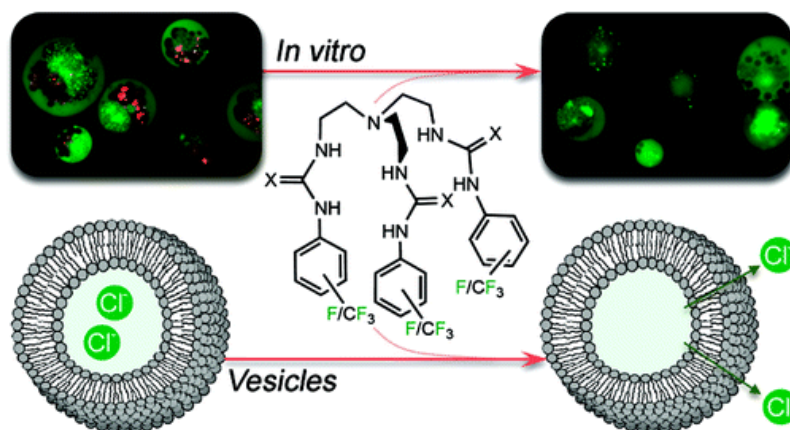


Figure 3.8. Urea and thiourea systems transporting anions across cell membranes. Image reproduced from reference⁹⁰.

The transport of ions, and in particular chloride and bicarbonate anions, is important to numerous biological processes, and is often mediated by proteins embedded within cellular lipid bilayers. Malfunction of these proteins can lead to diseases, such as cystic fibrosis⁹¹. Due to this, there is much synthetic research being conducted to produce small molecules capable of mimicking the role of such proteins. Although there are several examples of nonprotein natural products that can function as cation transporters, such as valinomycin⁹², only few examples of anion transporters can be found.

Gale and coworkers have discovered that bis- and tris- ureas and thioureas are capable of tightly binding small anions such as chloride, nitrate, and sulfate and transporting them across bi-lipid cell membranes. The systems function by facilitating the formation of multiple hydrogen bonds, which is allowed by the geometry of the bis- and tris- ureas and thioureas. An X-ray structure showing a bis-urea binding a chloride anion is given in **Figure 3.9**.

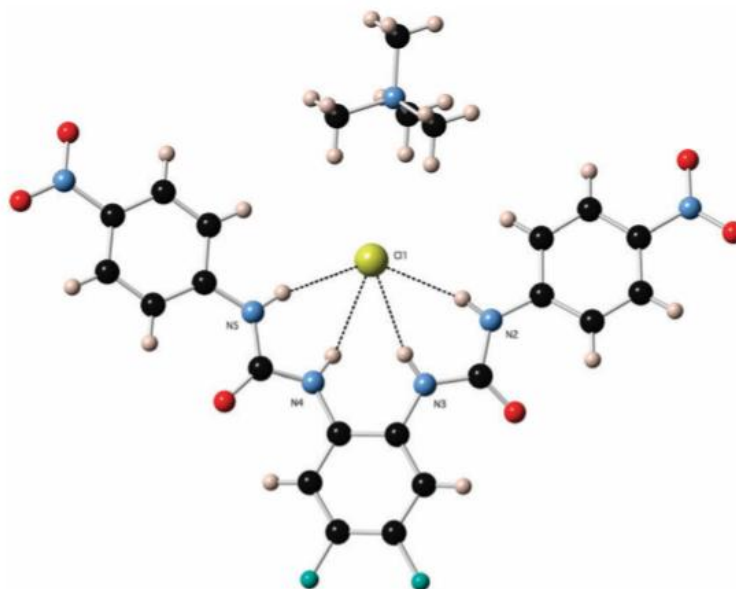


Figure 3.9. X-ray crystal structure showing binding of a chloride anion by a fluorinated bis-urea functionalised with nitro groups. Reproduced from reference⁹¹ (white spheres H; blue spheres N; black spheres C; red spheres O; light green sphere Cl; darker green spheres F).

The formation of multiple hydrogen bonds of the bis-urea in **Figure 3.9.** allows the partial encapsulation of the anion. This wrapping up would be ideal in combination with the cyanide groups ligated to [FeFe]-hydrogenase subsite analogues, as the cyanide behaving as a 'pseudo-halide' could be capped in protection against the problems associated with exposed cyanides outlined in **Section 3.1.3.**

Gale's bis-ureas are synthesised from a one step reaction involving the combination of an *ortho*-phenylenediamine with the appropriate phenyl isocyanate. The chemical properties and anion-binding potential of the bis-ureas are tuneable by functionalisation by different groups, and the fluorinated bis-ureas employed in this work are shown in **Figure 3.10.**

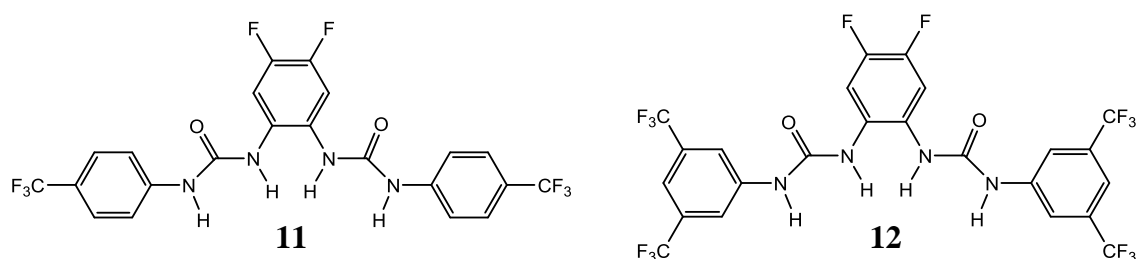


Figure 3.10. Fluorinated bis-ureas employed in this work.

Due to being highly electronegative, the fluorine atoms on these bis-ureas should draw electron density away from the urea hydrogens by inductive effects, making the protons more amenable to hydrogen bonding. Urea **12** was chosen in addition to **11** to examine the effect of additional trifluoromethyl groups on the binding strength to the cyanide group. In regard to the use of multiple fluorine atoms, and in the inherent risk of withdrawing considerable amounts of electron density away from the FeFe core, as was in the case of Rauchfuss' BAr^F experiments outlined in **Section 3.1.3.**, it was deemed appropriate to ensure that the bis-urea was sufficiently electron-withdrawing to ensure binding to the cyanide ligand, with tuneability of properties to be considered later, if necessary.

3.2 Results and discussion

3.2.1 Synthesis of diiron subsite analogues

It is well-established that the bridgehead of the naturally-occurring [FeFe]-hydrogenase is an azadithiolate (adt) derivative⁷⁸, and that the secondary amine involved participates in the catalytic cycle. However, in this work the propanedithiolate (pdt) derivatives were employed. The reasons for this are twofold. Firstly, the pdt derivatives have been extensively studied⁷⁷ and are straightforward to synthesise and handle using standard Schlenk techniques. The adt derivatives, on the other hand, are more difficult to synthesise and handle, and have the additional property that the bridging amine is capable of hydrogen bonding, as shown in **Figure 3.1**. As the focus of this work is to monitor hydrogen bonding interactions between fluorinated bis-ureas and the cyanide groups on the subsite derivatives, the presence of a further hydrogen bonding site would present additional complications.

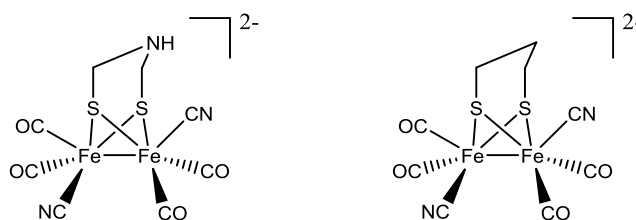
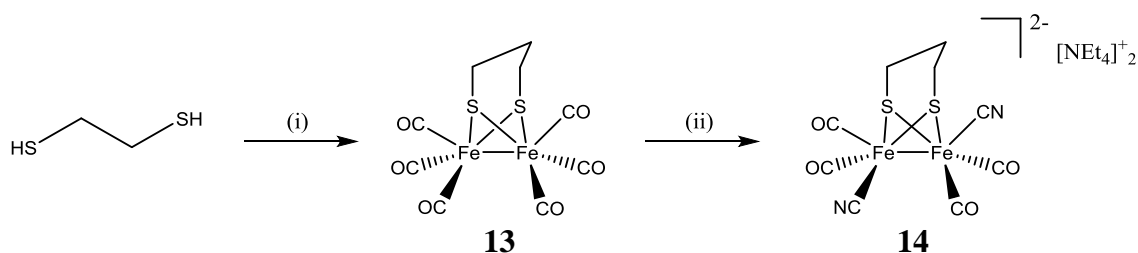


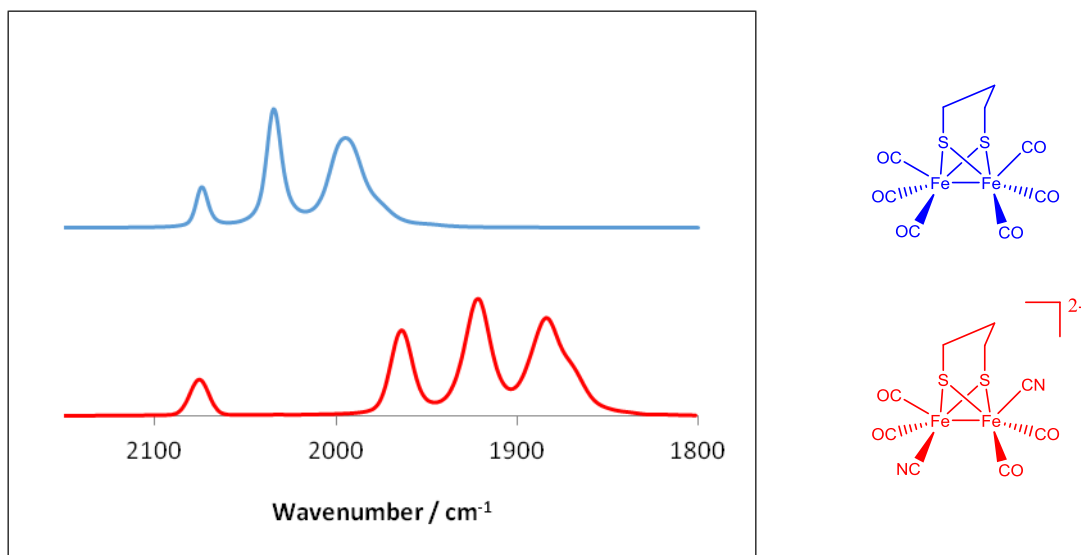
Figure 3.11. Structures of [FeFe]-hydrogenase subsite mimics $[\text{Fe}_2(\text{adt})(\text{CO})_4(\text{CN})_2]^{2-}$ (left) and $[\text{Fe}_2(\text{pdt})(\text{CO})_4(\text{CN})_2]^{2-}$ (right)

The standard method of preparation of the dicyanide diiron units is firstly the preparation of the hexacarbonyl derivative, followed by ligand substitution by the nucleophile CN^- . The hexacarbonyl starting material employed in this work, $[\text{Fe}_2(\text{pdt})(\text{CO})_6]$ **13**, was synthesised from reaction of 1,3-propanedithiol with triiron dodecacarbonyl, and was then combined with tetraethylammonium cyanide to give the dicyanide derivative, $(\text{Et}_4\text{N})_2[\text{Fe}_2(\text{pdt})(\text{CO})_4(\text{CN})_2]$ **14**, shown in **Scheme 3.3**.



Scheme 3.3. Synthesis of $(\text{Et}_4\text{N})_2[\text{Fe}_2(\text{pdt})(\text{CO})_4(\text{CN})_2]$ **14**. (i) 1.2 $\text{Fe}_3(\text{CO})_{12}$, THF, 70 °C, 3 h, 79%; (ii) 2.1 $[\text{Et}_4\text{N}][\text{CN}]$, MeCN, RT, 16 h, 95%. Procedures modified from those outlined by Rauchfuss and coworkers⁸².

The dicyanide complex **14** is water soluble and air-sensitive red crystalline solid, and was reported independently by three groups in 1999⁹³⁻⁹⁵. From the solution FTIR spectra of the dicyanide complex compared to the hexacarbonyl starting material it is clear to see the effects of the coordination of the cyanide groups on the electron density of the FeFe core, as shown in **Figure 3.12**.



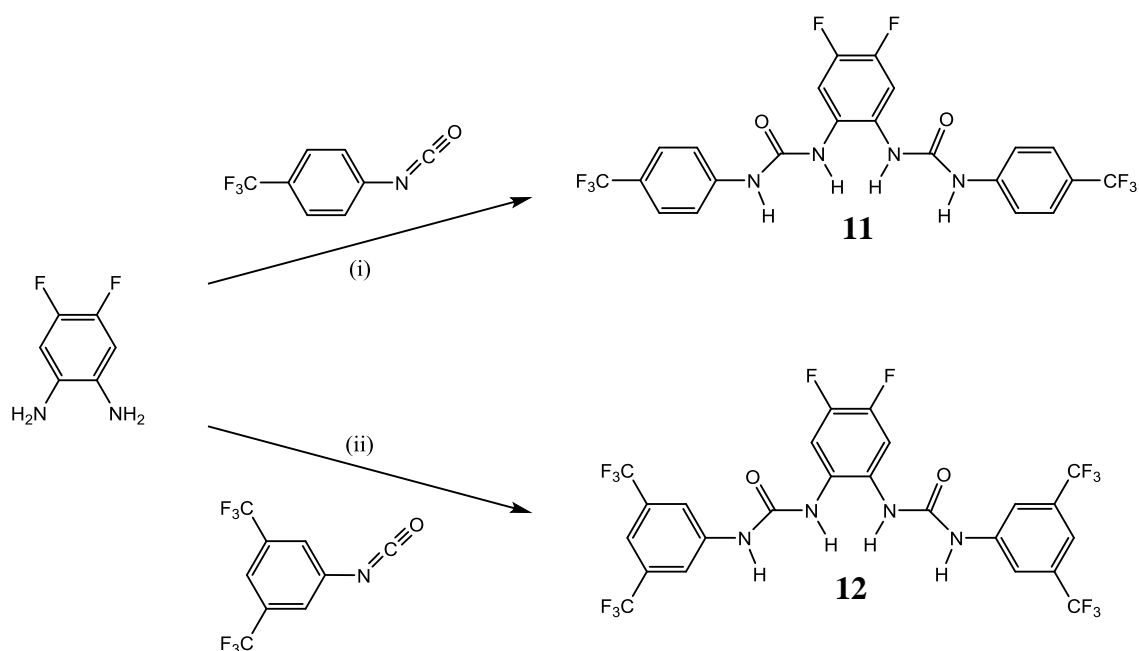
Compound	$\nu(\text{CN}) / \text{cm}^{-1}$	$\nu(\text{CO}) / \text{cm}^{-1}$
$[\text{Fe}_2(\text{pdt})(\text{CO})_6]$		2074, 2035, 1995
$(\text{NEt}_4)_2[\text{Fe}_2(\text{pdt})(\text{CO})_4(\text{CN})_2]$	2075	1963, 1921, 1884, 1870

Figure 3.12. Solution FTIR spectra in MeCN comparing $(\text{NEt}_4)_2[\text{Fe}_2(\text{pdt})(\text{CO})_4(\text{CN})_2]$ with the parent compound $[\text{Fe}_2(\text{pdt})(\text{CO})_6]$.

From the IR spectra it is clear that the carbonyl stretches are shifted to much lower wavenumbers on coordination of the cyanide ligands ($>100 \text{ cm}^{-1}$). This is due to the cyanide ligation greatly increasing the electron density on the FeFe core, which in turn increases the back bonding into the π^* antibonding orbitals of CO. This has the effect of decreasing the $\text{C}\equiv\text{O}$ bond order, shifting the CO stretches to lower stretching frequencies.

3.2.2 Synthesis of fluorinated bis-ureas

The fluorinated bis-ureas **11** and **12** were synthesised by reaction of 4,5-difluoro-*ortho*-phenylenediamine with the appropriate fluorinated phenyl isocyanate, in a one pot reaction using DCM as a solvent with pyridine acting as a base (**Scheme 3.4**).



Scheme 3.4. Synthesis of fluorinated bis-ureas **11** and **12**. (i) DCM, 5% pyridine, 53%; (ii) DCM, 5% pyridine, 59%. Procedures modified from those outlined by Gale *et al.*⁹¹.

Dichloromethane was the solvent used in the bis-urea synthesis with the poor solubility of urea species helping drive the reaction towards completion⁹⁶. The crude bis-ureas were then purified by passing through an SCX-2 column to remove starting material amine and pyridine, before recrystallising from ethyl acetate to give white powders.

3.2.3 The binding of fluorinated bis-ureas to $[\text{Fe}_2(\text{pdt})(\text{CO})_4(\text{CN})_2]^{2-}$

3.2.3.1 FTIR spectroscopy

Fluorinated bis-urea **11** was combined with $(\text{NEt}_4)_2[\text{Fe}_2(\text{pdt})(\text{CO})_4(\text{CN})_2]$ **14** in MeCN, and examined by FTIR spectroscopy. **Figure 3.13.** shows the evolution of the IR spectrum upon successive addition of aliquots.

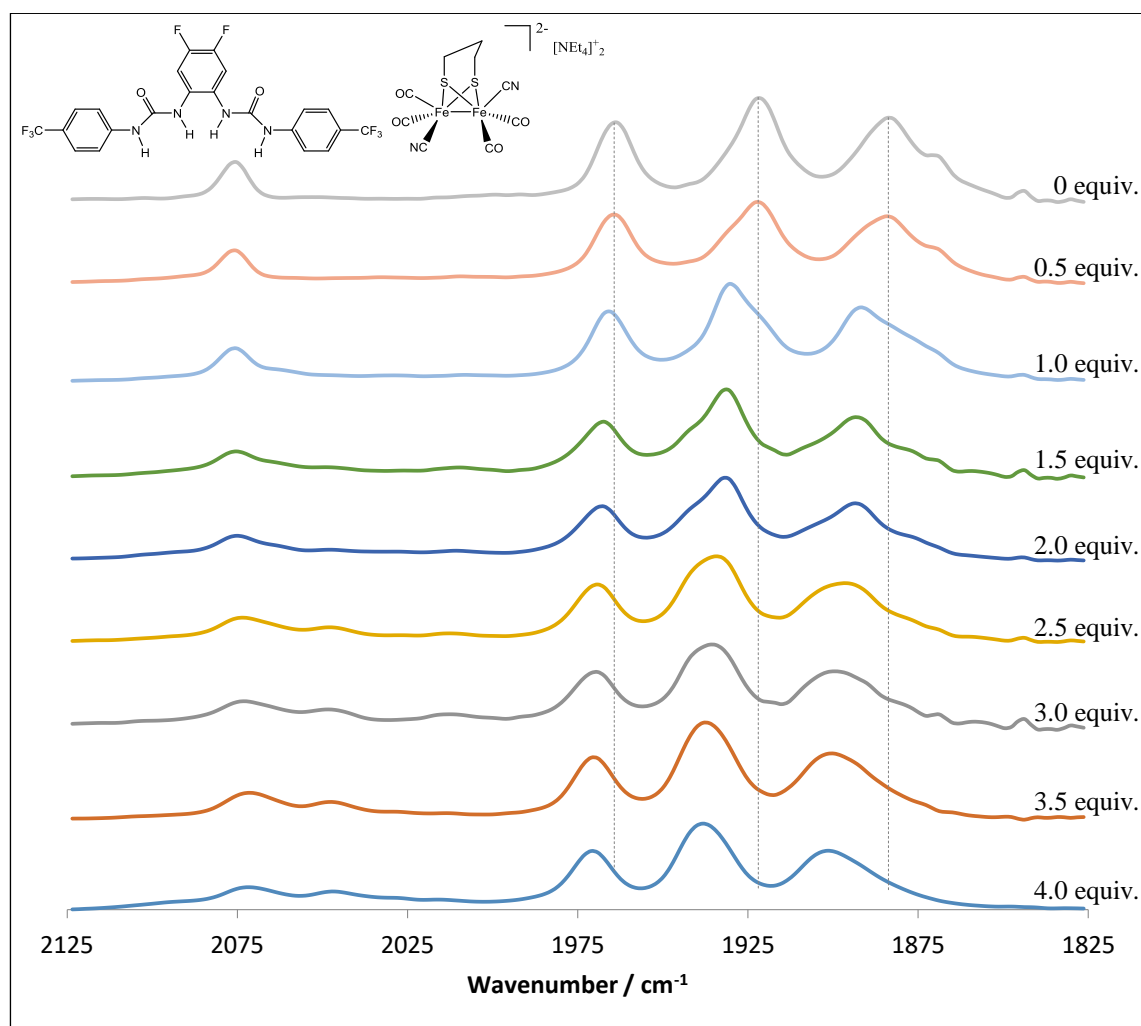


Figure 3.13. Solution FTIR spectra in MeCN showing the effect of 0.5 to 4.0 equivalents of fluorinated bis-urea **11** on the CO and CN stretches of the dicyanide compound **14**. The concentration of the diiron species was consistent across all measurements (1.0 mM).

After the addition of 1 equivalent a spectrum corresponding to the evolution of a single new species evolves. Upon further addition this species is consumed, and is replaced by a clean spectrum after addition of 4 equivalents; indicative of the formation of a successor species. The final spectrum shows two distinct cyanide bands.

Comparing the initial spectrum of the unreacted dicyanide species **14** with that obtained from the addition of 4 equivalents of the fluorinated bis-urea **11**, there is a substantial shift in the three major CO absorption bands (**Figure 3.14**). After the addition of a single equivalent the shifts in these bands are intermediate between that of the starting material and the final product.

Urea equiv.	$\nu(\text{CN}) / \text{cm}^{-1}$	$\nu(\text{CO}) / \text{cm}^{-1}$
0	2075	1963, 1921, 1884
0.5	2075	1963, 1923, 1884
1.0	2075	1965, 1931, 1892
1.5	2075	1967, 1931, 1894
2.0	2075, 2048	1967, 1933, 1894
2.5	2073, 2048	1969, 1934, 1896
3.0	2073, 2048	1971, 1938, 1900
3.5	2071, 2048	1971, 1938, 1900
4.0	2071, 2046	1971, 1938, 1900

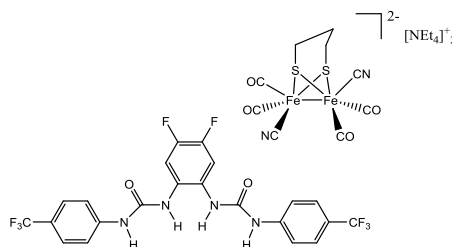


Figure 3.14. CO and CN stretch maxima of dicyanide compound **14** when subjected to increasing aliquots of fluorinated bis-urea **11**.

Whereas the magnitude of the shifts in IR frequency are considerable, they are less than those observed when using the powerful Lewis acid BAr^{F} groups to bond to cyanide as reported by Rauh fuss⁸¹, as shown in **Figure 3.15**.

Compound	$\nu(\text{CN}) / \text{cm}^{-1}$	$\nu(\text{CO}) / \text{cm}^{-1}$
$[\text{Fe}_2(\text{pdt})(\text{CO})_4(\text{CN})_2]^{2-}$	2077	1967, 1928, 1890
$[\text{Fe}_2(\text{pdt})(\text{CO})_4(\text{CNB}(\text{C}_6\text{F}_5)_3)_2]^{2-}$	2119	1989, 1951, 1916
$[\text{Fe}_2(\text{pdt})(\text{CO})_4(\text{CN})_2 \cdot (\text{urea } \mathbf{11})_2]^{2-}$	2071, 2046	1971, 1938, 1900

Figure 3.15. Solution FTIR spectra comparing the shifts of CO and CN stretch maxima of the dicyanide when subjected to fluorinated bis-urea **11** and Lewis acid $\text{BAr}^{\text{F}}_{15}$ groups⁸¹.

Similar results were observed with the fluorinated bis-urea **12** which has stronger Lewis acid properties. In this case the final spectrum was essentially fully developed after the addition of 2 equivalents of the bis-urea. The magnitude of the carbonyl shifts for bis-urea **12** were marginally larger than that of bis-urea **11**. Again two cyanide bands were observed. **Figures 3.16** clearly shows progression of the spectrum for the addition of bis-urea **12**.

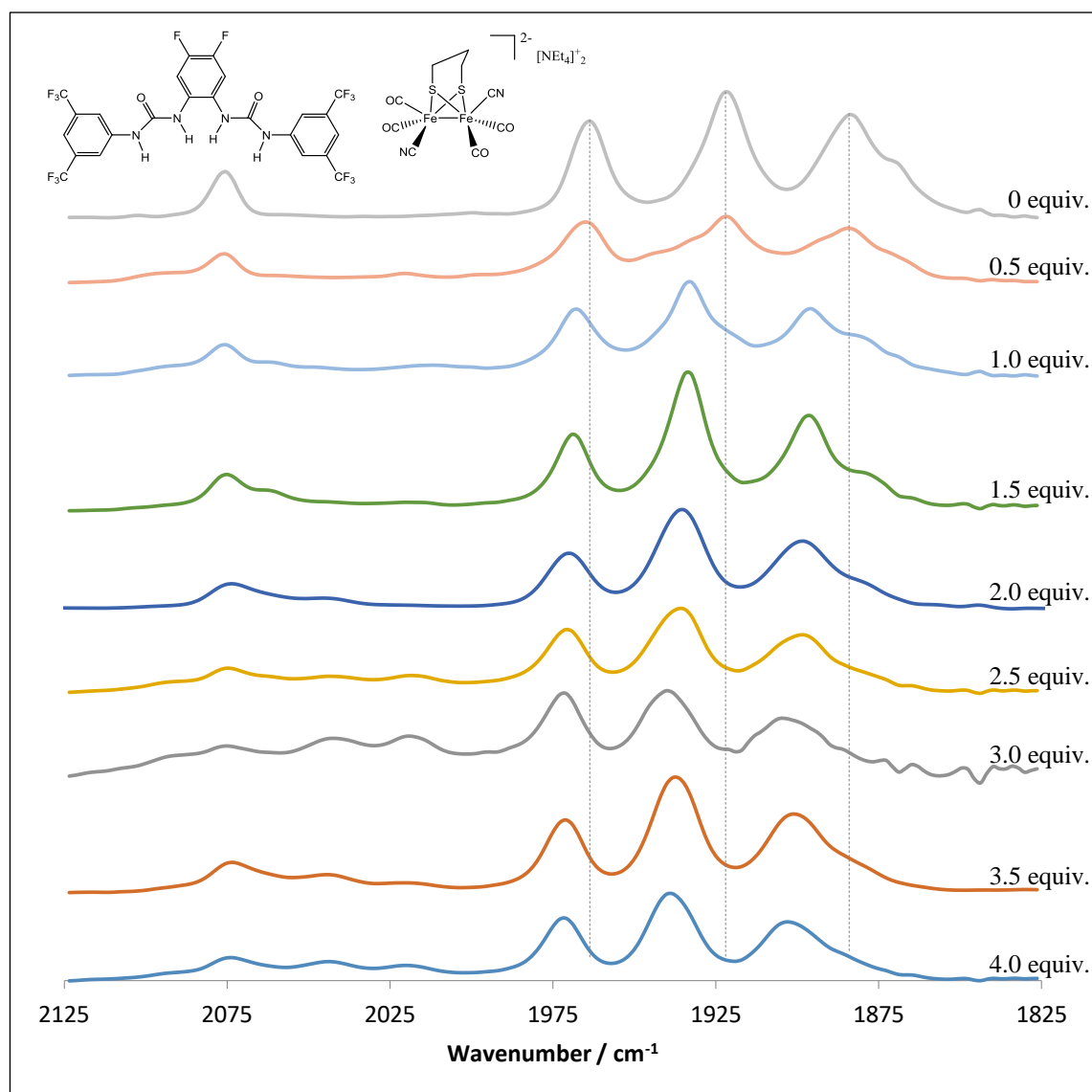


Figure 3.16. Solution FTIR spectra in MeCN showing the effect of 0.5 to 4.0 equivalents of fluorinated bis-urea **12** on the CO and CN stretches of the dicyanide compound **14**. The concentration of the diiron species was consistent across all measurements (1.0 mM). The band appearing at $\sim 2020 \text{ cm}^{-1}$ arises from decomposition.

Urea equiv.	$\nu(\text{CN}) / \text{cm}^{-1}$	$\nu(\text{CO}) / \text{cm}^{-1}$
0	2075	1963, 1921, 1884
0.5	2075	1965, 1921, 1884
1.0	2075	1967, 1932, 1896
1.5	2075	1969, 1934, 1896
2.0	2075, 2042	1969, 1934, 1898
2.5	2073, 2042	1971, 1936, 1898
3.0	2073, 2042	1971, 1937, 1900
3.5	2071, 2044	1971, 1938, 1902
4.0	2071, 2044	1971, 1938, 1904

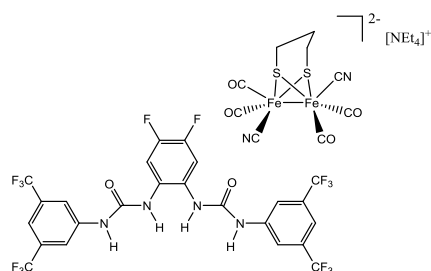


Figure 3.17. CO and CN stretch maxima of dicyanide compound **14** when subjected to increasing aliquots of fluorinated bis-urea **12**.

In summary, in MeCN both fluorinated bis-ureas interact strongly with the dicyanide species **14**. 1:1 adducts are essentially formed at a 1:1 stoichiometry of complex and bis-urea. Bis adducts are readily formed upon further addition of bis-urea; that only 2 equivalents of bis-urea **12** are required for formation of the bis adduct is indicative of successive tight equilibrium binding.

The observations of Rauchfuss of Lewis acid binding to cyanide⁸¹ clearly suggests that hydrogen-bonding to the basic nitrogen atom of the ligated cyanide is what is being observed. Importantly, this has been corroborated with additional studies in our laboratory⁹⁷ which have shown that the complex $[\text{Fe}_2(\text{pdt})(\text{CO})_6]$ and its electron-rich phosphine counterpart $[\text{Fe}_2(\text{pdt})(\text{CO})_4(\text{PMe}_3)_2]$ do not interact with the fluorinated bis-ureas.

To further probe the interactions of the fluorinated bis-ureas with the dicyanide complex NMR, mass spectrometry and DFT studies were undertaken.

3.2.3.2 NMR spectroscopy

In addition to the FTIR experiments, it was hoped that NMR spectroscopy could provide additional evidence towards the successful binding of the fluorinated bis-ureas **11** and **12** to the dicyanide diiron subsite analogue $(\text{NEt}_4)_2[\text{Fe}_2(\text{pdt})(\text{CO})_4(\text{CN})_2]$ **14**.

One equivalent of bis-urea **11** was combined with $(\text{NEt}_4)_2[\text{Fe}_2(\text{pdt})(\text{CO})_4(\text{CN})_2]$ **14** in MeCN, and stirred for 30 min before removal of the solvent *in vacuo*, and then sampling for NMR in $\text{DMSO-}d_6$. One equivalent of bis-urea was chosen due to the findings of the FTIR experiments outlined in **Section 3.2.3.1** where it was suggested that the first bis-urea binds to the cyanide groups strongly, and should therefore provide a 'cleaner' spectrum with less of a mixture of products.

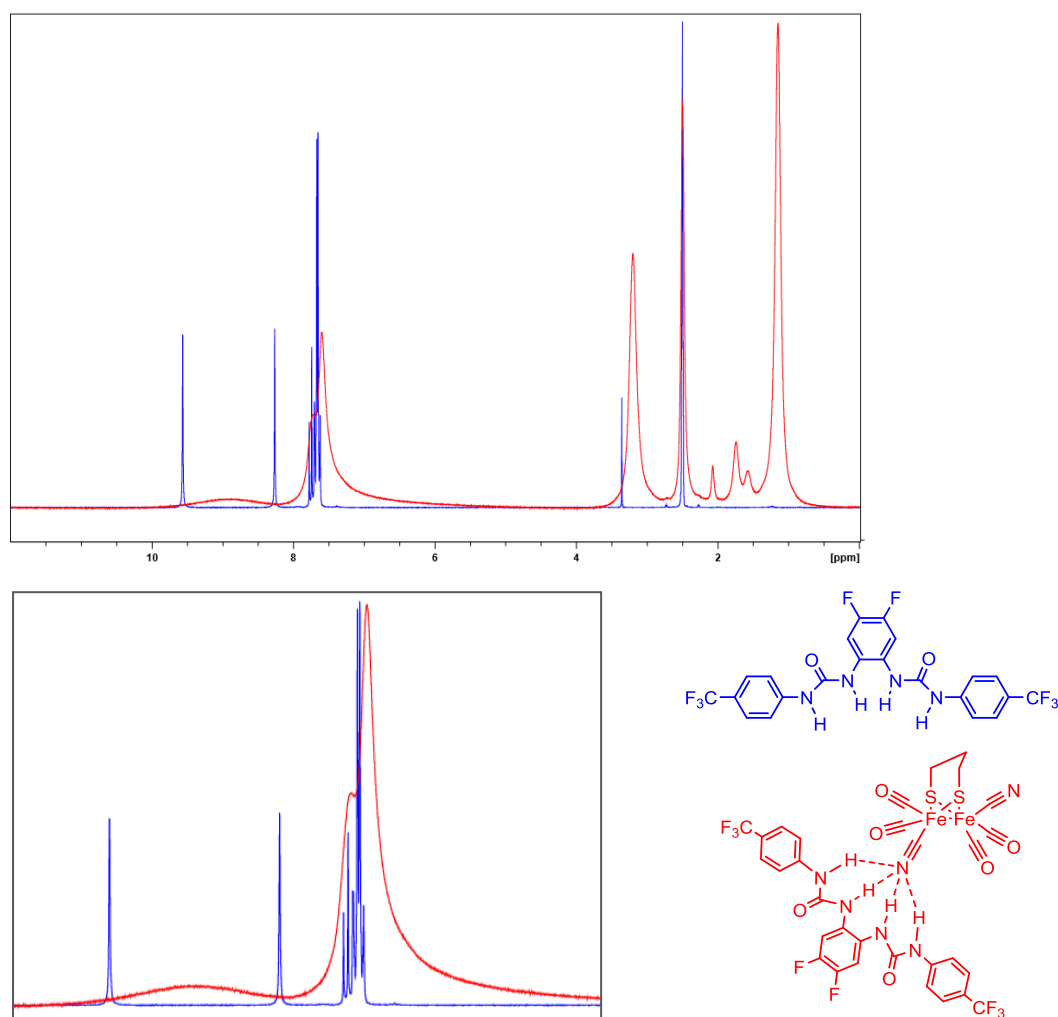


Figure 3.18. ^1H -NMR of bis-urea **11** compared to its hydrogen bonded product with $(\text{NEt}_4)_2[\text{Fe}_2(\text{pdt})(\text{CO})_4(\text{CN})_2]$ **14** in $\text{DMSO-}d_6$.

The ^1H -NMR of the starting material, bis-urea **11** is consistent with the reported data⁹¹; ^1H -NMR (DMSO- d_6 , 300.13 MHz): δ (ppm) = 9.54 (s, 2H), 8.26 (s, 2H), 7.72 (m, 2H), 7.69 (m, 4H), 7.64 (m, 4H). The coordination to the diiron complex **14** brought about the appearance of the pdt protons on the bridgehead as a broad multiplet at 1.81 ppm, along with a severe broadening of the aromatic and amine protons of bis-urea **11** to give one large multiplet at 7.93 ppm. This severe broadening would be consistent with coordination of the bis-urea to a transition metal complex, as the protons are now in the environment of a large metal centre.

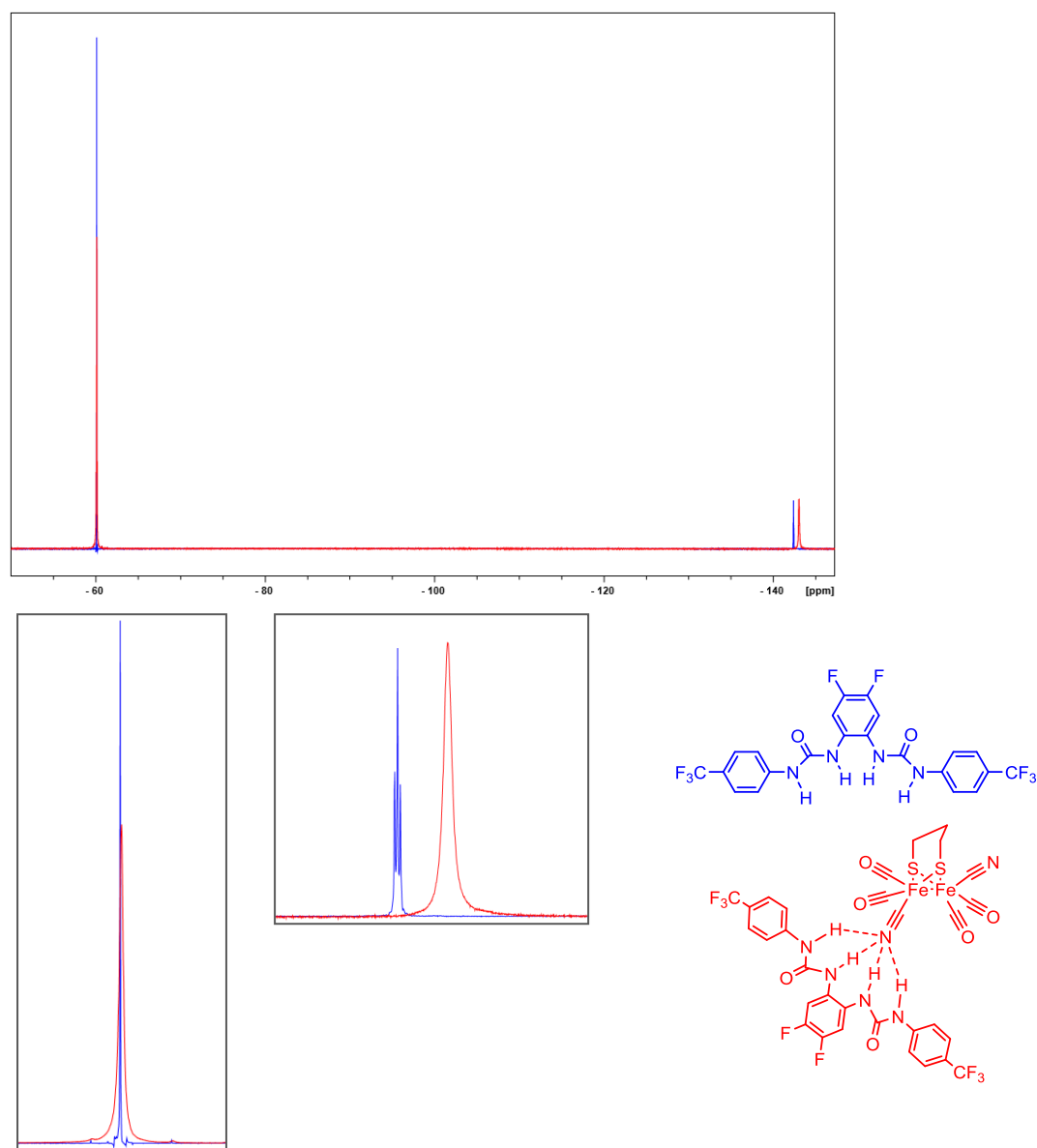


Figure 3.19. ^{19}F -NMR of bis-urea **11** compared to its hydrogen bonded product with $(\text{NEt}_4)_2[\text{Fe}_2(\text{pdt})(\text{CO})_4(\text{CN})_2]$ **14** in DMSO- d_6 .

The ^{19}F -NMR of the starting material, bis-urea **11** is consistent with the reported data⁹¹; ^{19}F -NMR ($\text{DMSO-}d_6$, 282.37 MHz): δ (ppm) = -60.18 (s, 6F), -142.44 (m, 2F). The coordination to the diiron complex **14** once again brought about signal broadening, with both fluorine signals becoming significantly broader. The six fluorine atoms on the trifluoromethyl groups underwent a tiny shift to -60.12 ppm, whereas the two fluorine atoms present on the 4,5-difluoro-ortho-phenylenediamine ring were shifted by a slightly larger amount to -143.05 ppm. This is interesting, as it suggests that the fluorine atoms present on the phenylenediamine ring are more greatly affected by the hydrogen bonding to the cyanide than the fluorine atoms present in the trifluoromethyl groups. This is consistent with the X-ray structure of bis-urea binding shown in **Figure 3.9.**, as the nitro *para*-phenyl groups in that example are shown to be pointing away from the coordinated chloride ion. In this case it is then not unreasonable to assume that the trifluoromethyl groups present on bis-urea **11** would adopt a similar position upon coordination to CN, so that the fluorines present on the phenylenediamine ring are more greatly affected by the coordination than the outward-facing trifluoromethyl groups. A structure showing this postulated binding geometry is shown in **Figure 3.20.**

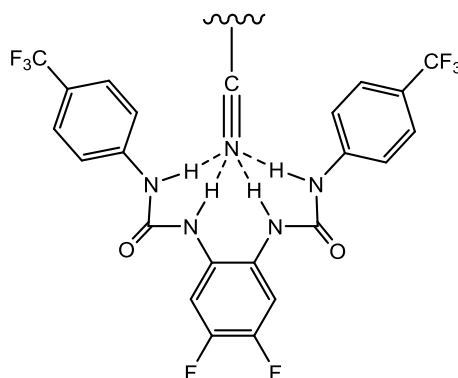


Figure 3.20. Suggested binding geometry of bis-urea **11** to a cyanide ligand, showing that the fluorines present on the phenylenediamine ring are more greatly affected by the coordination than the outward-facing trifluoromethyl groups.

That such binding effects can be inferred from the NMR data further suggests that successful hydrogen bonding between the fluorinated bis-urea **11** and the cyanide-containing diiron species has taken place. Bis-urea **12** was subjected to the same NMR experiments as bis-urea **11**.

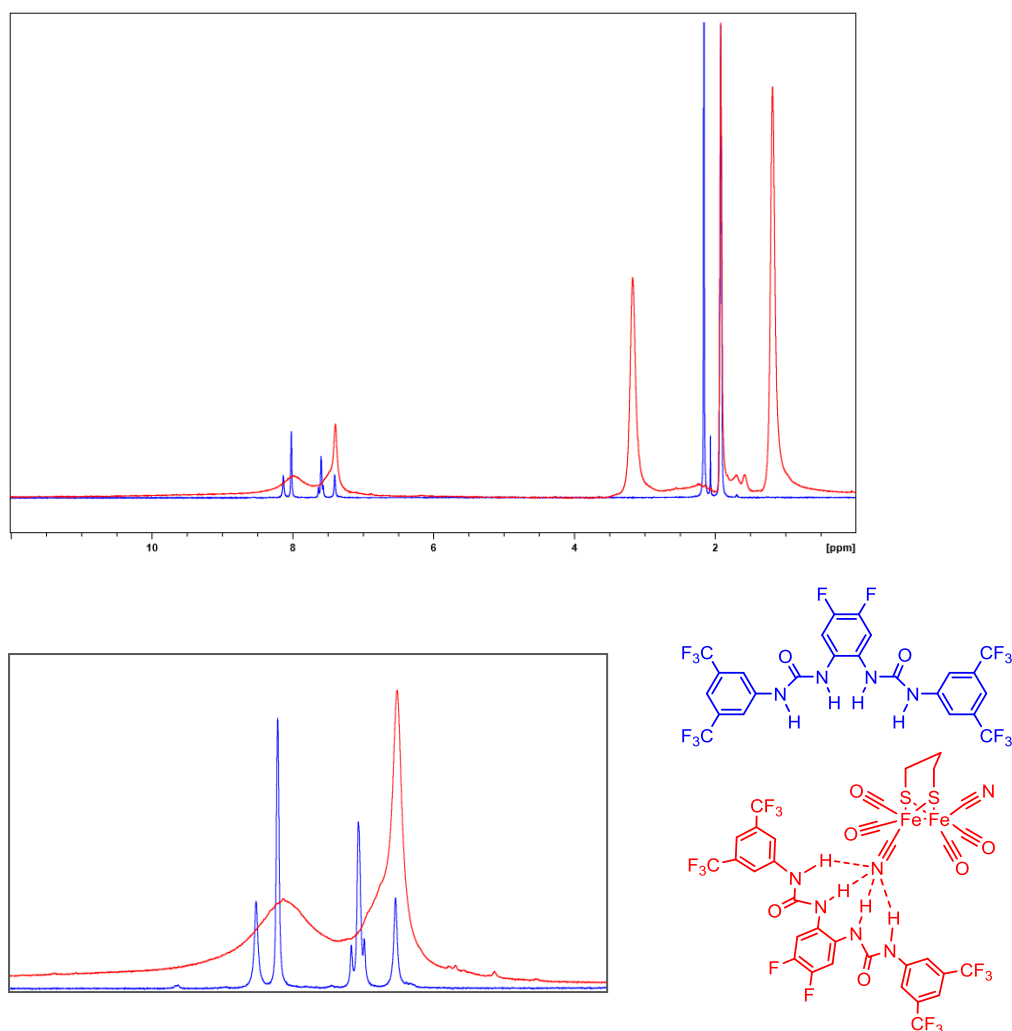


Figure 3.21. ¹H-NMR of bis-urea **12** compared to its hydrogen bonded product with (NEt₄)₂[Fe₂(pdt)(CO)₄(CN)₂] **14** in DMSO-*d*₆.

The ¹H-NMR of the starting material, bis-urea **12** is consistent with the reported data⁹¹; ¹H-NMR (DMSO-*d*₆, 300.13 MHz): δ (ppm) = 8.38 (s, 2H), 8.11 (s, 3H), 7.73 (m, 5H), 7.62 (s, 2H). As was in the case of bis-urea **11**, the coordination of the diiron complex **14** to bis-urea **12** brought about the appearance of the pdt protons on the bridgehead as a broad multiplet at 1.81 ppm, broadening of the aromatic and amine protons of bis-urea **12** to give one large multiplet at 7.76 ppm.

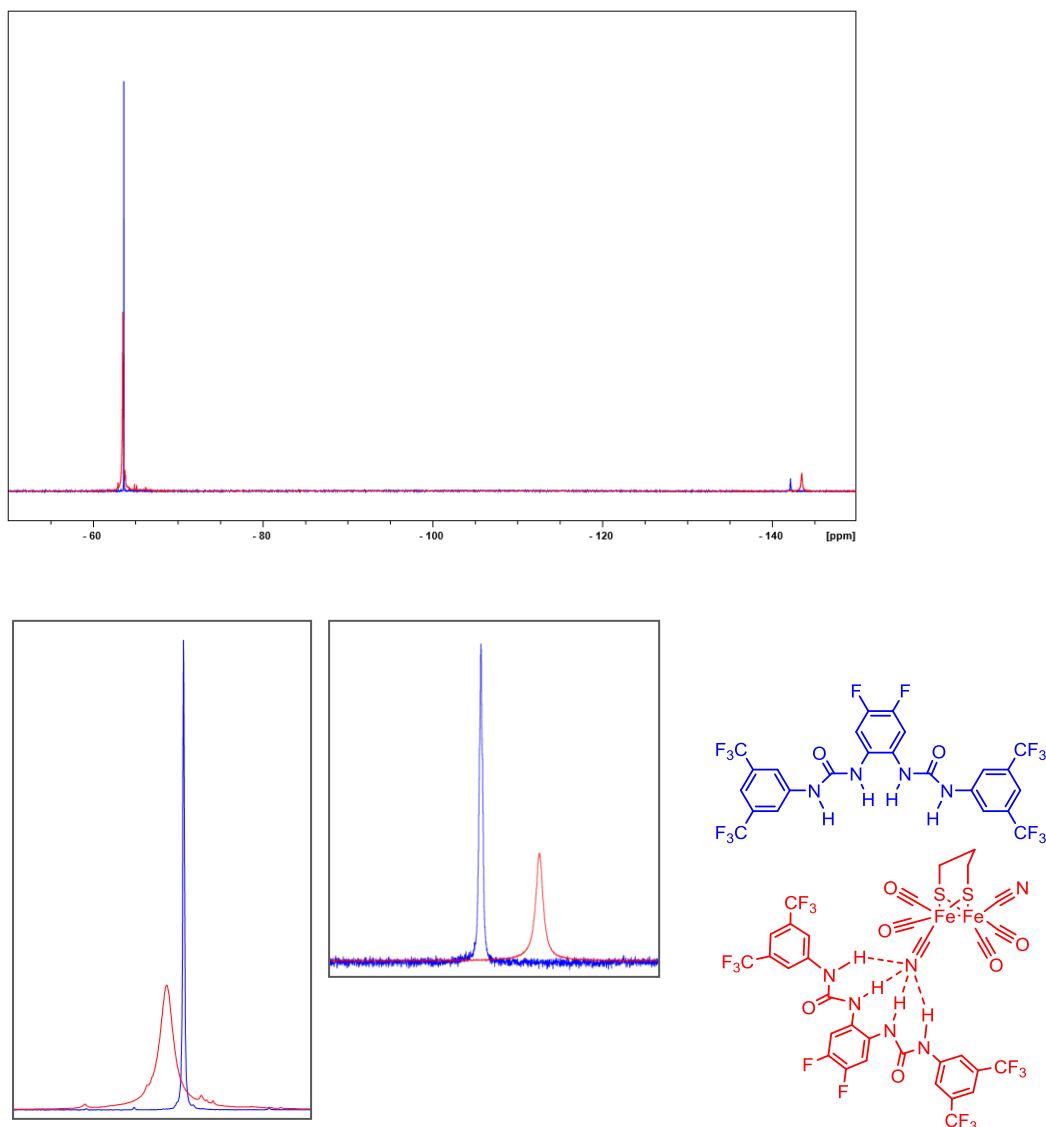


Figure 3.22. ^{19}F -NMR of bis-urea **12** compared to its hydrogen bonded product with $(\text{NEt}_4)_2[\text{Fe}_2(\text{pdt})(\text{CO})_4(\text{CN})_2]$ **14** in $\text{DMSO}-d_6$.

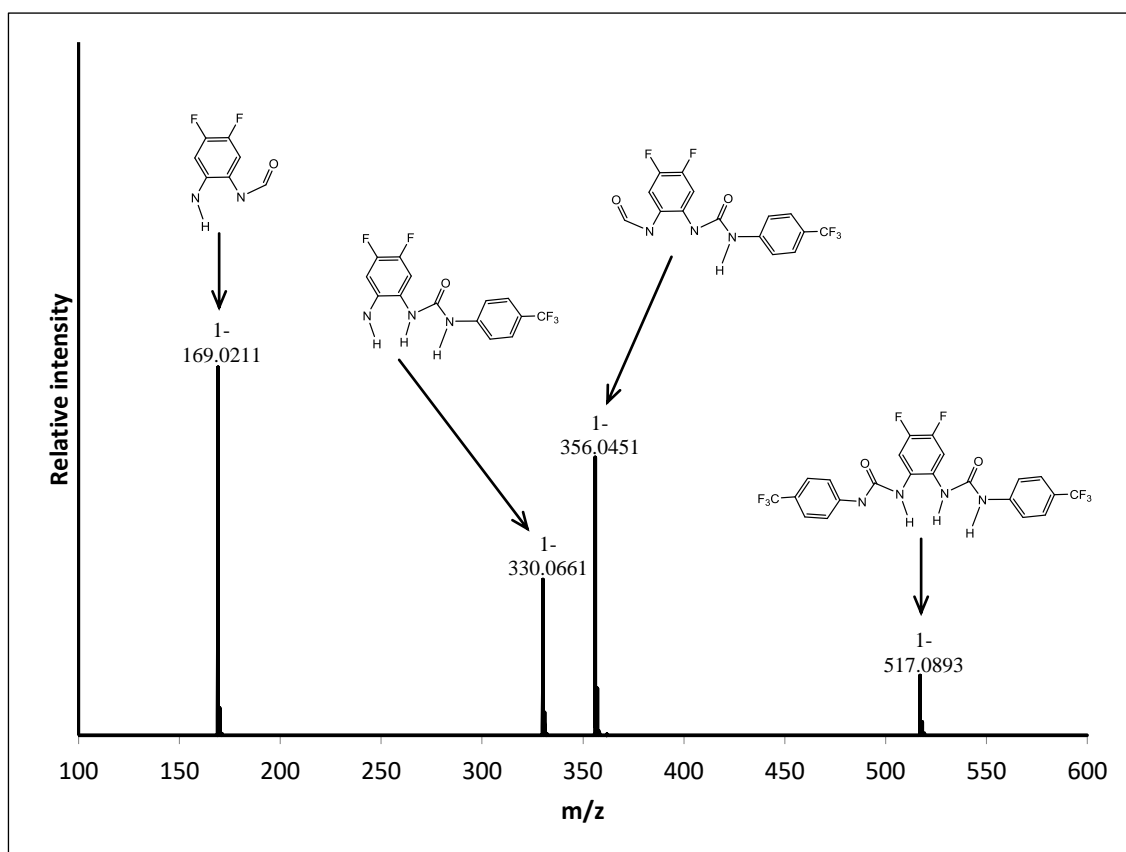
The ^{19}F -NMR of the starting material, bis-urea **12** is consistent with the reported data⁹¹; ^{19}F -NMR ($\text{DMSO}-d_6$, 282.37 MHz): δ (ppm) = -61.83 (s, 12F), -141.83 (s, 2F). The coordination to the diiron complex **14** once again brought about signal broadening, with both fluorine signals becoming significantly more broad. The twelve fluorine atoms on the trifluoromethyl groups underwent a small shift to -63.48 ppm, and the two fluorine atoms present on 4,5-difluoro-ortho-phenylenediamine ring were shifted to -144.29 ppm. Once again the shift of the fluorines present on the phenylenediamine ring suggested that they were being affected to a greater extent than the trifluoromethyl

group fluorines by coordination to CN, which is consistent with the effects seen with bis-urea **11**. However, the shifts for both fluorine signals for bis-urea **12** are larger than those observed for bis-urea **11**. This suggests that the fluorine atoms in bis-urea **12** are more affected by coordination to CN than the fluorine atoms in bis-urea **11**. This is a consistent result as this would be in agreement with the results observed by the FTIR experiments that bis-urea **12**, with its additional trifluoromethyl groups, binds to the cyanide ligands stronger than bis-urea **11**.

3.2.3.3 Mass spectrometry

Electron spray ionisation mass spectrometry (ESI-MS) was employed to demonstrate that the fluoroinated bis-ureas **11** and **12** were securely bound via hydrogen bonding to the ligated cyanides of $(\text{NEt}_4)_2[\text{Fe}_2(\text{pdtCO})_4(\text{CN})_2]$ **14**. For all of these experiments, a Bruker MicroTOF Q-III was employed, with the mass spectra recorded in the negative mode. Anaerobic and anhydrous MeCN was used as solvent, with the samples being injected using gas tight syringes, and of consistent 0.1 mM concentration.

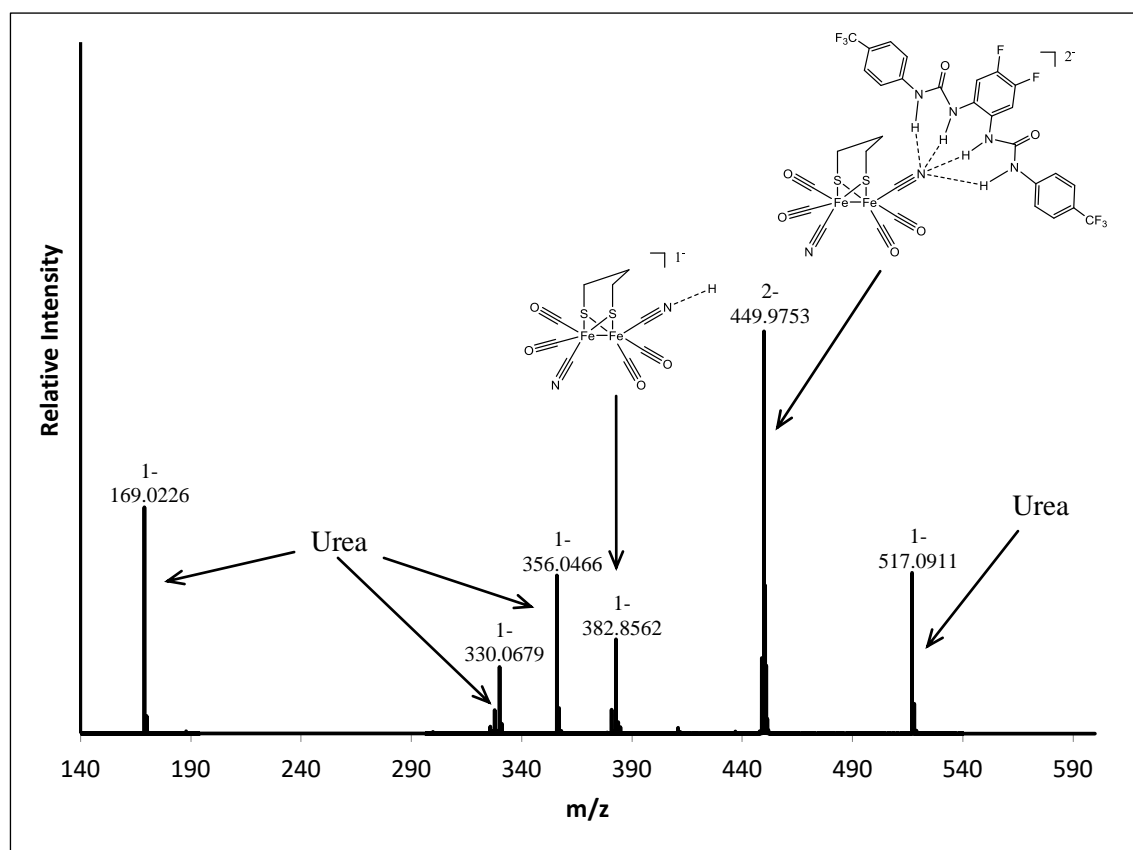
In order to accurately interpret the mass spectra obtained of the hydrogen-bonded complexes, it was a priority to first analyse the mass spectra of the bis-urea starting material. To this end, the ESI-MS spectrum of fluorinated bis-urea **11** is given in **Figure 3.23**.



m/z observed	Charge	Proposed fragment	Chemical Formula	Calculated ion m/z
517.0893	1-	Bis-urea - [H]	C ₂₂ H ₁₃ N ₄ F ₈ O ₂	(1-) 517.0916
356.0451	1-	Bis-urea - [(C ₇ H ₄ F ₃)N·H ₃]	C ₁₅ H ₇ N ₃ F ₅ O ₂	(1-) 356.0464
330.0661	1-	Bis-urea - [(C ₇ H ₄ F ₃)NCO·H]	C ₁₄ H ₉ N ₃ F ₅ O	(1-) 330.0671
169.0211	1-	Bis-urea - [(C ₇ H ₄ F ₃ N) ₂ ·CO·H ₃]	C ₇ H ₃ N ₂ F ₂ O	(1-) 169.0219

Figure 3.23. ESI-MS of bis-urea **11** at 13.9 eV collision energy, with identified fragments shown.

With the fragmentation pattern of bis-urea **11** obtained, it was then possible to conduct ESI-MS on mixtures on the hydrogen-bonded complexes. (NEt₄)₂[Fe₂(pdt)(CO)₄(CN)₂] **14** was combined with 1.5 equivalents of bis-urea **11**, and then analysed. 1.5 equivalents was chosen to ensure that the majority of complex existed in solution as the diiron system with one bis-urea attached, based on the results of the FTIR experiments in Section 3.2.3.1.



m/z observed	Charge	Proposed fragment	Chemical Formula	Calculated ion m/z
517.0911	1-	Bis-urea - [H]	C ₂₂ H ₁₃ N ₄ F ₈ O ₂	(1-) 517.0916
449.9753	2-	[Fe ₂ (pdt)(CO) ₄ (CN) ₂].bis-urea	C ₃₁ H ₂₀ N ₆ F ₈ O ₆ Fe ₂ S ₂	(2-) 449.9734
382.8562	1-	[Fe ₂ (pdt)(CO) ₄ (CN) ₂].H	C ₉ H ₇ N ₂ O ₄ Fe ₂ S ₂	(1-) 382.8552
356.0466	1-	Bis-urea - [(C ₇ H ₄ F ₃)N.H ₃]	C ₁₅ H ₇ N ₃ F ₅ O ₂	(1-) 356.0464
330.0679	1-	Bis-urea - [(C ₇ H ₄ F ₃)NCO.H]	C ₁₄ H ₉ N ₃ F ₅ O	(1-) 330.0671
169.0226	1-	Bis-urea - [(C ₇ H ₄ F ₃ N) ₂ .CO.H ₃]	C ₇ H ₃ N ₂ F ₂ O	(1-) 169.0219

Figure 3.24. ESI-MS of 1.5 equivalents of fluorinated bis-urea **11** with (NEt₄)₂[Fe₂(pdt)(CO)₄(CN)₂] **14** at 1.0 eV collision energy, and tuned for 449. Identified fragments shown.

These results give the strongest indication yet that the fluorinated bis-urea is hydrogen bonded to the cyanide ligand of the diiron complex. A 2- ion at 449.98 would be the ion expected if bis-urea **11** was attached to the diiron complex, and it is present. Another

point of interest is that the diiron unit $[\text{Fe}_2(\text{pdt})(\text{CO})_4(\text{CN})_2]$ is shown to travel with a proton as a 1- ion at 382.86; this suggests that the fragmentation has removed the coordinated bis-urea, though one of the urea's protons has been left behind due to its binding to the cyanide group. It is possible to argue that the proton may be present as a bridging hydride species between the two Fe atoms, though as the cyanide group is the most basic group present on the diiron molecule it is not an unreasonable assumption to infer that the proton remains attached to the cyanide ligand. Both of the suggested diiron species exhibit excellent isotope agreement between the calculated and experimental values, and are shown in **Figure 3.25**.

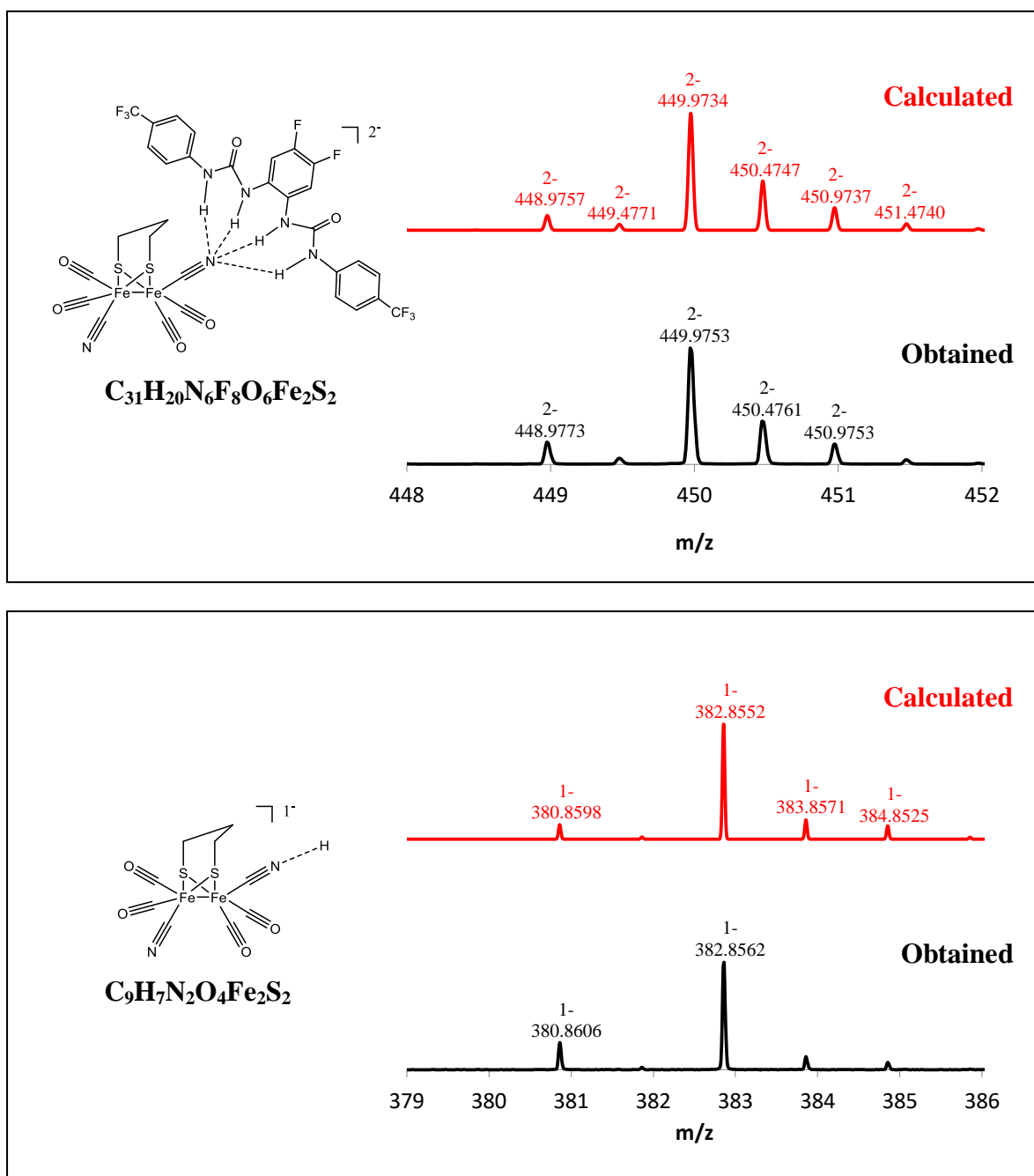
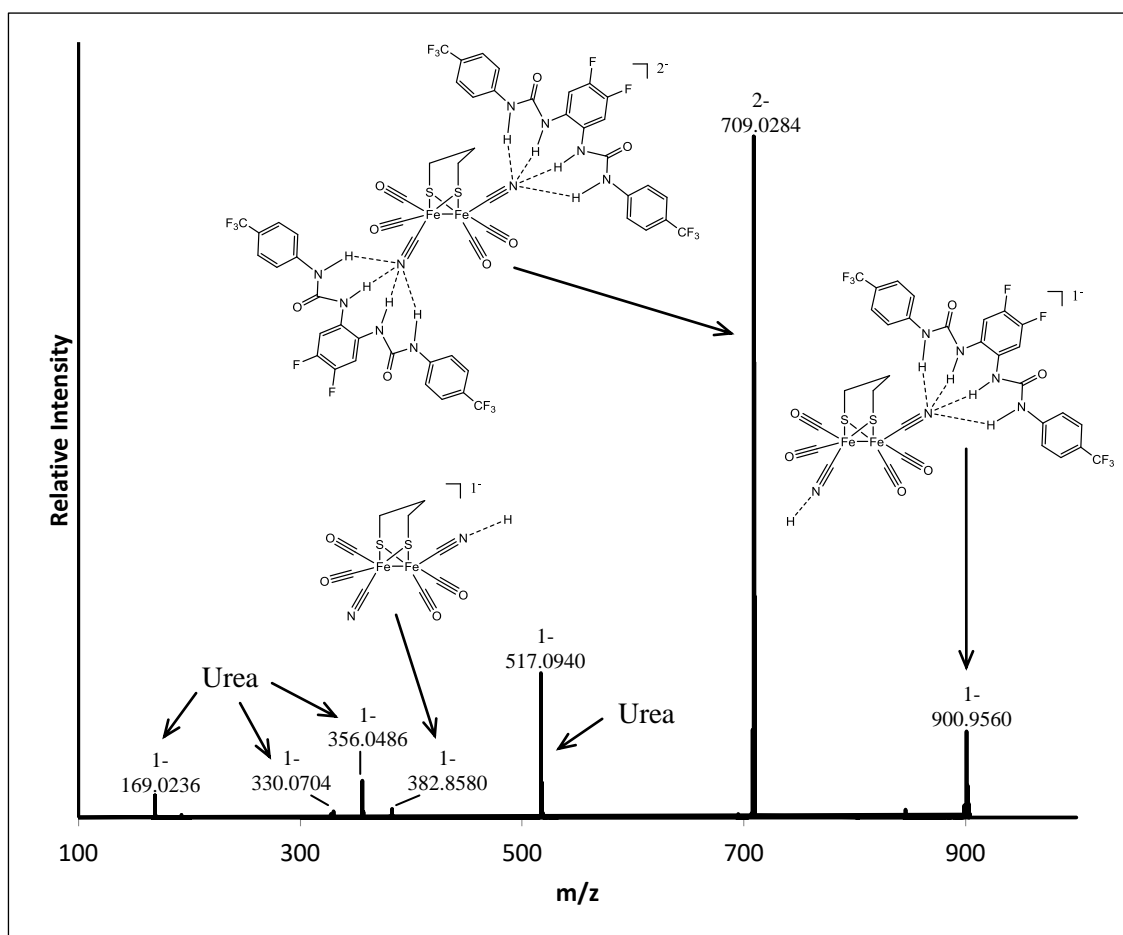


Figure 3.25. Isotope agreement between the obtained fragments and the calculated values for $[\text{Fe}_2(\text{pdt})(\text{CO})_4(\text{CN})_2 \cdot \text{urea } \mathbf{11}]^{2-}$ and $[\text{Fe}_2(\text{pdt})(\text{CO})_4(\text{CN})_2 \cdot \text{H}]^{1-}$.

With the binding of the of the first equivalent of bis-urea **11** proving successful, the binding of the second equivalent was attempted. $(\text{NEt}_4)_2[\text{Fe}_2(\text{pdt})(\text{CO})_4(\text{CN})_2]$ **14** was combined with 4.0 equivalents of bis-urea **11**, and then analysed. 4.0 equivalents was chosen to ensure that the majority of complex existed in solution as the diiron system with two bis-ureas attached, based on the results of the FTIR experiments in Section 3.2.3.1.



m/z observed	Charge	Proposed fragment	Chemical Formula	Calculated ion m/z
900.9560	1-	[Fe ₂ (pdt)(CO) ₄ (CN) ₂]·H·bis-urea	C ₃₁ H ₂₁ N ₆ F ₈ O ₆ Fe ₂ S ₂	(1-) 900.9541
709.0284	2-	[Fe ₂ (pdt)(CO) ₄ (CN) ₂]·(bis-urea) ₂	C ₅₃ H ₃₄ N ₁₀ F ₁₆ O ₈ Fe ₂ S ₂	(2-) 709.0230
517.0940	1-	Bis-urea - [H]	C ₂₂ H ₁₃ N ₄ F ₈ O ₂	(1-) 517.0916
382.8580	1-	[Fe ₂ (pdt)(CO) ₄ (CN) ₂]·H	C ₉ H ₇ N ₂ O ₄ Fe ₂ S ₂	(1-) 382.8552
356.0486	1-	Bis-urea - [(C ₇ H ₄ F ₃)N·H ₃]	C ₁₅ H ₇ N ₃ F ₅ O ₂	(1-) 356.0464
330.0704	1-	Bis-urea - [(C ₇ H ₄ F ₃)NCO·H]	C ₁₄ H ₉ N ₃ F ₅ O	(1-) 330.0671
169.0236	1-	Bis-urea - [(C ₇ H ₄ F ₃ N) ₂ ·CO·H ₃]	C ₇ H ₃ N ₂ F ₂ O	(1-) 169.0219

Figure 3.26. ESI-MS of 4.0 equivalents of fluorinated bis-urea **11** with (NEt₄)₂[Fe₂(pdt)(CO)₄(CN)₂] **14** at 12.0 eV collision energy, and tuned for 709. Identified fragments shown.

These mass spectra show that two molecules of bis-urea **11** will bind to the $[\text{Fe}_2(\text{pdt})(\text{CO})_4(\text{CN})_2]^{2-}$ unit in stable fashion. A 2- ion at 709.03 would be the expected ion if two equivalents of bis-urea **11** were attached to the diiron complex, and it is present. As seen with the one equivalent experiment, there are also traces present of species that had bis-urea(s) coordinated and then subsequently had them removed by fragmentation. The 1- ion at 900.96 is consistent with a species that originally had two bis-ureas coordinated, and then had one removed, leaving behind a complex with one bis-urea still attached and a proton remaining linked to the cyanide group having been previously hydrogen bonded between the cyanide and the removed bis-urea. The 1- ion at 382.86 caused by a diiron unit with one hydrogen still bound, as seen in the previous experiment, is present once again, presumably having originated from a diiron species with two bis-ureas attached only to have had them both of them removed by fragmentation. Both of these newly-identified diiron species exhibit excellent isotope agreement between the calculated and experimental values, and are shown in **Figure 3.27**.

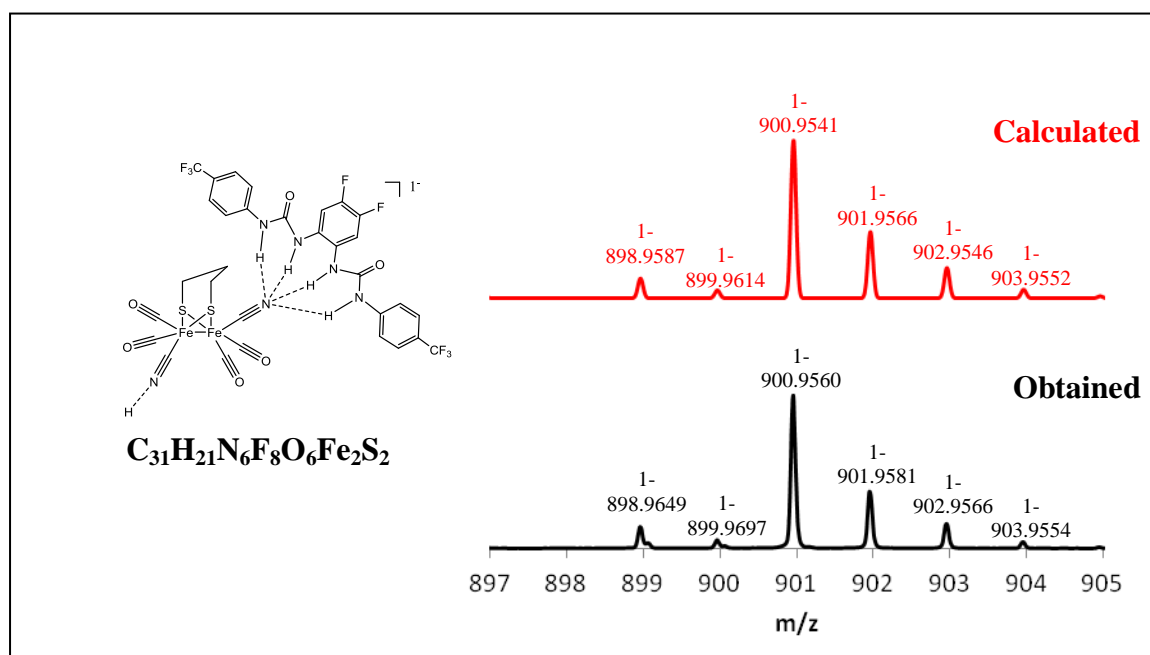
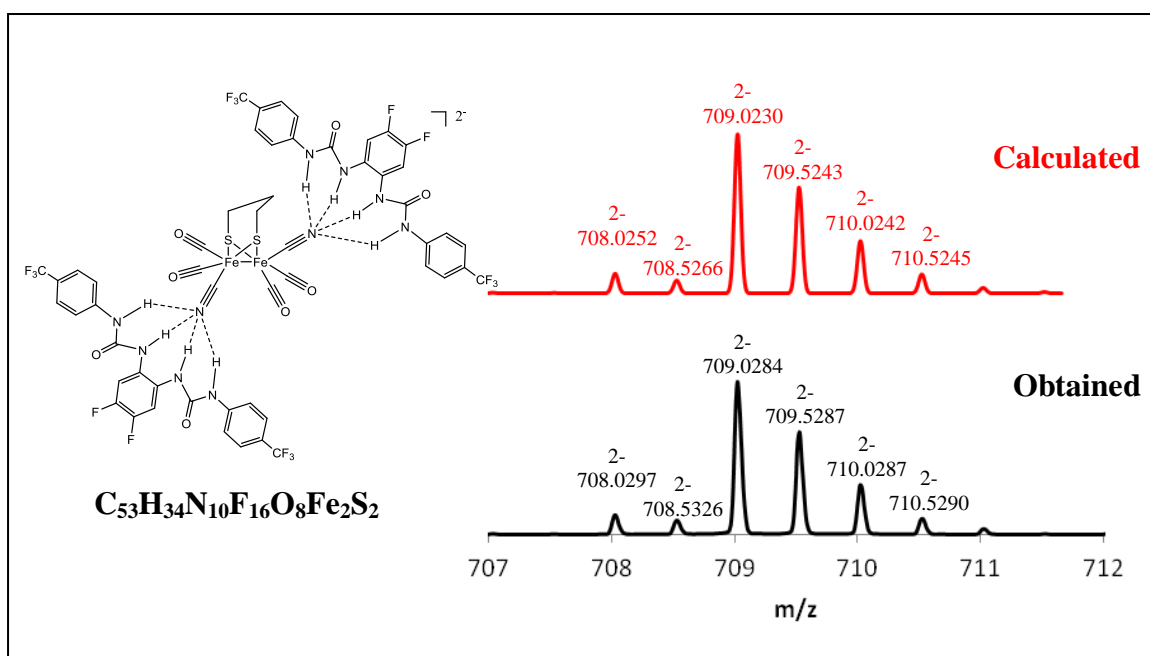


Figure 3.27. Isotope agreement between the obtained fragments and the calculated values for $[\text{Fe}_2(\text{pdt})(\text{CO})_4(\text{CN})_2 \cdot (\text{urea } \mathbf{1})_2]^{2-}$ and $[\text{Fe}_2(\text{pdt})(\text{CO})_4(\text{CN})_2 \cdot \text{H} \cdot \text{urea } \mathbf{11}]^{1-}$.

With the data suggesting that bis-urea molecules can be removed from a coordinated system by fragmentation to give the diiron subsite with proton residues, it should be possible to systematically remove one and then two bis-ureas. This was attempted using increasing collision energy and is shown in **Figure 3.28.** below.

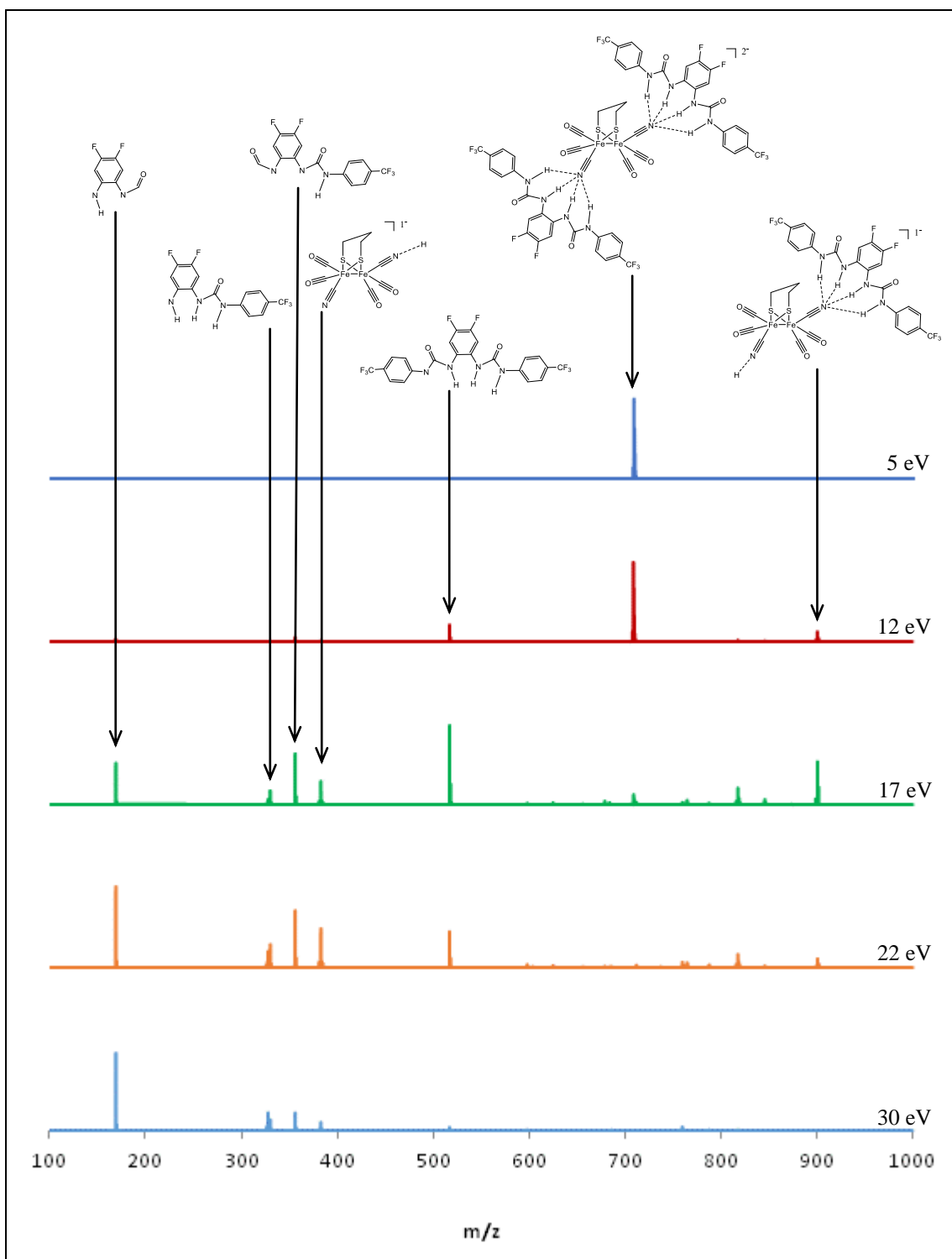
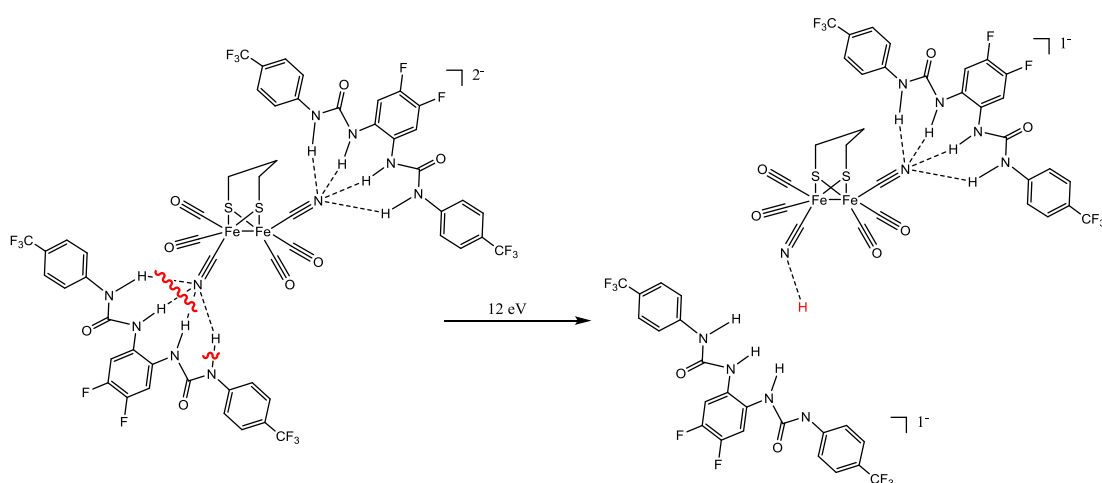


Figure 3.28. ESI-MS of 4.0 equivalents of fluorinated bis-urea **11** with $(\text{NEt}_4)_2[\text{Fe}_2(\text{pdt})(\text{CO})_4(\text{CN})_2]$ **14** tuned for 709 with increasing collision energies.

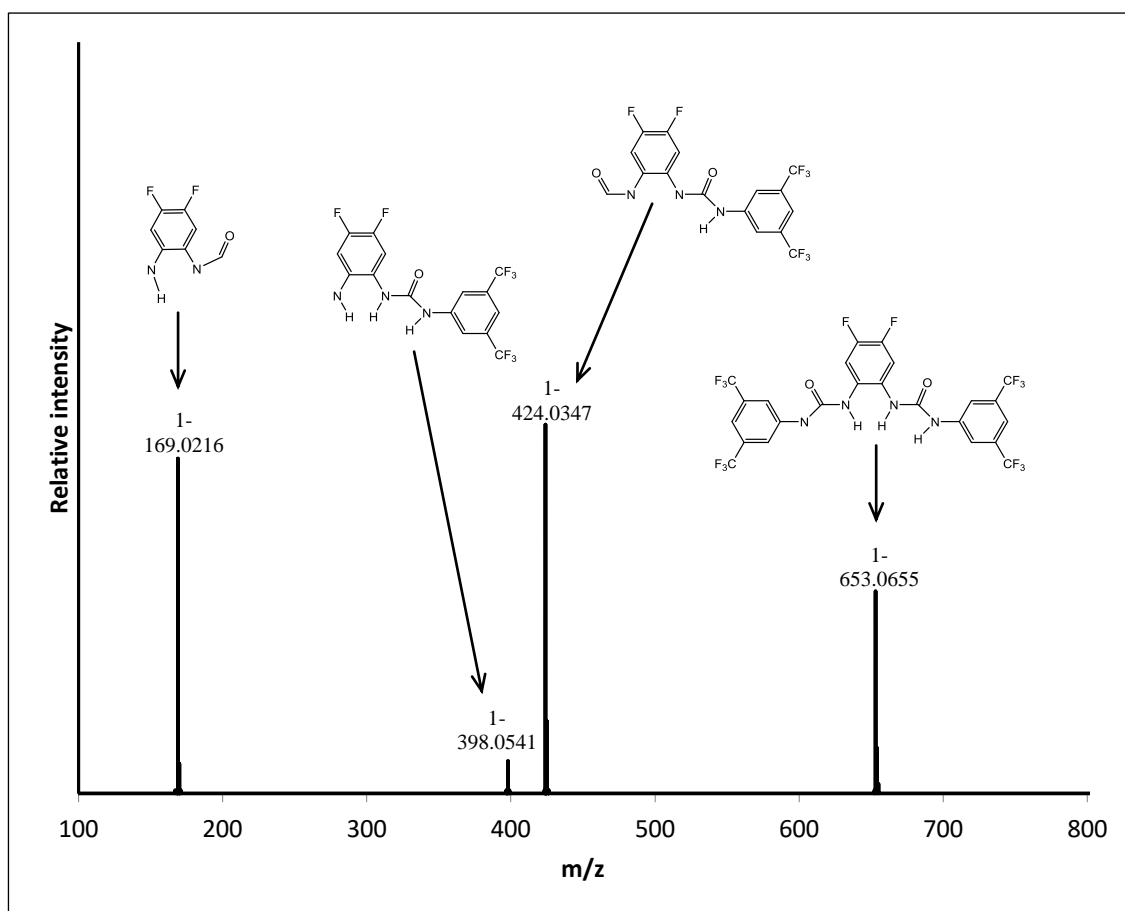
Increasing collision energies on the mass spectra samples had the desired effect: it was possible to systematically remove each of the coordinated bis-ureas before then

breaking up the fragments formed. This experiment also provided additional evidence to support the hypothesis that the additional proton present on the molecular ions after bis-urea removal is located as a hydrogen-bonded proton to the cyanide ligand(s). Increasing the collision energy from 5 eV to 12 eV is shown to remove one molecule of coordinated bis-urea, generating the protonated 1- ion with one bis-urea still attached at 900.96 *and* the 1- bis-urea fragment with one proton removed at 517.09. This would be consistent of a cleavage of the urea-proton bond, generating the diiron ion with a protonated cyanide group, and a bis-urea ion with a proton missing, which is essentially the conjugate base of the system. This is shown in **Scheme 3.5**. It should still be noted that it is still a distinct possibility for the additional proton to be present as a bridging hydride between the two Fe atoms, though this is appearing to be increasingly unlikely.



Scheme 3.5. Suggested fragmentation of $[\text{Fe}_2(\text{pdt})(\text{CO})_4(\text{CN})_2 \cdot (\text{urea } \mathbf{11})_2]^{2-}$ at 12.0 eV to give the protonated species $[\text{Fe}_2(\text{pdt})(\text{CO})_4(\text{CN})_2 \cdot \text{H} \cdot \text{urea } \mathbf{11}]^{1-}$.

The mass spectrometry experiments on bis-urea **11** appeared successful, demonstrating significant interaction between the bis-urea and the cyanide-containing diiron subsite analogue. The same series of experiments was then performed using bis-urea **12**, starting again with the mass spectrum of just the bis-urea itself as shown in **Figure 3.29**.

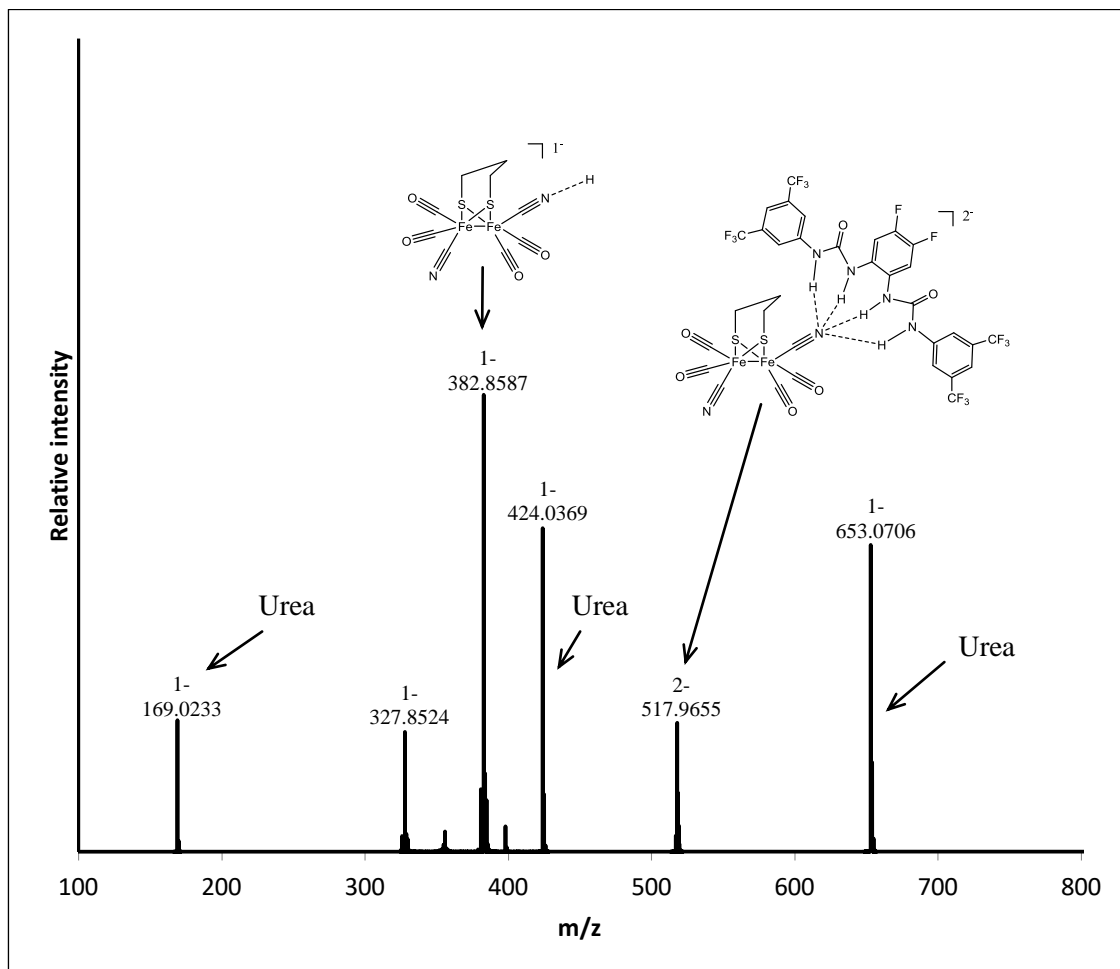


m/z observed	Charge	Proposed fragment	Chemical Formula	Calculated ion m/z
653.0655	1-	Bis-urea - [H]	C ₂₄ H ₁₁ N ₄ F ₁₄ O ₂	(1-) 653.0664
424.0347	1-	Bis-urea - [(C ₈ H ₃ F ₆)N·H ₃]	C ₁₆ H ₆ N ₃ F ₈ O ₂	(1-) 424.0338
398.0541	1-	Bis-urea - [(C ₈ H ₃ F ₆)NCO·H]	C ₁₅ H ₈ N ₃ F ₈ O	(1-) 398.0545
169.0216	1-	Bis-urea - [(C ₈ H ₃ F ₆ N) ₂ ·CO·H ₃]	C ₇ H ₃ N ₂ F ₂ O	(1-) 169.0219

Figure 3.29. ESI-MS of bis-urea **12** at 12.0 eV collision energy, with identified fragments shown.

The fragmentation pattern of bis-urea **12** gave very similar fragments to bis-urea **11**, with the molecules breaking in the same places and the only change being the additional mass of the extra trifluoromethyl groups. With the fragmentation pattern of bis-urea **12** obtained, it was again possible to conduct ESI-MS on mixtures on the hydrogen-bonded

complexes. $(\text{NEt}_4)_2[\text{Fe}_2(\text{pdt})(\text{CO})_4(\text{CN})_2]$ **14** was combined with 1.5 equivalents of bis-urea **12**, as was in the case for bis-urea **11**, and then analysed.



m/z observed	Charge	Proposed fragment	Chemical Formula	Calculated ion m/z
653.0706	1-	Bis-urea - [H]	$\text{C}_{24}\text{H}_{11}\text{N}_4\text{F}_{14}\text{O}_2$	(1-) 653.0664
517.9655	2-	$[\text{Fe}_2(\text{pdt})(\text{CO})_4(\text{CN})_2] \cdot \text{bis-urea}$	$\text{C}_{33}\text{H}_{18}\text{N}_6\text{F}_{14}\text{O}_6\text{Fe}_2\text{S}_2$	(2-) 517.9608
424.0369	1-	Bis-urea - $[(\text{C}_8\text{H}_3\text{F}_6\text{N}) \cdot \text{H}_3]$	$\text{C}_{16}\text{H}_6\text{N}_3\text{F}_8\text{O}_2$	(1-) 424.0338
382.8587	1-	$[\text{Fe}_2(\text{pdt})(\text{CO})_4(\text{CN})_2] \cdot \text{H}$	$\text{C}_9\text{H}_7\text{N}_2\text{O}_4\text{Fe}_2\text{S}_2$	(1-) 382.8552
169.0233	1-	Bis-urea - $[(\text{C}_8\text{H}_3\text{F}_6\text{N})_2 \cdot \text{CO} \cdot \text{H}_3]$	$\text{C}_7\text{H}_3\text{N}_2\text{F}_2\text{O}$	(1-) 169.0219

Figure 3.30. ESI-MS of 1.5 equivalents of fluorinated bis-urea **12** with $(\text{NEt}_4)_2[\text{Fe}_2(\text{pdt})(\text{CO})_4(\text{CN})_2]$ **14** at 10.0 eV collision energy, and tuned for 517. Identified fragments shown.

The desired 2- ion at 517.96 is present which demonstrates the binding of bis-urea **12** to the diiron complex. As was in the case of the bis-urea **11** experiments, the protonated $[\text{Fe}_2(\text{pdt})(\text{CO})_4(\text{CN})_2]\cdot\text{H}$ fragment is present as a 1- ion at 382.86, presumably generated by the removal of the attached bis-urea, leaving behind a hydrogen-bonded proton. The 2- 517.96 ion that demonstrates bis-urea attachment exhibits excellent correlation between the calculated and observed isotope pattern, and is shown in **Figure 3.31**.

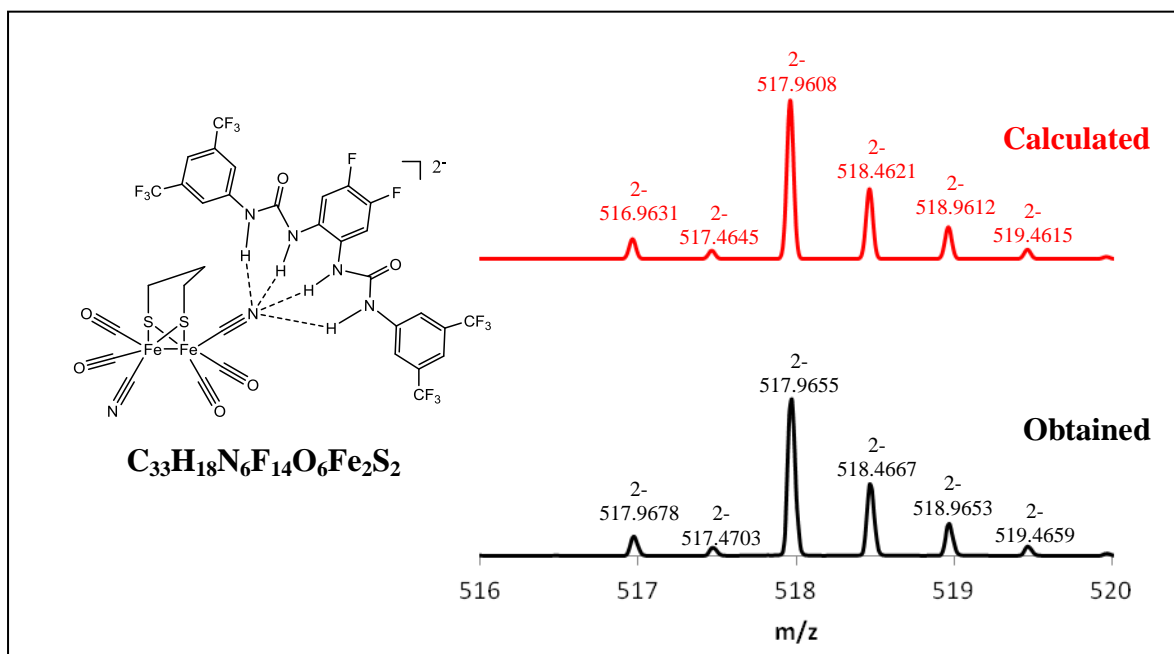
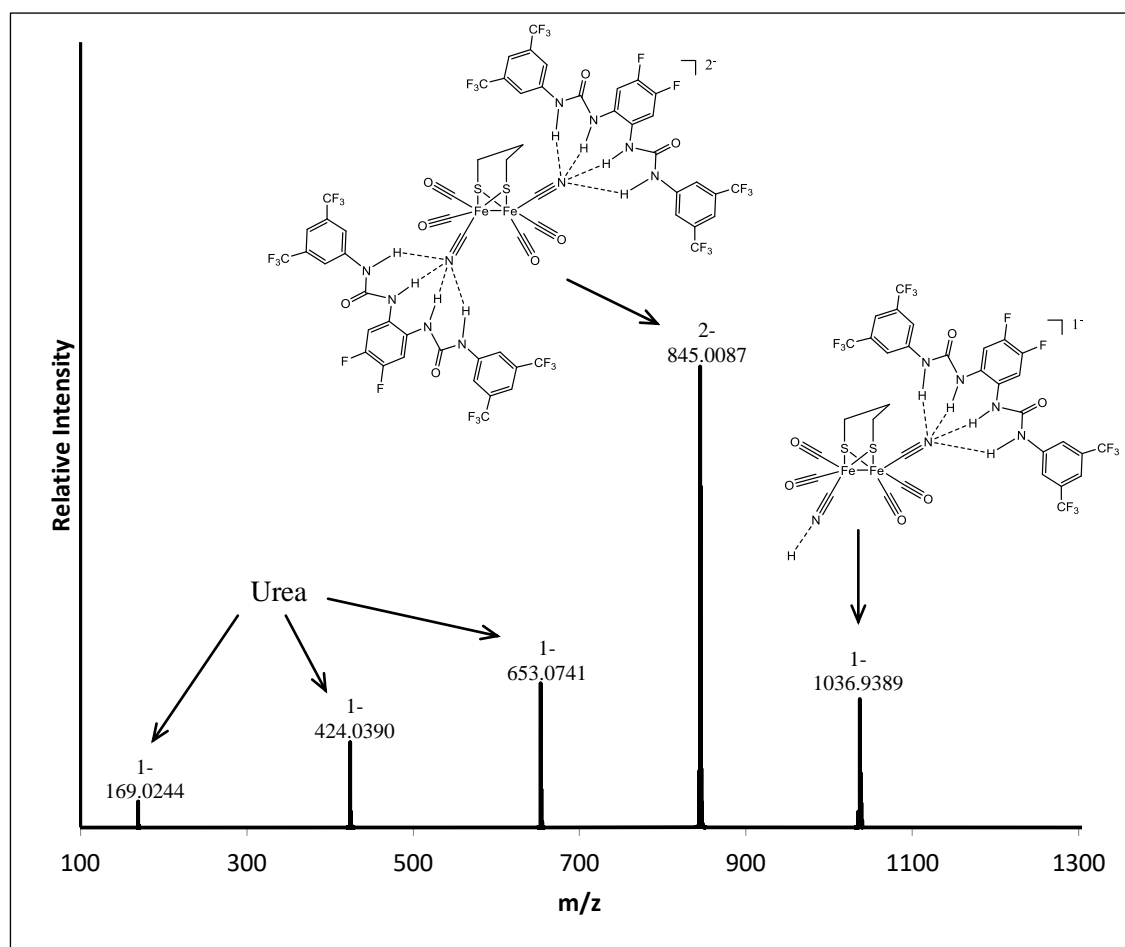


Figure 3.31. Isotope agreement between the obtained fragments and the calculated values for $[\text{Fe}_2(\text{pdt})(\text{CO})_4(\text{CN})_2\cdot\text{urea } \mathbf{12}]^{2-}$.

With the binding of the first equivalent of bis-urea **12** proving successful, the binding of the second equivalent was attempted. $(\text{NEt}_4)_2[\text{Fe}_2(\text{pdt})(\text{CO})_4(\text{CN})_2]$ **14** was combined with 4.0 equivalents of bis-urea **12**, and then analysed, as in the experiments conducted on bis-urea **11**.



m/z observed	Charge	Proposed fragment	Chemical Formula	Calculated ion m/z
1036.9389	1-	$[\text{Fe}_2(\text{pdt})(\text{CO})_4(\text{CN})_2] \cdot \text{H} \cdot \text{bis-urea}$	$\text{C}_{33}\text{H}_{19}\text{N}_6\text{F}_{14}\text{O}_6\text{Fe}_2\text{S}_2$	(1-) 1036.9289
845.0087	2-	$[\text{Fe}_2(\text{pdt})(\text{CO})_4(\text{CN})_2] \cdot (\text{bis-urea})_2$	$\text{C}_{57}\text{H}_{30}\text{N}_{10}\text{F}_{28}\text{O}_8\text{Fe}_2\text{S}_2$	(2-) 844.9978
653.0741	1-	Bis-urea - $[\text{H}]$	$\text{C}_{24}\text{H}_{11}\text{N}_4\text{F}_{14}\text{O}_2$	(1-) 653.0664
424.0390	1-	Bis-urea - $[(\text{C}_8\text{H}_3\text{F}_6)\text{N} \cdot \text{H}_3]$	$\text{C}_{16}\text{H}_6\text{N}_3\text{F}_8\text{O}_2$	(1-) 424.0338
169.0244	1-	Bis-urea - $[(\text{C}_8\text{H}_3\text{F}_6\text{N})_2 \cdot \text{CO} \cdot \text{H}_3]$	$\text{C}_7\text{H}_3\text{N}_2\text{F}_2\text{O}$	(1-) 169.0219

Figure 3.32. ESI-MS of 4.0 equivalents of fluorinated bis-urea **12** with $(\text{NEt}_4)_2[\text{Fe}_2(\text{pdt})(\text{CO})_4(\text{CN})_2]$ **14** at 15.0 eV collision energy, and tuned for 845. Identified fragments shown.

The desired 2- ion at 845.00 was present, indicating the presence of the diiron species with two equivalents of bis-urea **12** attached. As was in the case of bis-urea **11**, the species with one bis-urea molecule removed, leaving behind a hydrogen-bonded proton

is present as a 1- ion at 1036.94, and the calculated and experimental isotope patterns are in excellent agreement, as shown in **Figure 3.33**.

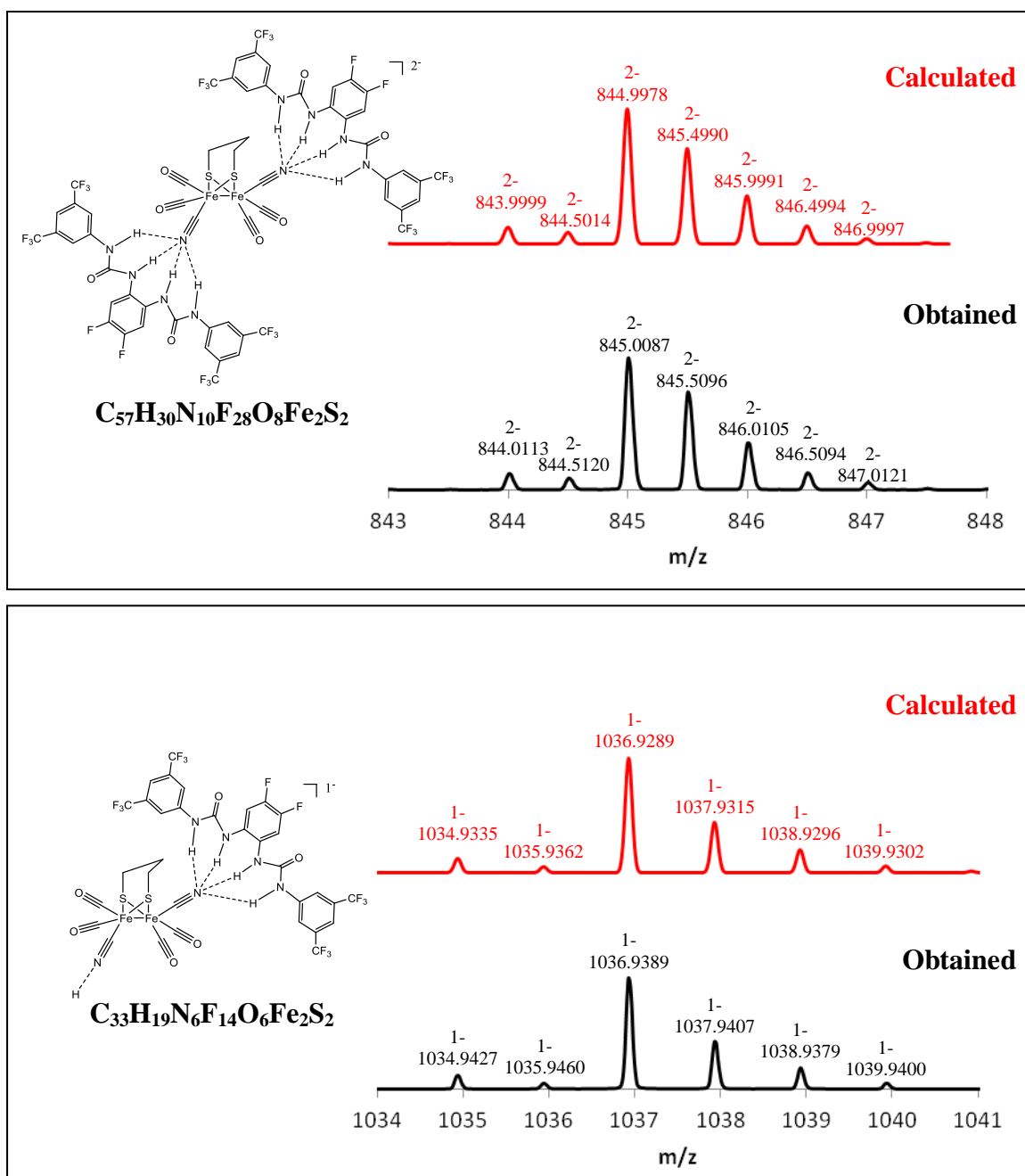
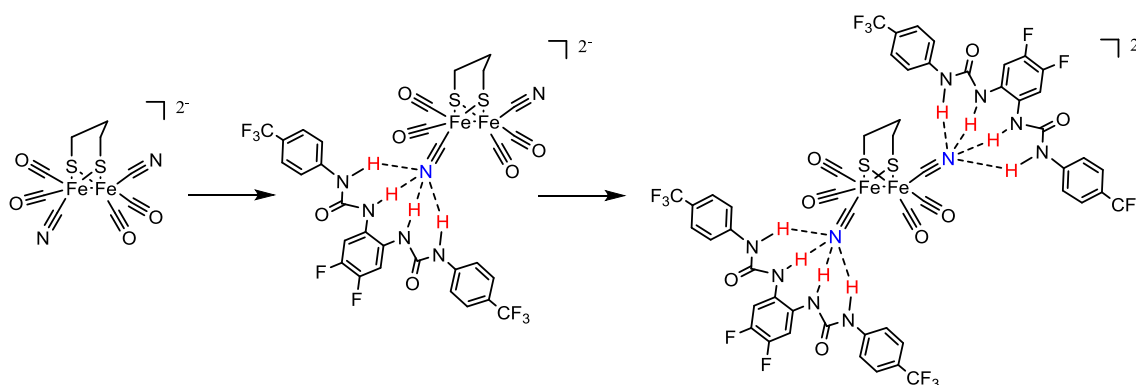


Figure 3.33. Isotope agreement between the obtained fragments and the calculated values for $[\text{Fe}_2(\text{pdt})(\text{CO})_4(\text{CN})_2 \cdot (\text{urea } \mathbf{12})_2]^{2-}$ and $[\text{Fe}_2(\text{pdt})(\text{CO})_4(\text{CN})_2 \cdot \text{H} \cdot \text{urea } \mathbf{12}]^{1-}$.

The mass spectrometry experiments have proven conclusive in that they have shown that the bis-ureas **11** and **12** can securely bind to $(\text{NEt}_4)_2[\text{Fe}_2(\text{pdt})(\text{CO})_4(\text{CN})_2]$ **14** via hydrogen bonding, and that it is possible to sequentially remove each of the attached ureas to leave behind hydrogen-bonded proton residues.

3.2.4 The nature of the interactions of a diiron dicyanide subsite analogue with fluorinated bis-ureas

All of the above spectroscopic studies by FTIR, NMR and mass spectrometry unequivocally demonstrate that in the solution and gas phase 1:1 and 1:2 hydrogen-bonding adducts are formed. This almost certainly involves hydrogen-bonding to cyanide ligand, as is observed in the crystal structures of the enzyme systems⁷⁵. The postulated binding of the bis-urea **11** to the diiron complex **14** is shown in **Scheme 3.6**.



Scheme 3.6. Suggested binding of bis-urea **11** to dicyanide diiron complex **14**.

To explore the degree of possible hydrogen-bonding in these systems, preliminary DFT calculations were undertaken with Dr Joseph Wright of the University of East Anglia.

All calculations were performed using the Gaussian 09⁹⁸ computational package. Geometry optimisations have been carried out using the Tao–Perdew–Staroverov–Scuseria⁹⁹ (TPSS) density functional. Sulfur and iron atoms are described by the Hay and Wadt LANL2DZ basis set with effective core potential (ECP). In the case of iron,

the two outermost p functions were replaced with reoptimised 4p functions. For sulfur, additional p and d polarisation functions were added. All other atoms employ the all electron 6-31+G** basis set. Structures were geometry optimised in the gas phase with the default convergence criteria.

Figure 3.34 shows the calculated structure for the mono-adduct $[\text{Fe}_2(\text{pdt})(\text{CO})_4(\text{CN})_2 \cdot \text{Bis-urea}(\mathbf{11})]^{2-}$ and **Figure 3.35** shows the equivalent bis-adduct. The optimised structures which converge in each case exhibit four hydrogen-bonding interactions to each cyanide to provide stable structures. The calculated hydrogen-bond lengths for the mono-adduct $[\text{Fe}_2(\text{pdt})(\text{CO})_4(\text{CN})_2 \cdot \text{Bis-urea}(\mathbf{11})]^{2-}$ are also shown in **Figure 3.34** and are fully consistent with strong hydrogen bonding to the N atom of cyanide, with the innermost amides having the shortest bond lengths.

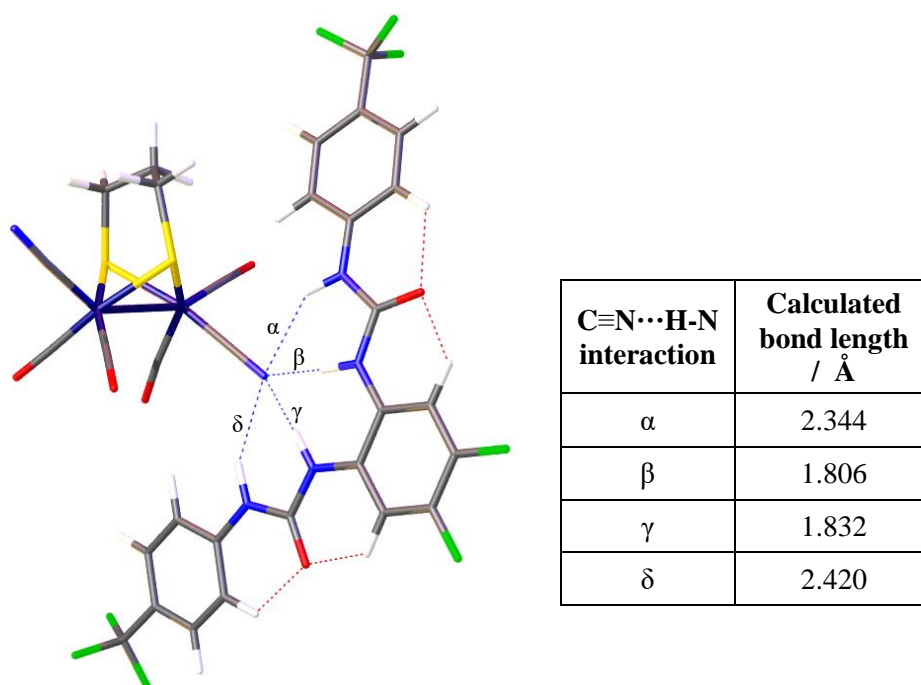


Figure 3.34. DFT optimised structure for $[\text{Fe}_2(\text{pdt})(\text{CO})_4(\text{CN})_2 \cdot \text{Bis-urea}(\mathbf{11})]^{2-}$ demonstrating the formation of four hydrogen-bonding interactions, with calculated bond lengths provided.

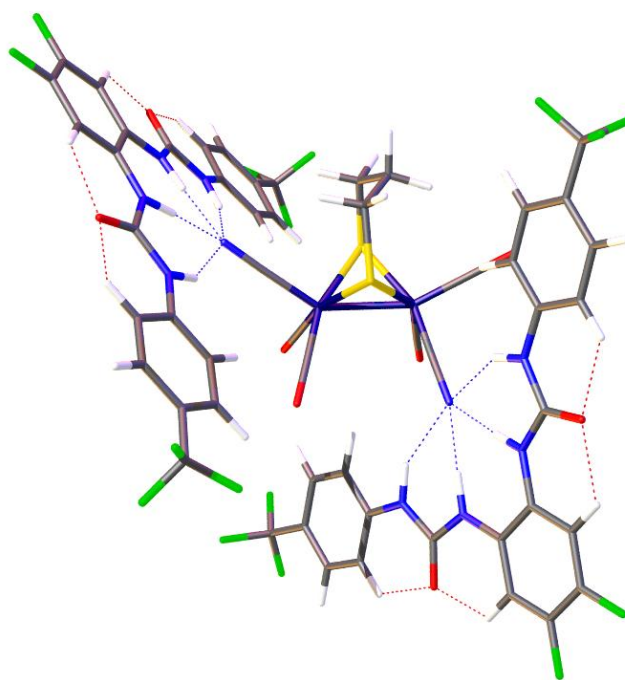
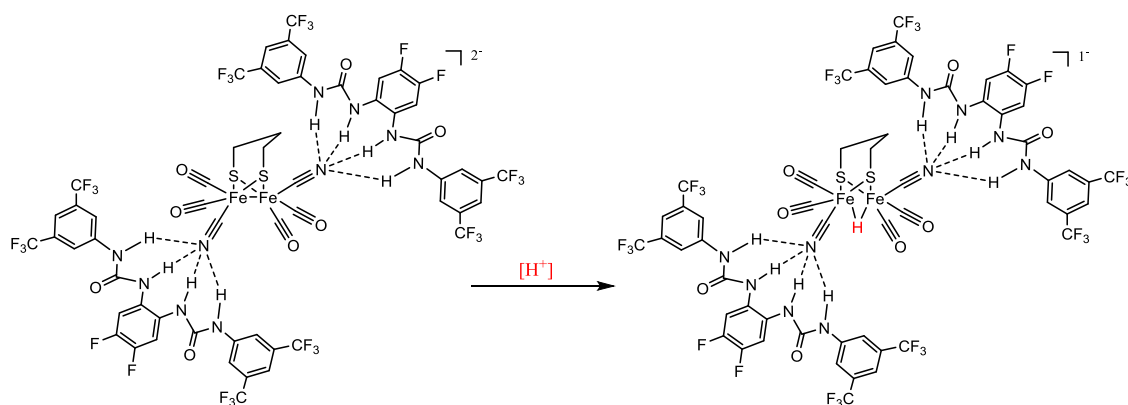


Figure 3.35. DFT optimised structure for $[\text{Fe}_2(\text{pdt})(\text{CO})_4(\text{CN})_2]^{2-} \cdot (\text{Bis-urea}(\mathbf{11}))_2^{2-}$. Again the formation of four hydrogen-bonding interactions is demonstrated.

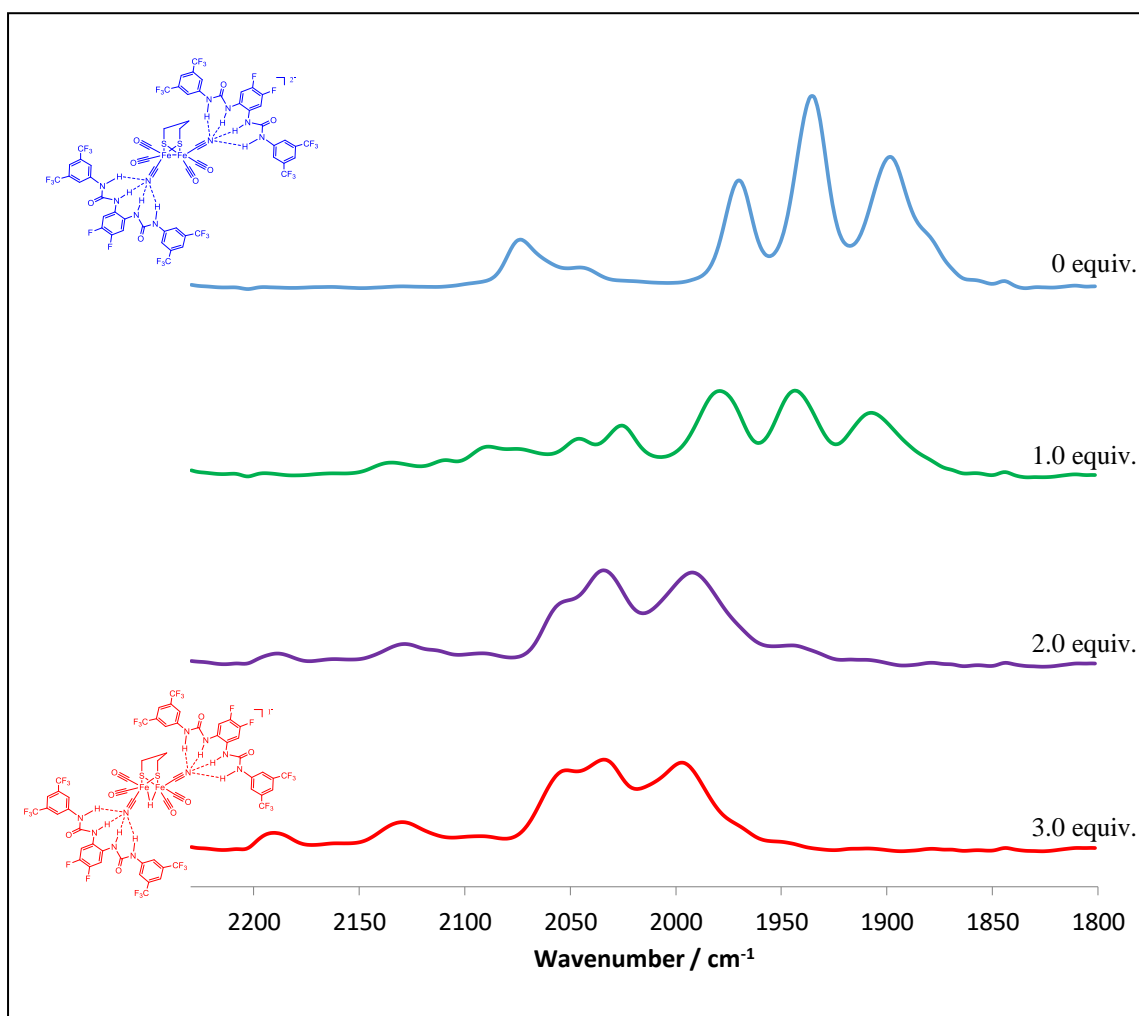
3.2.5 Protonation of $[\text{Fe}_2(\text{pdt})(\text{CO})_4(\text{CN})_2]^{2-} \cdot (\text{bis-urea})_2^{2-}$

After analysing the combined results of the FTIR, NMR and ESI-MS experiments, it is fairly conclusive that the fluorinated bis-ureas have been successfully bound to the diiron unit $[\text{Fe}_2(\text{pdt})(\text{CO})_4(\text{CN})_2]^{2-}$. The purpose of this work was to securely cap and protect the cyanide ligands, without a dramatic impact on the activity of the original system. The simplest way to examine the effectiveness of the fluorinated bis-urea capping is by protonation; ideally the system will still be capable of protonation at the metal-metal bond without the decomposition associated with protonation at the cyanide ligands, as explained in **Section 3.1.3**. The desired protonation of the bis-urea capped $[\text{Fe}_2(\text{pdt})(\text{CO})_4(\text{CN})_2]^{2-}$ species is shown in **Scheme 3.7**.



Scheme 3.7. Desired protonation of $[\text{Fe}_2(\text{pdt})(\text{CO})_4(\text{CN})_2(\text{bis-urea } \mathbf{12})_2]^{2-}$ to give the bridging hydride species $[\text{Fe}_2(\text{pdt})(\mu\text{-H})(\text{CO})_4(\text{CN})_2(\text{bis-urea } \mathbf{12})_2]^{1-}$.

For this protonation experiment a 1.0 mM solution of $(\text{NEt}_4)_2[\text{Fe}_2(\text{pdt})(\text{CO})_4(\text{CN})_2] \mathbf{14}$ with two equivalents of bis-urea $\mathbf{12}$ was prepared in MeCN, to which a stock solution of $\text{HBF}_4 \cdot \text{OEt}_2$ in MeCN was added. Two equivalents of the bis-urea were used to ensure that both the cyanide ligands were capped to hopefully protect from protonation. If the protonation is successful and gives a bridging hydride species, a large shift in the CO stretches in the IR spectrum should be apparent due to the large change of electron density on the FeFe core. The FTIR spectra recorded from the protonation experiment are given in **Figure 3.36**.



	$\nu(\text{CN}) / \text{cm}^{-1}$	$\nu(\text{CO}) / \text{cm}^{-1}$
Non-protonated	2075, 2042	1969, 1934, 1898
Protonated	2189, 2129	2052, 2035, 1996

Figure 3.36. Solution FTIR spectra (MeCN) monitoring the affects of equivalent additions of $\text{HBF}_4 \cdot \text{OEt}_2$ to $[\text{Fe}_2(\text{pdt})(\text{CO})_4(\text{CN})_2(\text{bis-urea } \mathbf{12})_2]^{2-}$ in order to protonate and generate the bridging hydride species, $[\text{Fe}_2(\text{pdt})(\mu\text{-H})(\text{CO})_4(\text{CN})_2(\text{bis-urea } \mathbf{12})_2]^{1-}$.

These IR spectra demonstrate that the diiron dicyanide species with capping bis-ureas, $[\text{Fe}_2(\text{pdt})(\text{CO})_4(\text{CN})_2(\text{bis-urea } \mathbf{12})_2]^{2-}$ undergoes stable protonation to give the bridging hydride species $[\text{Fe}_2(\text{pdt})(\mu\text{-H})(\text{CO})_4(\text{CN})_2(\text{bis-urea } \mathbf{12})_2]^{1-}$. This is shown by the CO and CN stretches moving to significantly higher wavenumbers ($\sim 80\text{-}110 \text{ cm}^{-1}$) as the electron density on the FeFe core is severely decreased with the attachment of the

bridging hydrogen atom, as there is much less back donation from the FeFe core into the π^* antibonding orbitals of CN and CO. These observed results are consistent with reported examples of protonation at the Fe-Fe bond^{80,81}.

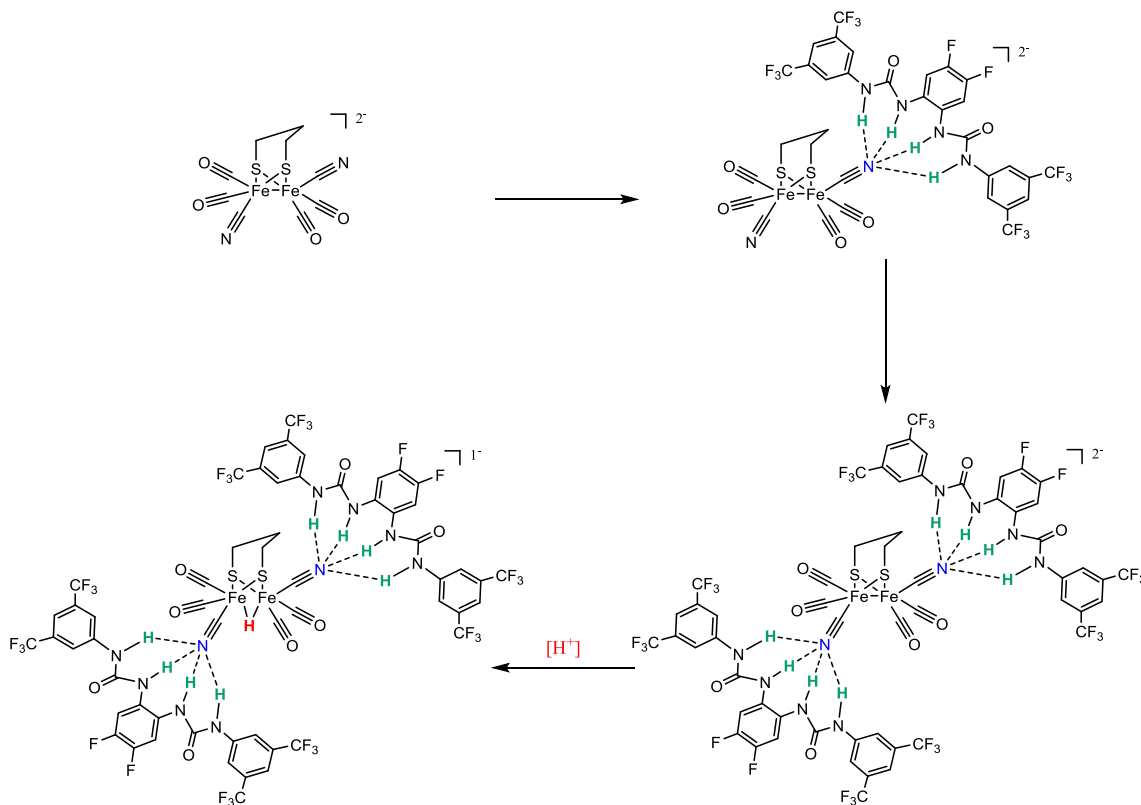
The fact that three equivalents of $\text{HBF}_4 \cdot \text{OEt}_2$ are required to fully protonate the system is in keeping with Rauchfuss' Bar^{F} experiments outlined in **Section 3.1.3**, which also required an excess of $[\text{H}^+]$. The binding of the substituents to the cyanide ligands shifts electron density away from the Fe-Fe bond, reducing its basicity.

3.2.6 Concluding remarks and future work

The FTIR and ESI-MS spectroscopic data obtained for the interactions between the diiron dicyanide subsite analogue and the fluorinated bis-ureas have provided compelling evidence for 1:1 and 1:2 subsite:bis-urea adduct formation. The FTIR data is consistent with hydrogen bonding involving the cyanide ligands of the subsite. The suggested hydrogen bonding interactions are those shown in **Scheme 3.6** and elsewhere, whereby the bis-urea unit is capable of multiple interactions with the CN group(s), which has some analogy with the bonding of Cl^- ion to electron deficient bis- and tris-ureas as demonstrated by Gale and coworkers⁹¹. Whereas it is clear that four lone pairs around a chloride anion can accommodate multiple H-bonding interactions from the bis-urea(s), the corresponding binding of ligated cyanide requires some consideration. The basic lone pair of electrons on the nitrogen of the cyanide ligand can clearly interact to form a single hydrogen bond, furthermore the $p-\pi$ electron density around the CN ligand may also contribute to hydrogen bonding. It has been noted in calculations for free cyanide that multiple hydrogen bonding to the pseudospherical anion can occur¹⁰⁰, which has been further corroborated with our own DFT calculations for these specific examples, as shown above.

The fluorinated bis-urea groups have protected the cyanide ligands whilst retaining the activity of the parent system, as demonstrated by protonation. The hydrogen bonding method of cyanide-capping employed has proven a milder mode of protection than the other reported system⁸¹, BAr^{F} -derived adduct formation, as demonstrated by the shifts in the CO stretches of the BAr^{F} system being $\sim 24 \text{ cm}^{-1}$ and the hydrogen bonding interactions resulting in shifts of $\sim 10\text{-}15 \text{ cm}^{-1}$, depending on the bis-urea employed.

A scheme depicting fluorinated bis-urea coordination to the cyanide ligands via hydrogen bonding, and then the species' subsequent protonation to form a bridging hydride derivative, is shown in **Scheme 3.8**.



Scheme 3.8. Fluorinated bis-urea attachment via hydrogen bonding and then subsequent protonation to form a bridging hydride species.

In regards to expanding this body of work, how such hydrogen bonding affects the electron transfer chemistry of these dicyanide species remains to be explored. Preliminary studies in our laboratory⁹⁷ employing tris-thioureas confirm substantial shifts in oxidation potentials to more positive values but with no additional stabilisation of the mixed-valence state.

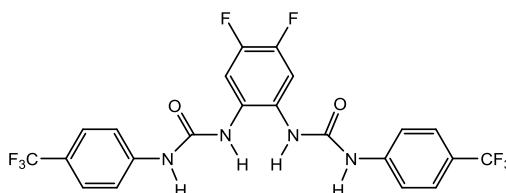
Another interesting avenue to pursue would be the synthesis of a molecule that incorporates two of these bis-ureas joined together, so that they must coordinate to the dicyanide species from the same face. This investigation, and the BAr^F experiments from the literature, report *apical-basal* geometries around the FeFe centre, whereas the

natural [FeFe]-hydrogenase system is believed to employ a *trans-(basal,basal)* orientation. A conjoined di-bis-urea system may just be capable of achieving such an arrangement.

A further area worth investigating would be to utilise the fluorinated bis-ureas for a purpose similar to which they were originally intended, and to help transport diiron dicyanide subsite analogues across cell membranes and into cells. The group of G. Berggren in Uppsala University, Sweden, has recently been able to activate apo-hydrogenases *in vivo* with FeFe subsites, with the mutant cells displaying activity for hydrogen production¹⁰¹. However, a limiting factor is uptake of the FeFe subsite into the cell. It is thought that the diiron dicyanide subsite analogues hydrogen bonded to fluorinated bis-ureas may be well-suited for cell uptake, and a collaboration to explore such chemistry is underway.

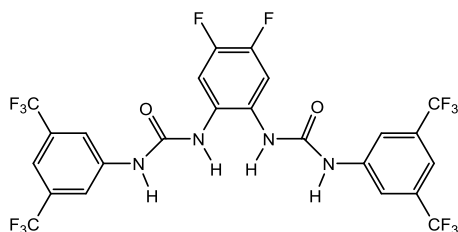
3.3 Experimental

3.3.1 Synthesis of 1,1'-(4,5-Difluoro-1,2-phenylene)bis(3-(4-(trifluoromethyl)phenyl)urea) (11)⁹¹



4,5-Difluoro-ortho-phenylenediamine (0.88 g, 6 mmol) was dissolved in dry degassed DCM (95 mL) and pyridine (5 mL). 4-(trifluoromethyl)phenyl isocyanate (1.80 mL, 13 mmol) was then added. The solution thickened immediately, forming a large amount of tan solid. Mixture left to stir for 16 h, before light brown precipitate obtained by filtration. Dissolved in MeOH with the aid of sonication before passing through an SCX-2 column. Drying in vacuo gave the *title compound* (1.67 g, 3 mmol, 53%) as white solid. ¹H-NMR (DMSO-*d*₆, 300.13 MHz): δ (ppm) = 9.54 (s, 2H), 8.26 (s, 2H), 7.72 (m, 2H), 7.69 (m, 4H), 7.64 (m, 4H). ¹⁹F-NMR (DMSO-*d*₆, 282.37 MHz): δ (ppm) = -60.18 (s, 6F), -142.44 (m, 2F).

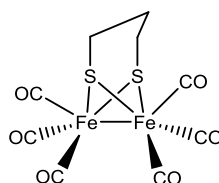
3.3.2 Synthesis of 1,1'-(4,5-Difluoro-1,2-phenylene)bis(3-(3,5-bis(trifluoromethyl)phenyl)urea) (12)⁹¹



4,5-Difluoro-ortho-phenylenediamine (0.78 g, 5 mmol) was dissolved in dry degassed DCM (190 mL) and pyridine (10 mL). 3,5-bis(trifluoromethyl)isocyanate (1.9 mL, 11 mmol) was then added, and the mixture left to stir for 16 h. A small amount of tan solid was produced, so the mixture was evaporated to dryness giving brown residues which were then taken up in ethyl acetate (200 mL). The organic layer was washed with H₂O (2 x 100 mL), before being dried over MgSO₄ and evaporated to dryness once again.

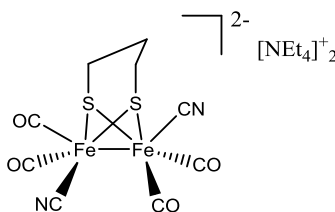
The resultant residues were then dissolved in MeOH with the aid of sonication before being passed through an SCX-2 column. The solvent was removed in vacuo before the product was recrystallised from DCM/ethyl acetate (5:1) to give the *title compound* (2.09 g, 3 mmol, 59%) as white fibrous solid. $^1\text{H-NMR}$ ($\text{DMSO-}d_6$, 300.13 MHz): δ (ppm) = 8.38 (s, 2H), 8.11 (s, 3H), 7.73 (m, 5H), 7.62 (s, 2H). $^{19}\text{F-NMR}$ ($\text{DMSO-}d_6$, 282.37 MHz): δ (ppm) = -61.83 (s, 12F), -141.83 (s, 2F).

3.3.3 Synthesis of $[\text{Fe}_2(\text{pdt})(\text{CO})_6]$ (**13**)⁸²



Triiron dodecacarbonyl (7.80 g, 15 mmol) was dissolved in dry degassed THF (250 mL) to give a green/black solution. 1,3-propanedithiol (1.30 mL, 13 mmol) was then added before the mixture was heated at 70 °C for 3 h, forming a red solution. The mixture was evaporated to dryness before the red/black residue was purified by column chromatography using hexane eluent to give the *title compound* (4.72 g, 12 mmol, 79%) as red crystalline solid. IR(MeCN): $\nu(\text{CO}) = 2074, 2035, 1995$.

3.3.4 Synthesis of $(\text{NEt}_4)_2[\text{Fe}_2(\text{pdt})(\text{CO})_4(\text{CN})_2]$ (**14**)⁸²



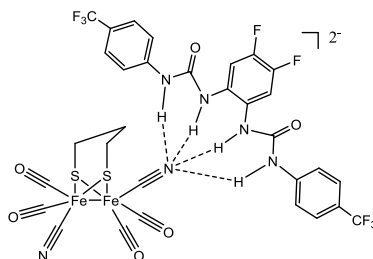
$[\text{Fe}_2(\text{pdt})(\text{CO})_6]$ **13** (1.28 g, 3 mmol) was dissolved in dry degassed MeCN (50 mL) to give a red solution. Tetraethylammonium cyanide (1.09 g, 7 mmol) in MeCN (50 mL) was then added over 15 mins to give a dark red solution. The solution was then stirred for 16 h, before being evaporated to dryness to give a sticky red solid. Stirring with

hexane (50 mL) for 6 h before filtration gave the *title compound* (2.02 g, 3 mmol, 95%) as red powder. IR(MeCN): $\nu(\text{CN}) = 2075$; $\nu(\text{CO}) = 1963, 1921, 1884, 1870$.

3.3.5 General procedure for generation of the $[\text{Fe}_2(\text{pdt})(\text{CO})_4(\text{CN})_2 \cdot \text{Bis-urea}_{(1,2)}]$ adducts

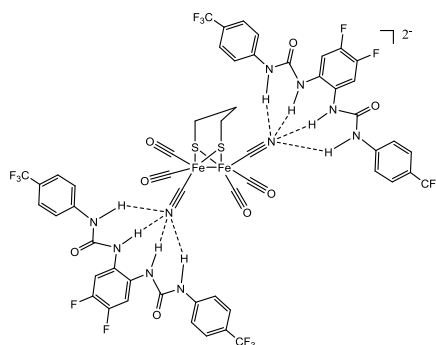
A solution of $(\text{NEt}_4)_2[\text{Fe}_2(\text{pdt})(\text{CO})_4(\text{CN})_2]$ **14** (12.85 mg, 0.02 mmol) in dry degassed MeCN (10 mL) was prepared, to which a solution of bis-urea **11** or **12** (1 equivalent: 10.37 mg or 13.09 mg, 0.02 mmol), (2 equivalents: 20.73 mg or 26.17 mg, 0.04 mmol) in MeCN (10 mL) was added. Samples for analysis were then removed by syringe as necessary. Characterisation of individual species outlined below.

3.3.6 Characterisation of the dianion $[\text{Fe}_2(\text{pdt})(\text{CO})_4(\text{CN})_2 \cdot \text{Bis-urea}(\mathbf{11})]$



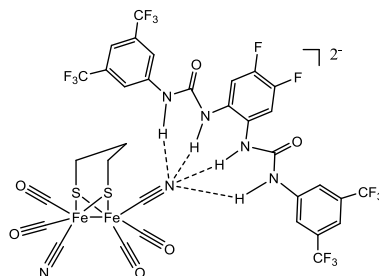
The *title anion* is formed in situ when bis-urea **11** is combined with $(\text{NEt}_4)_2[\text{Fe}_2(\text{pdt})(\text{CO})_4(\text{CN})_2]$ **14** in MeCN using a 1:1 ratio at room temperature. ^1H -NMR ($\text{DMSO-}d_6$, 300.13 MHz): δ (ppm) = 7.93 (m, 14H), 1.81 (m, 6H). ^{19}F -NMR ($\text{DMSO-}d_6$, 282.37 MHz): δ (ppm) = -60.12 (s, 6F), -143.05 (s, 2F). IR(MeCN): $\nu(\text{CN}) = 2075$; $\nu(\text{CO}) = 1965, 1931, 1892$. ESI-MS (m/z): 449.98 $[\text{M}]^{2-}$.

3.3.7 Characterisation of the dianion $[\text{Fe}_2(\text{pdt})(\text{CO})_4(\text{CN})_2 \cdot (\text{Bis-urea}(\mathbf{11}))_2]^{2-}$



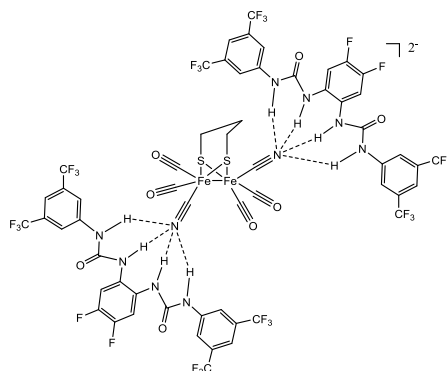
The *title anion* is formed in situ when bis-urea **11** is combined with $(\text{NEt}_4)_2[\text{Fe}_2(\text{pdt})(\text{CO})_4(\text{CN})_2]$ **14** in MeCN using a 2:1 ratio. IR(MeCN): $\nu(\text{CN}) = 2075, 2048; \nu(\text{CO}) = 1967, 1933, 1894$. ESI-MS (m/z): 709.03 $[\text{M}]^{2-}$.

3.3.8 Characterisation of the dianion $[\text{Fe}_2(\text{pdt})(\text{CO})_4(\text{CN})_2 \cdot \text{Bis-urea}(\mathbf{12})]^{2-}$



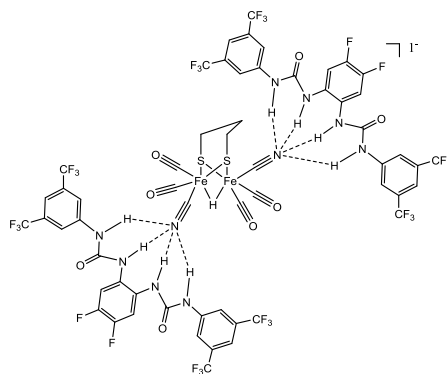
The *title anion* is formed in situ when bis-urea **12** is combined with $(\text{NEt}_4)_2[\text{Fe}_2(\text{pdt})(\text{CO})_4(\text{CN})_2]$ **14** in MeCN using a 1:1 ratio. ^1H -NMR ($\text{DMSO}-d_6$, 300.13 MHz): δ (ppm) = 7.76 (m, 12H), 1.81 (m, 6H). ^{19}F -NMR ($\text{DMSO}-d_6$, 282.37 MHz): δ (ppm) = -63.48 (s, 12F), -144.29 (s, 2F). IR(MeCN): $\nu(\text{CN}) = 2075; \nu(\text{CO}) = 1967, 1932, 1895$. ESI-MS (m/z): 517.97 $[\text{M}]^{2-}$.

3.3.9 Characterisation of the dianion $[\text{Fe}_2(\text{pdt})(\text{CO})_4(\text{CN})_2 \cdot (\text{Bis-urea}(\mathbf{12}))_2]^{2-}$



The *title anion* is formed in situ when bis-urea **12** is combined with $(\text{NEt}_4)_2[\text{Fe}_2(\text{pdt})(\text{CO})_4(\text{CN})_2]$ **14** in MeCN using a 2:1 ratio. IR(MeCN): $\nu(\text{CN}) = 2075, 2042$; $\nu(\text{CO}) = 1969, 1934, 1898$. ESI-MS (m/z): 845.01 $[\text{M}]^{2-}$.

3.3.10 Characterisation of the anion $[\text{Fe}_2(\text{pdt})(\mu\text{-H})(\text{CO})_4(\text{CN})_2 \cdot (\text{Bis-urea}(\mathbf{12}))_2]^{-}$



The *title anion* is formed in situ when bis-urea **12** is combined with $(\text{NEt}_4)_2[\text{Fe}_2(\text{pdt})(\text{CO})_4(\text{CN})_2]$ **14** in MeCN using a 2:1 ratio, and then 3 equivalents of $\text{HBF}_4 \cdot \text{OEt}_2$ are added. IR(MeCN): $\nu(\text{CN}) = 2189, 2129$; $\nu(\text{CO}) = 2052, 2035, 1996$.

4 Intimate linking of a photoactive Ru(II) centre to a diiron subsite analogue via bridging cyanide

4.1 Introduction

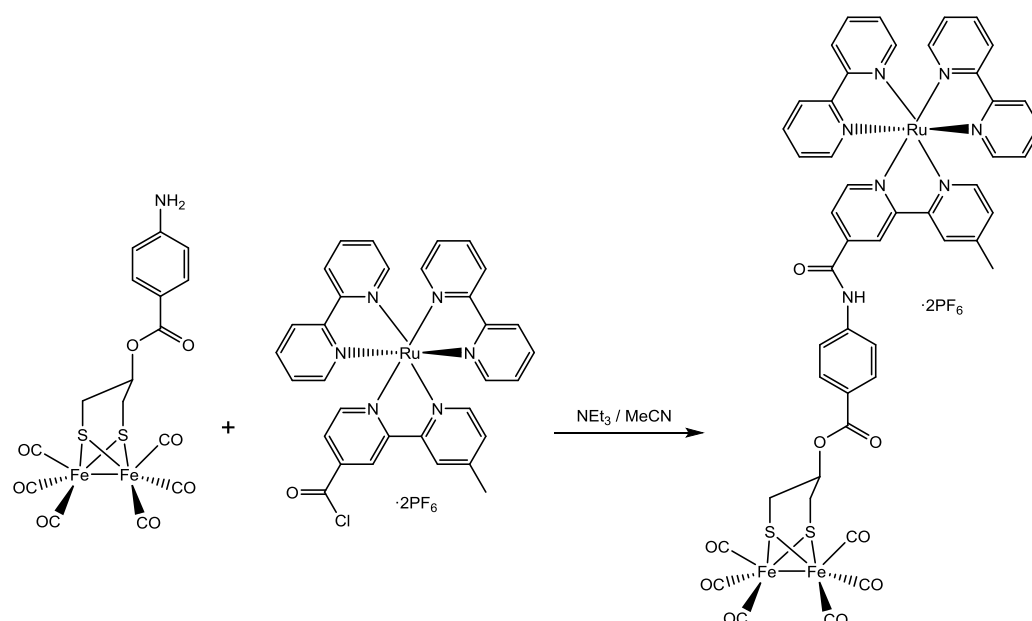
4.1.1 General aspects

This chapter is concerned with the second coordination sphere interactions of cyanide ligands with a ruthenium(II)-based photosensitiser system, in order to construct a cyanide-bridged dyad system. The importance of the interactions of the cyanide groups present in the natural system was explained in **Chapter 3**, though whereas previously in the fluorinated bis-urea work the H-bonding potential of the cyanide groups was exploited, in this chapter the Lewis basicity of the cyanide group is utilised in order to synthesise new compounds by adduct formation.

In the next sections the main reasons for interest in photosensitised hydrogenase mimic systems will be outlined, along with a brief summary of reported photosensitised systems and the reasons why Ru(II)-bipyridine derived systems are ideal candidates to use as photosensitisers. Following on from that, the successful synthesis of the novel $[\text{Fe}_2(\text{pdt})(\text{CO})_4(\text{CN})(\mu\text{-CN})\text{Ru}(\text{tpy})(\text{bpy})]$ dyad will be described, with the physical and electronic properties of this species being subsequently explored.

4.1.2 Photosensitised [FeFe]-hydrogenase mimic systems

There has been much interest in the utilisation of sunlight to drive hydrogenase subsite mimic systems, as this would truly allow a renewable alternative to fossil fuels¹⁰². To achieve photo-driven hydrogen evolution, a typical approach is the linking of a photosensitising group to the subsite analogue unit. Two different strategies have been put forward to achieve this linking: functionalisation of the dithiolate bridgehead, and anchoring the sensitiser to one of the Fe atoms in the diiron core¹⁰³. The first reported attempt at a photosensitised [FeFe]-hydrogenase subsite analogue system was by Sun and coworkers¹⁰⁴ in 2003 where the bridgehead functionalisation method was employed, with a Ru(II)-bipyridine unit covalently linked via a bridging 4-amino-benzoic acid group, as shown in **Scheme 4.1**.



Scheme 4.1. Synthesis of the first photosensitized [FeFe]-hydrogenase subunit analogue system, where a Ru(II)-bipyridine unit is covalently linked via the dithiolate bridgehead. Adapted from reference¹⁰⁴.

This was appealing experimental work as it proved the concept that attaching a photosensitising group was synthetically achievable, though the system was fundamentally flawed as the assembled complex was capable of minimal communication between the Ru and FeFe centres. This lack of communication is best illustrated using the IR spectrum of the complex when compared to that of a reference spectrum, the BOC-protected derivative of the 4-amino-benzoic acid bridgehead-functionalised starting material, as shown in **Figure 4.1**.

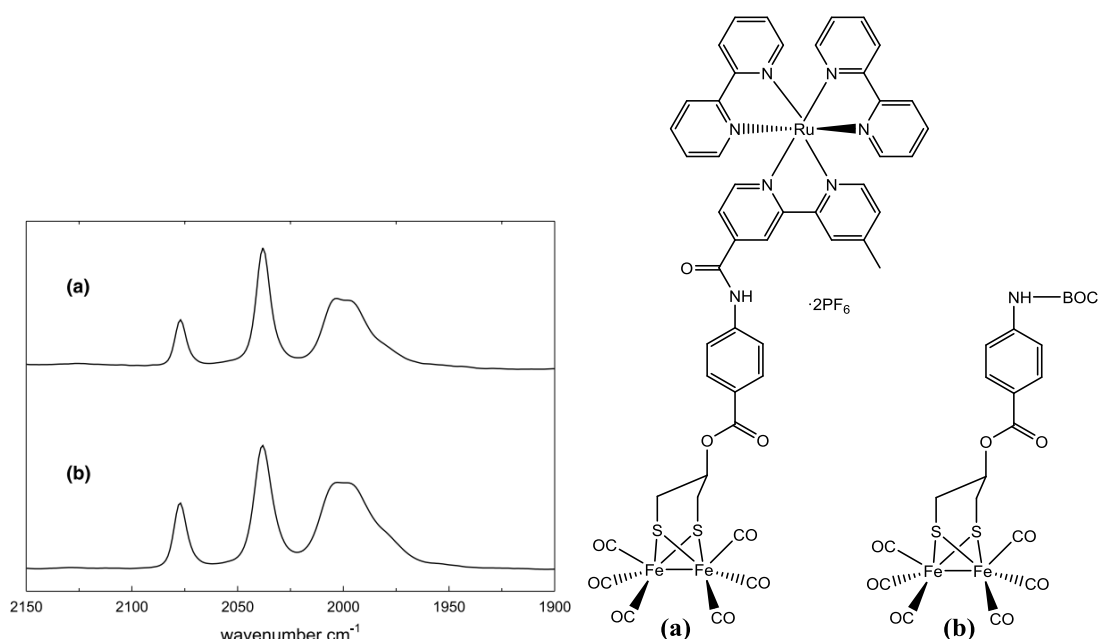
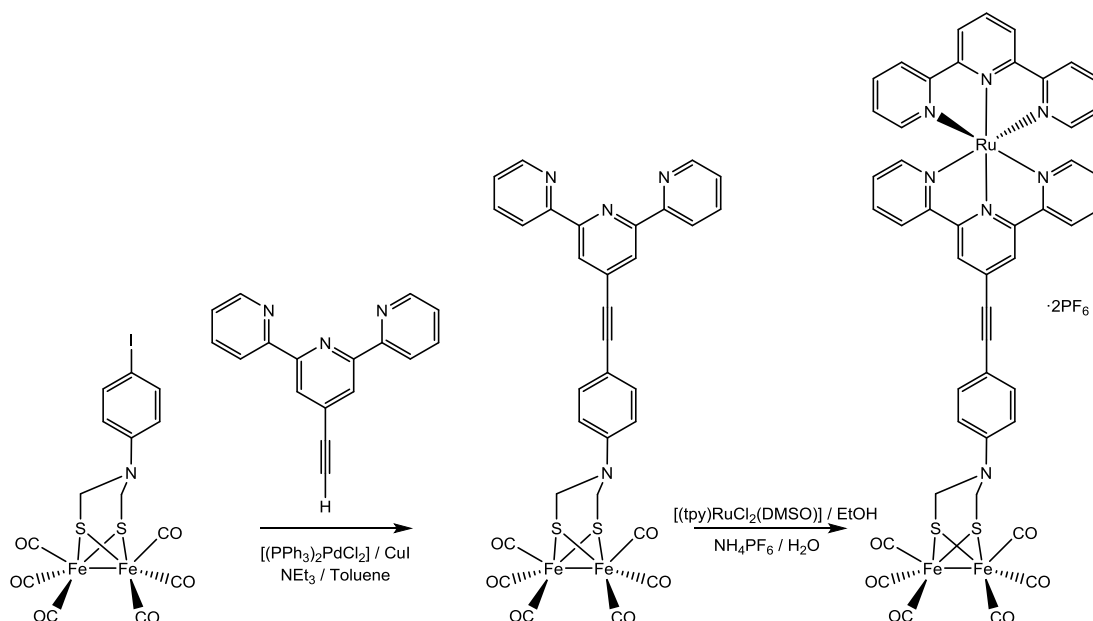


Figure 4.1. IR spectrum of the Ru(II)-coupled system compared to the reference BOC-protected analogue. Spectra reproduced from reference¹⁰⁴.

The IR spectrum of the Ru(II)-coupled system shows the characteristic peaks from the carbonyl ligands and is essentially identical to the non ruthenium-containing reference spectrum. As the carbonyl ligands act as antennae sensitive to changes in electron density on the FeFe core, if there was significant communication between the photosensitive component and the FeFe moiety, then the IR spectrum would be noticeably affected. Enabling strong communication between the photosensitising group and the diiron core has proven to be a major obstacle in the construction of photosensitised [FeFe]-hydrogenase subsite analogue systems, as without this the only significant benefit of such a non-communicating system is that the stoichiometry of photosensitiser and diiron unit can be accurately controlled. To synthesise a dyad system that exhibits good communication between the photosensitiser and the diiron moiety has become a target in this area of [FeFe]-hydrogenase subsite analogue chemistry, and one of the simplest and most effective methods of assessing this communication has been shown to be FTIR spectroscopy, due to the position of the CO stretches providing excellent indication of change (or lack of) in the electronic properties of the FeFe core.

The next attempt at a photosensitised [FeFe]-hydrogenase subsite analogue system by Sun and coworkers¹⁰⁵ aimed to improve the internal communication by means of a bridging acetylene group.



Scheme 4.2. Synthesis of the second photosensitised [FeFe]-hydrogenase subsite analogue system, where a Ru(II)-terpyridine unit is covalently linked via an acetylene moiety to the dithiolate bridgehead. Adapted from reference¹⁰⁵.

Despite the attempt to improve communication between the Ru(II) photosensitiser group and the FeFe centre by conjugation, the IR spectrum again showed no significant communication between the two centres. The most significant impact of this work was to show novel functionalisation of diiron units incorporating the azadithiolate (adt) bridgehead, which at this point in 2004 were known but not extensively explored¹⁰⁶⁻¹⁰⁸.

There have been many attempts to link a photosensitising group to a [FeFe]-hydrogenase subsite analogue system by means of functionalisation of the dithiolate bridgehead, including porphyrin¹⁰⁹, zinc¹¹⁰ and silicon¹¹¹-based systems, examples of which are shown in **Figure 4.2**; though they all suffer from the fundamental flaw that there is no significant communication between the photosensitiser and the FeFe core.

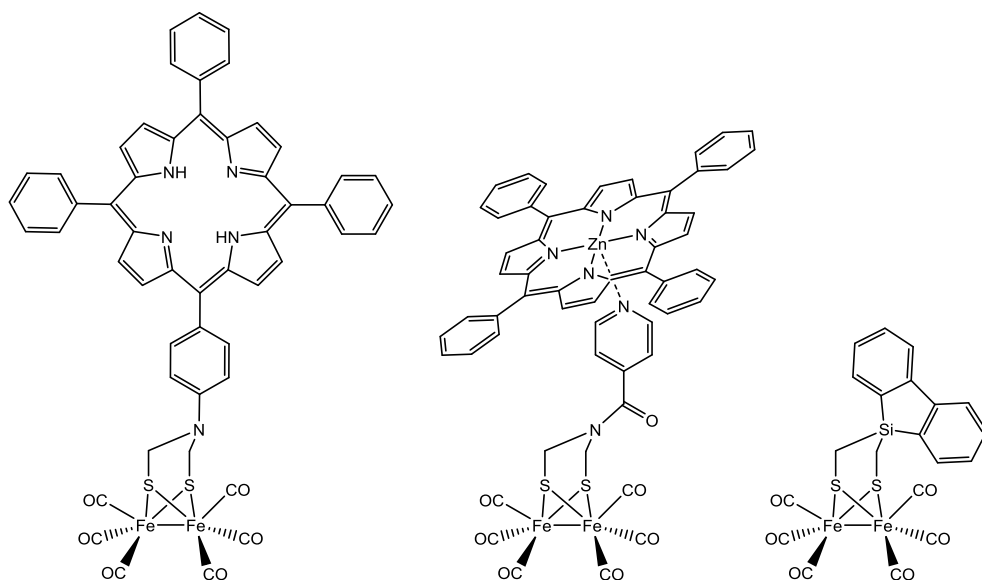


Figure 4.2. Porphyrin, zinc and silicon-based photosensitised FeFe systems where attachment of photosensitiser has been via bridgehead functionalisation. Adapted from references¹⁰⁹⁻¹¹¹.

Focus then switched to another approach; the anchoring of the sensitiser to one of the Fe atoms in the diiron core. In 2006, Ott and coworkers¹¹² were able to synthesise a FeFe subsite analogue with a Ru(II)-bipyridine unit attached via a phosphine group coordinated to one of the Fe atoms, as shown in **Figure 4.3**.

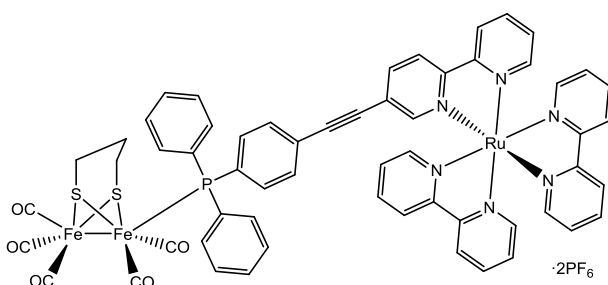


Figure 4.3. Ru(II)-bipyridine unit attached via a phosphine group to an Fe atom on a diiron subsite analogue. Adapted from reference¹¹².

Despite Ott's phosphine-linking approach allowing the attachment of the Ru(II)-bipyridine unit to one of the Fe atoms directly, the IR spectra of the complex still showed there was minimal communication between the diiron centre and the

photosensitiser moiety¹¹². The problem in this case was not the same as in the bridge-functionalised examples where communication was essentially non-existent via the thiolate groups, it was that electronic communication necessitated transmission through 10 atoms. This was a trend observed for many attempted systems that attached the photosensitising group via coordination to one of the Fe atoms at the diiron core; in order to incorporate the photosensitiser the required functionality was too complex and/or bulky to allow significant communication between the FeFe centre and the photosensitising group. Some reported examples of systems with the photosensitiser attached to one of the Fe atoms are given in **Figure 4.4**.

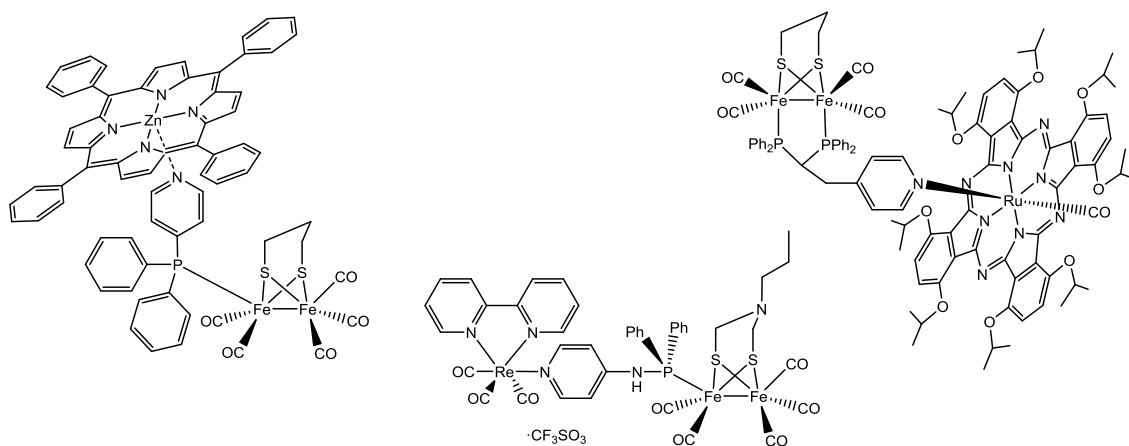
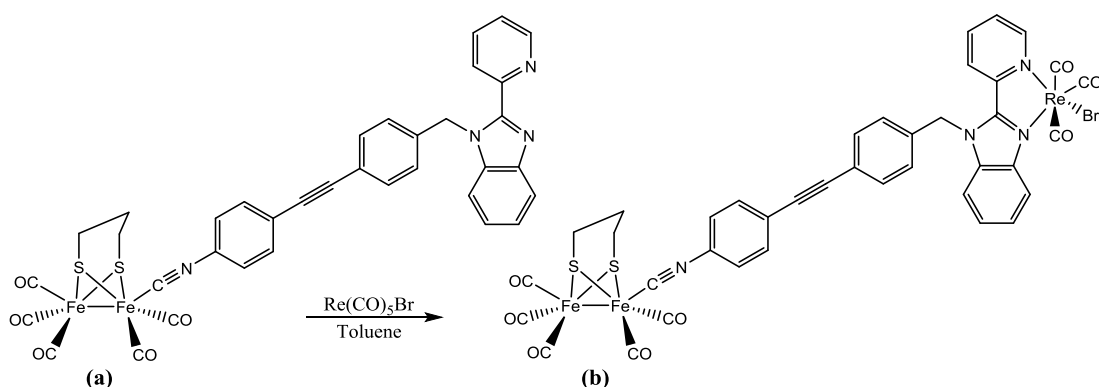


Figure 4.4. Example systems with the photosensitiser attached via anchoring to one of the Fe atoms in the diiron core. Adapted from references¹¹³⁻¹¹⁵.

In order to improve internal communication, in 2010 Wu and coworkers¹¹⁶ used cyanide as the linker ligand to the FeFe centre. They took their inspiration from nature, noticing that the natural system employed cyanide bridges, and the interactions of which, to help control the electron density on the diiron core (see **Chapter 3**). They believed that the cyanide group, with its linear, rigid and conjugated bridge would provide better communication between photosensitiser and FeFe core than the phosphine-derived systems. However this required additional functionality to introduce the photosensitising group (this time a rhenium moiety) meaning that communication within the system, as demonstrated by the IR spectra, was minimal.



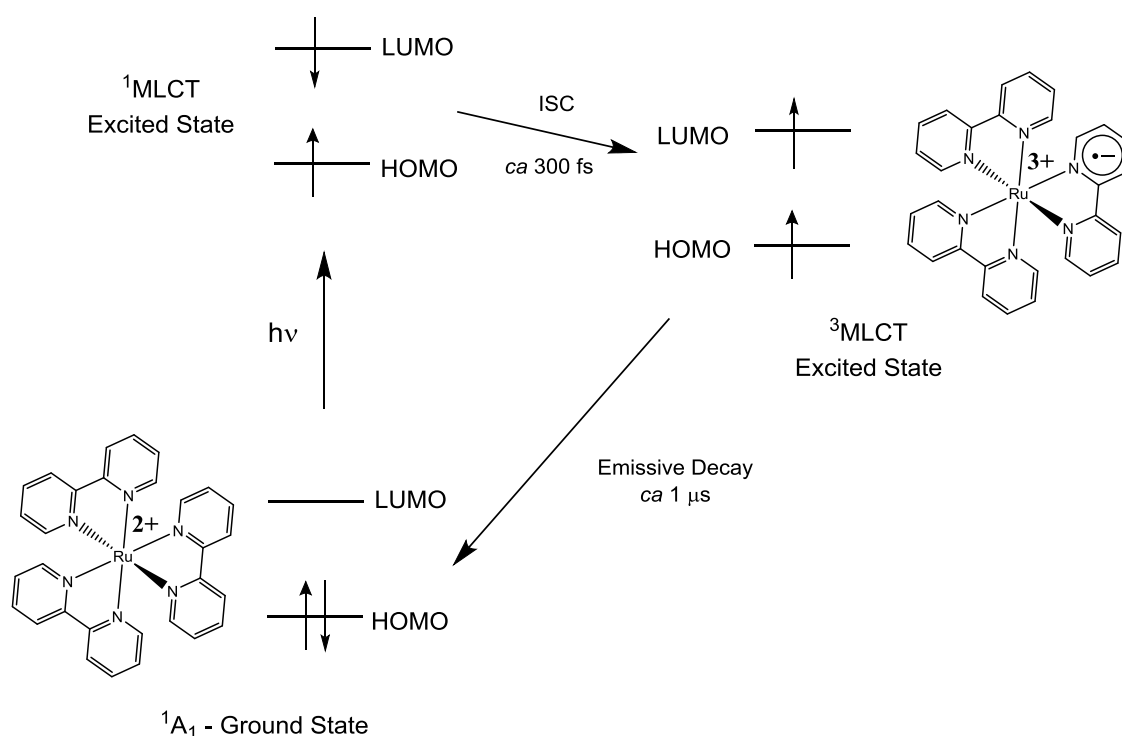
Compound	$\nu(\text{CN}) / \text{cm}^{-1}$	$\nu(\text{CO}) / \text{cm}^{-1}$
a $[\text{Fe}_2(\text{pdt})(\text{CO})_5(\text{CN})\cdot\text{Ligand}]$	2126	2038, 1997, 1967
b $[\text{Fe}_2(\text{pdt})(\text{CO})_5(\text{CN})\cdot\text{Ligand}\cdot\text{Re}(\text{CO})_3\text{Br}]$	2124	2038, 2020, 1998, 1967, 1896

Figure 4.5. Rhenium photosensitising group attached via bridging cyanide with IR data demonstrating minimal communication between the Re and FeFe centres. Adapted from reference¹¹⁶.

However, despite Wu's system not exhibiting much communication between the photosensitiser and the FeFe centre, the use of a bridging cyanide ligand could prove very interesting. In **Chapter 3** the coordination of fluorinated bis-ureas via hydrogen bonding was shown to have significant effects on the diiron core, and so linking a photosensitising group via a bridging cyanide with its linear, rigid and conjugated bridge may be a promising avenue to explore. However, instead of employing a complex and bulky system to attach the photosensitiser, *direct* linkage of the photosensitising group via a bonding arrangement Metal-N \equiv C-FeFe may provide an extremely intimate linking mechanism capable of significant communication between the photosensitising moiety and the FeFe core. At the time of writing no such systems have been reported, and in this work the creation of the first such system is attempted.

4.1.3 The advantages of Ru(II)-bipyridine systems as photosensitisers

There has been much interest in Ru(II) 2,2'-bipyridyl systems as it is one of the few transition metal complexes that luminesces strongly in solution at room temperature and exhibits powerful photosensitisation capacity for electron- and energy-transfer processes¹¹⁷. The advantages of $[\text{Ru}(\text{bpy})_3]^{2+}$ systems and their derivatives are numerous; they have good air and moisture stability, $[\text{Ru}(\text{bpy})_3]^{2+}$ systems absorb in a broad range of UV and visible light, and, most importantly, generated excited states have comparatively long lifetimes¹¹⁸. These long lifetimes are brought about by relatively fast intersystem crossing mechanisms, allowing further chemistry to take place before the complex relaxes to the ground state, as shown in **Scheme 4.3**.



Scheme 4.3. Diagram showing the photoexcitation and relaxation of a $[\text{Ru}(\text{bpy})_3]^{2+}$ system. Adapted from reference¹¹⁹.

The relatively fast intersystem crossing pathway (ca 300 fs) allows the singlet excited state formed on photoexcitation to generate a triplet excited state. This triplet state is then comparatively long-lived (ca 1 μs) as decay back to the singlet ground state is formally spin-forbidden, and is thus a slow process¹²⁰. Together with the structure of the

molecule allowing delocalisation of the excited electron across the bipyridine system, the generation of the excited triplet state allows an excited molecule of relatively long lifetimes; including 890 ns in acetonitrile and 650 ns in water¹²¹.

This comparatively long lifetime of the excited species allows further chemistry to take place before relaxation. The excited species essentially behaves as an Ru^{3+} complex containing a $(\text{bpy})^-$, which is not unlike the photosynthetic assembly, which features the separation of an electron and a hole¹²². This is particularly useful, as the $(\text{bpy})^-$ can then act as a strong reductant, as $\{\text{bpy}/\text{bpy}^{\bullet-}\} = -1.39 \text{ V (vs SCE)}^{123}$, and/or the Ru^{3+} can then act as a strong oxidant, as $\{\text{Ru}^{\text{III}}/\text{Ru}^{\text{II}}\} = +1.29 \text{ V (vs SCE)}^{124}$. Depending on the reaction environment, such as whether protons are present or not, these processes could cause interesting chemistry to occur in an attached redox-capable unit, such as a $[\text{FeFe}]$ -hydrogenase subsite analogue.

4.1.4 Further interest in ligated cyanide groups

In **Chapter 3** the research interest in the cyanide ligands coordinated to $[\text{FeFe}]$ -hydrogenase subsite analogues was discussed; namely the hydrogen bonding observed in the natural enzyme, Rauchfuss' BAr^{F} experiments, and the suggested CN linkage isomerism observed when a cyanide-functionalised diiron subsite analogue was incorporated into a HydF maturase. To further explore the effects of perturbing the cyanide ligands, some recent research has been towards studying interactions of these cyanide groups with Lewis acidic metal-containing moieties. During the undertaking of this body of work, Darensbourg and coworkers¹²⁵ reported the synthesis of a catalogue of compounds where piano-stool Fe moieties had been linked to $[\text{FeFe}]$ -hydrogenase subsite analogues via bridging cyanide ligands.

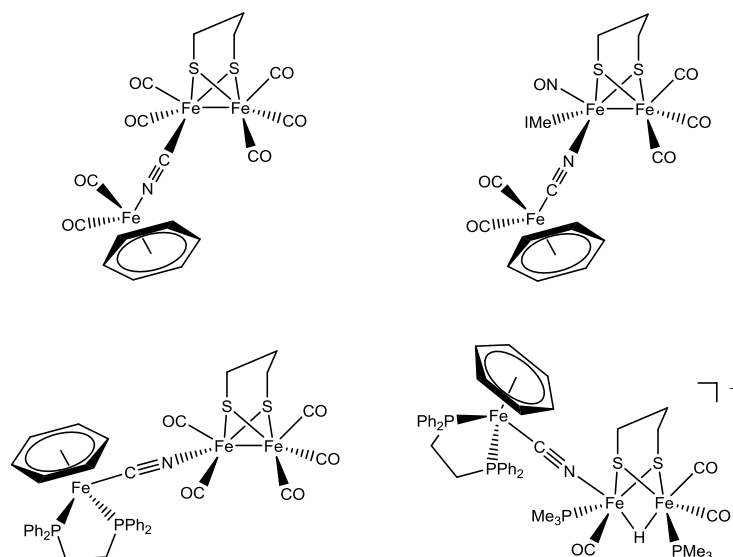


Figure 4.6. [FeFe]-hydrogenase subunit analogues joined to piano-stool Fe moieties via bridging cyanide. Adapted from reference¹²⁵.

The purpose of Darensbourg's work was to investigate the proposed CN linkage isomerism observed when a cyanide-functionalised diiron subunit analogue was incorporated into a HydF maturase (described in **Chapter 3**). As manoeuvres such as CN flipping subsequent to adduct formation are uncommon^{126,127}, a series of triiron systems was prepared. The orientation of the CN bridges was shown to be determined by the precursor agents, with no isomerisation observed. Furthermore, a series of DFT calculations were performed to evaluate the energetics of such systems, and found excessively high energy barriers accounting for the failure to observe any isomerisation.

The synthetic work reported by Darensbourg and coworkers was based on previous work of Zhu and Vahrenkamp¹²⁸ who reported the synthesis of many cyanide-bridged metal complexes of the type $M-N\equiv C-M'$ and $M-C\equiv N-M'$. Zhu and Vahrenkamp stated that the simplest method of forming cyanide-bridged species was by labile ligand substitution, and that the electropositive character of the two metal centres should be in a 'judicious balance'. Regarding this information, firstly, a labile ligand substitution approach would be employed in this work to attach the Ru(II) photosensitising group to the FeFe core. Secondly, the electropositive character of the proposed Ru and Fe metal centres were already known to be in 'balance' as the compound $(PPh_4)[Ru(tpy)(bpy)(\mu-NC)Fe(CN)_5]$ had been successfully synthesised and characterised by X-ray crystallography in 2011 by Baraldo and coworkers¹²⁹.

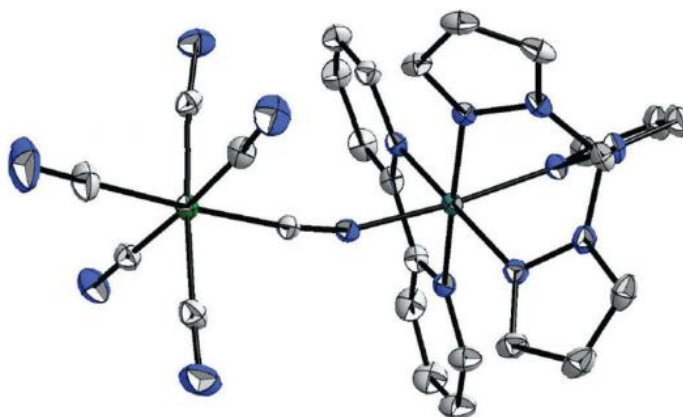


Figure 4.7. Thermal ellipsoid plot of $[\text{Ru}(\text{tpy})(\text{bpy})(\mu\text{-NC})\text{Fe}(\text{CN})_5]^{1-}$ at 30% probability with H atoms, counter ions and solvent molecules omitted for clarity. Image reproduced from reference¹²⁹.

In order to synthesise a successful photosensitised [FeFe]-hydrogenase subsite analogue system there must be significant communication between the photosensitising unit and the diiron subsite analogue. A bridging cyanide ligand, with its linear, rigid and conjugated system if linked directly to the photosensitising group via a bonding arrangement $\text{Metal-N}\equiv\text{C-FeFe}$ may provide an extremely intimate linking mechanism capable of such communication. The work of Darensbourg¹²⁵ has shown that Lewis acidic metal moieties can be adducted to the cyanide ligands on FeFe analogues, and the study of Ru(II)-bipyridine systems has shown that these would be ideal candidates to employ as the photosensitising moiety. Finally, the work of Baraldo¹²⁹ has demonstrated that $\text{Ru-N}\equiv\text{C-Fe}$ complexes are synthetically achievable, thus making a dyad system such as $[\text{Fe}_2(\text{pdt})(\text{CO})_4(\text{CN})(\mu\text{-CN})\text{Ru}(\text{tpy})(\text{bpy})]$ an attractive prospect.

4.1.5 Mechanistic advantages of a $[\text{Fe}_2(\text{pdt})(\text{CO})_4(\text{CN})(\mu\text{-CN})\text{Ru}(\text{tpy})(\text{bpy})]$ system

The proposed dyad to be synthesised is given in **Figure 4.8**. Such a system, with its bridging cyanide ligand could be capable of fast electron transfer between the FeFe core and the Ru(II) photosensitising group.

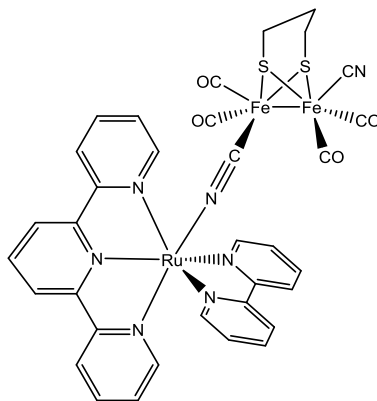


Figure 4.8. Proposed dyad $[\text{Fe}_2(\text{pdt})(\text{CO})_4(\text{CN})(\mu\text{-CN})\text{Ru}(\text{tpy})(\text{bpy})]$.

This possible fast electron transfer may allow the detection and isolation of a mixed valence bridging CO state. A CO switching from a terminal to a bridging mode is believed to be critical in opening a site for protonation¹³⁰⁻¹³⁵, and so there have been many attempts to achieve structures that contain such groups. In 2007, Pickett and coworkers¹³⁶ were able to obtain a X-ray structure of two diiron units bridged by CO ligands, shown in **Figure 4.9**.

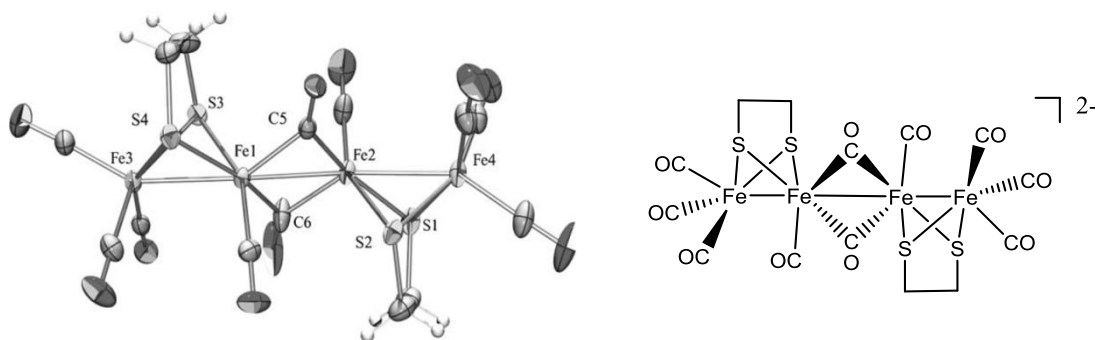
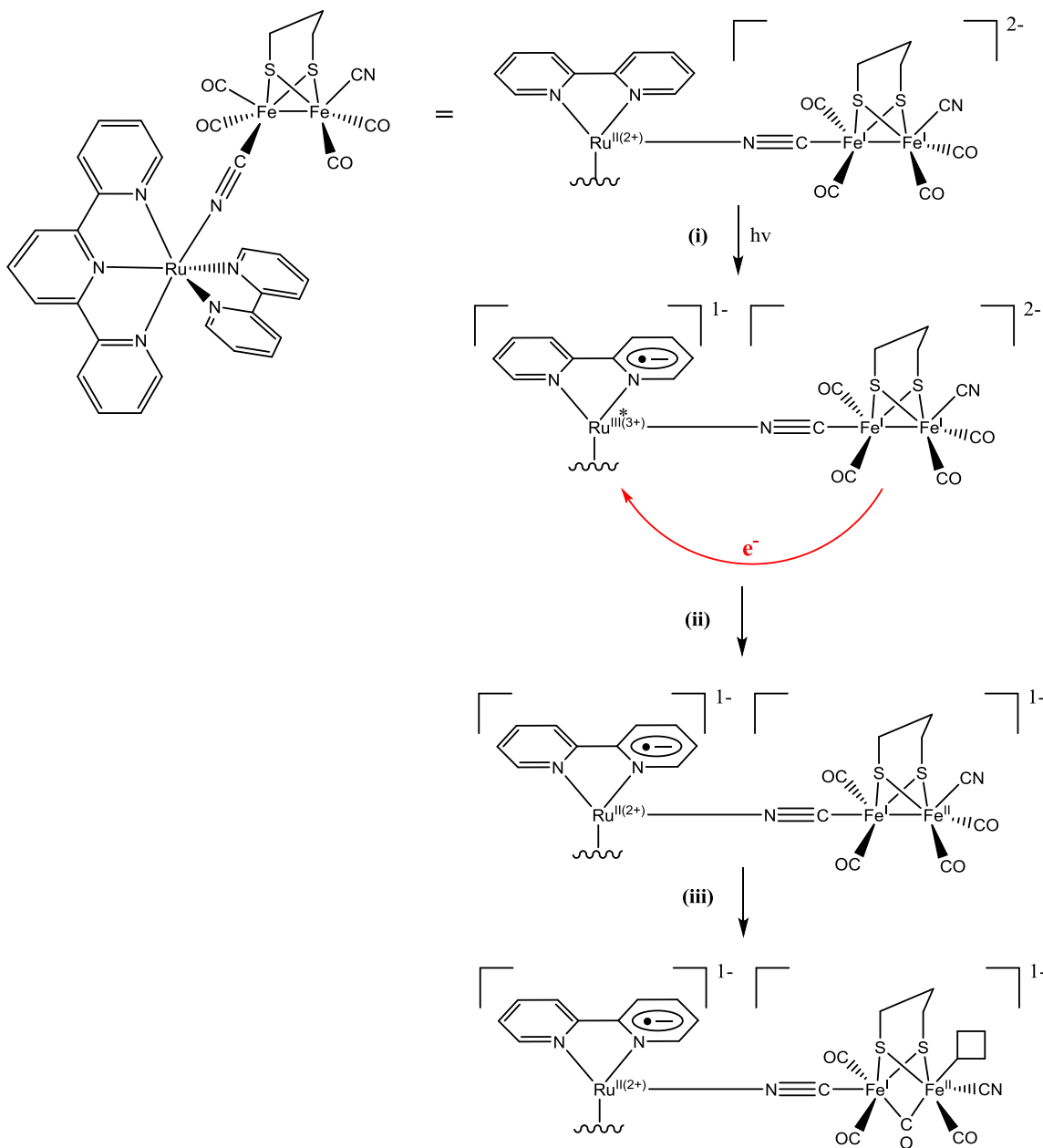


Figure 4.9. Ortep view (ellipsoids at 50% probability level) of $[\text{Fe}_4(\mu\text{-S}(\text{CH}_2)_2\text{S})_2\mu\text{-(CO)}_2(\text{CO})_8]^{2-}$. Image reproduced from reference¹³⁶.

Mixed-valence systems utilising phosphine-substituted diiron units are known^{131,137}, though mixed-valence systems incorporating cyanide ligands are much less common. Rauchfuss and coworkers^{138,139} were able to detect a transient bridging CO moiety after oxidising a cyanide-ligated system with ferrocene, but as yet this is the only reported example of this species. The proposed $[\text{Fe}_2(\text{pdt})(\text{CO})_4(\text{CN})(\mu\text{-CN})\text{Ru}(\text{tpy})(\text{bpy})]$ system may be capable of generating a bridging CO species, as shown by a suggested reaction pathway in **Scheme 4.4**.

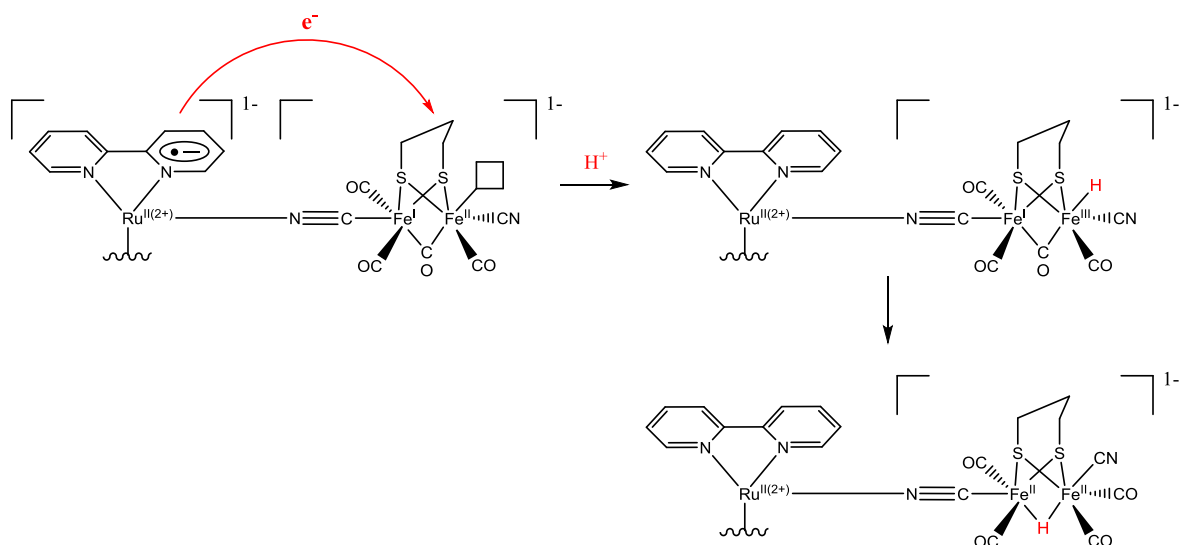


Scheme 4.4. Proposed excitation of a $[\text{Fe}_2(\text{pdt})(\text{CO})_4(\text{CN})(\mu\text{-CN})\text{Ru}(\text{tpy})(\text{bpy})]$ system to generate a bridging CO mixed valence state.

The proposed mechanism given in **Scheme 4.4.** is an idealised scheme that does not take into account competing pathways and it should be noted that at any point the system may relax from its excited state, via vibrational methods or otherwise. However, in the interest of discussing the potential for generating a mixed-valence bridging CO species **Scheme 4.4.** will suffice.

The photoexcitation step in (i) may generate the excited $\text{Ru}^{*3+}/(\text{bpy})^{\bullet-}$ system discussed in **Section 4.1.3.** which has a relatively long lifetime. Providing this excited $\text{Ru}^{*3+}/(\text{bpy})^{\bullet-}$ system exists for long enough, it may be possible for an electron from the FeFe moiety to quench the Ru^{*3+} centre in step (ii). Such a quench would depend on the cyanide bridge allowing electron transfer to take place very rapidly; though if the quenching was successful this would essentially 'lock' the excited electron in the $(\text{bpy})^{\bullet-}$ system. This quenching, if occurring, should be possible to monitor by emission spectroscopy, and would provide some very interesting scenarios. Firstly, the excited electron locked in the $(\text{bpy})^{\bullet-}$ system may be employed to reduce protons, if present in solution; a process which will be discussed shortly. Secondly, one of the Fe centres has been oxidised. As the Ru moiety is electron-withdrawing in nature, it would not be unreasonable to infer that the Fe atom distal to the Ru centre is the one oxidised to Fe^{II} . It may be possible that this Fe^{II} could rearrange its ligands in step (iii) in order to generate a mixed valence state with bridging CO. Such a species should be readily detectable by IR and would be a rare example of a mixed-valence species incorporating cyanide ligands. This is made possible by the combination of the components in the $[\text{Fe}_2(\text{pdt})(\text{CO})_4(\text{CN})(\mu\text{-CN})\text{Ru}(\text{tpy})(\text{bpy})]$ allowing the $\text{Fe}^{\text{I}}\text{Fe}^{\text{I}}$ system to be oxidised by Ru^{III} but not reduced by $(\text{bpy})^{\bullet-}$.

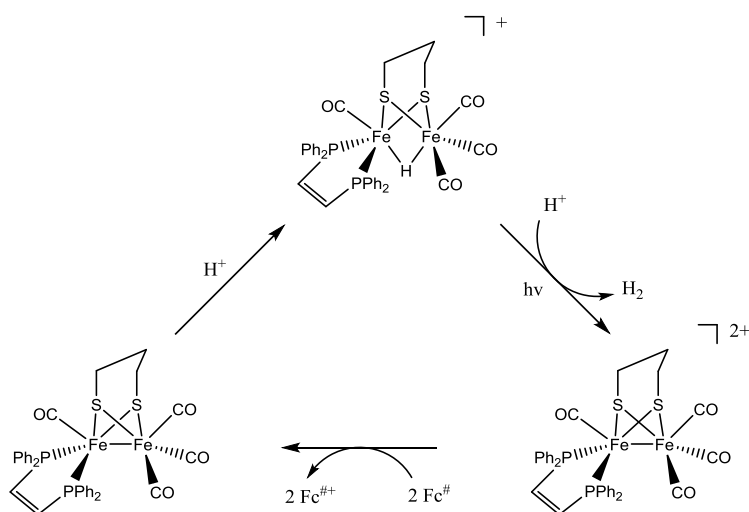
In regards to the electron locked in the $(\text{bpy})^{\bullet-}$ system being able to reduce protons, a continuation of the mechanism is given in **Scheme 4.5.** In this scheme the $\text{Fe}^{\text{I}}\text{-Fe}^{\text{II}}$ system could be protonated at the vacant site to formally give a $\text{Fe}^{\text{I}}\text{-Fe}^{\text{III}}$ species with a terminal hydride, which would then subsequently rearrange to give a bridging hydride $\text{Fe}^{\text{II}}\text{-Fe}^{\text{II}}$ system.



Scheme 4.5. Proposed action of the electron locked in the $(\text{bpy})^{\bullet-}$ system upon addition of protons to the system.

4.1.6 A photoactive unsensitised $[\text{FeFe}]$ -hydrogenase subsite system

As a final note to conclude this introduction, in 2012 Rauchfuss and coworkers¹⁴⁰ reported a diiron hydride species capable of generating hydrogen upon irradiation without the use of a photosensitiser.



Scheme 4.6. Proposed scheme of $[\text{Fe}_2(\text{pdt})(\text{CO})_4(\mu\text{-H})(\text{dppv})](\text{PF}_6)$ generating H_2 upon irradiation without the use of a photosensitiser. Adapted from reference¹⁴⁰.

Rauchfuss' proposed mechanism is given in **Scheme 4.6.** where $[\text{Fe}_2(\text{pdt})(\text{CO})_4(\mu\text{-H})(\text{dppv})]^+$ is shown to generate hydrogen when in the presence of protons and octamethylferrocene reductant and irradiated by a light source of wavelength >400 nm. Unsurprisingly such a proposed mechanism attracted a lot of research interest, prompting further investigation. In 2014, Pickett and Hunt¹⁴¹, after conducting $\text{UV}_{\text{pump}}\text{-IR}_{\text{probe}}$ experiments, in conjunction with DFT calculations, concluded that, instead of the generation of exciting photoproducts, irradiation of the sample was causing CO ligand dissociation, and that the hydrogen generation was caused by chance encounters of the compound with protons and/or octamethylferrocene in conjunction with utilising favourable redox potentials and the electronic environment of the diiron centre. Therefore the most promising method of photocatalytic hydrogen generation utilising [FeFe]-hydrogenase subsite analogues still remains to be the intimate attachment of an appropriate photosensitiser.

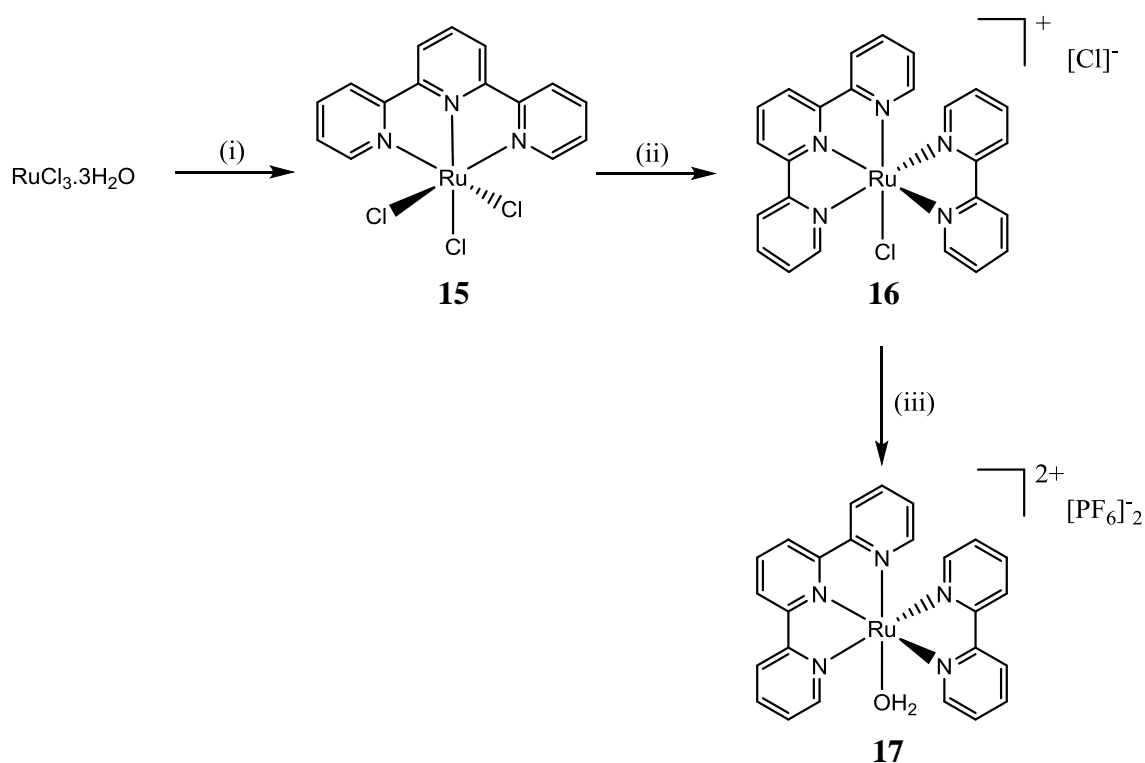
4.2 Results and discussion

4.2.1 Synthesis of the Ru(II)(tpy)(bpy).OH₂ system

The synthesis of the dicyanide subsite analogue system (Et₄N)₂[Fe₂(pdt)(CO)₄(CN)₂] **14** employed in this work was described in detail in **Chapter 3**. As was in the previous chapter where fluorinated bis-ureas were used to promote hydrogen-bonding interactions, the pdt bridgehead system was used here instead of the adt system to reduce unwanted side reactions.

A ruthenium-containing system of the type [Ru(tpy)(bpy)(OH₂)]²⁺ was employed in this work in order to promote coordination of the CN ligand to the Ru atom. Although [Ru(bpy)₃]²⁺ systems have been extensively studied, use of a terpyridine group would allow stepwise functionalisation of the Ru centre and a 'vacant' ligation site for the CN ligand to occupy. The OH₂ 'placeholder' ligand was chosen in accordance with the work of Zhu and Vahrenkamp¹²⁸ who had previously stated the merits of utilising a labile ligand substitution approach for cyanide coordination.

The synthesis of the ruthenium-containing moiety [Ru^{II}(tpy)(bpy)(OH₂)](PF₆)₂ **17** was performed stepwise from RuCl₃·3H₂O using procedures modified from the literature¹⁴²⁻¹⁴⁴.

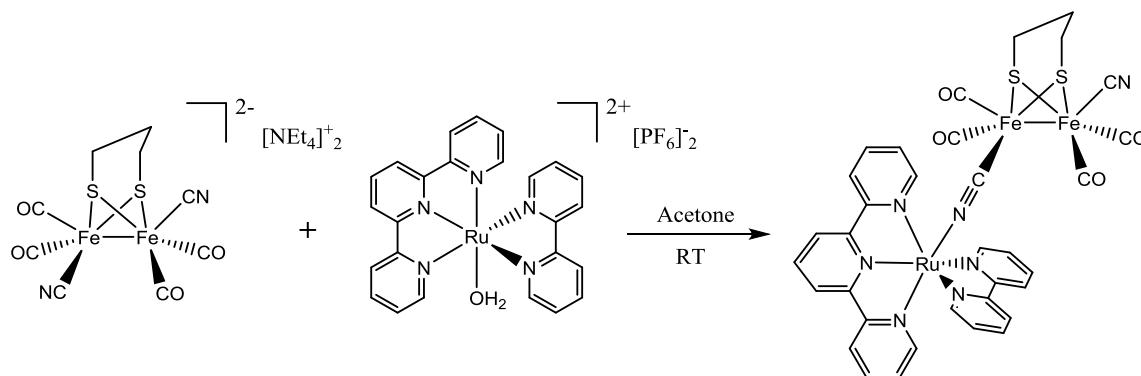


Scheme 4.7. Stepwise synthesis of $[\text{Ru}^{\text{II}}(\text{tpy})(\text{bpy})(\text{OH}_2)](\text{PF}_6)_2$ **17**. (i) 1.0 2,2',2''-terpyridine, EtOH, 90 °C, 3 h, 88%; (ii) 1.0 2,2'-bipyridine, 1.1 LiCl, 0.5% NEt₃, 3:1 EtOH/H₂O, 95 °C, 4.5 h, 55%; (iii) 2.2 AgPF₆, 3:1 Acetone/H₂O, 95 °C, 1.5 h, 92%. Procedures modified from those outlined by Meyer^{142,143} and Janiak¹⁴⁴.

The ethanol solvent helps drive step (i) to completion due to the insolubility of the $[\text{Ru}^{\text{III}}(\text{tpy})\text{Cl}_3]$ **15** product. In step (ii) lithium chloride is added to ensure a chloride ligand remains coordinated to the Ru centre, in order to prevent bipyridine-bridged dimer species. In step (iii) silver hexafluorophosphate is employed to remove the chloride ions, driving the reaction to completion by formation of the insoluble silver chloride, leaving the Ru(II) centre to ligate a water molecule which will act as a labile ligand in the subsequent reactions with diiron dicyanide species.

4.2.2 Formation of the $[\text{Fe}_2(\text{pdt})(\text{CO})_4(\text{CN})(\mu\text{-CN})\text{Ru}(\text{tpy})(\text{bpy})]$ dyad

With the starting materials $(\text{Et}_4\text{N})_2[\text{Fe}_2(\text{pdt})(\text{CO})_4(\text{CN})_2]$ **14** and $[\text{Ru}^{\text{II}}(\text{tpy})(\text{bpy})(\text{OH}_2)](\text{PF}_6)_2$ **17** in hand, it was possible to combine them to form a cyanide-bridged species. After much trial and error, it was discovered that combination of the two materials in dry degassed acetone at room temperature allowed the reaction to proceed as desired.



Scheme 4.8. Synthesis of $[\text{Fe}_2(\text{pdt})(\text{CO})_4(\text{CN})(\mu\text{-CN})\text{Ru}(\text{tpy})(\text{bpy})]$ **18**.

Upon dropwise addition of an acetone solution of $[\text{Ru}^{\text{II}}(\text{tpy})(\text{bpy})(\text{OH}_2)](\text{PF}_6)_2$ **17** to a vigorously-stirred acetone solution of $(\text{NEt}_4)_2[\text{Fe}_2(\text{pdt})(\text{CO})_4(\text{CN})_2]$ **14**, the dyad $\text{Ru-N}\equiv\text{C-FeFe}$ system precipitated out of the acetone solution as a purple powder. This purple powder is insoluble in most known solvents, except DMF and DMSO, and was shown to decompose upon dissolution in MeCN.

The initial reactions to produce $[\text{Fe}_2(\text{pdt})(\text{CO})_4(\text{CN})(\mu\text{-CN})\text{Ru}(\text{tpy})(\text{bpy})]$ **18** proved successful, though further adjustment of the reaction conditions allowed the isolation of the non-CN-bridged salt, $[\text{Fe}_2(\text{pdt})(\text{CO})_4(\text{CN})_2][\text{Ru}^{\text{II}}(\text{tpy})(\text{bpy})(\text{OH}_2)]$, also as a purple precipitate. This species was characterised by IR, and is formed by conducting the reaction at lower temperature $\sim 5\text{-}10^\circ\text{C}$ and using highly concentrated solutions of the starting materials. This non-CN-bridged salt only remains in its non-bridged form as a dry solid, with subsequent stirring in DMF allowing the bridging to take place. The non-CN-bridged salt is easily recognisable by its IR spectrum, which is almost identical to the $[\text{Fe}_2(\text{pdt})(\text{CO})_4(\text{CN})_2]^{2-}$ starting material and differs from the bridged $\text{Ru-N}\equiv\text{C-FeFe}$ system by only have one CN stretch, whereas the $\text{Ru-N}\equiv\text{C-FeFe}$ has two. To counteract the possible formation of small amounts of the non-CN-bridged salt, the revised

synthesis of $[\text{Fe}_2(\text{pdt})(\text{CO})_4(\text{CN})(\mu\text{-CN})\text{Ru}(\text{tpy})(\text{bpy})]$ **18** (given in **Section 4.3.4.**) incorporates an additional step of stirring the obtained precipitate in DMF, prior to re-isolation using dry acetone.

The synthesis of $[\text{Fe}_2(\text{pdt})(\text{CO})_4(\text{CN})(\mu\text{-CN})\text{Ru}(\text{tpy})(\text{bpy})]$ **18** has good yields (85%) and crystals suitable for X-ray diffraction were grown by slow diffusion of Et_2O into a DMF solution.

4.2.3 Structure and properties of $[\text{Fe}_2(\text{pdt})(\text{CO})_4(\text{CN})(\mu\text{-CN})\text{Ru}(\text{tpy})(\text{bpy})]$

4.2.3.1 X-ray crystallography

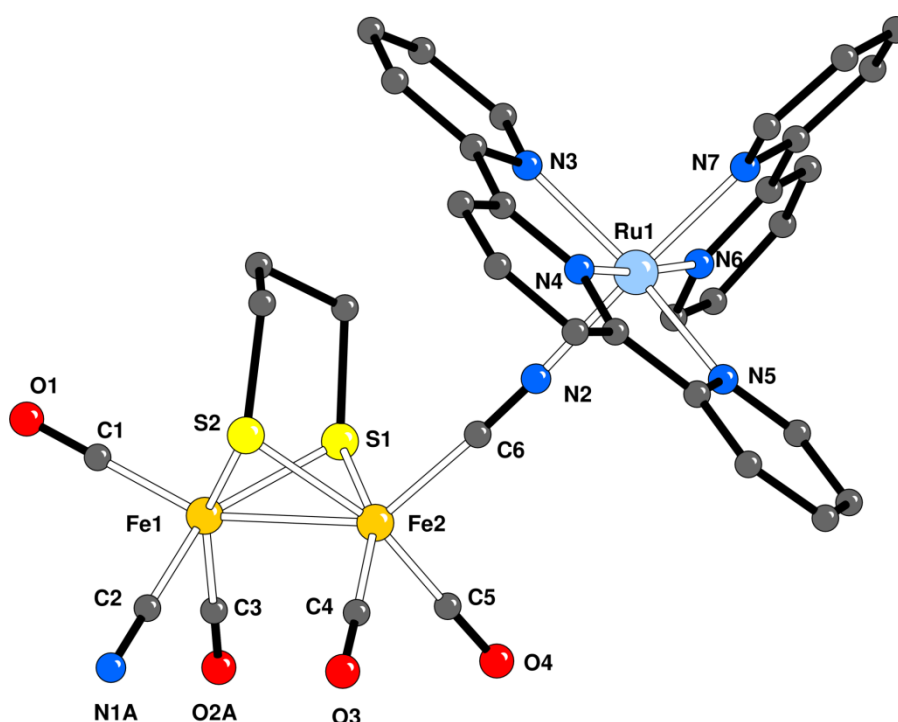


Figure 4.10 CAMERON representations of the structure of $[\text{Fe}_2(\text{pdt})(\text{CO})_4(\text{CN})(\mu\text{-CN})\text{Ru}(\text{tpy})(\text{bpy})]$ **18** with spheres of arbitrary size.

The solid state structure allows comparison of bond lengths between the $\text{Ru-N}\equiv\text{C-FeFe}$ dyad, the $[\text{Fe}_2(\text{pdt})(\text{CO})_4(\text{CN})_2]^{2-}$ starting material¹⁴⁵, the BAr^{F} complex⁸¹ $[\text{Fe}_2(\text{pdt})(\text{CO})_4(\text{CNB}(\text{C}_6\text{F}_5)_3)_2]^{2-}$ and the CN-bridged compounds synthesised by Darensbourg and coworkers¹²⁵. Some bond lengths of note are given in **Figure 4.11**.

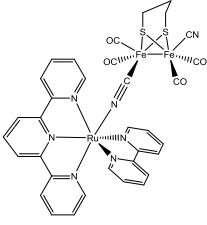
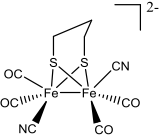
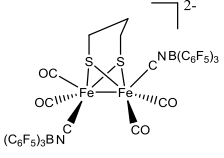
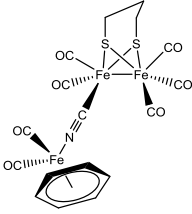
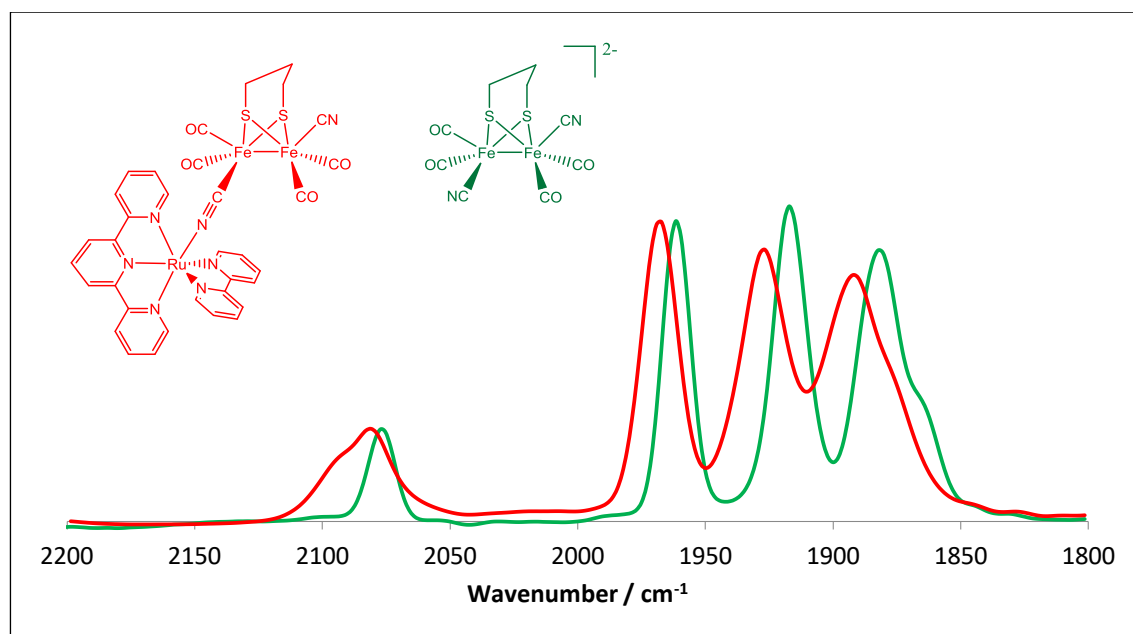
				
Bond or Equivalent				
M(Ru)···N2	2.043(5)			1.930(3)
C2···N1A	1.147(10)	1.159(7)	1.158(8)	
C6···N2	1.141(9)	1.159(7)	1.158(8)	1.152(4)
Fe2···C6	1.912(7)	1.933(7)	1.873(6)	1.918(3)
Fe1···Fe2	2.5102(15)	2.5171(12)	2.519(1)	2.522(1)

Figure 4.11 Selected bond lengths (Å) of $[\text{Fe}_2(\text{pdt})(\text{CO})_4(\text{CN})(\mu\text{-CN})\text{Ru}(\text{tpy})(\text{bpy})]$ compared to the $[\text{Fe}_2(\text{pdt})(\text{CO})_4(\text{CN})_2]^{2-}$ starting material¹⁴⁵, Rauchfuss' BARF complex⁸¹ and a comparative compound synthesised by Darensbourg and coworkers¹²⁵.

The C≡N bond lengths do not change significantly upon attachment of metal or boron Lewis acid. In the Ru-N≡C-FeFe complex the C≡N bond length of the rutheniated cyanide is essentially identical to that of the non-adducted cyanide. Fe-C bond lengths are identical within statistical error except for the BARF system where the Fe-C distances are statistically shorter by *ca* 0.04 Å. The Fe-Fe bond lengths for the four species show statistically different values at the 2σ level. The shortest bond is observed for the Ru-N≡C-FeFe species which is approximately 0.01 Å shorter than that in the Darensbourg complex.

4.2.3.2 FTIR spectroscopy

The solution FTIR spectrum of $[\text{Fe}_2(\text{pdt})(\text{CO})_4(\text{CN})(\mu\text{-CN})\text{Ru}(\text{tpy})(\text{bpy})]$ **18** was recorded in DMF and is shown in **Figure 4.12** compared to the equivalent IR spectrum of the $[\text{Fe}_2(\text{pdt})(\text{CO})_4(\text{CN})_2]^{2-}$ starting material.



Compound	$\nu(\text{CN}) / \text{cm}^{-1}$	$\nu(\text{CO}) / \text{cm}^{-1}$
$(\text{NEt}_4)_2[\text{Fe}_2(\text{pdt})(\text{CO})_4(\text{CN})_2]$	2077	1961, 1917, 1882, 1865
$[\text{Fe}_2(\text{pdt})(\text{CO})_4(\text{CN})(\mu\text{-CN})\text{Ru}(\text{tpy})(\text{bpy})]$	2093, 2081	1968, 1927, 1892

Figure 4.12 Solution FTIR spectra in DMF of $[\text{Fe}_2(\text{pdt})(\text{CO})_4(\text{CN})(\mu\text{-CN})\text{Ru}(\text{tpy})(\text{bpy})]$ **18** compared to $(\text{NEt}_4)_2[\text{Fe}_2(\text{pdt})(\text{CO})_4(\text{CN})_2]$ **14**.

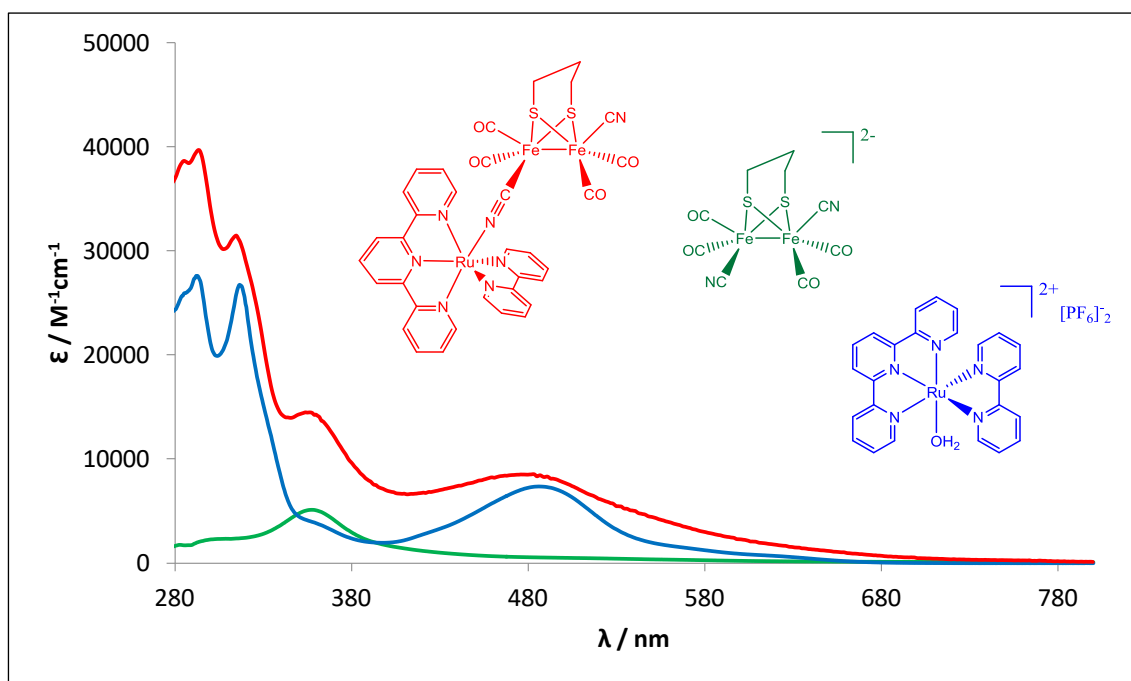
This IR data reveals several key pieces of information. Firstly, upon attachment of the Lewis acidic Ru(II) moiety the CO stretches have shifted to higher wavenumbers. This is consistent with the Ru(II) group binding to the cyanide ligand via adduct formation, withdrawing electron density from the FeFe core and reducing back donation into the π^* antibonding orbitals of CO. This is an important result as it demonstrates that there is direct and significant communication between the Ru centre and the FeFe core, a property much desired in photosensitised [FeFe]-hydrogenase subsite analogue systems,

as explained in **Section 4.1.2**. From the IR perspective, this implies that the photosensitising group and the diiron centre are linked by a more intimate system than those previously reported, and thus the potential of such a photosensitised system is very promising.

Secondly, upon attachment of the Ru(II) group there is an emergence of a second cyanide stretch. This would also be in agreement with the attachment of the photosensitiser, as the two cyanide groups ligated to the FeFe core are no longer equivalent. The new CN stretch appearing at higher wavenumber (2093 cm^{-1}) would be consistent with the kinematic effect of constraining the CN motion by double attachment¹⁴⁴, and the non-adducted CN stretch is shifted slightly (4 cm^{-1}) to higher wavenumbers in accordance with diminished back donation into the π^* orbitals of CN.

4.2.3.3 UV-vis spectroscopy

The UV-vis spectrum of $[\text{Fe}_2(\text{pdt})(\text{CO})_4(\text{CN})(\mu\text{-CN})\text{Ru}(\text{tpy})(\text{bpy})]$ **18** was recorded in degassed DMF and is shown in **Figure 4.13** compared to the equivalent UV-vis spectra of the two starting materials, $(\text{NEt}_4)_2[\text{Fe}_2(\text{pdt})(\text{CO})_4(\text{CN})_2]$ **14** and $[\text{Ru}^{\text{II}}(\text{tpy})(\text{bpy})(\text{OH}_2)](\text{PF}_6)_2$ **17**.



Compound	Transitions λ / nm, ϵ / $\text{M}^{-1}\text{cm}^{-1}$
$[\text{Fe}_2(\text{pdt})(\text{CO})_4(\text{CN})(\mu\text{-CN})\text{Ru}(\text{tpy})(\text{bpy})]$	294 nm, 39665 $\text{M}^{-1}\text{cm}^{-1}$ ($\pi - \pi^*$) 315 nm, 31457 $\text{M}^{-1}\text{cm}^{-1}$ ($\pi - \pi^*$) 356 nm, 14457 $\text{M}^{-1}\text{cm}^{-1}$ (Fe-Fe) 481 nm, 8492 $\text{M}^{-1}\text{cm}^{-1}$ (MLCT)
$(\text{NEt}_4)_2[\text{Fe}_2(\text{pdt})(\text{CO})_4(\text{CN})_2]$	358 nm, 5099 $\text{M}^{-1}\text{cm}^{-1}$ (Fe-Fe)
$[\text{Ru}^{\text{II}}(\text{tpy})(\text{bpy})(\text{OH}_2)](\text{PF}_6)_2$	292 nm, 27594 $\text{M}^{-1}\text{cm}^{-1}$ ($\pi - \pi^*$) 316 nm, 26739 $\text{M}^{-1}\text{cm}^{-1}$ ($\pi - \pi^*$) 486 nm, 7355 $\text{M}^{-1}\text{cm}^{-1}$ (MLCT)

Figure 4.13 UV-vis spectra of $[\text{Fe}_2(\text{pdt})(\text{CO})_4(\text{CN})(\mu\text{-CN})\text{Ru}(\text{tpy})(\text{bpy})]$ **18**, $(\text{NEt}_4)_2[\text{Fe}_2(\text{pdt})(\text{CO})_4(\text{CN})_2]$ **14** and $[\text{Ru}^{\text{II}}(\text{tpy})(\text{bpy})(\text{OH}_2)](\text{PF}_6)_2$ **17** in degassed DMF.

The UV-vis spectrum of the dyad species $[\text{Fe}_2(\text{pdt})(\text{CO})_4(\text{CN})(\mu\text{-CN})\text{Ru}(\text{tpy})(\text{bpy})]$ **18** exhibits characteristics of both the FeFe and Ru centres and is essentially an additive spectrum. There are no new bands indicative of Ru(II)-Fe CT, though this is not unexpected as remote metal ligand charge transfer (RMLCT) bands of Ru-NC species have been shown to have comparatively very low intensity and do not have a significant impact on absorption profiles¹⁴⁷.

4.2.3.4 Emission spectroscopy

In **Section 4.1.5.**, the potential mechanistic advantages of a $[\text{Fe}_2(\text{pdt})(\text{CO})_4(\text{CN})(\mu\text{-CN})\text{Ru}(\text{tpy})(\text{bpy})]$ system were outlined, with a possible mechanism leading towards a mixed-valence bridging CO species given in **Scheme 4.4**. An important part of that mechanism was the possibility of the $\text{Ru-N}\equiv\text{C-FeFe}$ system, via its bridging CN ligand, to allow fast electron transfer from the FeFe centre in order to quench the Ru^{*3+} moiety. If possible, this quenching may then allow the FeFe centre to rearrange into a bridging CO system and also 'lock' the excited electron in the $(\text{bpy})^{\bullet-}$ system for subsequent chemistry. If this quenching is able to occur then it should be possible to observe via emission spectroscopy.

1 mM solutions of $[\text{Fe}_2(\text{pdt})(\text{CO})_4(\text{CN})(\mu\text{-CN})\text{Ru}(\text{tpy})(\text{bpy})]$ **18** and $[\text{Ru}^{\text{II}}(\text{tpy})(\text{bpy})(\text{OH}_2)](\text{PF}_6)_2$ **17** were prepared in dry degassed DMF and subjected to emission spectroscopy. The Ru(II) centres in both compounds absorb strongly at 609 nm and 397 nm, wavelengths within the MLCT region, and so these wavelengths were used for excitation.

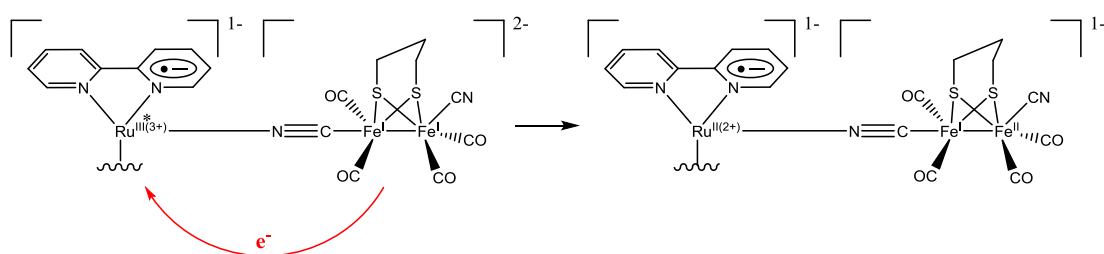
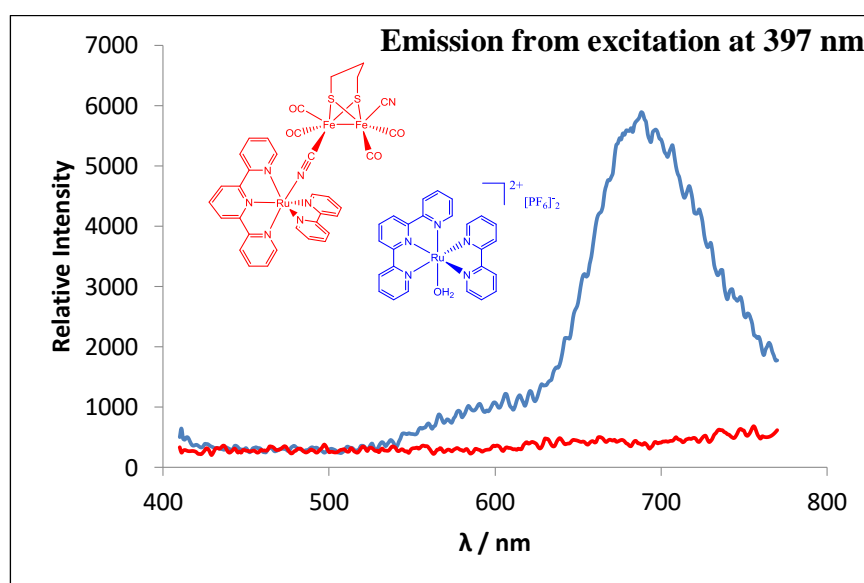
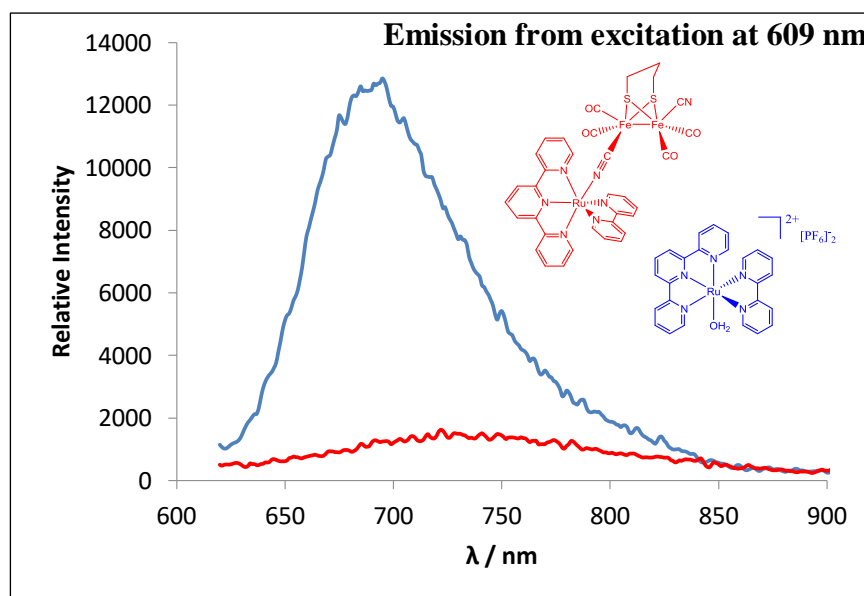


Figure 4.14 Emission spectra of $[\text{Fe}_2(\text{pdt})(\text{CO})_4(\text{CN})(\mu\text{-CN})\text{Ru}(\text{tpy})(\text{bpy})]$ **18** and $[\text{Ru}^{\text{II}}(\text{tpy})(\text{bpy})(\text{OH}_2)](\text{PF}_6)_2$ **17** from excitation at 609 nm and 397 nm. Solutions were 1 mM concentration in dry degassed DMF. Possible quenching mechanism shown.

In both cases, quenching of the emission of ~90% is observed. This is promising as it suggested that the presence of the FeFe unit offers an alternative non-radiative decay pathway. It is also of note that the emission in both cases is of approximately 700 nm. As the FeFe-containing species (both the dyad and the FeFe starting material) do not absorb at 700 nm, as shown in the UV-vis spectra given in **Figure 4.13.**, it is not unreasonable to infer that the quenching is due to electron transfer rather than an energy transfer pathway.

These are very interesting and promising optical properties which suggest that the $[\text{Fe}_2(\text{pdt})(\text{CO})_4(\text{CN})(\mu\text{-CN})\text{Ru}(\text{tpy})(\text{bpy})]$ compound may be capable of generating a mixed-valence bridging CO species upon excitation. As this would be a very rare example of a cyanide-ligated species of this type, proof of generation of this species is highly desirable. To this end a collaboration with Dr Neil Hunt of the University of Strathclyde is underway in order to attempt to observe such a species by employing $\text{UV}_{\text{pump}}\text{-IR}_{\text{probe}}$ experiments.

4.2.3.5 Electrochemistry

Electrochemistry of $[\text{Fe}_2(\text{pdt})(\text{CO})_4(\text{CN})(\mu\text{-CN})\text{Ru}(\text{tpy})(\text{bpy})]$ **18** was recorded in degassed DMF utilising tetrabutylammonium tetrafluoroborate electrolyte with a vitreous carbon working electrode. The diiron dicyanide starting material $(\text{NEt}_4)_2[\text{Fe}_2(\text{pdt})(\text{CO})_4(\text{CN})_2]$ **14** was subjected to the same conditions and the oxidation potentials of both systems compared, as shown in **Figure 4.15.**

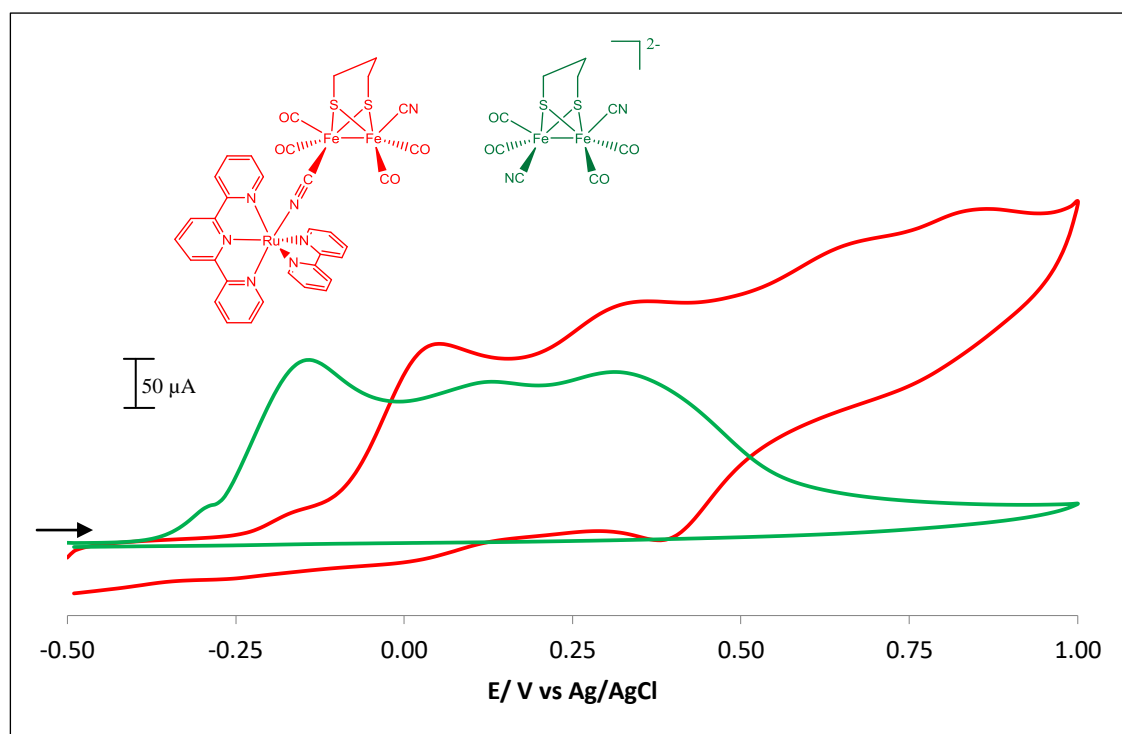


Figure 4.15 Electrochemistry of $[\text{Fe}_2(\text{pdt})(\text{CO})_4(\text{CN})(\mu\text{-CN})\text{Ru}(\text{tpy})(\text{bpy})]$ **18** and $(\text{NEt}_4)_2[\text{Fe}_2(\text{pdt})(\text{CO})_4(\text{CN})_2]$ **14**. Conditions: 1 mM of the complexes in DMF containing 0.1 M $[\text{Bu}_4\text{N}][\text{BF}_4]$ at a vitreous carbon working electrode, area 0.7 cm^2 ; scan-rate 100 mV s^{-1} at 21°C .

The one electron $\{\text{Fe}^{\text{II}}\text{-Fe}^{\text{I}}\}/\{\text{Fe}^{\text{I}}\text{-Fe}^{\text{I}}\}$ oxidation of $(\text{NEt}_4)_2[\text{Fe}_2(\text{pdt})(\text{CO})_4(\text{CN})_2]$ is an irreversible process¹⁴⁶. Upon formation of the $\text{Ru-N}\equiv\text{C-Fe}$ bridge in the $[\text{Fe}_2(\text{pdt})(\text{CO})_4(\text{CN})(\mu\text{-CN})\text{Ru}(\text{tpy})(\text{bpy})]$ species the $\{\text{Fe}^{\text{II}}\text{-Fe}^{\text{I}}\}/\{\text{Fe}^{\text{I}}\text{-Fe}^{\text{I}}\}$ oxidation is shifted positive by *ca* 200 mV. This is consistent with the other characterisations which demonstrate the effects of the Lewis acidic Ru moiety, as the shift in electron density towards the electron-withdrawing Ru unit lowers the energy of the HOMO making the species harder to oxidise.

4.2.3.6 Protonation and photocatalysed hydrogen evolution

A key property of a [FeFe]-hydrogenase system necessary to function as intended is the ability to form a bridging hydride upon protonation. Cyanide-functionalised diiron systems are known to protonate readily, though as explained in **Chapter 3**, a serious problem is protonation on a cyanide ligand itself, as opposed to the FeFe centre, which leads to decomposition of the system. This problem was addressed extensively in the preceding chapter by use of fluorinated bis-ureas to cap the cyanide ligands, though the new Ru-N≡C-FeFe system, with its one bound cyanide, may potentially form a stable bridging hydride species also. In addition to this, it is also important to investigate whether a bridging hydride species will even form on this system, as it may be possible that attachment of the photosensitiser may have reduced the activity of the system. The desired protonation of the Ru-N≡C-FeFe system is shown in **Figure 4.18**.

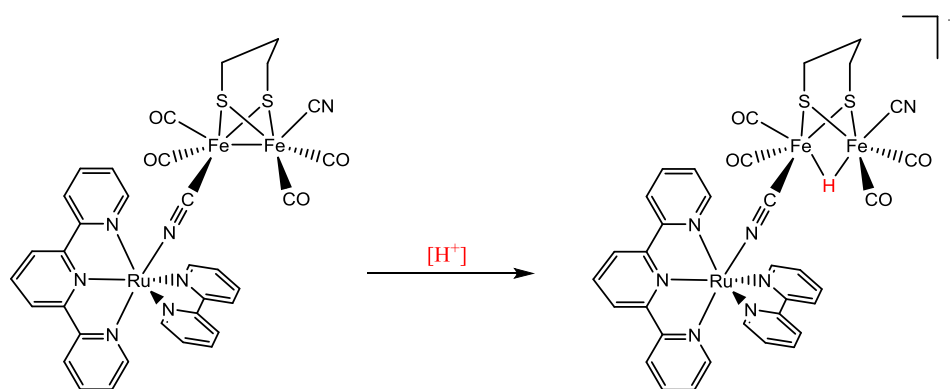
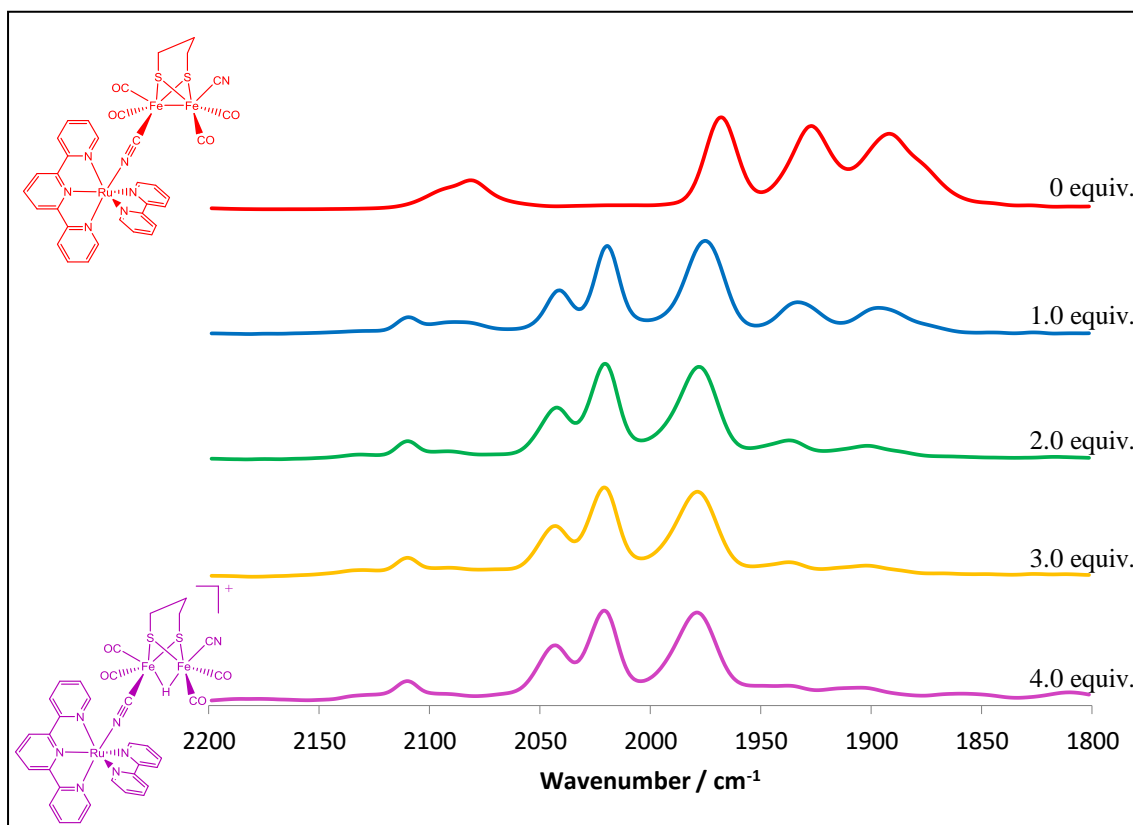


Figure 4.18. Desired protonation of $[\text{Fe}_2(\text{pdt})(\text{CO})_4(\text{CN})(\mu\text{-CN})\text{Ru}(\text{tpy})(\text{bpy})]$ to give the bridging hydride species $[\text{Fe}_2(\text{pdt})(\mu\text{-H})(\text{CO})_4(\text{CN})(\mu\text{-CN})\text{Ru}(\text{tpy})(\text{bpy})]^+$.

For this protonation experiment a 1.0 mM solution of $[\text{Fe}_2(\text{pdt})(\text{CO})_4(\text{CN})(\mu\text{-CN})\text{Ru}(\text{tpy})(\text{bpy})]$ **18** was prepared in DMF, to which a stock solution of $\text{HBF}_4 \cdot \text{OEt}_2$ in DMF was added. If the protonation is successful and gives a bridging hydride species, a large shift in the CO stretches in the IR spectrum should be apparent due to the large change of electron density on the FeFe core. The FTIR spectra recorded from the protonation experiment are given in **Figure 4.19**.



	$\nu(\text{CN}) / \text{cm}^{-1}$	$\nu(\text{CO}) / \text{cm}^{-1}$
Non-protonated	2093, 2081	1968, 1927, 1892
Protonated	2110	2043, 2020, 1979

Figure 4.19. Solution FTIR spectra (DMF) monitoring the affects of equivalent additions of $\text{HBF}_4 \cdot \text{OEt}_2$ to $[\text{Fe}_2(\text{pdt})(\text{CO})_4(\text{CN})(\mu\text{-CN})\text{Ru}(\text{tpy})(\text{bpy})]$ **18** in order to protonate and generate the bridging hydride species, $[\text{Fe}_2(\text{pdt})(\mu\text{-H})(\text{CO})_4(\text{CN})(\mu\text{-CN})\text{Ru}(\text{tpy})(\text{bpy})]^+$.

These IR spectra demonstrate that the $\text{Ru-N}\equiv\text{C-FeFe}$ species, $[\text{Fe}_2(\text{pdt})(\text{CO})_4(\text{CN})(\mu\text{-CN})\text{Ru}(\text{tpy})(\text{bpy})]$, undergoes stable protonation to give the bridging hydride species $[\text{Fe}_2(\text{pdt})(\mu\text{-H})(\text{CO})_4(\text{CN})(\mu\text{-CN})\text{Ru}(\text{tpy})(\text{bpy})]^+$. This is shown by the CO stretches moving to significantly higher wavenumbers ($\sim 75\text{-}90 \text{ cm}^{-1}$), and the CN stretches are also shifted to higher wavenumbers ($\sim 25 \text{ cm}^{-1}$). Interestingly the two different CN ligands are no longer distinguishable.

The stability of the protonation is slightly surprising given that only one of the cyanide ligands is bound to Ru, leaving the other cyanide ligand exposed to potential attack by protons. Possibly the binding of one cyanide ligand has the additional effect of rendering the second cyanide less Lewis basic due to a decrease in the electron density on the FeFe core. This would be in keeping with the fluorinated bis-urea work conducted in **Chapter 3**, where the second equivalent of bis-urea is shown to be less rapidly bound to the diiron dicyanide core than the first equivalent. At the time this was explained by steric effects, though it could very well be possible that there is an electronic contribution to this mechanism too.

The fact that four equivalents of $\text{HBF}_4\cdot\text{OEt}_2$ is required to fully protonate the system is in keeping with the fluorinated bis-urea work in **Chapter 3** and Rauchfuss' Bar^{F} experiments also outlined in that chapter, which also required an excess of $[\text{H}^+]$. Possibly, due to the inherent chemistry involved in binding protecting groups via the cyanide ligand, it is inevitable that some electron density is withdrawn from the FeFe system and thus some of the reactivity is lost.

However, it is evident that the IR data obtained for protonation of the $\text{Ru-N}\equiv\text{C-FeFe}$ species is consistent with other reported data for protonated diiron dicyanide units. **Figure 4.20** compares the values for the dyad system to the solution (MeCN) data measured by Rauchfuss' group¹⁴⁹ and the polymer-bound system analysed by Pickett and coworkers¹⁵⁰.

Protonated species	$\nu(\text{CN}) / \text{cm}^{-1}$	$\nu(\text{CO}) / \text{cm}^{-1}$
$[\text{Fe}_2(\text{pdt})(\mu\text{-H})(\text{CO})_4(\text{CN})_2]^-$ (solution)	2118, 2112	2045, 2024, 1985
$[\text{Fe}_2(\text{pdt})(\mu\text{-H})(\text{CO})_4(\text{CN})_2]^-$ (polymer)	2114	2044, 2020, 1980
$[\text{Fe}_2(\text{pdt})(\mu\text{-H})(\text{CO})_4(\text{CN})(\mu\text{-CN})\text{Ru}(\text{tpy})(\text{bpy})]^+$	2110	2043, 2020, 1979

Figure 4.20. Comparison of the CN and CO bands observed in FTIR upon treatment of $[\text{Fe}_2(\text{pdt})(\text{CO})_4(\text{CN})(\mu\text{-CN})\text{Ru}(\text{tpy})(\text{bpy})]$ **18** with $\text{HBF}_4\cdot\text{OEt}_2$ with reported values. Adapted from references^{149,150}.

There is undoubtedly a remarkable consistency in the IR stretches observed for protonation of the parent dicyanide observed in solution and in polymer matrices and

the set of frequencies observed for the rutheniated species. The protonation of the parent dicyanide species has been interpreted as taking place at the metal-metal bond^{149,150}. However some caution is required because we cannot exclude the possibility that protonation occurs both on the Fe-Fe bond and a cyanide ligand under the conditions of excess acid. The 'loss' of one CN stretching frequency would be consistent with protonation at CN. It is possible that one of the bands observed in the CO region is actually a CN-H (isocyanide) stretch. Isotopic labelling experiments would resolve this.

Photocatalysed hydrogen evolution was attempted using the photosensitised diiron system. A procedure similar to that employed by Sun and coworkers¹⁵¹ was used, where a 0.1 mM solution of the complex was irradiated by a pyrex-filtered Xe lamp (500 W) in the presence of 100 equivalents of HBF₄.OEt₂ and 500 equivalents of ascorbic acid. After 30 minutes 0.1 mol equivalent H₂ was detected by gas chromatography, with no additional H₂ produced after 6 hours. It was decided that the reaction conditions were far too severe and led to the immediate decomposition of the complex, as confirmed by IR spectroscopy of the resulting reaction mixture which displayed no identifiable peaks. To accurately assess the potential of this system for photocatalysed hydrogen production, less severe reaction conditions need to be employed; probably involving the gradual addition of acid feedstock so as not to destroy the complex.

4.2.4 Concluding remarks and future work

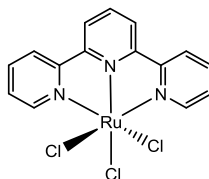
The linkage of a Ru(II)bipyridine-derived photosensitiser to a [FeFe]-hydrogenase subsite analogue has been achieved by using a bridging cyanide ligand, and the resulting [Fe₂(pdt)(CO)₄(CN)(μ-CN)Ru(tpy)(bpy)] species has been characterised crystallographically. The direct coordination of cyanide to the Ru centre by a bonding motif of the fashion Ru-N≡C-FeFe has proven to be a very intimate linking mechanism, as demonstrated by IR spectroscopy. The dyad complex has been studied electrochemically and with UV-vis spectroscopy, with features of both the Ru and FeFe centres observed. The complex also has the potential to generate a mixed-valence bridging CO species on photoexcitation due to its possible fast electron transfer pathway via the linking CN, which would be a rare example of a cyanide-ligated species of this type. The generation of this bridging CO species has been initially supported by emission spectroscopy, which has suggested that an electron transfer quenching

pathway may be present. Finally, the system is stable to protonation and forms bridging hydride species when exposed to $\text{HBF}_4\cdot\text{OEt}_2$, and has been shown to produce some dihydrogen, although some refinement of the reaction conditions are required in order to achieve an effective system.

In regards to expanding this body of work, a collaboration with Dr Neil Hunt of the University of Strathclyde is already underway in order to attempt to detect photogenerated species, in particular mixed-valence bridging CO species. This will be undertaken in October 2016 using the $\text{UV}_{\text{pump}}\text{-IR}_{\text{probe}}$ laser facilities at the Rutherford Appleton Laboratory. The potential for the new photosensitised diiron system to generate dihydrogen photocatalytically also requires much further investigation; with an obvious first avenue being to adjust the reaction conditions. However the most significant contribution of this work may well be the attachment of other metals via the cyanide ligands. Taking the recent work of Darensbourg¹²⁵ as an example, attachment of various metal-incorporating groups provides a means of modifying subsite structure and reactivity.

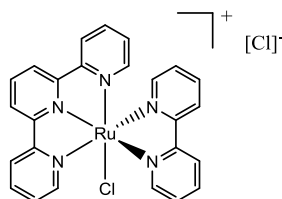
4.3 Experimental

4.3.1 Synthesis of $[\text{Ru}^{\text{III}}(\text{tpy})\text{Cl}_3]$ (**15**)¹⁴²



2,2',2''-terpyridine (0.81 g, 3 mmol) and $\text{RuCl}_3 \cdot 3\text{H}_2\text{O}$ (0.90 g, 3 mmol) were dissolved in ethanol (160 mL) and heated at 90 °C for 3 h with vigorous stirring. The reaction was allowed to cool to room temperature before the fine brown precipitate produced was obtained by filtration from the red solution. The powder was washed with ethanol (3 x 50 mL) and diethyl ether (3 x 50 mL) until the washings were colourless. Air drying gave the *title compound* (1.35 g, 3 mmol, 88%) as brown powder. m.p. >250 °C.

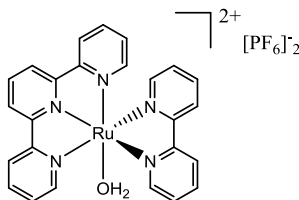
4.3.2 Synthesis of $[\text{Ru}^{\text{II}}(\text{tpy})(\text{bpy})\text{Cl}](\text{Cl})$ (**16**)¹⁴³



$[\text{Ru}^{\text{III}}(\text{tpy})\text{Cl}_3]$ **15** (1.34 g, 3 mmol), 2,2'-bipyridine (0.48 g, 3 mmol) and lithium chloride (0.13 g, 3.2 mmol) were added to a flask containing 3:1 ethanol/distilled water (280 mL). Triethylamine (0.8 mL) was added, and then the mixture heated at 95 °C for 4.5 h. The pot contents were filtered hot through celite before the resultant solution was concentrated to ~50 mL. The solution was then set to crystallise at 2 °C for 48 h. The black crystals obtained were then collected on a frit and washed with chilled 3 M HCl (2 x 8 mL), acetone (25 mL) and finally diethyl ether (200 mL). Air-drying gave the *title compound* (0.95 g, 2 mmol, 55%) as black crystals. $^1\text{H-NMR}$ ($\text{DMSO-}d_6$, 300.13 MHz): δ (ppm) = 10.09 (d, $^3J_{\text{HH}} = 5.2$ Hz, 1H, Ar-H), 8.96 (d, $^3J_{\text{HH}} = 8.2$ Hz, 1H, Ar-H), 8.85 (d, $^3J_{\text{HH}} = 8.1$ Hz, 2H, Ar-H), 8.73 (d, $^3J_{\text{HH}} = 8.1$ Hz, 2H, Ar-H), 8.68 (d, $^3J_{\text{HH}} = 8.1$ Hz, 1H, Ar-H), 8.36 (t, $^3J_{\text{HH}} = 7.5$ Hz, 1H, Ar-H), 8.21 (t, $^3J_{\text{HH}} = 8.0$ Hz, 1H, Ar-H), 8.07 (t, $^3J_{\text{HH}} = 6.6$ Hz, 1H, Ar-H), 7.98 (t, $^3J_{\text{HH}} = 7.5$ Hz, 2H, Ar-H), 7.77 (t, $^3J_{\text{HH}} = 7.5$

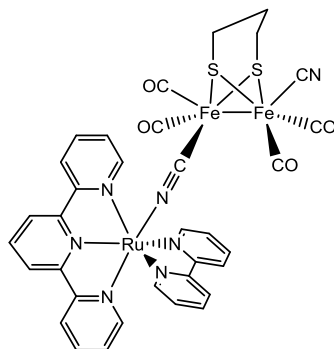
Hz, 1H, Ar-H), 7.62 (d, $^3J_{\text{HH}} = 5.2$ Hz, 2H, Ar-H), 7.38 (t, $^3J_{\text{HH}} = 6.3$ Hz, 2H, Ar-H), 7.31 (d, $^3J_{\text{HH}} = 5.4$ Hz, 1H, Ar-H), 7.08 (t, $^3J_{\text{HH}} = 6.4$ Hz, 1H, Ar-H).

4.3.3 Synthesis of $[\text{Ru}^{\text{II}}(\text{tpy})(\text{bpy})(\text{OH}_2)](\text{PF}_6)_2$ (**17**)¹⁴⁴



$[\text{Ru}^{\text{II}}(\text{tpy})(\text{bpy})\text{Cl}](\text{Cl})$ **16** (0.24 g, 0.4 mmol) and silver hexafluorophosphate (0.22 g, 0.9 mmol) were added to a flask containing 3:1 acetone/distilled water (30 mL), and the resultant mixture heated at 95 °C for 1.5 h. White AgCl had precipitated out, and this was removed by filtering the brown solution through celite. The solution was then concentrated to ~10 mL, and was then set to crystallise at 2°C for 16 h. The brown crystals obtained were then collected on a frit and washed with chilled 3:1 acetone/distilled water (2 mL). Air-drying gave the *title compound* (0.32 g, 0.4 mmol, 92%) as brown crystals. ^1H -NMR ($\text{DMSO-}d_6$, 300.13 MHz): δ (ppm) = 9.51 (d, $^3J_{\text{HH}} = 5.2$ Hz, 1H, Ar-H), 8.96 (d, $^3J_{\text{HH}} = 8.1$ Hz, 1H, Ar-H), 8.89 (d, $^3J_{\text{HH}} = 8.1$ Hz, 2H, Ar-H), 8.75 (d, $^3J_{\text{HH}} = 8.0$ Hz, 2H, Ar-H), 8.65 (d, $^3J_{\text{HH}} = 8.1$ Hz, 1H, Ar-H), 8.43 (t, $^3J_{\text{HH}} = 7.8$ Hz, 1H, Ar-H), 8.33 (t, $^3J_{\text{HH}} = 8.1$ Hz, 1H, Ar-H), 8.15 (t, $^3J_{\text{HH}} = 6.4$ Hz, 1H, Ar-H), 8.07 (t, $^3J_{\text{HH}} = 7.8$ Hz, 2H, Ar-H), 7.79 (t, $^3J_{\text{HH}} = 7.9$ Hz, 1H, Ar-H), 7.70 (d, $^3J_{\text{HH}} = 5.2$ Hz, 2H, Ar-H), 7.45 (t, $^3J_{\text{HH}} = 6.1$ Hz, 2H, Ar-H), 7.33 (d, $^3J_{\text{HH}} = 5.4$ Hz, 1H, Ar-H), 7.09 (t, $^3J_{\text{HH}} = 6.2$ Hz, 1H, Ar-H), 5.91 (s, 2H, Ru-OH₂). ^{19}F -NMR ($\text{DMSO-}d_6$, 282.37 MHz): δ (ppm) = -70.06 (d, $^1J_{\text{FP}} = 711$ Hz). ^{31}P -NMR ($\text{DMSO-}d_6$, 121.48 MHz): δ (ppm) = -144.19 (sept, $^1J_{\text{PF}} = 711$ Hz).

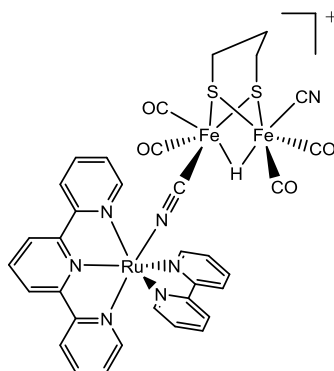
4.3.4 Synthesis of $[\text{Fe}_2(\text{pdt})(\text{CO})_4(\text{CN})(\mu\text{-CN})\text{Ru}(\text{tpy})(\text{bpy})]$ (**18**)



A brown solution of $[\text{Ru}^{\text{II}}(\text{tpy})(\text{bpy})(\text{OH}_2)](\text{PF}_6)_2$ **17** (137 mg, 0.17 mmol) in dry degassed acetone (30 mL) was added dropwise to a red solution of $(\text{NEt}_4)_2[\text{Fe}_2(\text{pdt})(\text{CO})_4(\text{CN})_2]$ **14** (110 mg, 0.17 mmol) in dry degassed acetone (40 mL) with vigorous stirring. A dark purple precipitate was formed on addition. The mixture was left to stir for 16 h at room temperature, and afterwards the precipitate was obtained via filtration. This isolated powder may contain the non-CN-bridged salt, $[\text{Fe}_2(\text{pdt})(\text{CO})_4(\text{CN})_2][\text{Ru}^{\text{II}}(\text{tpy})(\text{bpy})\text{OH}_2]$. IR(DMF): $\nu(\text{CN}) = 2077$; $\nu(\text{CO}) = 1964$, 1921, 1885.

To ensure the reaction progressed to completion, the precipitate was then dissolved in dry degassed DMF (30 mL) and stirred vigorously for 24 h at room temperature, whilst monitoring via IR. Upon completion of the reaction, the DMF solvent was evaporated to give a dark purple oil which was then stirred vigorously for 24 h with dry degassed acetone (60 mL). The resultant solid was obtained by filtration and drying in vacuo gave the *title compound* (128 mg, 0.15 mmol, 85%) as purple solid. Crystals suitable for X-ray diffraction were grown from slow diffusion of Et_2O into a DMF solution. ^1H -NMR ($\text{DMSO}-d_6$, 300.13 MHz): δ (ppm) = 9.95 - 7.06 (br m, 19H, Ar-H), 1.14 (s, 6H). IR(DMF): $\nu(\text{CN}) = 2093$, 2081; $\nu(\text{CO}) = 1968$, 1927, 1892. Anal. Calcd. for $\text{C}_{34}\text{H}_{25}\text{N}_7\text{O}_4\text{S}_2\text{Fe}_2\text{Ru}$: C, 46.80; H, 2.89; N, 11.24. Found: C, 46.76; H, 3.03; N, 11.12.

4.3.5 Generation of the cation $[\text{Fe}_2(\text{pdt})(\mu\text{-H})(\text{CO})_4(\text{CN})(\mu\text{-CN})\text{Ru}(\text{tpy})(\text{bpy})]^+$



A solution of $[\text{Fe}_2(\text{pdt})(\text{CO})_4(\text{CN})(\mu\text{-CN})\text{Ru}(\text{tpy})(\text{bpy})]$ **18** (17.5 mg, 0.02 mmol) in dry degassed DMF (20 mL) was prepared, to which 4 equivalents of $\text{HBF}_4 \cdot \text{OEt}_2$ via DMF (1:99) stock solution (0.27 mL, 0.08 mmol) were added. This gave the *title cation* in solution. IR(DMF): $\nu(\text{CN}) = 2110$; $\nu(\text{CO}) = 2043, 2020, 1979$.

4.3.6 X-ray diffraction

Crystals were suspended in oil, and one was mounted on a glass fibre and fixed in the cold nitrogen stream of the diffractometer. Data were collected on a Rigaku AFC12 goniometer equipped with an enhanced sensitivity (HG) Saturn724+ detector mounted at the window of an FR-E+ SuperBright molybdenum rotating anode generator with HF Varimax optics. Data were processed using the CrysAlisPro program¹⁵². Structures were determined by dual space routines in the SHELXT-2014/5 program¹⁵³ and refined by full-matrix least-squares methods on F^2 in SHELXL-2014/7¹⁵⁴. Non-hydrogen atoms were refined with anisotropic thermal parameters. Hydrogen atoms were included in idealized positions and their U_{iso} values were set to ride on the U_{eq} values of the parent carbon atoms. The cyanide ligand bound to Fe(1) was located by free refinement of a nitrogen atom in the three possible sites which established that it was best modelled in the two basal positions. For these two locations, the partial occupancy nitrogen atom was refined with position and thermal parameters equal to the co-located oxygen. The DMF solvent molecule was disordered around a special position. The distances in the molecule were restrained to 1.21(2) Å [C(101)–O(101)], 1.34(2) Å [C(101)–N(101)], 1.43(2) Å ([N101)–C(102)] and 1.43(1) Å [N(101)–C(103)]. A rigid bond restrain was applied to this molecule, with anisotropic displacement parameters restrained for

bonded atoms to an e.s.d. of 0.01 Å in the direction of the bond. The thermal parameters for all atoms in the molecule were also restrained to have U_{ij} components equal with an e.s.d. of 0.04 Å for N(101) and 0.08 Å for all other non-hydrogen atoms. The anisotropic thermal parameters for C(102) were restrained to approximate to isotropic with an e.s.d. of 0.1 Å.

Crystal data: C₃₄H₂₅Fe₂N₇O₄RuS₂, C_{1.5}H_{3.5}N_{0.5}O_{0.5}, $M = 909.0$, $T = 100(2)$ K, $\lambda(\text{Mo-K}\alpha) = 0.71075$ Å, monoclinic, space group $P2/c$, $a = 12.8337(5)$ Å, $b = 11.5308(4)$ Å, $c = 26.7635(9)$ Å, $\beta = 102.183(4)^\circ$, $V = 3871.3(2)$ Å³, $Z = 4$, total reflections 47019, independent reflections 6816, $R_{\text{int}} = 0.094$, $R_1 = 0.067$ [$F^2 > 2\sigma(F^2)$], wR2 (all data) 0.221.

5 Incorporation of *ortho*-carboranes into the backbone structure of Fe-Fe subsite analogues

5.1 Introduction

5.1.1 General aspects

O-carboranes (1,2-*closo*-C₂B₁₀H₁₂) are electron-deficient, redox active and bulky. This chapter describes work directed towards the incorporation of this type of moiety as an integral structural element of a diiron subsite unit.

In the next sections an overview of carboranes and background chemistry related to the work described in this chapter will be described. This will be followed by a description of the synthesis and X-ray structure of a novel diiron dithiolate complex possessing phosphine functionalised *o*-carboranes together with a consideration of key physical properties.

5.1.2 Interest in *ortho*-carboranes

Dicarba-*closo*-dodecaboranes, of the general formula C₂B₁₀H₁₂, are a class of compounds with high thermal and chemical stability that exhibit strong acceptor behaviour¹⁵⁵. Due to their unusual properties, since their discovery in the 1960s they have been employed in a wide range of fields, including catalysis¹⁵⁶, biomedicine¹⁵⁷, materials¹⁵⁸ and nuclear waste remediation¹⁵⁹, to give some examples.

There are three isomers of C₂B₁₀H₁₂ carborane that differ in the relative positions of both the carbon atoms in the clusters; namely *ortho*-, *meta*- and *para*-¹⁶⁰. The structures of these isomers are shown in **Figure 5.1**.

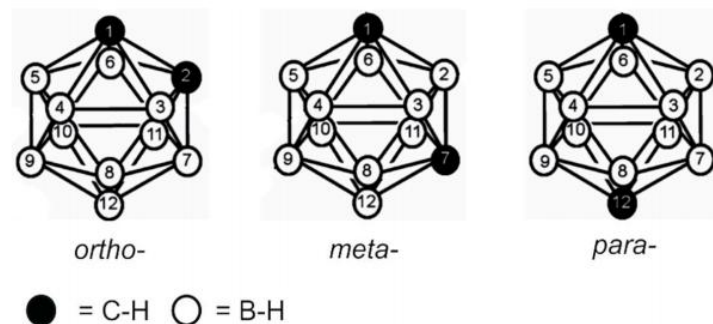


Figure 5.1. Three structural isomers of $\text{closo-C}_2\text{B}_{10}\text{H}_{12}$ with vertex numbering. Image reproduced from reference¹⁶⁰.

The relative positions of the carbon atoms have a significant impact on the properties of the carborane. The three isomers have very different dipole moments as a consequence of the carbon atoms' positions, with the *ortho*-, *meta*- and *para*- derivatives having values of 4.53 D, 2.85 D and 0 D respectively¹⁶¹. The presence of the ten boron atoms creates a very electron deficient molecule, and as such the carbon atoms exert an electron-withdrawing effect on attached substituents. The extent of electron-withdrawing behaviour decreases in the order *ortho*- > *meta*- > *para*-; with the *ortho*- isomer demonstrating an electron-withdrawing effect comparable to that of a fluorinated aryl group¹⁶². The electron-withdrawing behaviour also has the effect of making the C-H bonds relatively acidic, with the acidity again following the order of *ortho*- > *meta*- > *para*-. These acidic protons can be removed with strong bases, with the generated carboranyl nucleophiles being capable of reacting with a wide range of electrophiles¹⁶³. As the B-H vertices have reactivity reminiscent of arenes, most reactions that occur at the carbon atoms do not affect the boron atoms¹⁵⁵, and as the C-H protons on *ortho*-carboranes are the most acidic of the three *closo*-carborane isomers, the reactions of *ortho*-carboranes generally produce less side products and are therefore often preferred.

In addition, *closo*-carborane derivatives, with their rigid three-dimensional icosahedron structures, hold substituents in well-defined spatial relationships, with most transformations maintaining the underlying geometry¹⁶⁴. *Ortho*-carboranes, and in particular those functionalised with phosphine groups, exhibit especially attractive geometries for incorporation into transition metal complexes due to their orientation

allowing steric stabilisation of the complex¹⁶⁵. To this end, transition metal *ortho*-carborane complexes have attracted a lot of interest¹⁶⁶⁻¹⁶⁸.

5.1.3 Existing *ortho*-carborane [FeFe]-hydrogenase subsite analogue systems

Due to their interesting electron-withdrawing and steric properties it was inevitable that *ortho*-carborane moieties would be incorporated into [FeFe]-hydrogenase subsite analogue systems. At the time of writing two such systems are in the literature: the first synthesised by Ott and coworkers¹⁶⁹ in 2008 includes a dithiolate-*ortho*-carborane bridgehead; and the second synthesised by Lubitz's and Ott's groups in collaboration¹⁷⁰ in 2012 incorporates a bis(diphenylphosphine)-*ortho*-carborane moiety coordinated to one of the Fe atoms in the diiron core (**Figure 5.2**).

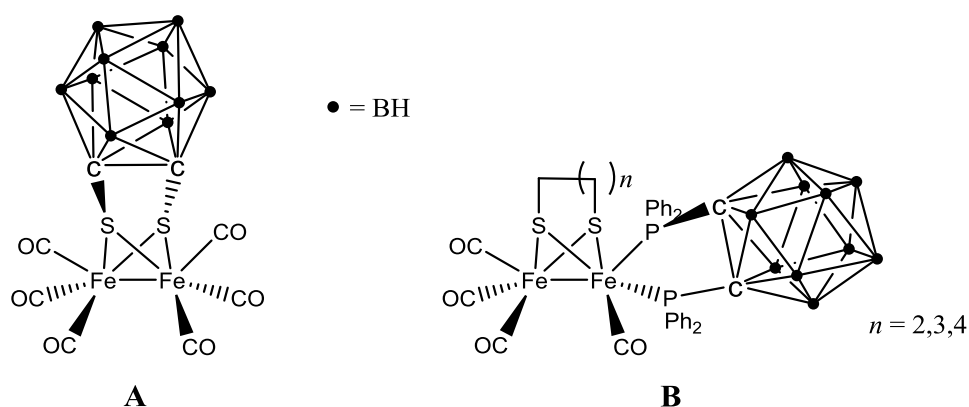
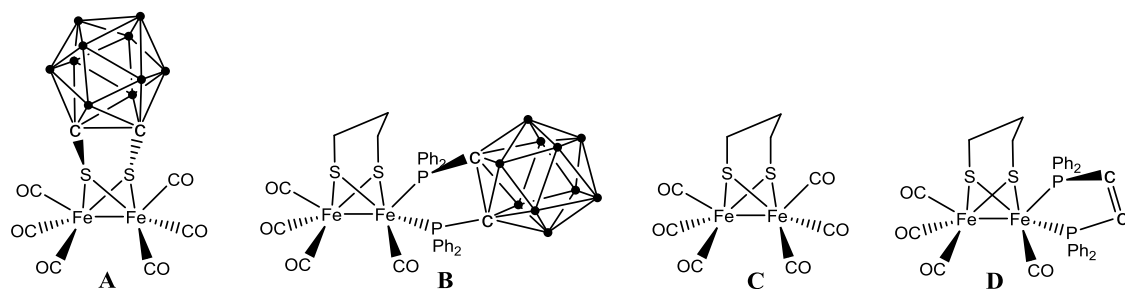


Figure 5.2. Existing subsite analogues incorporating *ortho*-carborane moieties; dithiolate-*ortho*-carborane bridgehead species **A** and bis(diphenylphosphine)-*ortho*-carborane coordinated species **B**. Adapted from references^{169,170}.

The electron-withdrawing character of the *ortho*-carborane units should remove electron density from the FeFe core of the subsite analogue. As the carbonyl groups present on the diiron centre are highly sensitive to change in electron density, FTIR should provide detailed information about the extent of electron withdrawal by the carborane groups. This is shown in **Figure 5.3** where a table of the CO stretches is given relative to some comparative FeFe systems.



Compound	$\nu(\text{CO}) / \text{cm}^{-1}$
A $[\text{Fe}_2(o\text{-carb-S}_2)(\text{CO})_6]$	2092, 2055, 2024
B $[\text{Fe}_2(\text{pdt})(\text{CO})_4((\text{PPh}_2)_2o\text{-carb})]$	2032, 1965, 1920
C $[\text{Fe}_2(\text{pdt})(\text{CO})_6]$	2074, 2035, 1995
D $[\text{Fe}_2(\text{pdt})(\text{CO})_4(\text{dppv})]$	2021, 1950, 1912

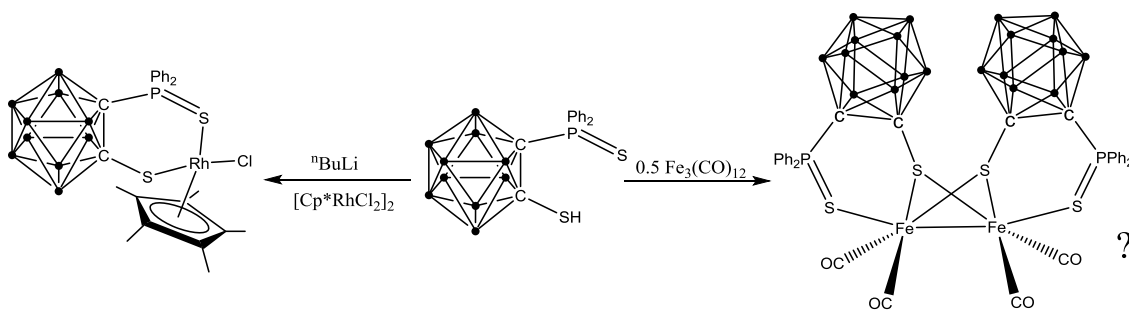
Figure 5.3. Solution FTIR comparison of the carborane-functionalised subsite systems^{169,170} compared to $[\text{Fe}_2(\text{pdt})(\text{CO})_6]$ and $[\text{Fe}_2(\text{pdt})(\text{CO})_4(\text{dppv})]$ ¹⁷¹.

The FTIR demonstrates that the carborane moieties are withdrawing electron density from the diiron centre. Comparing $[\text{Fe}_2(o\text{-carb-S}_2)(\text{CO})_6]$ **A** with $[\text{Fe}_2(\text{pdt})(\text{CO})_6]$ **C**, the CO stretches have shifted to higher wavenumbers ($\sim 20 \text{ cm}^{-1}$). For $[\text{Fe}_2(\text{pdt})(\text{CO})_4((\text{PPh}_2)_2o\text{-carb})]$ **B**, a suitable comparison is to $[\text{Fe}_2(\text{pdt})(\text{CO})_4(\text{dppv})]$ **D**, where dppv = *cis*-1,2-bis(diphenylphosphino)ethylene¹⁷¹. From $[\text{Fe}_2(\text{pdt})(\text{CO})_6]$ **C** to $[\text{Fe}_2(\text{pdt})(\text{CO})_4(\text{dppv})]$ **D**, the shift is $\sim 50\text{-}85 \text{ cm}^{-1}$. However, with the carborane moiety attached to the phosphines in $[\text{Fe}_2(\text{pdt})(\text{CO})_4((\text{PPh}_2)_2o\text{-carb})]$ **B**, the electron-withdrawing character of the carborane means the donation from the phosphine ligand is reduced, meaning that the shift to lower wavenumber is less, $\sim 30\text{-}75 \text{ cm}^{-1}$.

5.1.4 Bidentate *ortho*-carborane ligands

The two existing *ortho*-carborane systems described in **Section 5.1.3** are functionalised by incorporation into the bridgehead and by phosphine substitution onto the diiron centre. An appealing alternative would be to synthesise a FeFe system where bidentate carborane ligands are utilised to create a novel subsite analogue whereby the carborane is anchored to the bridgehead but can also interact with the diiron core by ligand

coordination to Fe. In 2011, Jin and coworkers¹⁷² reported a bidentate *ortho*-carborane ligand possibly capable of such an interaction. The phosphine-sulfide-*ortho*-carborane thiolate moiety in question was employed to make rhodium complexes for norbornene polymerisation, but could also be used to synthesise an attractive di-carborane system, as suggested in **Scheme 5.1**.

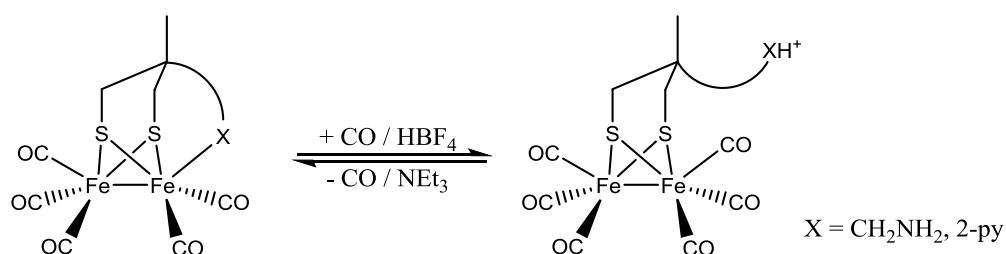


Scheme 5.1. Coordination of [1-S-2-SPPH₂-1,2-*closo*-C₂B₁₀H₁₀] bidentate carborane ligand to give a rhodium-based polymerisation catalyst and suggested coordination to iron to give the postulated di-carborane [FeFe]-hydrogenase subsite analogue. Adapted from reference¹⁷².

There are several reasons as to why this postulated di-carborane species would be attractive. Primarily, it would be a novel species and the characterisation and properties of which would prove very interesting; particularly in how the FTIR spectrum, and thus the relative amount of electron density on the FeFe core, relates to the other existing carborane-functionalised subsite analogues. The other reasons are more concerned with the structural properties of the species. Darensbourg and coworkers have shown that bulky ligands are capable of stabilising a bridging CO on the FeFe centre^{173,174}, which is believed to be mechanistic intermediates before protonation; and Pickett's research group have demonstrated that large bridgehead groups increase the rate of protonation, also due to a stabilisation of bridging CO species¹⁷⁵⁻¹⁷⁸. With two bidentate carboranes present, essentially adding bulk to both the diiron core and the bridgehead, protonation chemistry may be very interesting in this hypothetical species.

It is also possible that the phosphine-sulfide groups of the postulated di-carborane species would be hemi-labile, as they will be interacting with the Fe atoms via dative

bonding of the sulfur lone pairs. Pickett and coworkers have synthesised a range of subsite analogues with bridgehead-anchored pendant groups capable of interacting with the Fe atoms in labile fashion, and it was suggested that these were capable of acting as 'proton shuttles' to increase catalytic activity¹⁷⁷ (**Scheme 5.2**). If the postulated di-carborane compound was capable of such a mechanism this would be highly desirable.



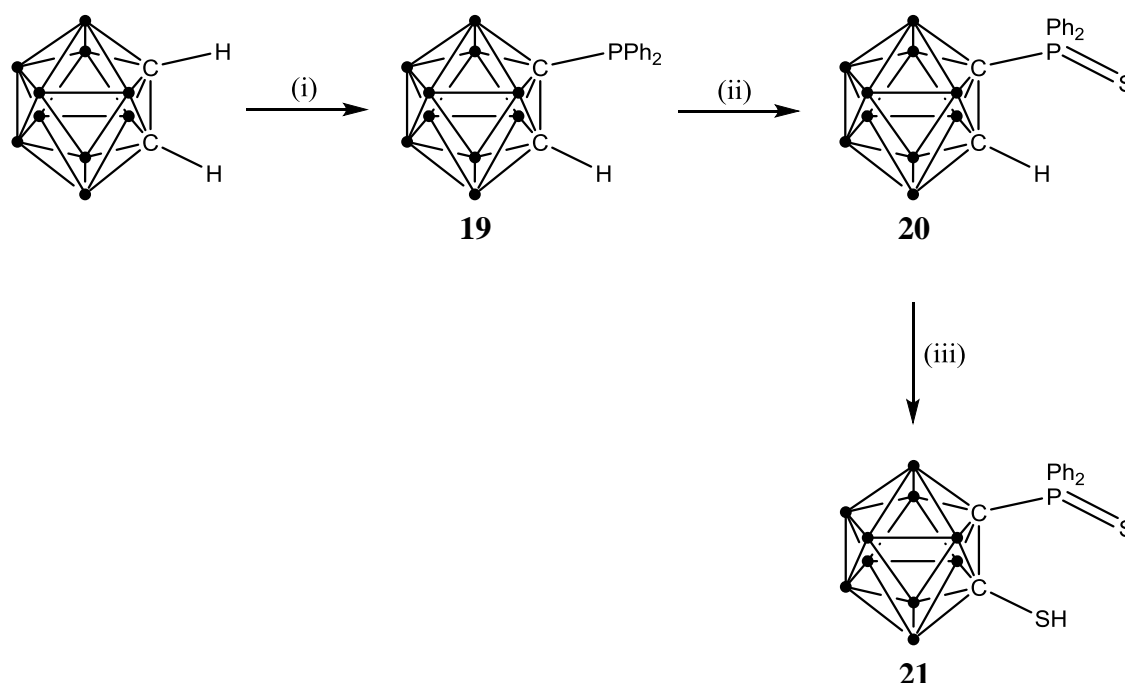
Scheme 5.2. Hemi-labile groups potentially acting as proton shuttles. Adapted from reference¹⁷⁷.

The incorporation of bidentate *ortho*-carboranes into a [FeFe]-hydrogenase subsite analogue offered the possibility of a species with potentially remarkable properties, and thus the synthesis was attempted.

5.2 Results and discussion

5.2.1 Synthesis of the bidentate *ortho*-carborane ligand

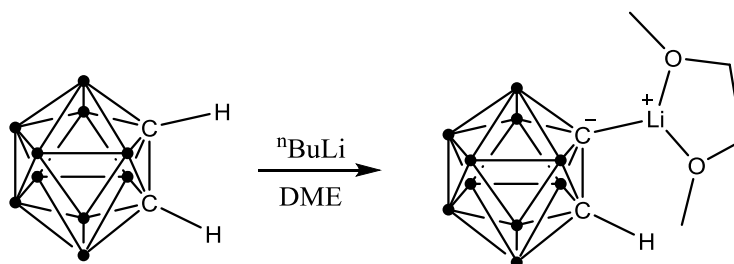
The synthesis of the bidentate phosphine-sulfide-*ortho*-carborane thiolate ligand **21** was performed stepwise from the parent carborane 1,2-C₂B₁₀H₁₂ using procedures modified from the literature^{179,172}.



Scheme 5.3. Stepwise synthesis of bidentate phosphine-sulfide-*ortho*-carborane thiolate ligand **21**. (i) a) 1.0 ⁿBuLi, DME, -78 °C, b) 1.0 Ph₂PCl, DME, 85 °C, 16 h, 61%; (ii) 1.2 S₈, Toluene, 2% NEt₃, 100 °C, 16 h, 55%; (iii) a) 1.0 ⁿBuLi, Et₂O, -78 °C, b) 1.2 S₈, Et₂O, RT, 16 h, 71%. Procedures modified from those outlined by Viñas¹⁷⁹ and Jin¹⁷².

Historically the synthesis of the mono-phosphine substituted *ortho*-carborane **19** has not proven trivial, with the reaction producing a significant amount of the di-substituted phosphine product. Various methods have been employed to ensure the reaction favours the mono-phosphine product, including using protecting/deprotecting groups and performing the reaction at very low concentrations¹⁶⁰, though in 1995 Viñas and coworkers¹⁷⁹ devised a simple and effective method using 1,2-dimethoxyethane (DME)

as the solvent. DME is believed to chelate to the Li atom in a bidentate fashion, generating a bulky Li(DME) moiety. This bulky group then helps prevent lithiation of the second carbon by steric constraints.

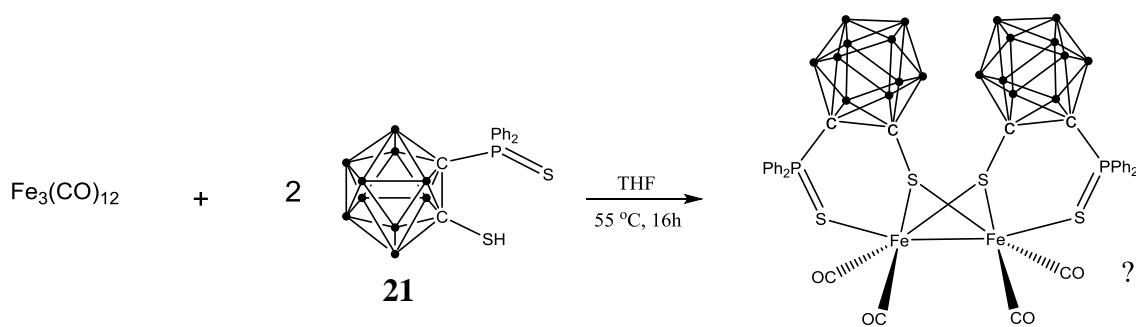


Scheme 5.4. Favours mono-phosphine substitution by use of DME as the reaction solvent. Adapted from reference¹⁷⁹.

Despite use of the mono-phosphine favouring DME solvent, reaction (i) still generated some di-substituted (and consequently some non-reacted starting material) which had to be removed by column chromatography (15:1 hexane/DCM), giving *ortho*-carborane **19** in 61% yield. Reactions (ii) and (iii) were both transformations employing sulfur powder as the electrophile, with the *ortho*-carborane products **20** and **21** being purified by column chromatography (6:1 hexane/DCM) and recrystallisation (from hexane) respectively to give yields of 55% and 71%.

5.2.2 Reaction of the bidentate *ortho*-carborane ligand to generate diiron species

The standard procedure for the synthesis of [FeFe]-hydrogenase subsite analogues is the reaction of triirondodecacarbonyl with the appropriate thiol¹⁸⁰. To this end, the *ortho*-carborane ligand **21** was reacted with Fe₃(CO)₁₂ to hopefully generate the desired species [Fe₂{*o*-carbP(S)(Ph)₂S}₂(CO)₄}], according to **Scheme 5.5**.



Scheme 5.5. Suggested synthesis of the diiron species $[\text{Fe}_2\{\text{o-carbP(S)(Ph)}_2\text{S}\}_2(\text{CO})_4]$.

However, this reaction did not proceed as expected. Instead of the desired product, the reaction solution contained a mixture of a vast array of varying carborane species and one prevalent purple solid. The purple solid was obtained from the reaction mixture using column chromatography (hexane eluent) and was both ^1H -NMR and ^{31}P -NMR silent. In order to identify the purple solid, crystals were obtained from slow evaporation of a hexane solution, and showed the purple solid to be a FeS cluster molecule, $\text{S}_2\text{Fe}_3(\text{CO})_9$.

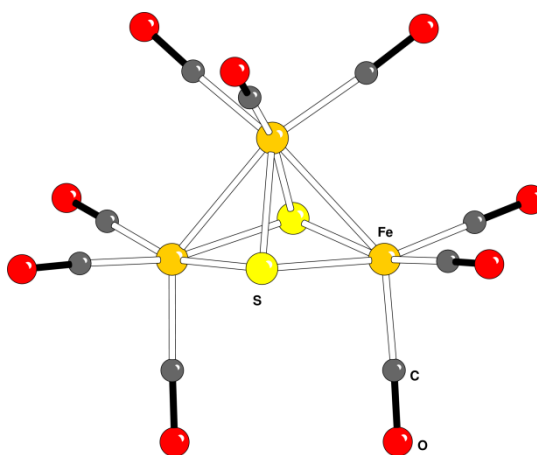
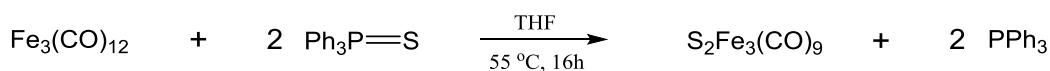


Figure 5.4. CAMERON representation of the structure of $\text{S}_2\text{Fe}_3(\text{CO})_9$ with spheres of arbitrary size. Image generated from the data provided from reference¹⁸¹.

This $\text{S}_2\text{Fe}_3(\text{CO})_9$ cluster molecule was crystallised in 1999 by Henkel and coworkers¹⁸¹, and was clearly being generated in preference to the desired diiron carborane species. It

was therefore important to deduce where the sulfur required to produce this $\text{S}_2\text{Fe}_3(\text{CO})_9$ molecule originated from.

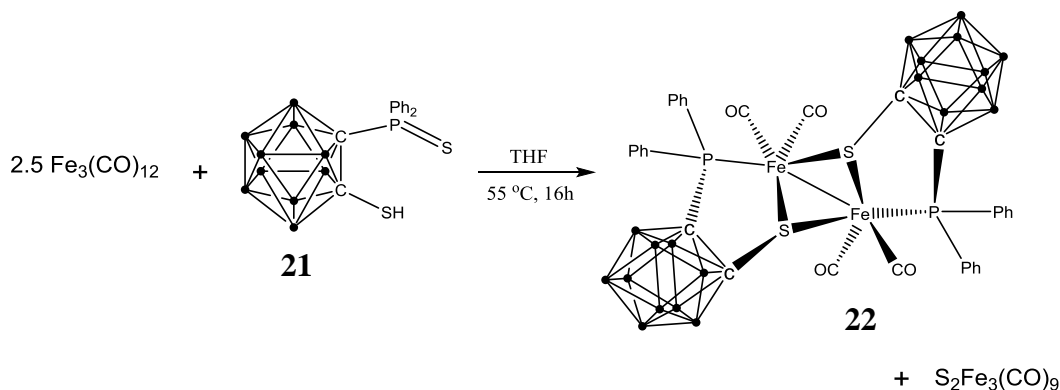
It was deemed unlikely that the sulfur atoms used to generate $\text{S}_2\text{Fe}_3(\text{CO})_9$ originated from excess sulfur powder residues present as impurities in the bidentate *ortho*-carborane ligand **21**, as this was purified by recrystallisation as part of the synthesis. It was therefore deduced that the source of the sulfur atoms required was the carborane ligand itself. The two possible sources of sulfur on the functionalised carborane are the diphenylphosphine sulfide group and the thiol group, and of these two functionalities, it was surmised that the sulfur atom on the diphenylphosphine sulfide group was the most labile and therefore the source of the sulfur for the $\text{S}_2\text{Fe}_3(\text{CO})_9$ cluster. This hypothesis was tested experimentally by the reaction of a suitable surrogate, triphenylphosphine sulfide, with $\text{Fe}_3(\text{CO})_{12}$.



Scheme 5.6. Test reaction of $\text{Ph}_3\text{P}=\text{S}$ with $\text{Fe}_3(\text{CO})_{12}$ to generate $\text{S}_2\text{Fe}_3(\text{CO})_9$.

The test reaction of $\text{Ph}_3\text{P}=\text{S}$ with $\text{Fe}_3(\text{CO})_{12}$ proved successful, with the $\text{S}_2\text{Fe}_3(\text{CO})_9$ cluster being the major product isolated by column chromatography and again being characterised by X-ray crystallography. This strongly suggested that in the presence of $\text{Fe}_3(\text{CO})_{12}$ the diphenylphosphine sulfide sulfur atom present in the carborane ligand **21** could be removed, and that the cluster product $\text{S}_2\text{Fe}_3(\text{CO})_9$ would be formed preferentially in any reaction attempting the coordination of the carborane ligand **21** to a diiron centre when using $\text{Fe}_3(\text{CO})_{12}$, as observed experimentally. These results are consistent with the literature, where similar desulfurisation reactions of phosphorus sulfides by iron carbonyls are known¹⁸²⁻¹⁸⁴. To this end, it was accepted that formation of a phosphine-sulfide complex, namely $[\text{Fe}_2\{o\text{-carbP}(\text{S})(\text{Ph})_2\text{S}\}_2(\text{CO})_4]$, was unfavourable, and instead the synthesis of the phosphine complex $[\text{Fe}_2\{o\text{-carbP}(\text{Ph})_2\text{S}\}_2(\text{CO})_4]$ should be attempted. To achieve this it was decided that an excess of $\text{Fe}_3(\text{CO})_{12}$ should be employed, in order to first remove all of the sulfur atoms present on the phosphine-sulfide groups as $\text{S}_2\text{Fe}_3(\text{CO})_9$, and then the remainder of the

$\text{Fe}_3(\text{CO})_{12}$ reagent could react with the exposed phosphines to form the desired $[\text{Fe}_2\{o\text{-carbP(Ph)}_2\text{S}\}_2(\text{CO})_4]$ product.



Scheme 5.7. Synthesis of $[\text{Fe}_2\{o\text{-carbP(Ph)}_2\text{S}\}_2(\text{CO})_4]$ **22** from *o*-carborane ligand **21** and excess $\text{Fe}_3(\text{CO})_{12}$.

The reaction proved successful with the excess $\text{Fe}_3(\text{CO})_{12}$ serving to first generate the $\text{S}_2\text{Fe}_3(\text{CO})_9$ cluster and then the di-carborane phosphine-coordinated product $[\text{Fe}_2\{o\text{-carbP(Ph)}_2\text{S}\}_2(\text{CO})_4]$ **22**. The diiron carborane species **22** is air-sensitive and was obtained via fractional crystallisation from hexane at -20 °C where the $\text{S}_2\text{Fe}_3(\text{CO})_9$ cluster was removed first, leaving dark red block crystals of **22** to form in 39% yield. These crystals were suitable for X-ray diffraction.

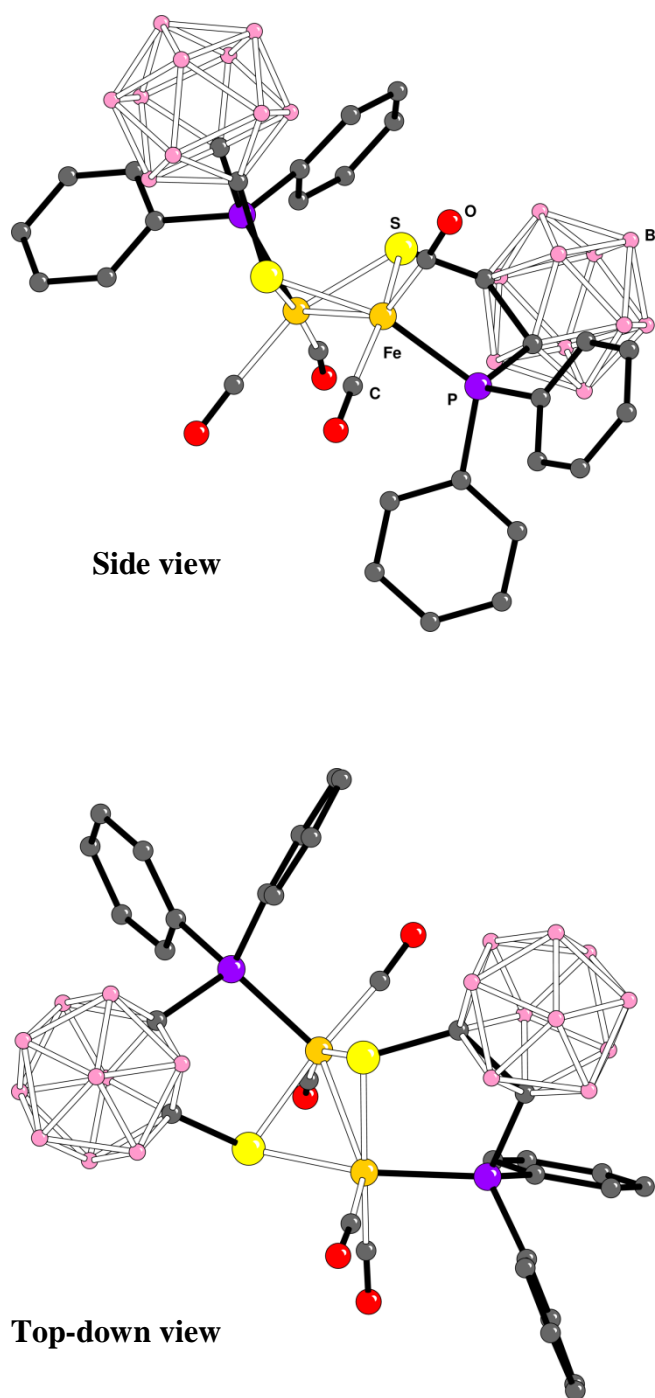


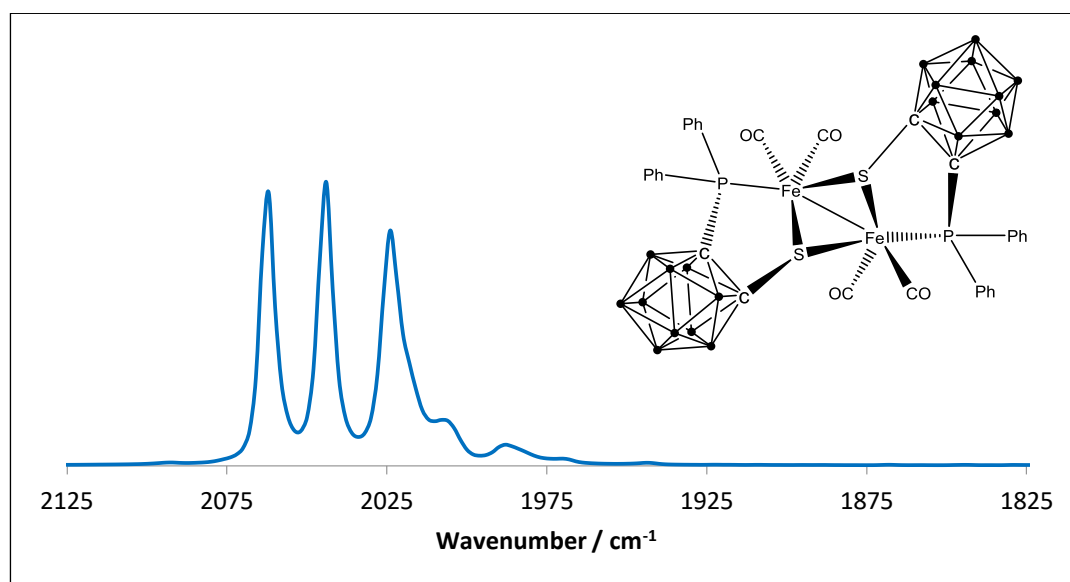
Figure 5.5. CAMERON representations of the structure of $[\text{Fe}_2\{\text{o-carbP}(\text{Ph})_2\text{S}\}_2(\text{CO})_4]$ **22** with spheres of arbitrary size.

$[\text{Fe}_2\{\text{o-carbP}(\text{Ph})_2\text{S}\}_2(\text{CO})_4]$ **22**, with its incorporation of two *ortho*-carborane units, displays interesting chemical and physical properties, particularly when compared to the two reported carborane systems.

5.2.3 Spectroscopic properties of $[\text{Fe}_2\{o\text{-carbP(Ph)}_2\text{S}\}_2(\text{CO})_4]$

5.2.3.1 FTIR spectroscopy

The solution FTIR spectrum of $[\text{Fe}_2\{o\text{-carbP(Ph)}_2\text{S}\}_2(\text{CO})_4]$ **22** was recorded in hexane and is shown in **Figure 5.6** along with a table comparing the CO stretches of the two reported *ortho*-carborane $[\text{FeFe}]$ -hydrogenase subsite analogue systems.



Compound	$\nu(\text{CO}) / \text{cm}^{-1}$
$[\text{Fe}_2\{o\text{-carbP(Ph)}_2\text{S}\}_2(\text{CO})_4]$	2062, 2043, 2020
A $[\text{Fe}_2(o\text{-carb-S}_2)(\text{CO})_6]$	2092, 2055, 2024
B $[\text{Fe}_2(\text{pdt})(\text{CO})_4((\text{PPh}_2)_2o\text{-carb})]$	2032, 1965, 1920

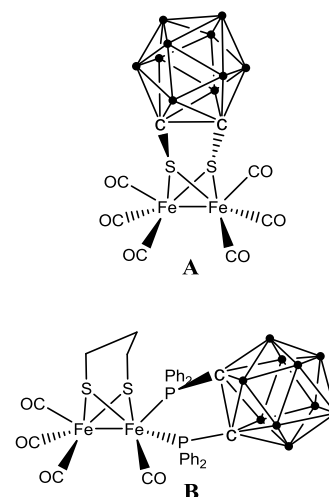


Figure 5.6. FTIR spectra comparing the CO stretches of $[\text{Fe}_2\{o\text{-carbP(Ph)}_2\text{S}\}_2(\text{CO})_4]$ **22** to those of the two reported *ortho*-carborane $[\text{FeFe}]$ -hydrogenase subsite analogue systems^{169,170}.

The IR spectrum of $[\text{Fe}_2\{o\text{-carbP(Ph)}_2\text{S}\}_2(\text{CO})_4]$ **22** provided some interesting information. The CO stretches of **22** appear at relatively high wavenumbers, but not as high as those of the dithiolate ortho-carborane species, $[\text{Fe}_2(o\text{-carb-S}_2)(\text{CO})_6]$ **A**. This suggests that although the carborane moieties of **22** are providing an electron-withdrawing effect, reducing electron density on the FeFe core and decreasing back donation into the π^* antibonding orbitals of CO, this is counteracted to some extent by the coordination of the electron-donating phosphine groups. This is significant, as the fact that the CO stretches of **22** are at lower wavenumbers than those of **A**, despite **22** containing two carborane moieties as opposed to **A** only containing one carborane, demonstrates that the phosphine donating effects outweigh the electron-withdrawing effects of the carborane groups.

Comparing the CO stretches of $[\text{Fe}_2\{o\text{-carbP(Ph)}_2\text{S}\}_2(\text{CO})_4]$ **22** to the diphosphine carborane species $[\text{Fe}_2(\text{pdt})(\text{CO})_4((\text{PPh}_2)_2o\text{-carb})]$ **B**, the wavenumbers of the CO stretches are higher for **22** than **B**. This is due to the structural effect of the carborane moieties in **22** being attached to the FeFe centre via thiolate groups in addition to the electron-donating phosphine groups, so that more electron-withdrawing character of the carborane species is exerted on the FeFe core, reducing the extent of back bonding into the π^* antibonding orbitals of CO, and increasing the CO bond order.

The overall effect of the presence of the bidentate *ortho*-carborane ligands incorporated into $[\text{Fe}_2\{o\text{-carbP(Ph)}_2\text{S}\}_2(\text{CO})_4]$ **22**, which contain both thiolate-bridgehead groups and electron-donating phosphine groups on the FeFe core, is an IR spectrum with CO bands displaying both the character of the carborane dithiolate system $[\text{Fe}_2(o\text{-carb-S}_2)(\text{CO})_6]$ **A** and the diphosphine carborane species $[\text{Fe}_2(\text{pdt})(\text{CO})_4((\text{PPh}_2)_2o\text{-carb})]$ **B**. Although this result was not unexpected, it is significant in that it has provided validation to both the new system $[\text{Fe}_2\{o\text{-carbP(Ph)}_2\text{S}\}_2(\text{CO})_4]$ **22** and the previously reported *ortho*-carborane systems.

5.2.3.1 Electrochemistry

The electrochemistry of $[\text{Fe}_2\{o\text{-carbP(Ph)}_2\text{S}\}_2(\text{CO})_4]$ **22** was examined in MeCN containing 0.1 M $[\text{Bu}_4\text{N}][\text{BF}_4]$ at a vitreous carbon electrode. A typical response obtained at room temperature at a scan-rate of 50 mVs^{-1} is shown in **Figure 5.7** over the potential range 0 to -1.5 V versus Fc^+/Fc .

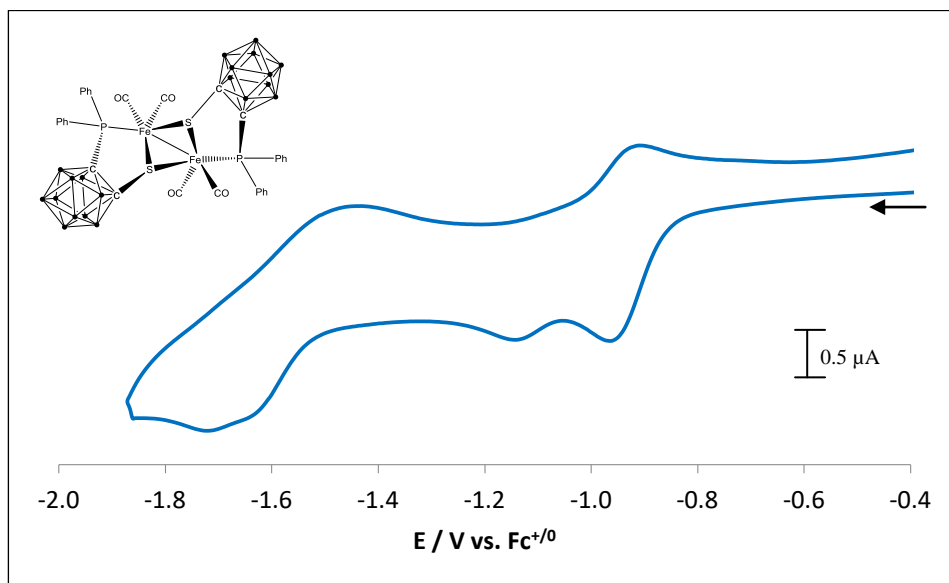


Figure 5.7. Electrochemistry of $[\text{Fe}_2\{o\text{-carbP(Ph)}_2\text{S}\}_2(\text{CO})_4]$ **22**. Conditions: 1 mM of the complex in MeCN containing 0.1 M $[\text{Bu}_4\text{N}][\text{BF}_4]$ at a vitreous carbon working electrode, area 0.7 cm^2 ; scan-rate 50 mV s^{-1} at 21°C .

An apparently partially reversible primary process with a peak separation, $|E_p^{\text{ox}} - E_p^{\text{red}}|$ of 74 mV, close to the theoretical value for a one-electron process, is observed at -0.96 V . Near -1.1 V another peak is observed which probably arises from chemistry associated with the partially reversible chemistry primary step. Near -1.7 V a major process occurs which may involve quasi-reversible (slow) electron-transfer chemistry and/or overlapping redox processes. The system is much simplified when recorded at -40°C as is shown by **Figure 5.8**. Firstly, the primary one-electron process appears fully reversible with the reverse peak current of similar magnitude to the forward step. Secondly, the minor redox process near -1.1 V is substantially suppressed as is consistent with a slowing down of the chemistry following the primary electron-transfer.

Finally, the more negative process at observed at -1.66 V has a shape consistent with a quasi-reversible one-electron step.

If we consider the major redox processes as essentially two successive one-electron steps then the separation in $E^{o/}$ – values of 700 mV is typical of that involving sequential addition to an orbital without major structural change.

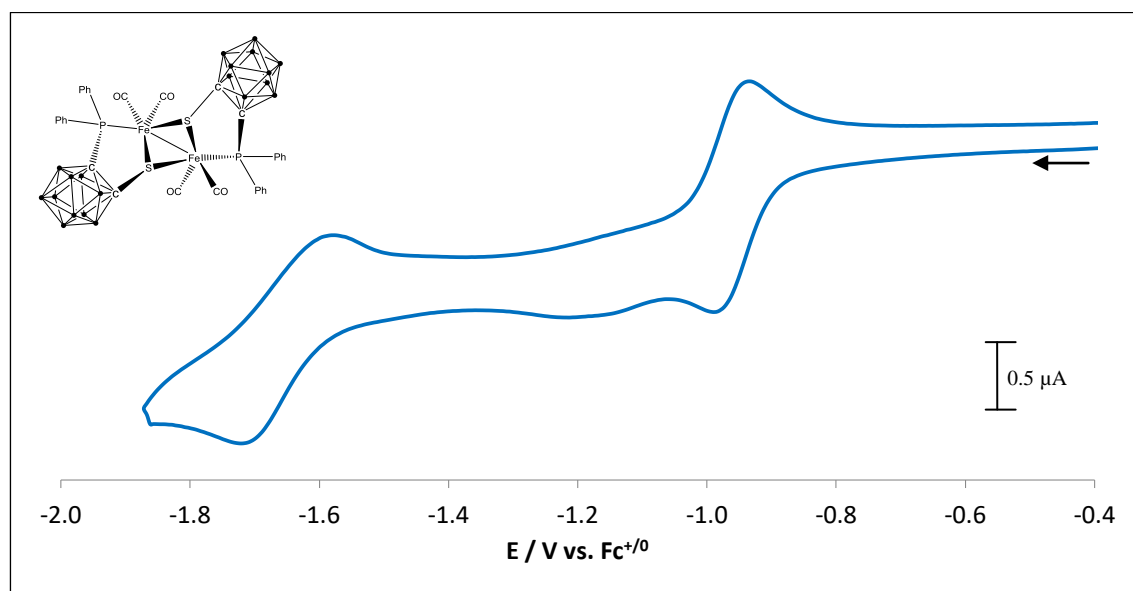
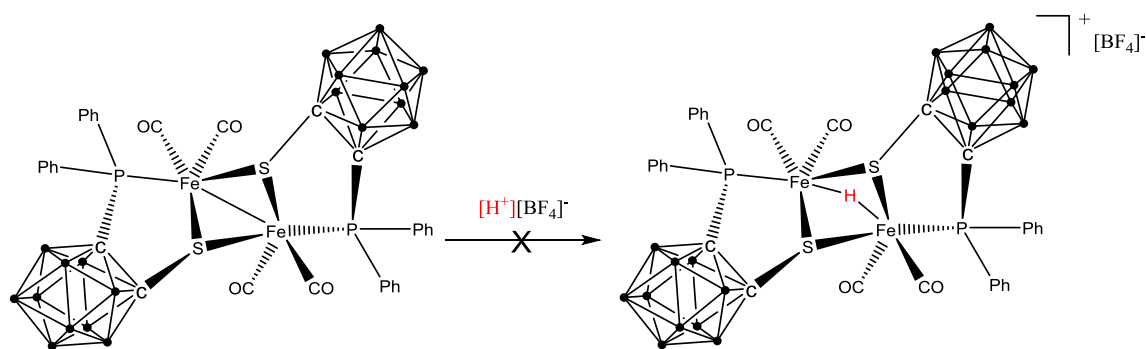


Figure 5.9. Low temperature electrochemistry of $[\text{Fe}_2\{\text{o-carbP}(\text{Ph})_2\text{S}\}_2(\text{CO})_4]$ **22**. Conditions: 1 mM of the complex in MeCN containing 0.1 M $[\text{Bu}_4\text{N}][\text{BF}_4]$ at a vitreous carbon working electrode, area 0.7 cm^2 ; scan-rate 50 mV s^{-1} at -40°C .

The observed relative ease of reduction is strongly indicative of the electron withdrawing capacity of the carborane unit as is consistent with the high frequencies of the CO stretches as discussed above. Moreover, the draining of electron density from the diiron unit onto the carborane explains the inactivity of **22** with respect to protonation. Thus treatment of $[\text{Fe}_2\{\text{o-carbP}(\text{Ph})_2\text{S}\}_2(\text{CO})_4]$ **22** with $\text{HBF}_4 \cdot \text{OEt}_2$ does not lead to reaction as is observed with other bis-phosphine systems¹⁶⁸.

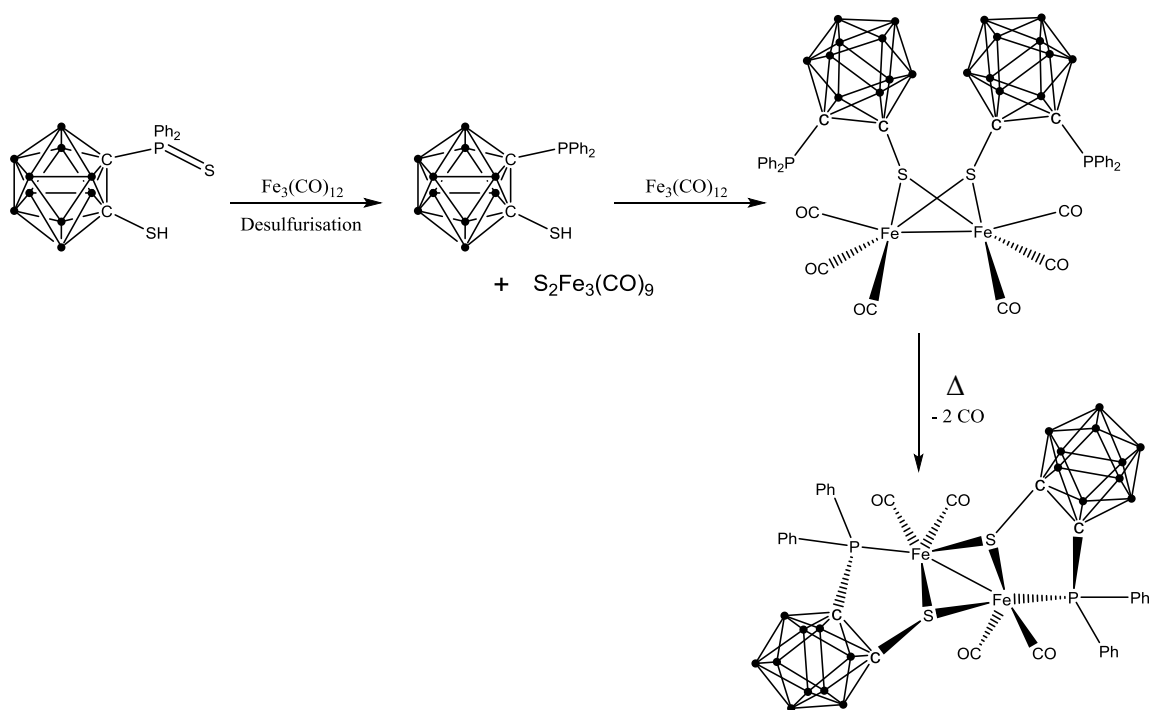


Scheme 5.8. $[\text{Fe}_2\{\text{o-carbP(Ph)}_2\text{S}\}_2(\text{CO})_4]$ **22** is not protonated on addition of $\text{HBF}_4\cdot\text{OEt}_2$.

5.2.4 Concluding remarks and future work

In this chapter we have shown that it is possible to construct a di-carborane FeFe subsite system where the bidentate *ortho*-carborane ligands are anchored to the bridgehead via thiolate groups but also interact with the diiron core through *tertiary* phosphine moieties. The new system $[\text{Fe}_2\{\text{o-carbP(Ph)}_2\text{S}\}_2(\text{CO})_4]$ **22** was characterised crystallographically.

The formation of **22** must involve multi-step chemistry, notably a desulfurisation reaction step whereby the cluster molecule $\text{S}_2\text{Fe}_3(\text{CO})_9$ was produced as a co-product in the first step of the reaction process, together with the phosphino thiol. Subsequent attack of this species on $\text{Fe}_3(\text{CO})_{12}$ is likely to lead to the formation of a dithiolate intermediate with subsequent substitution of CO by the appended phosphine ligands giving the final product, $[\text{Fe}_2\{\text{o-carbP(Ph)}_2\text{S}\}_2(\text{CO})_4]$ **22**, **Scheme 5.9**. However, an alternative pathway which proceeds via an CO substitution by phosphine and subsequent formation of the bis-thiolate cannot be excluded.



Scheme 5.9. Possible mechanism for the formation of $[\text{Fe}_2\{\text{o-carbP(Ph)}_2\text{S}\}_2(\text{CO})_4]$ **22**.

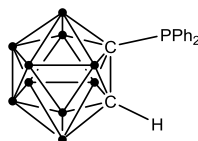
The FTIR and electrochemical data show that the *ortho*-carborane moieties are strongly electron withdrawing. The CO stretches are substantial higher than in related bis-phosphine systems and a primary reduction process can be accessed at -0.96 V.

The withdrawing carborane ligands are responsible for the lowering of the energy of the metal-metal bond (the probable homo) and consequently the inability to protonate this bond under conditions that other phosphine complexes readily protonate.

An exploration of the electron-transfer chemistry in the presence of a proton source is a clear avenue for further work. The primary electron-transfer step would be expected to raise the basicity of the HOMO allowing protonation and possible electrocatalysis.

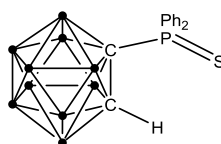
5.3 Experimental

5.3.1 Synthesis of 1-PPh₂-1,2-*closo*-C₂B₁₀H₁₁ (**19**)¹⁷⁹



1,2-*closo*-C₂B₁₀H₁₂ (0.86 g, 6 mmol) was dissolved in dry degassed DME (50 mL) and cooled to -78 °C. *n*-butyllithium 1.6 M in hexane solution (3.73 mL, 6 mmol) was then added, and the resultant mixture left to stir at -78 °C for 30 min. The solution was then warmed to room temperature and left to stir for a further 2 h. The solution was then cooled to 0 °C and chlorodiphenylphosphine (1.07 mL, 6 mmol) was added. The solution was then left to stir at 0 °C for a further 30 min before being heated to 85 °C for 16 h. The solvents were then removed in vacuo to give an off-white oil. Column chromatography (15:1 hexane/DCM) and subsequent drying in vacuo gave the *title compound* (1.19 g, 4 mmol, 61%) as colourless crystals. ¹H-NMR (CDCl₃, 300.13 MHz): δ (ppm) = 7.78 (m, 4H, Ar-H), 7.35 (m, 6H, Ar-H), 3.45 (s, 1H, BC-H), 2.10 (m, 10H, B-H). ³¹P-NMR (CDCl₃, 121.48 MHz): δ (ppm) = 25.08 (s).

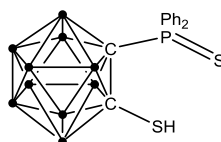
5.3.2 Synthesis of 1-SPPH₂-1,2-*closo*-C₂B₁₀H₁₁ (**20**)¹⁷²



1-PPh₂-1,2-*closo*-C₂B₁₀H₁₁ **19** (1.19 g, 4 mmol) was dissolved in dry degassed toluene (50 mL) and sulfur powder (0.14 g, 4 mmol) was added. Dry degassed triethylamine (1 mL) was then added before the mixture was heated to 100 °C for 16 h. The solvents were then removed in vacuo to give a yellow oil. Column chromatography (6:1 hexane/DCM) and subsequent drying in vacuo gave the *title compound* (0.71 g, 2 mmol, 55%) as white crystals. ¹H-NMR (CDCl₃, 300.13 MHz): δ (ppm) = 8.24 (m, 4H, Ar-H),

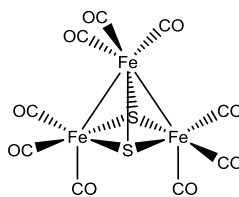
7.60 (m, 6H, Ar-H), 4.65 (s, 1H, BC-H), 2.20 (m, 10H, B-H). ^{31}P -NMR (CDCl_3 , 121.48 MHz): δ (ppm) = 50.72 (s).

5.3.3 Synthesis of 1-SH-2-SPPH₂-1,2-*closo*-C₂B₁₀H₁₀ (**21**)¹⁷²



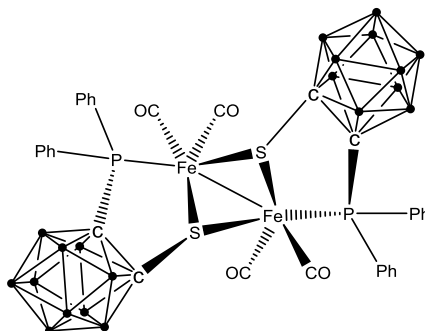
1-SPPH₂-1,2-*closo*-C₂B₁₀H₁₁ **20** (0.71 g, 2 mmol) was dissolved in dry degassed diethyl ether (50 mL) and cooled to -78 °C. *n*-butyllithium 1.6 M in hexane solution (1.24 mL, 2 mmol) was then added, and the resultant mixture left to stir at -78 °C for 30 min. The solution was then warmed to room temperature and left to stir for a further 2 h. Sulfur powder (0.08 g, 2mmol) was then added, and the resultant mixture left to stir for 16 h. 3 M HCl (40 mL) was then added, and after 10 min stirring the organic Et₂O layer was obtained. The aqueous layer was extracted with more Et₂O (2 x 50 mL) and then the organic layers were combined, with the Et₂O solvent subsequently being removed in vacuo to give a foamy off-white solid. With the aid of sonication, the solid was dissolved in hexane (100 mL) and recrystallised at -20 °C. Obtaining the crystals formed by filtration gave the *title compound* (0.55 g, 1 mmol, 71%) as slightly yellow crystals. ^1H -NMR (CDCl_3 , 300.13 MHz): δ (ppm) = 8.38 (m, 4H, Ar-H), 7.61 (m, 6H, Ar-H), 5.54 (s, 1H, S-H), 2.26 (m, 10H, B-H). ^{31}P -NMR (CDCl_3 , 121.48 MHz): δ (ppm) = 49.35 (s).

5.3.4 Test synthesis of $\text{S}_2\text{Fe}_3(\text{CO})_9$



Triphenylphosphine sulfide (0.27 g, 1 mmol) and triirondodecacarbonyl (0.23 g, 0.5 mmol) were dissolved in dry degassed THF (40 mL). The mixture was then heated to 55 °C for 16 h. Removal of the solvent in vacuo gave a red/purple oil and column chromatography (hexane eluent) and subsequent drying in vacuo gave the *title compound* (0.10 g, 0.2 mmol, 44%) as purple powder. Crystals suitable for X-ray diffraction were grown by slow evaporation of a hexane solution.

5.3.5 Synthesis of $[\text{Fe}_2\{o\text{-carbP(Ph)}_2\text{S}\}_2(\text{CO})_4]$ (**22**)



1-SH-2-SPPPh₂-1,2-*closo*-C₂B₁₀H₁₀ **21** (0.22 g, 0.6 mmol) and triirondodecacarbonyl (0.71 g, 1.4 mmol) were dissolved in dry degassed THF (75 mL) and heated to 55 °C for 16 h. Removal of the solvent in vacuo gave a red/black oil. Dry degassed hexane was then added (100 mL) and the mixture sonicated for 1 h. The resultant dark red solution was then filtered through celite into another flask, removing insoluble Fe salts, and the solution was cooled at -20 °C for 24 h. The resultant solution had precipitated the cluster $\text{S}_2\text{Fe}_3(\text{CO})_9$, which was removed by another filtration through celite. The subsequent solution was then cooled to -20 °C for 72 h, producing dark red block crystals suitable for X-ray diffraction of the *title compound* (0.11 g, 0.1 mmol, 39%). ¹H-NMR (C₆D₆, 300.13 MHz): δ (ppm) = 7.68 (m, 8H, Ar-H), 7.01 (m, 12H, Ar-H), 2.75 (m, 20H, B-H).

^{31}P -NMR (CDCl_3 , 121.48 MHz): δ (ppm) = -122.50 (s, 1P), -110.72 (s, 1P). IR(hexane): $\nu(\text{CO}) = 2062, 2043, 2020$. Anal. Calcd. for $\text{C}_{32}\text{H}_{40}\text{O}_4\text{S}_2\text{P}_2\text{B}_{20}\text{Fe}_2$: C, 40.78; H, 4.28. Found: C, 40.60; H, 4.15.

5.3.6 X-ray diffraction

Crystals were suspended in oil, and one was mounted on a glass fibre and fixed in the cold nitrogen stream of the diffractometer. Data were collected on a Bruker Apex DUO diffractometer. Data were process using the SAINT program¹⁸⁵. Structures were determined by direct methods in the SHELXS-97 program¹⁸⁶ and refined by full-matrix least-squares methods on F^2 in SHELXL-2013¹⁸⁶. Non-hydrogen atoms were refined with anisotropic thermal parameters. Hydrogen atoms were included in idealized positions and their U_{iso} values were set to ride on the U_{eq} values of the parent carbon atoms. Three carbon atoms of the solvent hexane molecule were disordered over two positions: occupancy for the major position was 0.728(15) at the end of refinement. The carbon–carbon distances in the disordered part were restrained to a length of 1.52(2) Å.

Crystal data: $\text{C}_{32}\text{H}_{40}\text{B}_{20}\text{Fe}_2\text{O}_4\text{P}_2\text{S}_2$, $0.5(\text{C}_6\text{H}_{14})$, $M = 985.7$, $T = 173(2)$ K, $\lambda(\text{Mo-K}\alpha) = 0.71073$ Å, triclinic, space group $P\bar{1}$, $a = 10.8183(19)$, Å, $b = 14.130(3)$ Å, $c = 16.628(3)$ Å, $\alpha = 90.494(3)^\circ$, $\beta = 95.619(3)^\circ$, $\gamma = 106.934(2)^\circ$, $V = 2418.0(7)$ Å³, $Z = 2$, total reflections 14988, independent reflections 9335, $R_{\text{int}} = 0.030$, $R_1 = 0.056$ [$F^2 > 2\sigma(F^2)$], wR2 (all data) 0.182.

6 Towards heterolytic hydrogen splitting: attachment of electron-deficient boranes

6.1 Introduction

6.1.1 General aspects

This chapter is concerned with steps undertaken towards synthesising a system where a [FeFe]-hydrogenase subsite analogue is linked to an electron-deficient borane functionality with the view that this might allow heterolytic cleavage of dihydrogen.

In the next sections the interest in a hydrogen cleaving system will be explained, along with a brief introduction into the use of borane groups for hydrogen splitting. Subsequently, the steps taken towards the synthesis of such a system are outlined.

6.1.2 Interest in a diiron system capable of hydrogen cleavage

The heterolytic cleavage of dihydrogen by hydrogenase systems is fairly well-known; except by utilising the [Fe]-hydrogenase as opposed to the [FeFe]-hydrogenase. The [Fe]-hydrogenase, otherwise known as hydrogen-forming methylene-tetrahydromethanopterin dehydrogenase (Hmd), is known to heterolytically split H_2 into a hydride and a proton, with the hydride transferred to the carbocation-containing substrate, methenyl-tetrahydromethanopterin (methenyl- H_4MPT^+)¹⁸⁷⁻¹⁹⁰. The active site of the [Fe]-hydrogenase is shown in **Figure 6.1**, along with its heterolytic dihydrogen splitting reaction to transfer hydride to methylene- H_4MPT^+ .

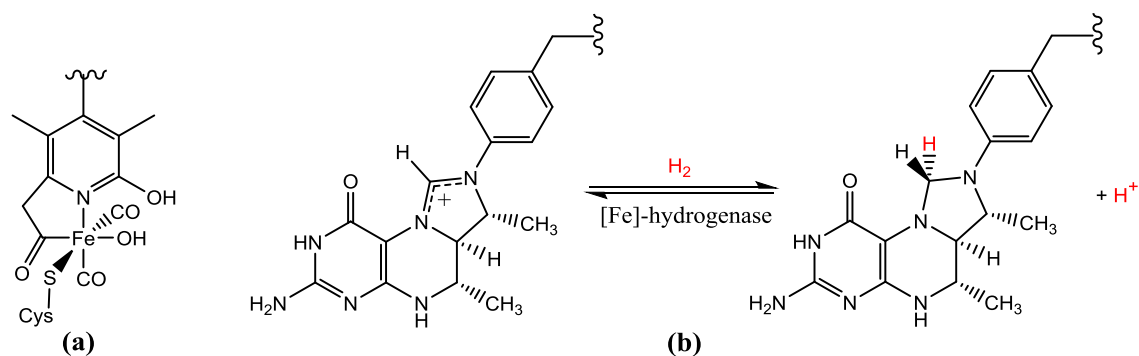
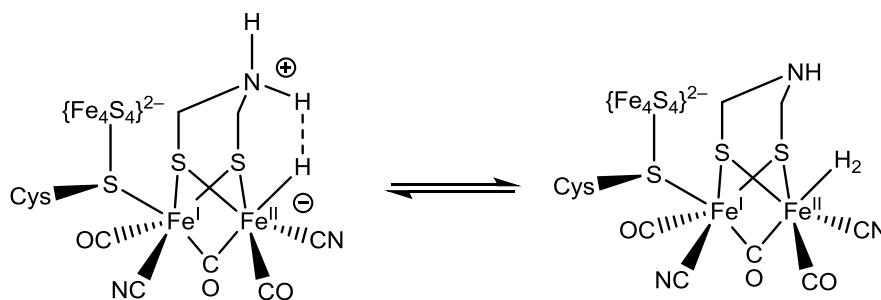


Figure 6.1. The active site of the [Fe]-hydrogenase enzyme (a) and its heterolytic H₂ splitting to stereoselectively transfer hydride to methenyl-H₄MPT⁺ to yield methenyl-H₄MPT plus a proton (b). Adapted from references¹⁸⁷⁻¹⁹⁰.

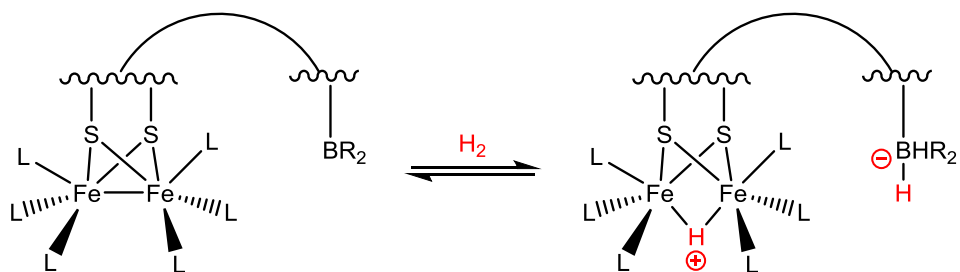
[Fe]-hydrogenases, in contrast to [FeFe]- and [NiFe]-hydrogenases, do not catalyse the splitting of H₂ into protons and electrons (or the reverse reaction). In addition, they cannot facilitate a H/D exchange reaction at a significant rate unless methenyl-H₄MPT⁺ or methenyl-H₄MPT is present¹⁹¹.

The [FeFe]-hydrogenase system employs an entirely different system to generate dihydrogen. It is fairly well-established that the bridgehead of the naturally-occurring [FeFe]-hydrogenase is an azadithiolate (adt) derivative¹⁹², and that the secondary amine involved participates in the catalytic cycle. With the amine bridgehead acting as a proton shuttle, it is believed that H₂ formation step occurs in a fashion to that shown in **Scheme 6.1**, where the proton interacts with a hydridic species at the diiron core^{193,194}.



Scheme 6.1. Putative mechanistic step for reversible formation of dihydrogen in the catalytic cycle of the [FeFe]-hydrogenase. Adapted from references^{193,194}.

Much synthetic work has been carried out on enhancing this mechanism, including the incorporation of additional Lewis basic moieties into the surrounding environment (see **Chapter 2**). However, in this work the aim is to progress towards an inversion of the inherent chemistry by the attachment of a pendant Lewis acidic borane group to cleave hydrogen heterolytically; with the borane accepting a hydride and the FeFe core being protonated, as according to **Scheme 6.2**.

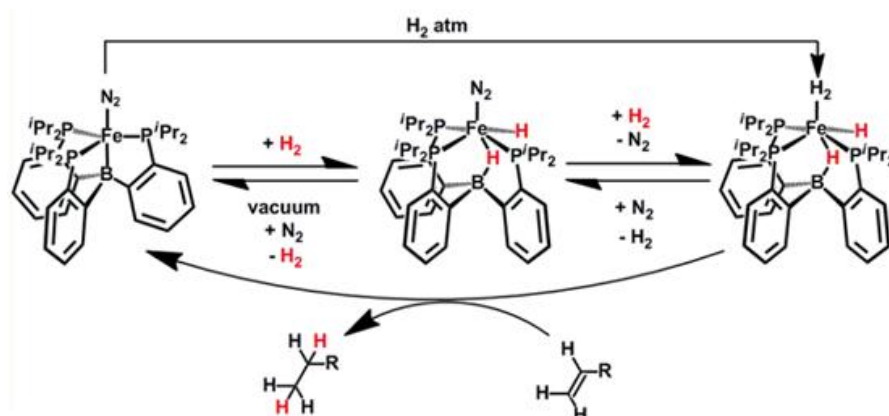


Scheme 6.2. Postulated heterolytic dihydrogen cleavage by a [FeFe]-hydrogenase subsite analogue with pendant Lewis acidic borane group.

This scheme of hydrogen splitting is not altogether unreasonable. The basicity of these diiron systems is fairly well established, with ligand coordination providing a means of control¹⁹⁵⁻¹⁹⁷. As a general rule, the presence of more electron-donating ligands on the FeFe core renders the diiron system more basic, thus making protonation more favourable. Pickett and coworkers¹⁹⁸ were able to demonstrate this concept by establishing that there is a linear free energy correlation between the rate of protonation and the basicity of the FeFe bond. This was achieved by measuring the energy of the HOMO, which is an acceptable method as photoelectron spectroscopy and DFT calculations have shown that in a typical Fe₂S₂(CO)₆ unit the character of the HOMO corresponds closely to the classical 'bent' Fe-Fe bond¹⁹⁹⁻²⁰¹. Therefore protonation of the Fe-Fe bond and the oxidation of diiron complexes can be assumed to engage the HOMO directly.

The requirement for electron-donating ligands to promote protonation in a heterolytic dihydrogen cleaving system was echoed in a recent publication by Peters and coworkers²⁰². In this not entirely-unrelated work, a ferraboratrane moiety was employed

for heterolytic addition of H₂, giving iron-borohydrido-hydride complexes as shown in **Scheme 6.3**.

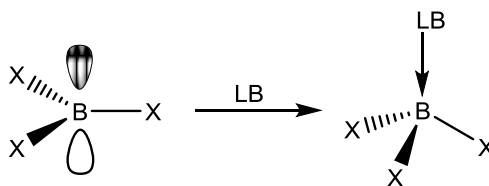


Scheme 6.3. Mechanism of heterolytic dihydrogen splitting by the system synthesised by Peters and coworkers. Image reproduced from reference²⁰².

The Peters system depends upon exposing a Lewis acidic borane site by decoordination of the donor iron atom; thereby generating a Lewis acid / Lewis Base system which can heterolytically split H₂. This has some analogy to the system proposed for development, thus some key ideas can be taken forward: an Fe + B system is indeed capable of cleaving H₂, electron-donating ligands (phosphines) are important for inducing sufficient electron density on the Fe centre to allow protonation, and ideally the Fe and B moieties are within reasonable proximity to each other to make H₂ cleavage as favourable as possible.

6.1.3 Borane groups for hydrogen splitting

Boranes are small, neutral molecules formed from a central boron atom surrounded by three covalently bound groups. Boron has only three valence electrons and therefore boranes have an empty p-orbital which is usually employed in their chemistry²⁰³. The empty p-orbital allows boranes to behave as Lewis acids and accept a pair of electrons from a Lewis base, which has the effect of changing the essentially planar borane into a nearly tetrahedral geometry²⁰⁴.



Scheme 6.4. Adduct formation upon coordination of a Lewis Base to a borane.

Boranes are incredibly useful for Lewis acid applications, though the standard method of tuning electrophilicity; the incorporation of electron-withdrawing halogen atoms, is not so straight forward for these moieties. Usually the Lewis acidity of a compound increases with the use of more electron-withdrawing halides following the series $F > Cl > Br$. However, with the case of the boron trihalides the order of Lewis acidity is in fact $BF_3 < BCl_3 < BBr_3$. This is because the Lewis acidity of these species is mainly controlled by the extent of π -bonding from the lone pairs of the halide ligand into the empty boron p-orbital²⁰⁵. The extent of π -donation is determined by the size of the electron donating orbital. The p-orbital on a fluoride is closest in size to the vacant boron p-orbital, meaning that orbital overlap is most effective in the BF_3 species and thus the boron p-orbital is less available to accept electrons from a Lewis base^{206,207}.

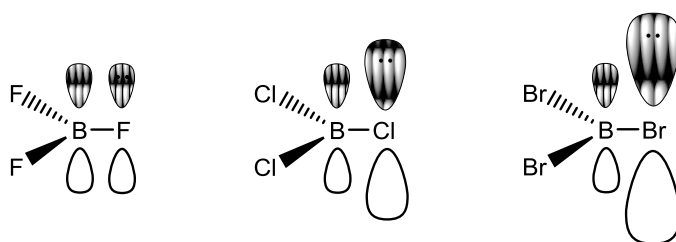


Figure 6.2. Lewis acidity of the boron trihalides is determined by the relative size of the p-orbitals on the halide ligands. Adapted from reference²⁰⁸.

The desire for more tuneable Lewis acidity and more thermally robust and water-tolerant boranes led to the development of organoboranes, and more specifically, fluorinated organoboranes. The presence of organic groups increased stability due to the B-C bond being more resistant to hydrolysis than the B-halide bonds²⁰⁹, and the organic groups introduced new possibilities for functionalisation in order to tailor the Lewis

acidic properties. To this end, pentafluorophenyl groups were soon employed. Tris(pentafluorophenyl)boron, $\text{B}(\text{C}_6\text{F}_5)_3$, was first synthesised in 1963 by Stone and Massey²¹⁰ and has since become one of the most popular Lewis acids^{211,212} due to its ease of preparation and handling²¹³ and high Lewis acidity, which is found to fall between BF_3 and BCl_3 ^{213,214}.

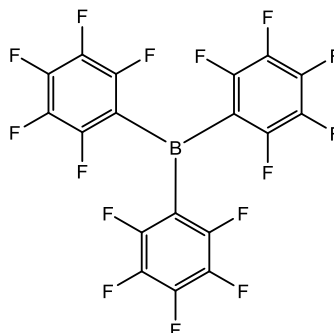
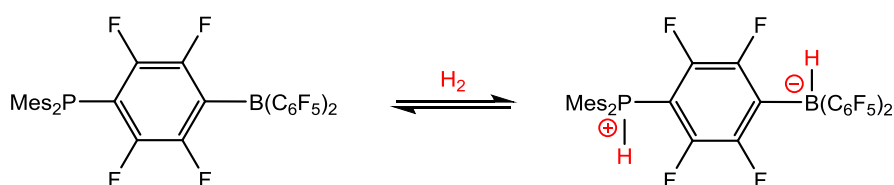


Figure 6.3. Structure of tris(pentafluorophenyl)boron, $\text{B}(\text{C}_6\text{F}_5)_3$.

In the last decade $\text{B}(\text{C}_6\text{F}_5)_3$ and other perfluoroaryl boranes have found employment in Frustrated Lewis Pair (FLP) systems²¹⁵. FLPs consist of Lewis acid and Lewis base components that are unable to form adducts due to steric congestion. This 'frustrated' reactivity has demonstrated the ability to cleave dihydrogen heterolytically. In 2006 Stephan and coworkers²¹⁶ reported the first example of reversible metal-free dihydrogen activation by using an intramolecular FLP system, as shown in **Scheme 6.5**.



Scheme 6.5. Heterolytic dihydrogen cleavage by $(\text{Mes})_2\text{P}(\text{C}_6\text{F}_4)\text{B}(\text{C}_6\text{F}_5)_2$ intramolecular FLP system. Adapted from reference²¹⁷.

The action of the FLP system shown in **Scheme 6.5** is not too dissimilar from the desired reactivity of a $[\text{FeFe}]$ -hydrogenase subsite analogue with pendant Lewis acidic borane group. A pendant bis(pentafluorophenyl)boron group would be ideal for accepting a hydride in a heterolytic dihydrogen splitting system. A convenient method

of introducing this functionality would be to utilise the equivalent hydride reagent, bis(pentafluorophenyl)boron hydride, $\text{HB}(\text{C}_6\text{F}_5)_2$. $\text{HB}(\text{C}_6\text{F}_5)_2$, commonly referred to as Piers' borane after its inventor²¹⁸, due to its inherent reactivity has found much employment in hydroboration chemistry²¹⁹, FLP assemblies²²⁰, and introducing bis(pentafluorophenyl)boron groups by adduct formation²²¹. However, non-adducted Piers' borane has some associated difficulties; namely the synthesis of which incorporates undesirably toxic tin reagents²¹⁸ or slow reaction speeds²¹⁹; and that it exists in its dimeric form due to the hydride groups satisfying the vacant p-orbital of another borane molecule. To this end Lancaster and coworkers²²⁰ have reported the synthesis of $\text{HB}(\text{C}_6\text{F}_5)_2$ isolated as its dimethyl sulfide adduct in its monomeric form, $\text{HB}(\text{C}_6\text{F}_5)_2 \cdot \text{SMe}_2$. This highly crystalline solid is synthetically easier to prepare and more soluble in hydrocarbon solvents than Piers borane, and most importantly retains the activity of the original system²²².

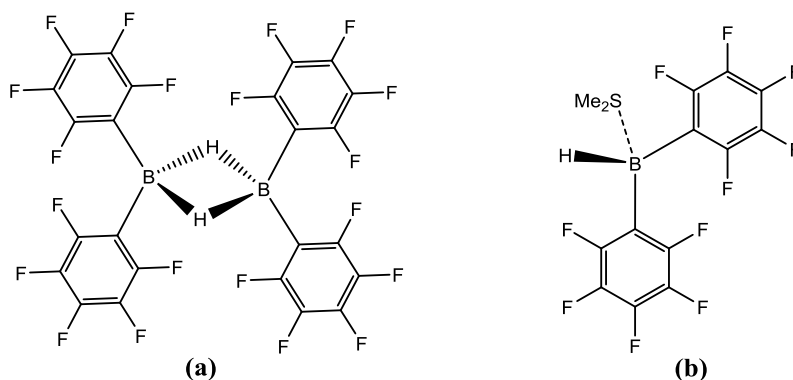


Figure 6.4. Dimeric Piers' borane (a) and monomeric $\text{HB}(\text{C}_6\text{F}_5)_2 \cdot \text{SMe}_2$ (b).

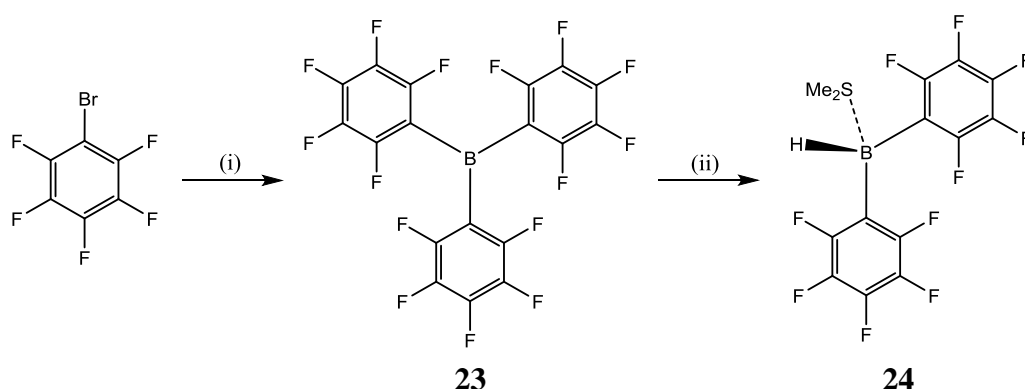
A [FeFe]-hydrogenase subsite analogue system capable of heterolytically cleaving dihydrogen is a desirable but synthetically challenging prospect. To construct such a system would involve an inversion of the inherent chemistry, though with electron-donating groups present on the diiron core to make the Fe-Fe bond more susceptible to protonation and a Lewis acidic pendant borane group present to accept a hydride, it could very well prove a possibility. As the control of the basicity of the diiron core is fairly well understood¹⁹⁵⁻¹⁹⁸, the priority was to achieve successful attachment of a pendant borane moiety. The attempts to achieve such an attachment are detailed in the following sections.

6.2 Results and discussion

Scheme 6.8. shows a proposed synthetic route to a target molecule possessing a borane moiety appended to a diiron subsite. The synthesis of the precursor compounds for this synthetic pathway are first described.

6.2.1 Synthesis of perfluoroaryl boranes

The synthesis of the bis(pentafluorophenyl)boron hydride dimethyl sulfide adduct, $\text{HB}(\text{C}_6\text{F}_5)_2 \cdot \text{SMe}_2$, **24** was performed stepwise using procedures modified from the literature^{223,221}.

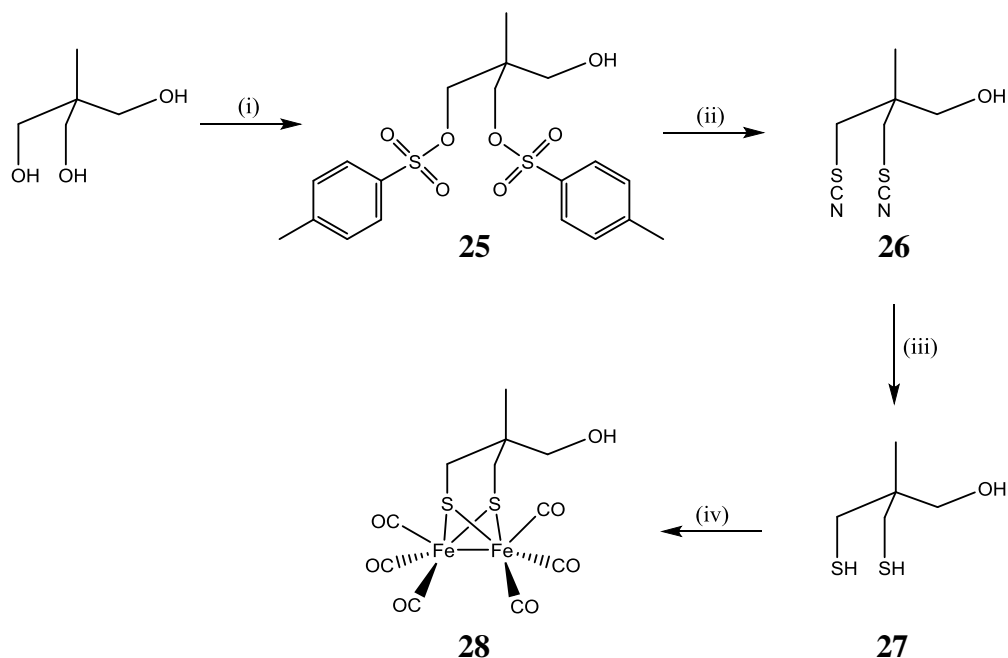


Scheme 6.6. Stepwise synthesis of $\text{HB}(\text{C}_6\text{F}_5)_2 \cdot \text{SMe}_2$, **24**. (i)a) 1.0 Mg, Et_2O , 0 °C, b) 0.33 $\text{BF}_3 \cdot \text{OEt}_2$, Et_2O /toluene, 0 °C, c) Toluene, 95 °C, 2 h, 43%; (ii)a) 0.5 $\text{BH}_3 \cdot \text{SMe}_2$, hexane, 50 °C, 1 h, b) 1.0 SMe_2 , hexane, RT, 82%. Procedures modified from those outlined by Lancaster and coworkers^{223,221}.

In step (i) the $\text{B}(\text{C}_6\text{F}_5)_3$ **23** product is formed by reaction of $\text{BF}_3 \cdot \text{OEt}_2$ with the Grignard species BrMgC_6F_5 which is generated in situ. The product is originally obtained via crystallisation of the diethyl ether adduct, $\text{Et}_2\text{O} \cdot \text{B}(\text{C}_6\text{F}_5)_3$, with the non-adducted form obtained through sublimation. In step (ii) the desired hydride product, $\text{HB}(\text{C}_6\text{F}_5)_2 \cdot \text{SMe}_2$ **24** is produced by facile exchange of hydride and pentafluorophenyl groups between the two borane reagents.

6.2.2 Synthesis of a hydroxyl-functionalised diiron subsite analogue

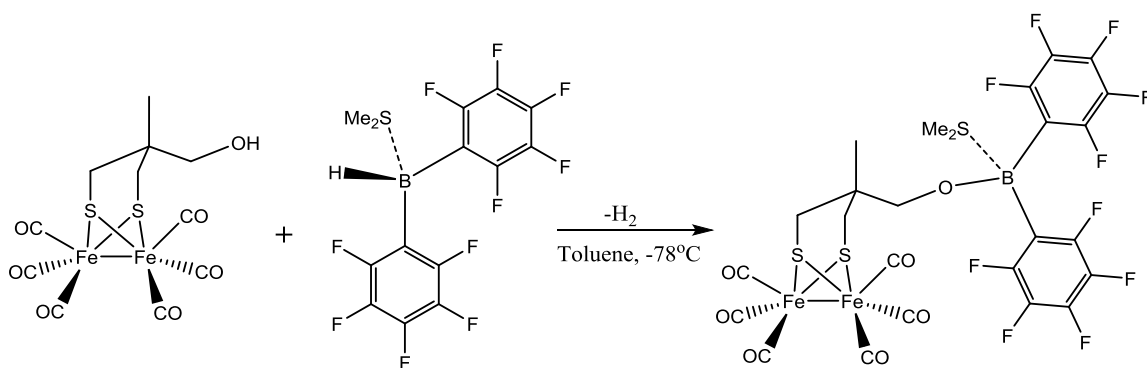
As demonstrated in **Chapter 2**, modification of [FeFe]-hydrogenase subsite analogues with pendant hydroxyl moieties is a convenient and simple method of introducing new functional groups. As the borane reagent employed readily forms adducts with Lewis bases, attaching the borane via a B-O bond to form a borinic ester moiety, R₂BOR', is a convenient and attractive option. However, whereas in **Chapter 2** [Fe₂(dmp)(CO)₆] **1** was used, considering the work of Peters and coworkers²⁰² where a successful system was shown to have Fe and B atoms in close proximity, another hydroxyl-functionalised diiron subsite analogue will be employed, namely [Fe₂{CH₃C(CH₂OH)(CH₂S)₂}(CO)₆] **28**. This diiron system, with its additional carbon chain length, should allow intimate proximity between the FeFe core and the borane moiety. The synthesis of [Fe₂{CH₃C(CH₂OH)(CH₂S)₂}(CO)₆] **28** was performed stepwise from the parent 1,1,1-tris(hydroxymethyl)ethane using procedures modified from the literature²²⁴.



Scheme 6.7. Stepwise synthesis of [Fe₂{CH₃C(CH₂OH)(CH₂S)₂}(CO)₆] **28**. (i) 2.0 Tos-Cl, pyridine, RT, 24 h, 54%; (ii) 10 KSCN, DMF, 140 °C, 6 h, 45%; (iii)a) 2 LiAlH₄, THF, 0 °C, b) THF, 40 °C, 48 h, 71%; (iv) 1.2 Fe₃(CO)₁₂, THF, 70 °C, 3 h, 83%. Procedures modified from those outlined by Pickett and coworkers²²⁴.

6.2.3 Combination of $[\text{Fe}_2\{\text{CH}_3\text{C}(\text{CH}_2\text{OH})(\text{CH}_2\text{S})_2\}(\text{CO})_6]$ with $\text{HB}(\text{C}_6\text{F}_5)_2\cdot\text{SMe}_2$

With the starting materials $[\text{Fe}_2\{\text{CH}_3\text{C}(\text{CH}_2\text{OH})(\text{CH}_2\text{S})_2\}(\text{CO})_6]$ **28** and $\text{HB}(\text{C}_6\text{F}_5)_2\cdot\text{SMe}_2$ **24** in hand, an attempt to synthesise the target borane functionalised species via the pathway proposed in **Scheme 6.8** was undertaken. Toluene was chosen as the solvent because it dissolves both reagents and because it is non-coordinating. The reaction was conducted at -78°C in an attempt to minimise undesired side reactions.



Scheme 6.8. Proposed synthetic route to $[\text{Fe}_2\{\text{CH}_3\text{C}(\text{CH}_2\text{OB}(\text{C}_6\text{F}_5)_2)(\text{CH}_2\text{S})_2\}(\text{CO})_6\cdot\text{SMe}_2]$.

After the addition of the diiron complex to the borane the reaction was allowed to warm to room temperature over 16 h, at which point volatiles were removed under vacuum to give a red oil. This oil was taken up in hexane and cooled to -20°C which afforded red crystals suitable for X-ray diffraction.

The crystallographic structure obtained revealed that the product was not the target monomer but instead the trimer; $[(\text{Fe}_2\{\text{C}_5\text{H}_9\text{S}_2\}(\text{CO})_6\text{O})_3\text{B}]$ **29**. Evidently the C_6F_5 substituents are susceptible to alcoholysis and/or facile exchange (scrambling). Attempts to modify the reaction by using a large excess of the borane **24** failed, the only crystalline material obtained was again the trimer, albeit this time as a different polymorph (structure **29'**, see experimental for crystallographical details). An explanation for this maybe that in the toluene solvent there is strong intramolecular hydrogen bonding of the hydroxyl groups of the diiron unit and they are pre-arranged for attack by the boron reagent. Such intramolecular H-bonding has been structurally characterised in the solid-state²²⁵.

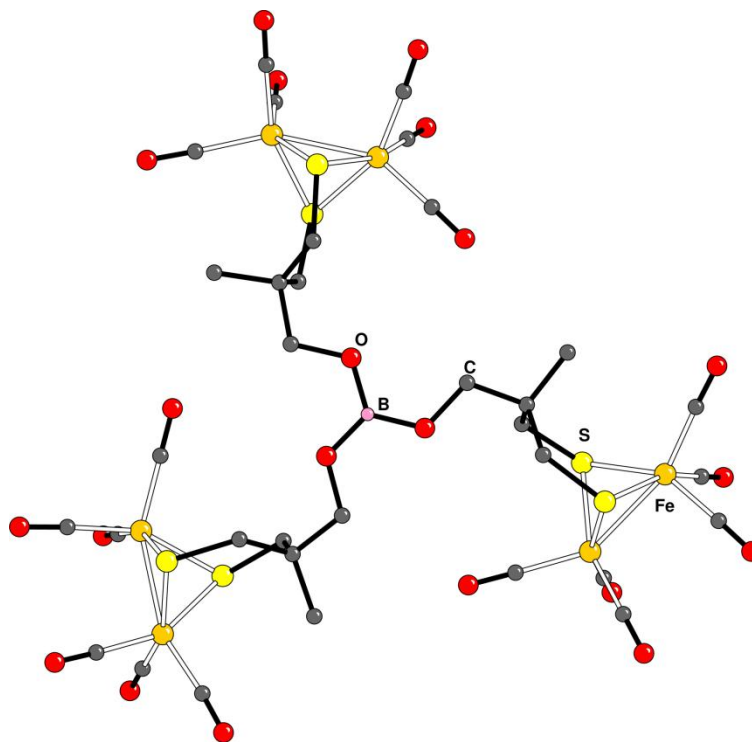
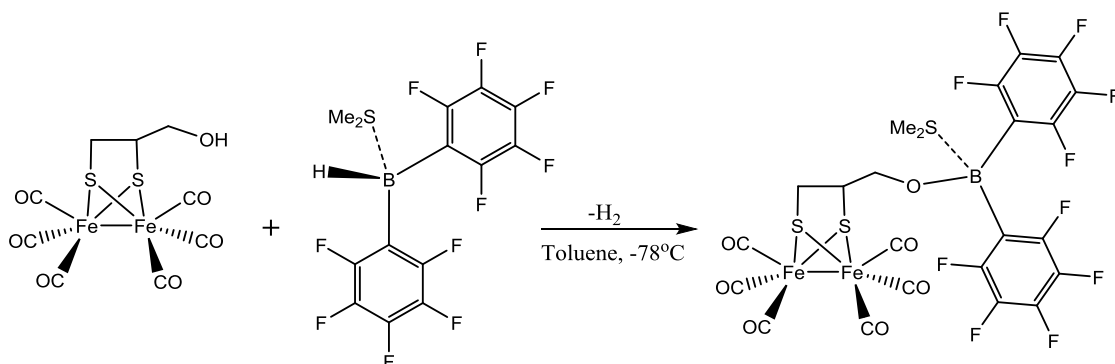


Figure 6.5. CAMERON representation of the structure of $[(\text{Fe}_2\{\text{C}_5\text{H}_9\text{S}_2\}(\text{CO})_6\text{O})_3\text{B}]$ **29** with spheres of arbitrary size.

There is evidently sufficient flexibility in $[\text{Fe}_2\{\text{CH}_3\text{C}(\text{CH}_2\text{OH})(\text{CH}_2\text{S})_2\}(\text{CO})_6]$ **28** with respect to the deployment of the hydroxyl group to allow three diiron moieties to be comfortably accommodated around the central boron atom. It was therefore thought that the 2,3-dimercapto-1-propanol derivative, $[\text{Fe}_2(\text{dmp})(\text{CO})_6]$ **1**, with its shorter alkoxy carbon chain length should sterically restrict the number of diiron moieties that can be accommodated around the central boron atom.

6.2.4 Combination of $[\text{Fe}_2(\text{dmp})(\text{CO})_6]$ with $\text{HB}(\text{C}_6\text{F}_5)_2 \cdot \text{SMe}_2$

The complex $[\text{Fe}_2(\text{dmp})(\text{CO})_6]$ **1** and $\text{HB}(\text{C}_6\text{F}_5)_2 \cdot \text{SMe}_2$ **24** were reacted under the same conditions as for **28** above with the objective of synthesising the assembly shown in **Scheme 6.9**.



Scheme 6.9. Proposed synthesis of $[\text{Fe}_2(\text{dmp})(\text{CO})_6\{\text{OB}(\text{C}_6\text{F}_5)_2\} \cdot \text{SMe}_2]$.

As before, after mixing the reagents at -78°C , the reaction mixture was allowed to warm to room temperature over 16 h, at which point volatiles were removed under vacuum to give a red oil. This oil was taken up in hexane from which red crystals were isolated upon cooling to -20°C . X-ray crystallography showed that the approach was partially successful in so far as that the isolated material possessed a bi-functionalised borane rather than the trimer derivative obtained using **28**. The structure of this dimeric product **30** which retains one C_6F_5 group bound to the boron is shown in **Figure 6.6**.

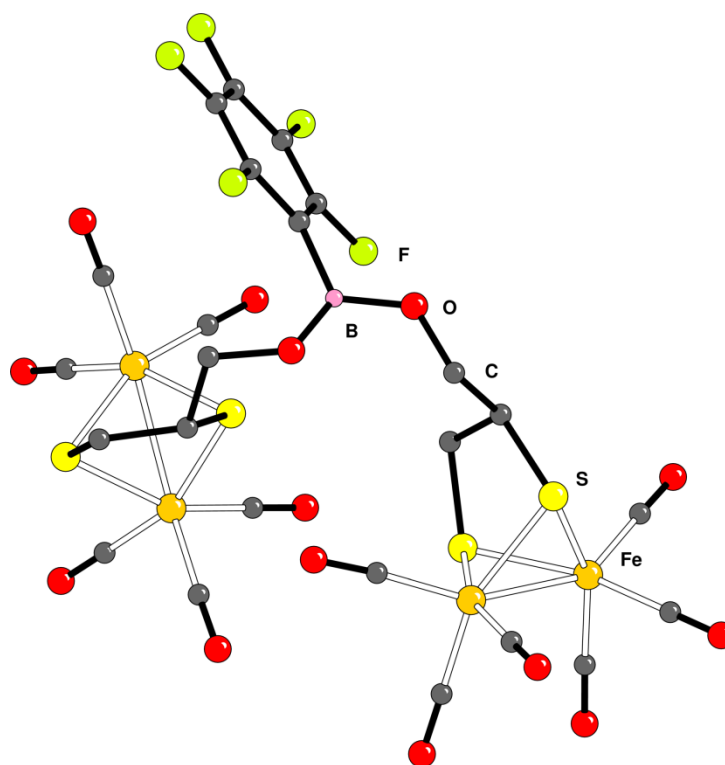
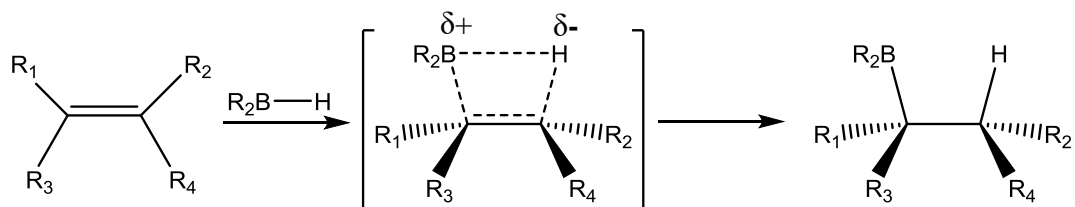


Figure 6.6. CAMERON representation of the structure of $[\{Fe_2(dmp)CO\}_6O]_2BC_6F_5$ **30** with spheres of arbitrary size.

At this point there were three potential avenues towards achieving the desired [FeFe]-hydrogenase subsite analogue with a pendant bis(pentafluorophenyl) borane moiety: develop a new even more sterically-hindered diiron unit with hydroxyl group, synthesise a more bulky borane group to attach, or try a new method of coupling. It was decided that synthesising new hydroxyl-functionalised diiron units and bulky boranes would require a lot of additional synthetic work; perhaps to only achieve the same result of trimeric/dimeric products. It was therefore resolved that a new approach would be adopted, namely hydroboration of an alkene functionality.

6.2.5 Synthesis of a diiron subsite analogue with alkene functionality

In order to test the activity of the monomeric Piers' borane dimethyl sulfide adduct, in 2012 Lancaster and coworkers²²² utilised $\text{HB}(\text{C}_6\text{F}_5)_2\cdot\text{SMe}_2$ for hydroboration. Hydroboration is the addition of a boron hydride across an alkene bond, proceeding through a four-centred transition state to generate a new organoborane species^{226,227}.

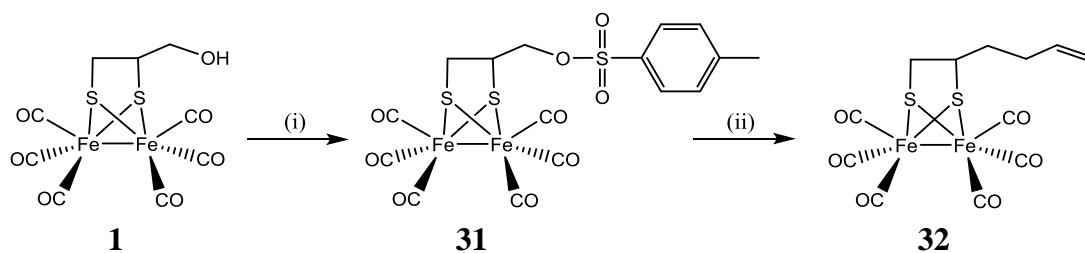


Scheme 6.10. General mechanism of a hydroboration reaction. Adapted from references^{226,227}.

Hydroboration is finding increasing use in synthetic chemistry due to its high favourability for anti-Markovnikov addition, as the borane moiety prefers to reside on the least substituted carbon. Subsequent oxidation reactions allow the formation of anti-Markovnikov alcohols and ketones^{228,229}.

In order to achieve hydroboration, it was first necessary to construct a suitable alkene-functionalised [FeFe]-hydrogenase subsite analogue. At the time of writing no carbon-backbone alkene functionalised diiron systems have been reported, so in this work the first species of this kind is introduced.

To construct the alkene moiety, inspiration was taken from the synthetic route for the production of $[\text{Fe}_2\{\text{CH}_3\text{C}(\text{CH}_2\text{OH})(\text{CH}_2\text{S})_2\}(\text{CO})_6]$ **28**, where tosylate groups were employed as a means of essentially replacing a hydroxyl group with another nucleophile. The stepwise synthesis of the alkene functionalised diiron system $[\text{Fe}_2\{\text{C}_4\text{H}_7\text{CH}(\text{S})\text{CH}_2\text{S}\}(\text{CO})_6]$ **32** from $[\text{Fe}_2(\text{dmp})(\text{CO})_6]$ **1** via a tosylate species, $[\text{Fe}_2(\text{dmp-Tos})(\text{CO})_6]$ **31**, is outlined in **Scheme 6.11**.



Scheme 6.11. Stepwise synthesis of $[\text{Fe}_2\{\text{C}_4\text{H}_7\text{CH}(\text{S})\text{CH}_2\text{S}\}(\text{CO})_6]$ **32**. (i) 1.2 Tos-Cl, pyridine, RT, 24 h, 87%; (ii) 1.0 $\text{C}_3\text{H}_5\text{MgCl}$, THF, -78°C , 14%.

In step (i) $[\text{Fe}_2(\text{dmp})(\text{CO})_6]$ **1** readily tosylates in the presence of pyridine to give the species $[\text{Fe}_2(\text{dmp-Tos})(\text{CO})_6]$ **31**. Crystals of **31** suitable for X-ray diffraction were grown from a hexane solution cooled to 2°C . In step (ii) the tosylate group is attacked by nucleophilic allylmagnesium chloride Grignard reagent. This reaction was conducted at -78°C to prevent side reactions, although the black reaction mixture and poor yield of 14% suggest that decomposition reactions were occurring; most likely due to attack of the Grignard reagent at the diiron centre. The new alkene-functionalised system has been characterised by $^1\text{H-NMR}$, FTIR, elemental analysis and mass spectrometry. Regarding the IR of the new species **31** and **32**, the tosylate compound **31** has CO bands comparable to the parent compound $[\text{Fe}_2(\text{dmp})(\text{CO})_6]$ **1**, though the alkene species **32** has CO bands of slightly lower wavenumber ($\sim 5\text{-}10\text{ cm}^{-1}$). This is due to the electronegative oxygen atom on the backbone being replaced with a more electron-donating carbon chain, increasing electron density on the diiron core and back donation into the π^* antibonding orbitals of CO, decreasing the $\text{C}\equiv\text{O}$ bond order.

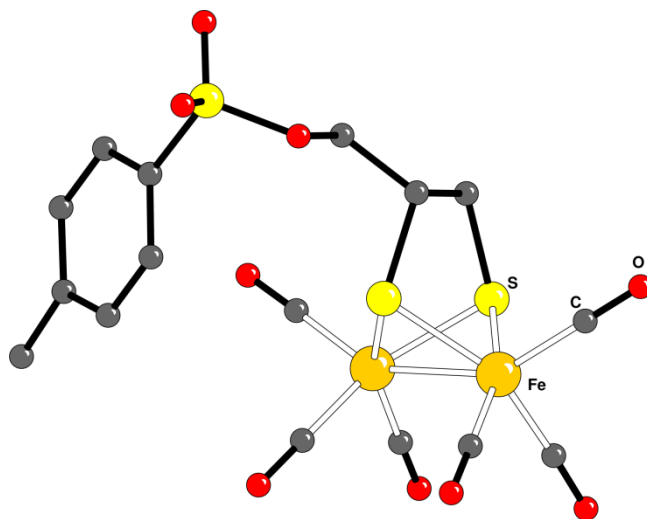
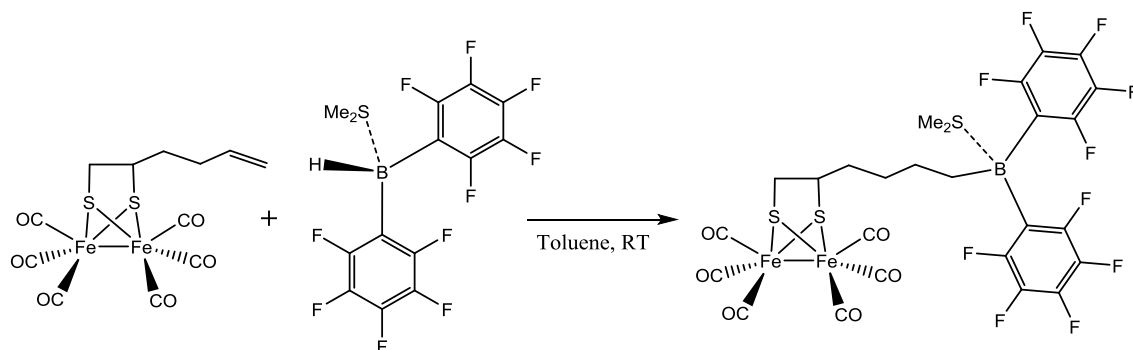


Figure 6.7. CAMERON representation of the structure of $[\text{Fe}_2(\text{dmp-Tos})(\text{CO})_6]$ **31** with spheres of arbitrary size.

6.2.6 Attempted hydroboration of $[\text{Fe}_2\{\text{C}_4\text{H}_7\text{CH}(\text{S})\text{CH}_2\text{S}\}(\text{CO})_6]$ with $\text{HB}(\text{C}_6\text{F}_5)_2\cdot\text{SMe}_2$

The hydroboration of $[\text{Fe}_2\{\text{C}_4\text{H}_7\text{CH}(\text{S})\text{CH}_2\text{S}\}(\text{CO})_6]$ **32** with $\text{HB}(\text{C}_6\text{F}_5)_2\cdot\text{SMe}_2$ **24** was attempted using the procedure outlined by Lancaster and coworkers²¹⁹. A toluene solution of **32** was added dropwise to a toluene solution of **24** at room temperature, with toluene again being used as solvent due to mutual solubility and the fact it was non-coordinating.



Scheme 6.12. Proposed hydroboration reaction to form the pendant borane species $[\text{Fe}_2\{(\text{C}_6\text{F}_5)_2\text{BC}_4\text{H}_8\text{CH}(\text{S})\text{CH}_2\text{S}\}(\text{CO})_6\cdot\text{SMe}_2]$ **33**.

After the addition, the reaction was stirred at room temperature for 1 h, at which point volatiles were removed under vacuum to give a red oil. This red oil was characterised by ^1H -NMR, ^{11}B -NMR, ^{19}F -NMR and FTIR, which suggested the possible formation of the hydroborated species $[\text{Fe}_2\{(\text{C}_6\text{F}_5)_2\text{BC}_4\text{H}_8\text{CH}(\text{S})\text{CH}_2\text{S}\}(\text{CO})_6\cdot\text{SMe}_2]$ **33**.

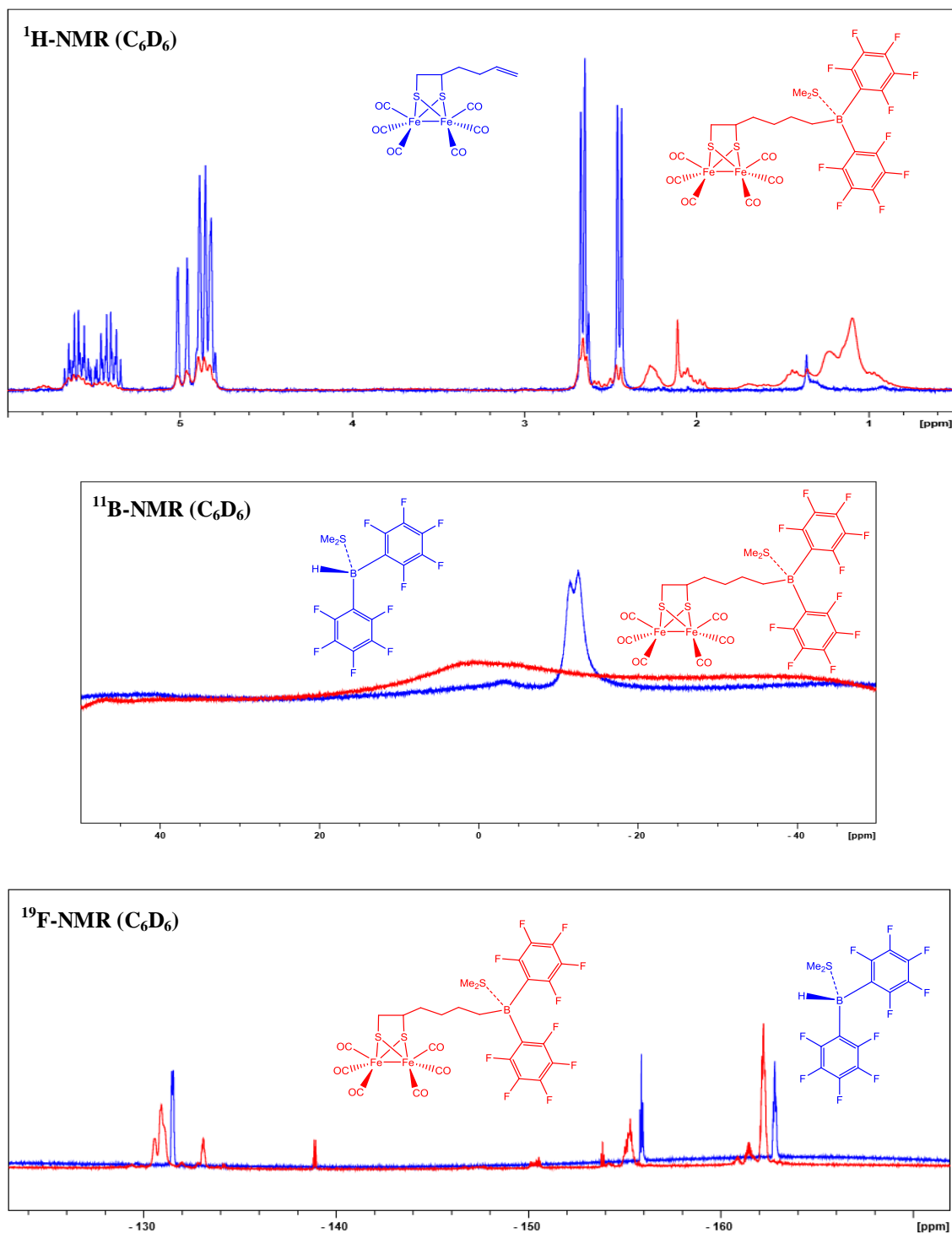


Figure 6.8. NMR characterisation of the red oil product of the reaction between $[\text{Fe}_2\{\text{C}_4\text{H}_7\text{CH}(\text{S})\text{CH}_2\text{S}\}(\text{CO})_6]$ **32** and $\text{HB}(\text{C}_6\text{F}_5)_2\cdot\text{SMe}_2$ **24**.

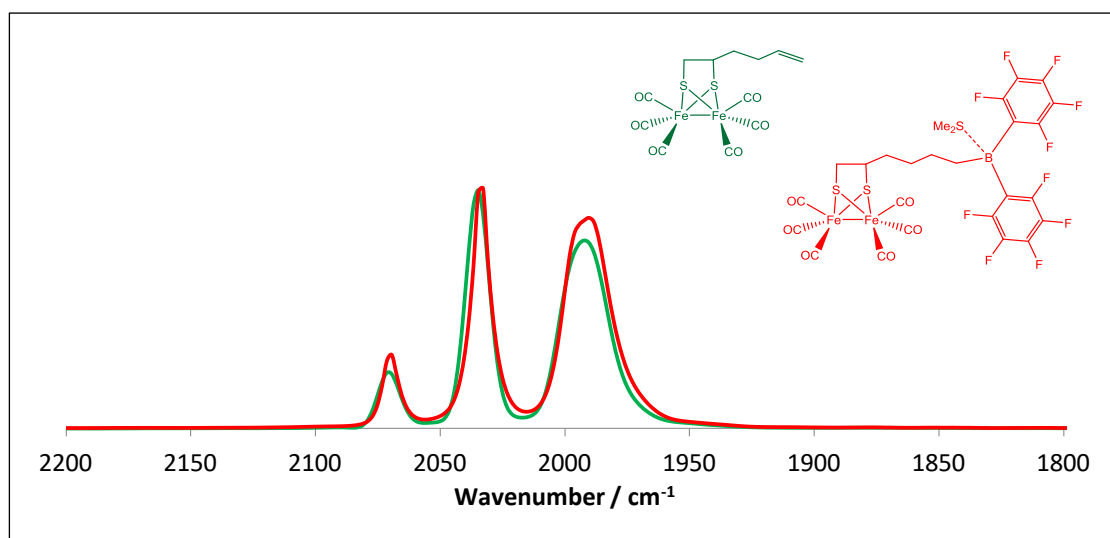


Figure 6.9. Solution FTIR spectrum (in C_6D_6) of the red oil product of the reaction between $[Fe_2\{C_4H_7CH(S)CH_2S\}(CO)_6]$ **32** and $HB(C_6F_5)_2 \cdot SMe_2$ **24**.

According to the characterisation performed, the reaction had potentially formed the hydroborated species $[Fe_2\{(C_6F_5)_2BC_4H_8CH(S)CH_2S\}(CO)_6 \cdot SMe_2]$ **33**. From the 1H -NMR it was observed that there was a slight excess of the alkene starting material present in the reaction, though the new proton signals at ~ 2 ppm are indicative of a saturated carbon chain. From the ^{11}B -NMR spectra, it was observed that the B-H signal of the starting material at -11.96 ppm had disappeared to be replaced with a very broad signal at 0.8 ppm. This broad signal is consistent with a four-coordinate dimethyl sulfide adduct species $(C_6F_5)_2B-R \cdot (SMe_2)$ as reported by Lancaster and coworkers²²². The ^{19}F -NMR exhibited major product peaks at -131.02 (4F), -155.32 (2F) and -162.31 ppm (4F), which is also consistent with a hydroborated species²²². The IR spectrum exhibited CO stretches at 2069 , 2033 and 1990 cm^{-1} , which are comparable to those of the starting material.

The hydroboration method seems as though it is effective for attaching pendant borane moieties, though further characterisation and crystallisation attempts would be required in order to firstly indentify the major species produced, and/or whether another rearrangement reaction to give a dimeric/trimeric species will take place.

6.2.7 Concluding remarks and future work

A [FeFe]-hydrogenase subsite analogue system capable of heterolytically cleaving dihydrogen is a desirable but synthetically challenging prospect. To construct such a system would involve an inversion of the inherent chemistry, though with electron-donating groups present on the diiron core to make the Fe-Fe bond more susceptible to protonation and a Lewis acidic pendant borane group present to accept a hydride, it could very well prove a possibility.

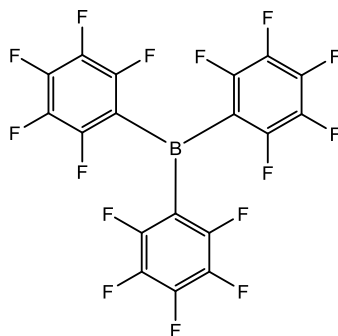
To this end, attachment of a bis(pentafluorophenyl)boron group was attempted using hydroxyl-functionalised diiron subsite analogues to form borinic ester groups of the system $(\text{C}_6\text{F}_5)_2\text{B-OR}$. Attachment of the borane group via this pathway proved unsuccessful due to these reactions yielding trimeric and dimeric diiron species around a central boron atom. However, two new diiron systems have been characterised crystallographically; $[(\text{Fe}_2\{\text{C}_5\text{H}_9\text{S}_2\})(\text{CO})_6\text{O})_3\text{B}]$ **29** and $[\text{Fe}_2(\text{dmp})(\text{CO})_6\text{O}]_2\text{BC}_6\text{F}_5]$ **30**.

An alternative method using the hydroboration of an alkene functionality was then employed, with this scheme tentatively proving successful and generating the pendant borane species $[\text{Fe}_2\{(\text{C}_6\text{F}_5)_2\text{BC}_4\text{H}_8\text{CH}(\text{S})\text{CH}_2\text{S}\}(\text{CO})_6\cdot\text{SMe}_2]$ **33**. Further characterisation and crystallisation attempts are required to formally identify the formed species, and/or whether another rearrangement reaction to give a dimeric/trimeric species will take place. However, the synthetic route to allow this hydroboration attempt involved the synthesis of two new species, $[\text{Fe}_2(\text{dmp-Tos})(\text{CO})_6]$ **31** and $[\text{Fe}_2\{\text{C}_4\text{H}_7\text{CH}(\text{S})\text{CH}_2\text{S}\}(\text{CO})_6]$ **32**, with the tosylate species **31** being characterised crystallographically and the new alkene species **32** being the first of its kind and thus introducing new possible synthetic reactions.

In regards to expanding this body of work, the synthetic journey to achieve a [FeFe]-hydrogenase subsite analogue system capable of heterolytically cleaving dihydrogen still continues. The steps undertaken in this body of work have provided some scope for incorporation of the required pendant borane moiety, though this will have to be employed in conjunction with electron-donating groups on the FeFe core in order to actually split H_2 . The formation of the new alkene-containing species also opens up novel functionalisation of diiron subsite analogues, with hydrosilylation and polymerisation possibly being exciting avenues for future exploration.

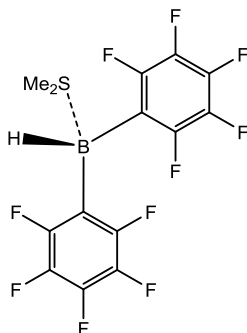
6.3 Experimental

6.3.1 Synthesis of tris(pentafluorophenyl)boron, B(C₆F₅)₃ (23)²²³



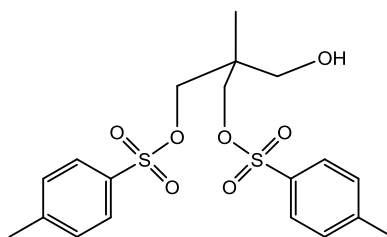
A suspension of magnesium metal (7.20 g, 0.3 mmol) in dry degassed Et₂O (500 mL) was cooled to 0 °C and bromopentafluorobenzene (37.4 mL, 0.3 mol) was added dropwise. The dark brown resultant solution was warmed to room temperature and stirred for 1 h. A second solution of boron trifluoride diethyl etherate (12.5 mL, 0.1 mol) in dry degassed toluene (200 mL) was prepared and cooled to 0 °C. The first solution was then added slowly to the second, with care being taken to leave remaining unreacted magnesium metal behind. The combined dark brown solution was warmed to room temperature and stirred for 1 h before being concentrated to *ca* 200 mL. The resultant concentrated solution was then heated to 95 °C for 2 h before being evaporated to dryness to give an orange-white cake. The solid was then extracted using dry degassed hexanes (600 mL) heated at 45 °C, with the extracted solution obtained being added to a flask containing Et₂O (30 mL) to aid crystallisation. The resulting mixture was then cooled to -20 °C for 24 h, producing colourless block crystals of the Et₂O adduct, (Et₂O)B(C₆F₅)₃. Sublimation at 100 °C and <0.1 mmHg gave the *title compound* (22.40 g, 0.04 mol, 43%). ¹⁹F-NMR (C₆D₆, 282.37 MHz): δ (ppm) = -130.03 (d, ³J_{FF} = 19.8 Hz, 6F, *o*-F), -143.27 (t, ³J_{FF} = 20.6 Hz, 3F, *p*-F), -161.44 (m, 6F, *m*-F). ¹¹B-NMR (C₆D₆, 96.29 MHz): δ (ppm) = 63.

6.3.2 Synthesis of bis(pentafluorophenyl)boron hydride dimethyl sulfide adduct, $\text{HB}(\text{C}_6\text{F}_5)_2 \cdot \text{SMe}_2$ (**24**)²²¹



$\text{B}(\text{C}_6\text{F}_5)_3$ **23** (5.77 g, 11 mmol) was combined with dry degassed hexane (150 mL) and heated to 50 °C to give a colourless solution. Borane dimethyl sulfide complex (0.53 mL, 6 mmol) was then added with the reaction mixture being stirred at 50 °C for a further 1 h. The resulting colourless mixture was then cooled to ~40 °C before dry degassed dimethyl sulfide (0.83 mL, 11 mmol) was added. The solution was then allowed to cool gradually to room temperature before the solution was concentrated to *ca* 100 mL in vacuo. The resulting mixture was then cooled to -20 °C for 72 h, producing colourless block crystals of the *title compound* (5.67 g, 14 mmol, 82%). ^1H -NMR (C_6D_6 , 300.13 MHz): δ (ppm) = 3.62 (m, 1H, B-H), 1.11 (s, 6H, SMe_2). ^{19}F -NMR (C_6D_6 , 282.37 MHz): δ (ppm) = -131.50 (bd, $^3J_{\text{FF}} = 20.7$ Hz, 4F, *o*-F), -156.01 (t, $^3J_{\text{FF}} = 20.7$ Hz, 2F, *p*-F), -162.89 (m, 4F, *m*-F). ^{11}B -NMR (C_6D_6 , 96.29 MHz): δ (ppm) = -11.96 (bd, $^1J_{\text{BH}} = 99.1$ Hz, B-H).

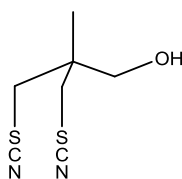
6.3.3 Synthesis of $\text{CH}_3\text{C}(\text{CH}_2\text{OH})(\text{CH}_2\text{OTos})_2$ (**25**)²²⁴



A solution of 1,1,1-tris(hydroxymethyl)ethane (34.20 g, 0.28 mol) in dry pyridine (150 mL) was cooled to 0 °C before a solution of *p*-toluenesulfonyl chloride (108.53 g, 0.57 mol) in dry pyridine (150 mL) was slowly added. The resultant mixture was allowed to warm to room temperature and stirred for 24 h. The mixture was then poured into ice-water (400 mL) and then 1 M HCl (50 mL) was added to form an off-

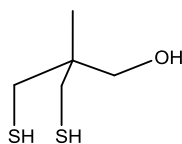
white oil. The aqueous solution was then decanted off before the residue was taken up in ethyl acetate (400 mL). The resulting solution was then washed with 1 M HCl (3 x 100 mL), saturated sodium hydrogen carbonate solution (3 x 100 mL) and finally brine (3 x 100 mL) before being dried over MgSO_4 and evaporated to give a yellow oil. Column chromatography (1:1 hexane/ethyl acetate) gave the compound as a colourless oil, which was then vigorously stirred in hexane (500 mL) to obtain the *title compound* (65.87 g, 0.15 mmol, 54%) as white solid. $^1\text{H-NMR}$ (CDCl_3 , 300.13 MHz): δ (ppm) = 7.74 (d, $^3J_{\text{HH}} = 8.2$ Hz, 4H, Tos-H), 7.35 (d, $^3J_{\text{HH}} = 8.2$ Hz, 4H, Tos-H), 3.86 (m, 4H, CH_2OS), 3.44 (d, $^3J_{\text{HH}} = 6.3$ Hz, 2H, CH_2OH), 2.14 (s, 6H, Tos- CH_3) 0.88 (s, 3H, CH_3).

6.3.4 Synthesis of $\text{CH}_3\text{C}(\text{CH}_2\text{OH})(\text{CH}_2\text{SCN})_2$ (**26**)²²⁴



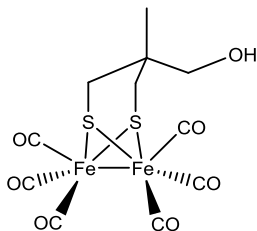
$\text{CH}_3\text{C}(\text{CH}_2\text{OH})(\text{CH}_2\text{OTos})_2$ **25** (8.15 g, 19 mmol) and potassium thiocyanate (18.62 g, 192 mmol) were combined in a flask and dry degassed DMF (50 mL) was added to give a yellow solution with some undissolved solid. The mixture was then heated at 140 °C for 6 h to give brown solution. After cooling to room temperature, H_2O (200 mL) was added to give an orange solution, which was then extracted with ethyl acetate (4 x 50 mL), with the combined organic layers then being washed with 1 M HCl (3 x 50 mL), saturated sodium hydrogen carbonate solution (3 x 50 mL) and finally brine (3 x 50 mL) before being dried over MgSO_4 and evaporated to give an orange oil. Column chromatography (1:1 hexane/ethyl acetate) gave the *title compound* (1.73 g, 9 mmol, 45%) as a yellow oil. $^1\text{H-NMR}$ (CDCl_3 , 300.13 MHz): δ (ppm) = 3.70 (d, $^3J_{\text{HH}} = 4.2$ Hz, 2H, CH_2O), 3.23 (m, 4H, CH_2S), 1.21 (s, 3H, CH_3).

6.3.5 Synthesis of $\text{CH}_3\text{C}(\text{CH}_2\text{OH})(\text{CH}_2\text{SH})_2$ (**27**)²²⁴



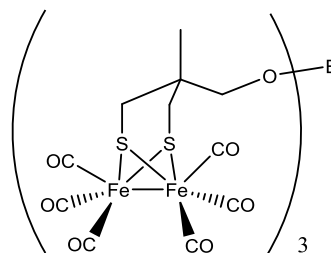
A suspension of lithium aluminium hydride (2.60 g, 69 mmol) in dry degassed THF (100 mL) was cooled to 0 °C before a solution of $\text{CH}_3\text{C}(\text{CH}_2\text{OH})(\text{CH}_2\text{SCN})_2$ **26** (6.41 g, 32 mmol) in dry degassed THF (50 mL) was added dropwise. The yellow resultant mixture was allowed to gradually warm to room temperature before being heated at 40 °C for 48 h. The mixture was then cooled to 0 °C before being slowly quenched with saturated ammonium chloride solution (100 mL). The aqueous solution was then extracted with ethyl acetate (3 x 50 mL) before being dried over MgSO_4 and evaporated to give an orange oil. Column chromatography (1:1 hexane/ethyl acetate) gave the *title compound* (3.43 g, 22 mmol, 71%) as a yellow oil. $^1\text{H-NMR}$ (CDCl_3 , 300.13 MHz): δ (ppm) = 3.63 (m, 2H, CH_2O), 2.58 (m, 4H, CH_2S), 1.26 (m, 1H, SH), 0.91 (s, 3H, CH_3).

6.3.6 Synthesis of $[\text{Fe}_2\{\text{CH}_3\text{C}(\text{CH}_2\text{OH})(\text{CH}_2\text{S})_2\}(\text{CO})_6]$ (**28**)²²⁴



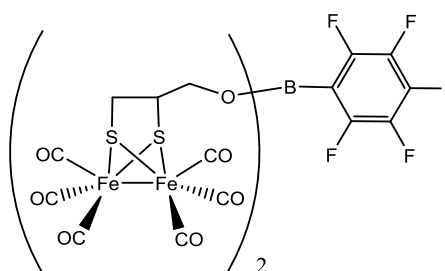
A solution of $\text{CH}_3\text{C}(\text{CH}_2\text{OH})(\text{CH}_2\text{SH})_2$ **27** (2.52 g, 17 mmol) in dry degassed THF (100 mL) was added to a green/black solution of triiron dodecacarbonyl (10.04 g, 20 mmol) in dry degassed THF (150 mL). The mixture was then heated at 70 °C for 3 h, forming a red solution. The mixture was evaporated to dryness before the red/black residue was purified by column chromatography (3:1 hexane/ethyl acetate) to give the *title compound* (5.91 g, 14 mmol, 83%) as red solid. $^1\text{H-NMR}$ ($\text{Acetone-}d_6$, 300.13 MHz): δ (ppm) = 3.23 (m, 2H, CH_2O), 2.45 (m, 2H, CH_2S), 2.20 (m, 2H, CH_2S), 0.94 (s, 3H, CH_3). IR(toluene): $\nu(\text{CO}) = 2073, 2033, 2002, 1988$.

6.3.7 Synthesis of $[(\text{Fe}_2\{\text{C}_5\text{H}_9\text{S}_2\})(\text{CO})_6\text{O})_3\text{B}]$ (**29**)



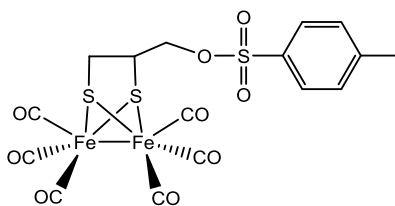
A solution of $[\text{Fe}_2\{\text{CH}_3\text{C}(\text{CH}_2\text{OH})(\text{CH}_2\text{S})_2\}(\text{CO})_6]$ **28** (86.0 mg, 0.20 mmol) in toluene (10 mL) was cooled to $-78\text{ }^\circ\text{C}$ and added dropwise to a solution of $\text{HB}(\text{C}_6\text{F}_5)_2\cdot\text{SMe}_2$ **24** (81.6 mg, 0.20 mmol) in toluene (10 mL) which was also cooled to $-78\text{ }^\circ\text{C}$. The mixture was allowed to warm to room temperature over 16 h, at which point volatiles were removed in vacuo to give a red oil. ^{11}B -NMR (C_6D_6 , 96.29 MHz): δ (ppm) = 39.1. IR(C_6D_6): $\nu(\text{CO}) = 2073, 2033, 2002, 1988$. Crystals suitable for X-ray diffraction were grown by cooling of a hexane solution to $-20\text{ }^\circ\text{C}$.

6.3.8 Synthesis of $[\text{Fe}_2(\text{dmp})(\text{CO})_6\text{O}]_2\text{BC}_6\text{F}_5$ (**30**)



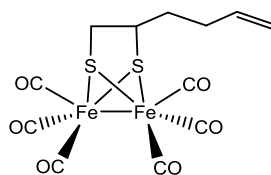
A solution of $[\text{Fe}_2(\text{dmp})(\text{CO})_6]$ **1** (112.5 mg, 0.28 mmol) in toluene (10 mL) was cooled to $-78\text{ }^\circ\text{C}$ and added dropwise to a solution of $\text{HB}(\text{C}_6\text{F}_5)_2\cdot\text{SMe}_2$ **24** (114.2 mg, 0.28 mmol) in toluene (10 mL) which was also cooled to $-78\text{ }^\circ\text{C}$. The mixture was allowed to warm to room temperature over 16 h, at which point volatiles were removed in vacuo to give a red oil. ^{11}B -NMR (C_6D_6 , 96.29 MHz): δ (ppm) = 26.5. IR(C_6D_6): $\nu(\text{CO}) = 2075, 2035, 2002, 1994$. Crystals suitable for X-ray diffraction were grown by cooling of a hexane solution to $-20\text{ }^\circ\text{C}$.

6.3.9 Synthesis of $[\text{Fe}_2(\text{dmp-Tos})(\text{CO})_6]$ (**31**)



A solution of $[\text{Fe}_2(\text{dmp})(\text{CO})_6]$ **1** (1.37 g, 3.4 mmol) and *p*-toluenesulfonyl chloride (0.84 g, 4.4 mmol) in dry degassed pyridine (100 mL) was prepared and stirred at room temperature for 24 h. Volatiles were then removed in vacuo to give a red oil which was dissolved in ethyl acetate (200 mL) before being washed with 1 M HCl (3 x 100 mL), saturated sodium hydrogen carbonate solution (3 x 100 mL) and finally brine (3 x 100 mL). Drying over MgSO_4 and removal of solvent gave a red oil. Column chromatography (3:1 hexane/ethyl acetate) gave the compound as a red oil, which was then vigorously stirred in hexane (200 mL) to obtain the *title compound* (1.65 g, 3.0 mmol, 87%) as red solid. Crystals suitable for X-ray diffraction were grown from a hexane solution cooled to 2 °C. $^1\text{H-NMR}$ (C_6D_6 , 300.13 MHz): δ (ppm) = 7.72 (d, $^3J_{\text{HH}} = 8.3$ Hz, 2H, Ar-H), 6.72 (d, $^3J_{\text{HH}} = 8.3$ Hz, 2H, Ar-H), 3.44 (d, $^3J_{\text{HH}} = 7.0$ Hz, 2H, CH- CH_2 -O), 2.10 (m, 1H, CH_2 -CH- CH_2), 1.85 (s, 3H, CH_3), 1.58 (m, 1H, SH-CHH-CH), 1.03 (m, 1H, SH-CHH-CH). IR(DCM): $\nu(\text{CO}) = 2079, 2039, 2006, 1999$.

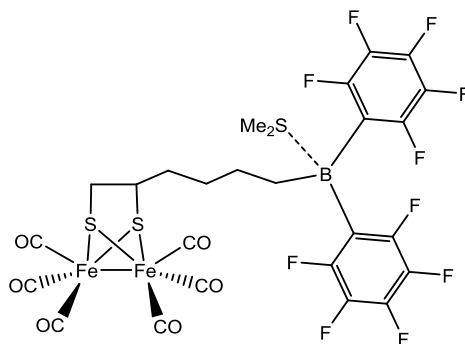
6.3.10 Synthesis of $[\text{Fe}_2\{\text{C}_4\text{H}_7\text{CH}(\text{S})\text{CH}_2\text{S}\}(\text{CO})_6]$ (**32**)



A solution of $[\text{Fe}_2(\text{dmp-Tos})(\text{CO})_6]$ **31** (1.48 g, 2.7 mmol) in dry degassed THF (80 mL) was cooled to -78 °C. Allylmagnesium chloride 2.0 M in THF solution (1.33 mL, 2.7 mmol) was then added dropwise. The mixture was allowed to warm to room temperature over 16 h, at which point volatiles were removed in vacuo to give a black foamy solid. Column chromatography using hexane eluent gave the *title compound* (0.16 g, 0.4 mmol, 14%) as a red oil. $^1\text{H-NMR}$ (C_6D_6 , 300.13 MHz): δ (ppm) = 5.60 (m,

1H), 5.41 (m, 1H), 4.98 (d, $^3J_{\text{HH}} = 16.9$ Hz, 1H), 4.85 (m, 3H), 2.66 (d, $^3J_{\text{HH}} = 7.0$ Hz, 2H), 2.45 (d, $^3J_{\text{HH}} = 7.4$ Hz, 2H). IR(C₆D₆): $\nu(\text{CO}) = 2071, 2035, 1992$. Anal. Calcd. for C₁₂H₁₀O₆S₂Fe₂: C, 33.83; H, 2.37. Found: C, 34.01; H, 2.29. ESI-MS: m/z 425.8 [M]⁺.

6.3.11 Synthesis of [Fe₂{(C₆F₅)₂BC₄H₈CH(S)CH₂S}(CO)₆·SMe₂] (33)



A red solution of [Fe₂{C₄H₇CH(S)CH₂S}(CO)₆] **32** (44.0 mg, 0.10 mmol) in toluene (5 mL) was added dropwise to a solution of HB(C₆F₅)₂·SMe₂ **24** (42.1 mg, 0.10 mmol) in toluene (5 mL). The reaction was stirred at room temperature for 1 h at which point volatiles were removed in vacuo to give a red oil. Characterisation of the red oil suggested formation of the *title compound* as the major product. ¹⁹F-NMR (C₆D₆, 282.37 MHz): δ (ppm) = -131.02 (m, 4F), -155.32 (m, 2F), -162.31 (m, 4F). ¹¹B-NMR (C₆D₆, 96.29 MHz): δ (ppm) = 0.8. IR(C₆D₆): $\nu(\text{CO}) = 2069, 2033, 1990$.

6.3.12 X-ray diffraction

Crystals were suspended in oil, and one was mounted on a glass fibre and fixed in the cold nitrogen stream of the diffractometer. Data were collected on a Rigaku AFC12 goniometer equipped with an enhanced sensitivity (HG) Saturn724+ detector mounted at the window of an FR-E+ SuperBright molybdenum rotating anode generator with HF Varimax optics (**29**, **29'**, **30**) or an Oxford Diffraction Xcalibur-3 CCD diffractometer equipped with Mo-K α radiation and graphite monochromator (**31**). Data were processed using the CrystalClear-SM Expert program (**29**, **29'**, **30**)²³⁰ or CrysAlisPro (**31**)²³¹. Structures were determined by charge flipping routines in the SUPERFLIP program (**29**, **29'**, **30**)²³² or by direct methods in the SIR-92 program²³³, and refined by full-

matrix least-squares methods on F^2 in SHELXL-2012 (**29**, **29'**, **30**)²³⁴ or SHELXL-2014 (**31**)²³⁵. Non-hydrogen atoms were refined with anisotropic thermal parameters. Hydrogen atoms were included in idealized positions and their U_{iso} values were set to ride on the U_{eq} values of the parent carbon atoms. Complex **29** crystallised in two polymorphs, one in space group $P\bar{1}$ and a second in space group $P2_1/n$. Complex **30** was a non-merohedral twin (a 180° rotation about $[0\ 0\ 1]$) with final occupancy for the minor component of 0.33. Bond distances and thermal parameters in complex **30** were restrained to the same values with e.s.d. values of 0.02 Å and 0.04 Å, respectively. A summary of the data collection parameters is given in **Figure 6.10**.

	29	29'	30	31
Formula	$\text{C}_{33}\text{H}_{27}\text{BFe}_6\text{O}_{21}\text{S}_6$	$\text{C}_{33}\text{H}_{27}\text{BFe}_6\text{O}_{21}\text{S}_6$	$\text{C}_{24}\text{H}_{10}\text{B}_1\text{F}_3\text{Fe}_4\text{O}_{14}\text{S}_4$	$\text{C}_{16}\text{H}_{12}\text{Fe}_2\text{O}_9\text{S}_3$
Molecular weight	1297.81	1297.81	979.81	556.10
T/K	100(2)	100(2)	100(2)	140(5)
$\lambda/\text{\AA}$	0.71075	0.71075	0.71075	0.71073
Crystal system	Triclinic	Monoclinic	Triclinic	Monoclinic
Space group	$P\bar{1}$	$P2_1/n$	$P\bar{1}$	$P2_1/c$
$a/\text{\AA}$	11.3576(8)	9.6164(7)	8.8653(5)	15.3039(6)
$b/\text{\AA}$	12.1137(9)	27.817(2)	13.0487(9)	11.5182(5)
$c/\text{\AA}$	18.6487(13)	18.3311(13)	15.6360(11)	12.2989(5)
$\alpha/^\circ$	103.654(5)	90	99.618(8)	90
$\beta/^\circ$	91.309(4)	99.190(2)	91.352(8)	102.736(4)
$\gamma/^\circ$	98.582(5)	90	101.604(8)	90
$V/\text{\AA}^3$	2460.8(3)	4840.6(6)	1743.8(2)	2114.63(15)
Z	2	4	2	4
Reflections collected	31680	60028	7755	31355
Independent reflections	11208	11058	7755	4817
R_{int}	0.061	0.110	—	0.029
$R_1 [F^2 > 2\sigma(F^2)]$	0.047	0.058	0.088	0.024
wR_2 (all data)	0.129	0.150	0.219	0.061

Figure 6.10. Summary of X-ray parameters for complexes **29**, **30** and **31**.

7 References

1. R.K Thauer, *Eur. J. Inorg. Chem.*, **2011**, 919
2. T.R. Simmons, G. Berggren, M. Bacchi, M. Fontecave, V. Artero, *Coord. Chem. Rev.*, **2014**, 270, 127
3. K.A. Vincent, A. Parkin, F.A. Armstrong, *Chem. Rev.*, **2007**, 107, 4366
4. J.C. Fontecilla-Camps, A. Volbeda, C. Cavazza, Y. Nicolet, *Chem. Rev.*, **2007**, 107, 4273
5. R.K. Thauer, A.K. Kaster, M. Goenrich, M. Schick, T. Hiromoto, S. Shima, *Annu. Rev. Biochem.*, **2010**, 79, 507.
6. M. Stephenson, L.H. Stickland, *Biochemical Journal*, **1931**, 25, 205
7. P.M. Vignais, B. Billoud, J. Meyer, *FEMS Microbiology Reviews*, **2001**, 25, 455
8. T. Hiromoto, K. Ataka, O. Pilak, S. Vogt, M.S. Stagni, W. Meyer-Klaucke, E. Warkentin, R.K. Thauer, S. Shima, U. Ermler, *FEBS Lett.*, **2009**, 583, 585
9. C. Zirngibl, R. Hedderich, R.K. Thauer, *FEBS Lett.*, **1990**, 261, 112
10. C. Zirngibl, W. van Dongen, B. Schworer, R. von Bunau, M. Richter, A. Klein, R.K. Thauer, *Eur. J. Biochem.*, **1992**, 208, 511
11. H.R. Pershad, J.L.C. Duff, H.A. Heering, E.C. Duin, S.P.J. Albracht, F.A. Armstrong, *Biochemistry*, **1999**, 38, 8992
12. C. Madden, M.D. Vaughn, I. Diez-Perez, K.A. Brown, P.W. King, D. Gust, A.L. Moore, T.A. Moore, *J. Am. Chem. Soc.*, **2012**, 134, 1577
13. A.J. Pierik, M. Hulstein, W.R. Hagen, S.P. Albracht, *Eur. J. Biochem.*, **1998**, 258, 572
14. A.J. Pierik, W. Roseboom, R.P. Happe, K.A. Bagley, S.P. Albracht, *J. Biol. Chem.*, **1999**, 274, 3331
15. T. Krämer, M. Kampa, W. Lubitz, M. van Gastel, F. Neese, *ChemBioChem*, **2013**, 14, 1898
16. A. Volbeda, L. Martin, E. Barbier, O. Gutiérrez-Sanz, A.L. Lacey, P.P. Liebgott, S. Dementin, M. Rousset, J.C. Fontecilla-Camps, *J. Biol. Inorg. Chem.*, **2014**, 20, 11
17. J.W. Peters, W.N. Lanzilotta, B.J. Lemon, L.C. Seefeldt, *Science*, **1998**, 282, 1853
18. K.A. Vincent, A. Parkin, F.A. Armstrong, *Chem. Rev.*, **2007**, 107, 4366
19. M. Frey, *ChemBioChem*, **2002**, 3, 153
20. M.W.W. Adams, *Biochim. Et. Biophys. Acta.*, **1990**, 1020, 115

21. Y.Nicolet, C.Piras, P.Legrand, C.E. Hatchikian, J.C. Fontecilla-Camps, *Struct. Fold. Des.*, **1999**, 7, 13
22. A. Jablonskyté, PhD thesis, University of East Anglia, **2014**
23. Y. Nicolet, A.L. de Lacey, X. Vernede, V.M. Fernandez, E.C. Hatchikian, J.C. Fontecilla-Camps, *J. Am. Chem. Soc.*, **2001**, 123, 1596
24. A Silakov, B. Wenk, E. Reijerse, W. Lubitz, *Phys. Chem. Chem. Phys.*, **2009**, 11, 6592
25. W. Lubitz, E. Reijerse, M. van Gastel, *Chem. Rev.*, **2007**, 107, 4331
26. Ö.F. Erdem, L. Schwartz, M. Stein, A. Silakov, S. Kaur-Ghumaan, P. Huang, S. Ott, E. Reijerse, W. Lubitz, *Angew. Int. Ed.*, **2011**, 50, 1439
27. G. Berggren, A. Adamska, C. Lambertz, T.R. Simmons, J. Esselborn, M. Atta, S. Gambarelli, J.M. Mouesca, E. Reijerse, W. Lubitz, T. Happe, V. Artero, M. Fontecave, *Nature*, **2013**, 499, 66
28. A. Adamska, A Silakov, C. Lambertz, O. Rüdiger, T. Happe, E. Reijerse, W. Lubitz, *Angew. Chem. Int. Ed.*, **2012**, 51, 11458
29. C.Tard, X. Liu, S.K. Ibrahim, M. Bruschi, L. De Gioia, S.C. Davies, X. Yang, L.-S. Wang, G. Sawers, C.J. Pickett, *Nature*, **2005**, 433, 610
30. H. Reihlen, A. Gruhl, G.V. Hessling, J. Liebigs, *Ann. Chem.*, **1929**, 472, 268
31. A. Winter, L. Zsolnai, G. Huttner, *Z. Naturforsch. B: Anorg. Chem., Org. Chem.*, **1982**, 37B, 1430
32. A. Le Cloiree, S.C. Davies, D.J. Evans, D.L. Hughes, C.J. Pickett, S.P. Best, *Chem. Commun.*, **1999**, 2285
33. M. Schmidt, S.M. Contakes, T.B. Rauchfuss, *J. Am. Chem. Soc.*, **1999**, 121, 9736
34. E.J. Lyon, I.P. Georgakaki, J.H. Reibenspies, M.Y. Darensbourg, *Angew. Chem. Int. Ed.*, **1999**, 38, 3178
35. D. Schilter, J.M. Camara, M.T. Huynh, S. Hammes-Schiffer, T.B. Rauchfuss, *Chem. Rev.*, **2016**, 116, 8693
36. Y. Li, T.B. Rauchfuss, *Chem. Rev.*, **2016**, 116, 7043
37. W. Lubitz, H. Ogata, O. Ruediger, *Chem. Rev.*, **2014**, 114, 4081
38. T.R. Simmons, G. Berggren, M. Bacchi, M. Fontecave, V. Artero, *Coord. Chem. Rev.*, **2014**, 270, 127
39. A.M. Lunsford, C.C. Beto, S. Ding, Ö.F. Erdem, N. Wang, N. Bhuvanesh, M.B. Hall, M.Y. Darensbourg, *Chem. Sci.*, **2016**, 7, 3710
40. B.C. Manor, M.R. Ringenberg, T.B. Rauchfuss, *Inorg. Chem.*, **2014**, 53, 7241

41. G.S. Girolami, T.B. Rauchfuss, R.J. Angelici, *Synthesis and Technique in inorganic chemistry: A laboratory manual*, University Science Books, **1999**
42. W.L. Armarego, C.L.L. Chai, *Purification of laboratory chemicals*, Butterworth-Heinemann, Amsterdam; London, 5th edition., **2003**
43. G. Berggren, A. Adamska, C. Lambertz, T.R. Simmons, J. Esselborn, M. Attal, S. Gambarelli, J.-M. Mouesca, E. Reijerse, W. Lubitz, T. Happe, V. Artero, M. Fontecave, *Nature*, **2013**, 499, 66
44. X. Liu, S.K. Ibrahim, C. Tard, C.J. Pickett, *Coord. Chem. Rev.*, **2005**, 249, 1641
45. A. Adamska, A. Silakov, C. Lambertz, O. Rüdiger, T. Happe, E. Reijerse, W. Lubitz, *Angew. Chem. Int. Ed.*, **2012**, 51, 11458
46. S. Ezzaher, J.-F. Capon, F. Gloaguen, F.Y. Pétillon, P. Schollhammer, J. Talarmin, *Inorg. Chem.*, **2009**, 48, 2
47. Y. Wang, Z. Li, Z. Zeng, X. Wang, C. Zhan, Y. Liu, Z. Zeng, Q. Luob, X. Liu, *New J. Chem.*, **2009**, 33, 1780
48. P. Li, M. Wang, L. Chen, J. Liu, Z. Zhao, L. Sun, *Dalton Trans.*, **2009**, 1919
49. J.A. Wright, L. Webster, A. Jablonskyté, P.M. Woi, S.K. Ibrahim, C.J. Pickett, *Faraday Discuss.*, **2011**, 148, 359
50. H.E. Morris, *Chem. Rev.*, **1932**, 10, 465
51. W.E. Bissinger, F.E. Kung, *J. Am. Chem. Soc.*, **1947**, 69, 2158
52. T. Turek, D.L. Trimm, N.W. Cant, *Catalysis Reviews*, **1994**, 36, 4
53. F. Xu, C. Tard, X. Wang, S.K. Ibrahim, D.L. Hughes, W. Zhong, X. Zeng, Q. Luo, X. Liu, C.J. Pickett, *Chem. Commun.*, **2008**, 606
54. U.-P. Apfel, Y. Halpin, H. Görls, J.G. Vos, B. Schweizer, G. Linti, W. Weigand, *Chem. Biodivers.*, **2007**, 2138
55. X. Zhu, W. Zhong, X. Liu, *Int. J. Hydrogen Energy*, **2016**, 41, 14068
56. S.K. Ibrahim, X. Liu, C. Tard, C.J. Pickett, *Chem. Commun.*, **2007**, 1535
57. M. Razavet, A. Le Cloirec, S.C. Davies, D. L. Hughes, C.J. Pickett, *J. Chem. Soc., Dalton Trans.*, **2001**, 3551
58. H. Wolpher, M. Borgström, L. Hammarström, J. Bergquist, V. Sundström, S. Styring, L. Sun, B. Åkermark, *Inorg. Chem. Commun.*, **2003**, 6, 989
59. X. Zeng, Z. Li, Z. Xiao, Y. Wang, X. Liu, *Electrochemistry Communications*, **2010**, 12, 342
60. S.K. Ibrahim, X. Liu, C. Tard, C.J. Pickett, *Chem. Commun.*, **2007**, 1535

61. F. Gloaguen, J.D. Lawrence, M. Schmidt, S.R. Wilson, T.B. Rauchfuss, *J. Am. Chem. Soc.*, **2001**, *123*, 12518
62. B. Neises, W. Steglich, *Angew. Chem. Int. Ed. Engl.*, **1978**, *17*, 522
63. G. Höfle, W. Steglich, H. Vorbrüggen, 1978, *Angew. Chem. Int. Ed. Engl.*, **1978**, *17*, 569
64. F. Chen, J. Guo, Z. Qu, J. Wei, *J. Mater. Chem.*, **2011**, *21*, 8574
65. L.A. Babadzhanova, N.V. Kirij, Y.L. Yagupolskii, W. Tyrre, D. Naumann, *Tetrahedron*, **2005**, *61*, 1813
66. A. Jablonskyté, L.R. Webster, T.R. Simmons, J.A. Wright, C.J. Pickett, *J. Am. Chem. Soc.*, **2014**, *136*, 13038
67. S.J. Borg, T. Behrsing, S.P. Best, M. Razavet, X. Liu, C.J. Pickett, *J. Am. Chem. Soc.*, **2004**, *126*, 16988
68. I.A. de Carcer, A. DiPasquale, A.L. Rheingold, D.M. Heinekey, *Inorg. Chem.*, **2006**, *45*, 8000
69. T. Liu, D.L. DuBois, R.M. Bullock, *Nat. Chem.*, **2013**, *5*, 228
70. *CrystalClear-SM Expert*, Rigaku Corporation, Tokyo, Japan, **2013**
71. L. Palatinus and G.J. Chapuis, *J. Appl. Cryst.*, **2007**, *40*, 786
72. G.M. Sheldrick, *Acta Cryst. A*, **2008**, *64*, 112
73. G.M. Sheldrick, *Acta Cryst. C*, **2015**, *71*, 3
74. A.S. Pandey, T.V. Harris, L.J. Giles, J.W. Peters, R.K. Szilagy, *J. Am. Chem. Soc.*, **2008**, *130*, 4533
75. T.R. Simmons, G. Berggren, M. Bacchi, M. Fontecave, V. Artero, *Coord. Chem. Rev.*, **2014**, *270*, 127
76. M. Winkler, J. Esselborn, T. Happe, *Biochim. Biophys.*, **2013**, *1827*, 974
77. C. Tard, C.J. Pickett, *Chem. Rev.*, **2009**, *109*, 2245
78. G. Berggren, A. Adamska, C. Lambert, T.R. Simmons, J. Esselborn, M. Attal, S. Gambarelli, J.-M. Mouesca, E. Reijerse, W. Lubitz, T. Happe, V. Artero, M. Fontecave, *Nature*, **2013**, *499*, 66
79. W. Lubitz, H. Ogata, O. Rüdiger, E. Reijerse, *Chem. Rev.*, **2014**, *114*, 4081
80. J.A. Wright, L. Webster, A. Jablonskyté, P.M. Woi, S.K. Ibrahim, C.J. Pickett, *Faraday Discuss.*, **2011**, *148*, 359
81. B.C. Manor, M.R. Ringenberg, T.B. Rauchfuss, *Inorg. Chem.*, **2014**, *53*, 7241
82. F. Gloaguen, J.D. Lawrence, M. Schmidt, S.R. Wilson, T.B. Rauchfuss, *J. Am. Chem. Soc.*, **2001**, *123*, 12518

83. IUPAC, 'Hydrogen bond', *Compendium of Chemical Terminology, 2nd Edition*, 'The Gold Book', **1997**
84. J.W. Larson, T.B. McMahon, *Inorg. Chem.*, **1984**, 23, 2029
85. J. Emsley, *Chem. Soc. Rev.*, **1980**, 9, 91
86. O. Markovitch, N. Agmon, *J. Phys. Chem. A.*, **2007**, 111, 2253
87. N. Stahl, W.P. Jencks, *J. Am. Chem. Soc.*, **1986**, 108, 4196
88. W. Saenger, *Principles of Nucleic Acid Structure*, New York, **1984**
89. P.V. Bernhardt, G.A. Lawrance, B.W. Skelton, A.H. White, *Aust. J. Chem.*, **1989**, 42, 1035
90. N. Busschaert, M. Wenzel, M.E. Light, P. Iglesias-Hernández, R. Pérez-Tomás, P.A. Gale, *J. Am. Chem. Soc.*, **2011**, 133, 14136
91. L.E. Karagiannidis, C.J.E. Haynes, K.J. Holder, I.L. Kirby, S.J. Moore, N.J. Wells, P.A. Gale, *Chem. Commun.*, **2014**, 50, 12050
92. M. Dobler, *Ionophores and Their Structures*, Wiley: New York, **1981**
93. A. Le Cloiree, S.C. Davies, D.J. Evans, D.L. Hughes, C.J. Pickett, S.P. Best, *Chem. Commun.*, **1999**, 2285
94. M. Schmidt, S.M. Contakes, T.B. Rauchfuss, *J. Am. Chem. Soc.*, **1999**, 121, 9736
95. E.J. Lyon, I.P. Georgakaki, J.H. Reibenspies, M.Y. Darensbourg, *Angew. Chem. Int. Ed.*, **1999**, 38, 3178
96. J. Tang, T. Mohan, J.G. Verkade, *J. Org. Chem.*, **1994**, 59, 4931
97. F.S. Aljohani, PhD thesis, University of East Anglia, **2016**
98. M.J. Frisch, G.W. Trucks, H.B. Schlegel, G.E. Scuseria, M.A. Robb, J.R. Cheeseman, G. Scalmani, V. Barone, B. Mennucci, G.A. Petersson, H. Nakatsuji, M. Caricato, X. Li, H.P. Hratchian, A.F. Izmaylov, J. Bloino, G. Zheng, J.L. Sonnenberg, M. Hada, M. Ehara, K. Toyota, R. Fukuda, J. Hasegawa, M. Ishida, T. Nakajima, Y. Honda, O. Kitao, H. Nakai, T. Vreven, J. A. Montgomery, Jr., J.E. Peralta, F. Ogliaro, M. Bearpark, J.J. Heyd, E. Brothers, K.N. Kudin, V.N. Staroverov, R. Kobayashi, J. Normand, K. Raghavachari, A. Rendell, J.C. Burant, S.S. Iyengar, J. Tomasi, M. Cossi, N. Rega, J.M. Millam, M. Klene, J.E. Knox, J.B. Cross, V. Bakken, C. Adamo, J. Jaramillo, R. Gomperts, R.E. Stratmann, O. Yazyev, A.J. Austin, R. Cammi, C. Pomelli, J.W. Ochterski, R.L. Martin, K. Morokuma, V.G. Zakrzewski, G.A. Voth, P. Salvador, J.J. Dannenberg, S. Dapprich, A.D. Daniels, Ö. Farkas, J.B. Foresman, J.V. Ortiz, J. Cioslowski, D.J. Fox, *Gaussian 09 Revision C.01*, Gaussian, Inc., Wallingford, CT, **2009**

99. J. Tao, J.P. Perdew, V.N. Staroverov, G.E. Scuseria, *Phys. Rev. Lett.*, **2003**, *91*, 146401
100. R.O. Ramabhadran, Y. Hua, A.H. Flood, K. Raghavachari, *J. Phys. Chem. A.*, **2014**, *118*, 7418
101. L.S. Mészáros, N. Khanna, C. Esmieu, P. Lindblad, G. Berggren, Oral presentation at the 11th International Hydrogenase Conference 2016, Marseille, France, 13th July **2016**
102. F. Wang, W.-G. Wang, H.-Y. Wang, G. Si, C.-H. Tung, L.-Z. Wu, *ACS Catal.*, **2012**, *2*, 407
103. W.-G. Wang, F. Wang, H.-Y. Wang, G. Si, C.-H. Tung, L.-Z. Wu, *Chem. Asian J.*, **2010**, *5*, 1796
104. H. Wolpher, M. Borgström, L. Hammarström, J. Bergquist, V. Sundström, S. Styring, L. Sun, B. Åkermark, *Inorg. Chem. Commun.*, **2003**, *6*, 989
105. S. Ott, M. Borgström, M. Kritikos, R. Lomoth, J. Bergquist, B. Åkermark, L. Hammarström, L. Sun, *Inorg. Chem.*, **2004**, *43*, 4683
106. J.D. Lawrence, H. Li, T.B. Rauchfuss, *Chem. Commun.*, **2001**, 1482
107. J.D. Lawrence, H. Li, T.B. Rauchfuss, M. Benard, M.M. Rohmer, *Angew. Chem., Int. Ed.*, **2001**, *40*, 1768
108. H. Li, T.B. Rauchfuss, *J. Am. Chem. Soc.*, **2002**, *124*, 726
109. L.-C. Song, M.-Y. Tang, F.-H. Su, Q.-M. Hu, *Angew. Chem., Int. Ed.*, **2006**, *45*, 1130
110. L.-C. Song, M.-Y. Tang, S. -Z. Mei, J.-H. Huang, Q.-M. Hu, *Organometallics*, **2007**, *26*, 1575
111. R. Goy, U.-P. Apfel, C. Elleouet, D. Escudero, M. Elstner, H. Görls, J. Talarmin, P. Schollhammer, L. González, W. Weigand, *Eur. J. Inorg. Chem.*, **2013**, 4466
112. J. Ekström, M. Abrahamsson, C. Olson, J. Bergquist, F.B. Kaynak, L. Eriksson, L. Sun, H.-C. Becker, B. Åkermark, L. Hammarström, S. Ott, *Dalton Trans.*, **2006**, 4599
113. A.M. Kluwer, R. Kapre, F. Hartl, M. Lutz, A.L. Spek, A.M. Brouwer, P.W.N.M. van Leeuwen, J.N.H. Reek, *Proc. Natl. Acad. Sci. U.S.A.*, **2009**, *106*, 10460
114. W. Gao, J. Liu, W. Jiang, M. Wang, L. Weng, B. Åkermark, L. Sun, *C. R. Chimie*, **2008**, *11*, 915
115. L.-C. Song, F.-X. Luo, B.-B. Liu, Z.-C. Gu, H. Tan, *Organometallics*, **2016**, *35*, 1399

116. W.-G. Wang, F. Wang, H.-Y. Wang, G. Si, C.-H. Tung, L.-Z. Wu, *Chem. Asian J.*, **2010**, 5, 1796
117. K. Kalyanasundaram, *Coord. Chem. Rev.*, **1982**, 46, 159
118. A. Juris, V. Balzani, F. Barigello, S. Campagna, P. Belser, A. von Zelewsky, *Coord. Chem. Rev.*, **1988**, 84, 85
119. F. Telpý, *Collect. Czech. Chem. Commun.*, **2011**, 76, 859
120. V. Balzani, A. Juris, M. Venturi, S. Campagna, S. Serroni, *Chem. Rev.*, **1996**, 96, 759
121. M. Marco, A. Cedi, L. Prodi, M.T. Gandolfi, *Handbook of Photochemistry 3rd Edition*, CRC Press: Boca Raton, **2006**
122. A.J. Bard, M.A. Fox, *Acc. Chem. Res.*, **1995**, 28, 141
123. K. Kobayashi, H. Ohtsu, K. Nozaki, S. Kitagawa, K. Tanaka, *Inorg. Chem.*, **2016**, 55, 2076
124. C.K. Prier, D.A. Rankic, D.W.C. MacMillan, *Chem. Rev.*, **2013**, 113, 5322
125. A.M. Lunsford, C.C. Beto, S. Ding, Ö.F. Erdem, N. Wang, N. Bhuvanesh, M.B. Hall, M.Y. Darensbourg, *Chem. Sci.*, **2016**, 7, 3710
126. M.J. Scott, R.H. Holm, *J. Am. Chem. Soc.*, **1994**, 116, 11357
127. M. Shatruk, A. Dragulescu-Andrasi, K.E. Chambers, S.A. Stoian, E.L. Bominaar, C. Achim, K.R. Dunbar, *J. Am. Chem. Soc.*, **2007**, 129, 6104
128. N. Zhu, H. Vahrenkamp, *Chem. Ber.*, **1997**, 130, 1241
129. A. Cadranel, P. Alborés, S. Yamazaki, V.D. Kleiman, L.M. Baraldo, *Dalton Trans.*, **2012**, 41, 5343
130. T. Liu, M.Y. Darensbourg, *J. Am. Chem. Soc.*, **2007**, 129, 7008
131. C.-H. Hsieh, Ö.F. Erdem, S.D. Harman, M.L. Singleton, E. Reijerse, W. Lubitz, C.V. Popescu, J.H. Reibenspies, S.M. Brothers, M.B. Hall, M.Y. Darensbourg, *J. Am. Chem. Soc.*, **2012**, 134, 13089
132. M. Razavet, S.C. Davies, D.L. Hughes, C.J. Pickett, *Chem. Commun.*, **2001**, 847
133. M. Razavet, S.C. Davies, D.L. Hughes, J.E. Barclay, D.J. Evans, S.A. Fairhurst, X. Liu, C.J. Pickett, *Dalton Trans.*, **2003**, 586
134. F. Xu, C. Tard, X. Wang, S.K. Ibrahim, D.L. Hughes, W. Zhong, X. Zeng, Q. Luo, X. Liu, C.J. Pickett, *Chem Commun.*, **2008**, 606
135. A. Jablonskyté, L.R. Webster, T.R. Simmons, J.A. Wright, C.J. Pickett, *J. Am. Chem. Soc.*, **2014**, 136, 13038

136. S.P. Best, S.J. Borg, J.M. White, M. Razavet, C.J. Pickett, *Chem. Commun.*, **2007**, 4348
137. A.K. Justice, T.B. Rauchfuss, S.R. Wilson, *Angew. Chem., Int. Ed.*, **2007**, *46*, 6152
138. A.K. Justice, G. Zampella, L. De Gioia, T.B. Rauchfuss, J.I. van der Vlugt, S.R. Wilson, *Inorg. Chem.*, **2007**, *46*, 1655
139. A.K. Justice, L. De Gioia, M.J. Nilges, T.B. Rauchfuss, S.R. Wilson, G. Zampella, *Inorg. Chem.*, **2008**, *47*, 7405
140. W. Wang, T.B. Rauchfuss, L. Bertini, G. Zampella, *J. Am. Chem. Soc.*, **2012**, *134*, 4525
141. P.W.J.M. Frederix, K. Adamczyk, J.A. Wright, T. Tuttle, R.V. Ulijn, C.J. Pickett, N.T. Hunt, *Organometallics*, **2014**, *33*, 5888
142. B.P. Sullivan, J.M. Calvert, T.J. Meyer, *Inorg. Chem.*, **1980**, *19*, 1404
143. K.J. Takeuchi, M.S. Thompson, D.W. Pipes, T.J. Meyer, *Inorg. Chem.*, **1984**, *23*, 1845
144. X.J. Yang, F. Drepper, B. Wu, W.H. Sun, W. Haehnel, C. Janiak, *Dalton Trans.*, **2005**, *2*, 256
145. M. Schmidt, S.M. Contakes, T.B. Rauchfuss, *J. Am. Chem. Soc.*, **1999**, *121*, 9736
146. S. Alvarez, C. López, M.J. Bermejo, *Trans. Met. Chem.*, **1984**, *9*, 123
147. A. Cadranel, B.M.A. Trošelj, S. Yamazaki, P. Alborés, V.D. Kleiman, L.M. Baraldo, *Dalton Trans.*, **2013**, *42*, 16723
148. F. Gloaguen, J.D. Lawrence, M. Schmidt, S.R. Wilson, T.B. Rauchfuss, *J. Am. Chem. Soc.*, **2001**, *123*, 12518
149. J.A. Wright, L. Webster, A. Jablonskyté, P.M. Woi, S.K. Ibrahim, C.J. Pickett, *Faraday Discuss.*, **2011**, *148*, 359
150. B.C. Manor, M.R. Ringenberg, T.B. Rauchfuss, *Inorg. Chem.*, **2014**, *53*, 7241
151. Y. Na, M. Wang, J. Pan, P. Zhang, B. Åkermark, L. Sun, *Inorg. Chem.*, **2008**, *47*, 2805
152. *CrysAlisPro*, Rigaku Oxford Diffraction, Abingdon, UK, **2015**
153. G.M. Sheldrick, *Acta Cryst. A*, **2015**, *71*, 3
154. G.M. Sheldrick, *Acta Cryst. C*, **2015**, *71*, 3
155. M.F. Hawthorne, Z.-P. Zheng, *Acc. Chem. Res.*, **1997**, *30*, 267
156. Z. Xie, *Acc. Chem. Res.*, **2003**, *36*, 1
157. R.N. Grimes, *Coord. Chem. Rev.*, **2000**, *200*, 773

158. B.P. Dash, R. Satapathy, J.A. Maguire, N.S. Hosmane, *New J. Chem.*, **2011**, 35, 1955
159. B. Grüner, J. Plešek, J. Báča, I. Císařová, J.F. Dozol, H. Rouquette, C. Viñas, P. Selucký, J. Rais, *New J. Chem.*, **2002**, 26, 1519
160. J.G. Planas, F. Teixidor, C. Viñas, *Crystals*, **2016**, 6, 50
161. M. Scholz, E. Hey-Hawkins, *Chem. Rev.*, **2011**, 111, 7035
162. R.N. Grimes, *Carboranes, Third Edition*, Academic Press: London, **2016**
163. L.I. Zakharkin, A.V. Grebennikov, A.V. Kazantsev, *Bull. Acad. Sci. USSR Div. Chem. Sci.*, **1968**, 16, 1991
164. M.F. Hawthorne, X. Yang, Z. Zheng, *Pure Appl. Chem.*, **1994**, 66, 245
165. X.-K. Huo, G. Su, G.-X. Jin, *Chem. Eur. J.*, **2010**, 16, 12017
166. M. Juhasz, S. Hoffman, E. Stoyanov, K.C. Kim, C.A. Reed, *Angew. Chem. Int. Ed.*, **2004**, 43, 5352
167. J.F. Valliant, K.J. Guenther, A.S. King, P. Morel, P. Schaffer, O.O. Sogbein, K.A. Stephenson, *Coord. Chem. Rev.*, **2002**, 232, 173
168. Y. Zhu, A.T. Peng, K. Carpenter, J.A. Maguire, N.S. Hosmane, M. Takagaki, *J. Am. Chem. Soc.*, **2005**, 127, 9875
169. L. Schwartz, L. Eriksson, R. Lomoth, F. Teixidor, C. Viñas, S. Ott, *Dalton Trans.*, **2008**, 2379
170. M. Karnahl, S. Tschierlei, O.F. Erdem, S. Pullen, M.-P. Santoni, E.J. Reijerse, W. Lubitz, S. Ott, *Dalton Trans.*, **2012**, 41, 12468
171. A.K. Justice, G. Zampella, L. De Gioia, T.B. Rauchfuss, J.I. van der Vlugt, S.R. Wilson, *Inorg. Chem.*, **2007**, 46, 1655
172. Z.-J. Yao, G.-X. Jin, *Organometallics*, **2011**, 30, 5365
173. T. Liu, M.Y. Darensbourg, *J. Am. Chem. Soc.*, **2007**, 129, 7008
174. C.-H. Hsieh, Ö.F. Erdem, S.D. Harman, M.L. Singleton, E. Reijerse, W. Lubitz, C.V. Popescu, J.H. Reibenspies, S.M. Brothers, M.B. Hall, M.Y. Darensbourg, *J. Am. Chem. Soc.*, **2012**, 134, 13089
175. M. Razavet, S.C. Davies, D.L. Hughes, C.J. Pickett, *Chem. Commun.*, **2001**, 847
176. M. Razavet, S.C. Davies, D.L. Hughes, J.E. Barclay, D.J. Evans, S.A. Fairhurst, X. Liu, C.J. Pickett, *Dalton Trans.*, **2003**, 586
177. F. Xu, C. Tard, X. Wang, S.K. Ibrahim, D.L. Hughes, W. Zhong, X. Zeng, Q. Luo, X. Liu, C.J. Pickett, *Chem Commun.*, **2008**, 606

178. A. Jablonskyté, L.R. Webster, T.R. Simmons, J.A. Wright, C.J. Pickett, *J. Am. Chem. Soc.*, **2014**, *136*, 13038
179. C. Viñas, R. Benakki, F. Teixidor, J. Casabó, *Inorg. Chem.*, **1995**, *34*, 3844
180. F. Gloaguen, J.D. Lawrence, M. Schmidt, S.R. Wilson, T.B. Rauchfuss, *J. Am. Chem. Soc.*, **2001**, *123*, 12518
181. R. Seidel, B. Schnautz, G. Henkel, *Angew. Chem. Int. Ed.*, **1996**, *35*, 1710
182. G. Hogarth, N.J. Taylor, A.J. Carty, A. Meyer, *J. Chem. Soc., Chem. Commun.*, **1988**, *12*, 834
183. W. Imhof, G. Huttner, *J. Organomet. Chem.*, **1993**, *448*, 247
184. O.S. Şentürk, *J. Coord. Chem.*, **2008**, *61*, 776
185. SAINT, Bruker AXS Inc., Madison, Wisconsin, USA, **2012**
186. G.M. Sheldrick, *Acta Cryst. A.*, **2008**, *64*, 112
187. T.R. Simmons, G. Berggren, M. Bacchi, M. Fontecave, V. Artero, *Coord. Chem. Rev.*, **2014**, *270*, 127
188. T. Hiromoto, K. Ataka, O. Pilak, S. Vogt, M.S. Stagni, W. Meyer-Klaucke, E. Warkentin, R.K. Thauer, S. Shima, U. Ermler, *FEBS Lett.*, **2009**, *583*, 585
189. C. Zirngibl, R. Hedderich, R.K. Thauer, *FEBS Lett.*, **1990**, *261*, 112
190. C. Zirngibl, W. van Dongen, B. Schworer, R. von Bunau, M. Richter, A. Klein, R.K. Thauer, *Eur. J. Biochem.*, **1992**, *208*, 511
191. S. Vogt, E.J. Lyon, S. Shima, R.K. Thauer, *J. Biol. Inorg. Chem.*, **2008**, *13*, 97
192. G. Berggren, A. Adamska, C. Lambertz, T.R. Simmons, J. Esselborn, M. Attal, S. Gambarelli, J.-M. Mouesca, E. Reijerse, W. Lubitz, T. Happe, V. Artero, M. Fontecave, *Nature*, **2013**, *499*, 66
193. X. Liu, S.K. Ibrahim, C. Tard, C.J. Pickett, *Coord. Chem. Rev.*, **2005**, *249*, 1641
194. A. Adamska, A. Silakov, C. Lambertz, O. Rüdiger, T. Happe, E. Reijerse, W. Lubitz, *Angew. Chem. Int. Ed.*, **2012**, *51*, 11458
195. J.W. Tye, M.Y. Darensbourg, M.B. Hall, *Inorg. Chem.*, **2006**, *45*, 1552
196. S. Tschierlei, S. Ott, R. Lomoth, *Energy Environ. Sci.*, **2011**, *4*, 2340
197. G.A.N. Felton, C.A. Mebi, B.J. Petro, K.A. Vannucci, D.H. Evans, R.S. Glass, D.L.J. Lichtenberger, *Organomet. Chem.*, **2009**, *694*, 2681
198. A. Jablonskyté, L.R. Webster, T.R. Simmons, J.A. Wright, C.J. Pickett, *J. Am. Chem. Soc.*, **2014**, *136*, 13038
199. B.K. Teo, M.B. Hall, R.F. Fenske, L.F. Dahl, *Inorg. Chem.*, **1975**, *14*, 3103

200. E.L. Andersen, T.P. Fehlner, A.E. Foti, D.R. Salahub, *J. Am. Chem. Soc.*, **1980**, *102*, 7422
201. B. Walther, H. Hartung, J. Reinhold, P.G. Jones, C. Mealli, H.C. Bottcher, U. Baumeister, A. Krug, A. Mockelt, *Organometallics*, **1992**, *11*, 1542
202. H. Fong, M.-E. Moret, Y. Lee, J.C. Peters, *Organometallics*, **2013**, *32*, 3053
203. N.N. Greenwood, *Coord. Chem. Rev.*, **2002**, *226*, 61
204. R.G. Pearson, *Inorg. Chem.*, **1988**, *27*, 734
205. H. Hirao, K. Omoto, H. Fujimoto, *J. Phys. Chem. A.*, **1999**, *103*, 5807
206. H.C. Brown, R.R. Holmes, *J. Am. Chem. Soc.*, **1956**, *78*, 2173
207. D.F. Shriver, B. Swanson, *Inorg. Chem.*, **1971**, *10*, 1354
208. E.A. Jacobs, PhD thesis, University of East Anglia, **2014**
209. K. Smith, *Chem. Soc. Rev.*, **1974**, *3*, 443
210. A.G. Massey, A.J. Park, F.G.A. Stone, *Proc. Chem. Soc.*, **1963**, 212
211. W.E. Piers, T. Chivers, *Chem. Soc. Rev.*, **1997**, *26*, 345
212. G. Erker, *Dalton Trans.*, **2005**, 1883
213. A.A. Danopoulos, J.R. Galsworthy, M.L.H. Green, S. Cafferkey, L.H. Doerrer, M.B. Hursthouse, *Chem. Commun.*, **1998**, 2529
214. S. Döring, G. Erker, R. Fröhlich, O. Meyer, K. Bergander, *Organometallics*, **1998**, *17*, 2183
215. M.A. Beckett, D.S. Brassington, S.J. Coles, M.B. Hursthouse, *Inorg. Chem. Commun.*, **2000**, *3*, 530
216. D.W. Stephan, *Org. Biomol. Chem.*, **2008**, *6*, 1535
217. G.C. Welch, R.R. San Juan, J.D. Masuda, D.W. Stephan, *Science*, **2006**, *314*, 1124
218. D.J. Parks, R.E. von H. Spence, W.E. Piers, *Angew. Chem. Int. Ed. Engl.*, **1995**, *34*, 809
219. D.J. Parks, W.E. Piers, G.P.A Yap, *Organometallics*, **1998**, *17*, 5492
220. C. Jiang, O. Blacque, H. Berke, *Organometallics*, **2009**, *28*, 5233
221. A.-M. Fuller, D.L. Hughes, S.J. Lancaster, C.M. White, *Organometallics*, **2010**, *29*, 2194
222. E.A. Jacobs, R. Chandrasekar, D.A. Smith, C.M. White, M. Bochmann, S.J. Lancaster, *J. Organomet. Chem.*, **2013**, *730*, 44
223. S.J. Lancaster, **2003**, "Alkylation of boron trifluoride with pentafluorophenyl Gignard reagent; Tris(pentafluorophenyl)boron; borane", *ChemSpider Synthetic Pages*, SyntheticPage 215, DOI: 10.1039/SP215

- 224. F. Xu, C. Tard, X. Wang, S.K. Ibrahim, D.L. Hughes, W. Zhong, X. Zeng, Q. Luo, X. Liu, C.J. Pickett, *Chem. Commun.*, **2008**, 606
- 225. M. Razavet, A. Le Cloirec, S.C. Davies, D. L. Hughes, C.J. Pickett, *J. Chem. Soc., Dalton Trans.*, **2001**, 3551
- 226. H.C. Brown, G. Zweifel, *J. Am. Chem. Soc.*, **1961**, 83, 2544
- 227. H.C. Brown, J. Chandrasekharan, K.K. Wang, *Pure Appl. Chem.*, **1983**, 55, 1387
- 228. H.C. Brown, B.C.S. Rao, *J. Am. Chem. Soc.*, **1956**, 78, 5694
- 229. H.C. Brown, G. Zweifel, *J. Am. Chem. Soc.*, **1959**, 81, 247
- 230. *CrystalClear-SM Expert*, Rigaku Corporation, Tokyo, Japan, **2013**
- 231. *CrysAlisPro*, Agilent Technologies, Abingdon, UK, **2014**
- 232. L. Palatinus, G. J. Chapuis, *J. Appl. Cryst.*, **2007**, 40, 786
- 233. A. Altomare, G. Cascarano, C. Giacovazzo, A. Guagliardi, M. C. Burla, G. Polidori, M. Camalli, *J. Appl. Cryst.*, **1994**, 27, 435
- 234. G. M. Sheldrick, *Acta Cryst. A*, **2008**, 64, 112
- 235. G. M. Sheldrick, *Acta Cryst. C*, **2015**, 71, 3